UNIVERSITÉ DE NANTES
FACULTÉ DES SCIENCES ET DES TECHNIQUES

ÉCOLE DOCTORALE : SPIGA

Année 2012

Probabilistic analysis of shallow foundations resting on spatially varying soils

THÈSE DE DOCTORAT

Discipline : Génie Civil

Spécialité : Géotechnique

Présentée
et soutenue publiquement par

Tamara AL-BITTAR

Le 19 Novembre 2012, devant le jury ci-dessous

Rapporteurs	M. Denys BREYSSE	Professeur, Université Bordeaux 1
	M. Bruno SUDRET	Professeur, ETH Zürich
Examinateurs	M. Isam SHAHROUR	Professeur, Université Lille 1
	M. Panagiotis KOTRONIS	Professeur, Ecole Centrale de Nantes
	M. Shadi NAJJAR	Assistant Professor, American University of Beirut
	Mme. Dalia YOUSSEF	Assistant Professor, Notre Dame University

Directeur de thèse : Pr. Abdul-Hamid SOUBRA

Co-directeur de thèse : Pr. Fadi HAGE CHEHADE

ACKNOWLEDGEMENTS

First and foremost I offer my most sincere gratitude to my thesis supervisor, Pr. Abdul-Hamid Soubra, for his exceptional support and guidance throughout my research work. I attribute the level of my Ph.D degree to his permanent encouragement and involvement, which allowed among others the publication of many journal and conference papers. I could just not expect a better supervisor.

I would also like to thank my Lebanese supervisor, Pr Fadi Hege Chehade for his confidence during my work in Lebanon. My grateful thanks are also extended to Dr. Dalia Youssef for her help in realizing the simulation of stochastic Ground-Motion, to Pr. Panagiotis Kotronis, who helped me introduce the time variability of Ground-Motion in his macro-element and to Ms. Nicolas Humbert and Mrs. Pauline Billion from EDF and Pr. Daniel Dias with whom we had a scientific collaboration on the stochastic dymanic behaviour of a free field soil mass.

I wish to thank the members of my dissertation committe, namely Pr. Isam Shahrour for having accepted to be its president, Pr. Bruno Sudret and Pr. Denys Breysse for their careful reading and rating of my thesis report. I also thank all the jury members for having accepted to be part of the jury and for their relevant questions after my presentation.

Throughout my three years of Ph.D I have meat my second half and the love of my life Rachid Cortas to whom I would like to say thank you.

Last not least, I thank my parents, Antoine and Daad, for their support throughout all my studies. Your encouragement always gave me the confidence to continue to pursue my goals. I also wish to thank my brothers Michel and Fadi, and my sister Mira for their own way support. Your sense of humor always gave me the power to continue what I started.

Finally, I am grateful to my big family and friends for their constant support through all the important step of my life.

ABSTRACT

The aim of this thesis is to study the performance of shallow foundations resting on spatially varying soils and subjected to a static or a dynamic (seismic) loading using probabilistic approaches. In the first part of this thesis, a static loading was considered in the probabilistic analysis. In this part, only the soil spatial variability was considered and the soil parameters were modelled by random fields. In such cases, Monte Carlo Simulation (MCS) methodology is generally used in literature. In this thesis, the Sparse Polynomial Chaos Expansion (SPCE) methodology was employed. This methodology aims at replacing the finite element/finite difference deterministic model by a meta-model. This leads (in the present case of highly dimensional stochastic problems) to a significant reduction in the number of calls of the deterministic model with respect to the crude MCS methodology. Moreover, an efficient combined use of the SPCE methodology and the Global Sensitivity Analysis (GSA) was proposed. The aim is to reduce once again the probabilistic computation time for problems with expensive deterministic models. In the second part of this thesis, a seismic loading was considered. In this part, the soil spatial variability and/or the time variability of the earthquake Ground-Motion (GM) were considered. In this case, the earthquake GM was modelled by a random process. Both cases of a free field and a Soil-Structure Interaction (SSI) problem were investigated. The numerical results have shown the significant effect of the time variability of the earthquake GM in the probabilistic analysis.

TABLE OF CONTENTS

TABLE OF FIGURES

TABLE OF TABLES

GENERAL INTRODUCTION

Traditionally, the analysis and design of geotechnical structures are based on deterministic approaches. In these approaches, constant conservative values of the soil and/or the loading parameters are considered with no attempt to characterize and model the uncertainties related to these parameters. In such approaches, a global safety factor is applied to take into account the soil and loading uncertainties. The choice of this factor is based on the judgment of the engineer based on his past experience.

During the last recent years, much effort has been paid for the establishment of more reliable and efficient methods based on probabilistic analysis. It should be mentioned here that in any probabilistic analysis, there are two tasks that must be performed. First, it is necessary to identify and quantify the soil and/or loading uncertainties. This task is usually carried out through experimental investigations and expert judgment. Although this first step is extremely important, it will not be considered throughout this work. The values of the soil and loading uncertainties used in the analysis are taken from the literature. After the input uncertainties have been appropriately quantified, the task remains to quantify the influence of these uncertainties on the output of the model. This task is referred to as uncertainty propagation. In other words, the uncertainty propagation aims to study the impact of the input uncertainty on the variation of a model output (response).

In nature, the soil parameters (shear strength parameters, elastic properties, etc.) vary spatially in both the horizontal and the vertical directions as a result of depositional and post-depositional processes. On the other hand, the seismic loading is time varying due to the fact that the fault break is random which gives the earthquake this variable aspect. This leads to the necessity of modeling the soil uncertain parameters by random fields and the seismic loading by a random process. As for the uncertainty propagation, different approaches (especially the meta-modeling techniques) were developed during the recent years. Of particular interest are the Polynomial Chaos Expansion (PCE) methodology and its extension the Sparse Polynomial Chaos Expansion (SPCE) methodology which are used in the framework of this thesis to perform the probabilistic analysis.

The ultimate aim of this work is to study the performance of shallow foundations resting on spatially varying soils and subjected to static or dynamic (seismic) loading using probabilistic approaches. In the first part of this thesis (i.e. chapters II, III and IV), static loading cases were considered in the probabilistic analysis. In this part, only the soil spatial variability was considered and the soil parameters were modelled by random fields. The system responses were the ultimate bearing capacity of the foundation and the footing displacement. However, in the second part of this thesis (i.e. chapter V), dynamic (or seismic) loading cases were considered in the probabilistic analysis. In this part, both the soil spatial variability and/or the time variability of the earthquake Ground-Motion (GM) were considered. The system response was the amplification of the acceleration.

Before the presentation of the different probabilistic analyses performed in this thesis, a literature review is presented in chapter I. It presents (i) the different sources of uncertainties, (ii) the soil spatial variability and the time variability of the earthquake ground-motion, (iii) the different meta-modeling techniques for uncertainty propagation and finally, (iv) the PCE and the SPCE methodologies which are the methods used in this thesis.

Contrary to the existing literature where the very computationally-expensive Monte Carlo Simulation (MCS) methodology is generally used to determine the probability density function (PDF) of a high-dimensional stochastic system involving spatially varying soil/rock properties; in chapters II, III and IV, the Sparse Polynomial Chaos Expansion (SPCE) and its extension 'the combined use of the SPCE and the Global Sensitivity Analysis (GSA)' are employed in the framework of the probabilistic analysis. Notice that the sparse polynomial chaos expansion is an extension of the Polynomial Chaos Expansion (PCE). A PCE or a SPCE methodology aims at replacing the finite element/finite difference deterministic model by a meta-model (i.e. a simple analytical equation). Thus, within the framework of the PCE or the SPCE methodology, the PDF of the system response can be easily obtained. This is because MCS is no longer applied on the original computationally-expensive deterministic model, but on the meta-model. The deterministic models used to calculate the system responses are based on numerical simulations using the commercial software FLAC^{3D}.

Contrary to the SLS analysis where the computation time of a footing deterministic displacement is not significant, the computational time of the deterministic ultimate bearing capacity varies in a wide range depending on the soil type and the footing geometry. The computation time of the ultimate bearing capacity of a rectangular or a circular footing is several times greater than that of a strip footing. For a given footing geometry, the time cost is the smallest in the case of a purely cohesive soil (i.e. for the computation of the N_c coefficient for φ=0). It increases in the case of a weightless soil (i.e. for the computation of the N_c coefficient for φ#0) and becomes the most significant in the case of a ponderable soil. The time cost is thus the most significant in the case of a 3D (circular or rectangular) foundation resting on a ponderable soil.

In chapter II, the SPCE methodology was employed to perform a probabilistic analysis at both ultimate limit state (ULS) and serviceability limit state (SLS) of strip footings. Relatively non-expensive deterministic models were used in this chapter since the ULS analysis was performed in the case of a weightless material. Two case studies were considered. The first one involves the case of strip footings resting on a weightless spatially varying soil mass obeying the Mohr-Coulomb failure criterion and the second one considers the case of strip footings resting on a weightless spatially varying rock mass obeying the Hoek-Brown (HB) failure criterion.

As for chapter III, the SPCE methodology was used to investigate the effect of the spatial variability in three dimensions (3D) through the study of the ultimate bearing capacity of strip and square foundations resting on a purely cohesive soil with a spatially varying cohesion in the three dimensions. Although a 3D mechanical problem (with a greater computation time with respect to the models of chapter II) was considered herein, the deterministic model can still be classified as a relatively non-expensive model because it considers a purely cohesive soil.

Chapter IV presents a combination between the SPCE methodology and the Global Sensitivity Analysis (GSA). This combination is refered to in this thesis as SPCE/GSA procedure. The aim of this procedure is to reduce the probabilistic computation time of high-dimensional stochastic problems involving expensive deterministic models. This procedure was illustrated through the probabilistic analysis at ULS of a strip footing resting on a ponderable soil with 2D and 3D random fields and subjected to a central vertical load.

Finally, chapter V is devoted to the presentation of the probabilistic analysis performed when a dynamic (or seismic) loading is considered. The soil spatial variability and/or the time variability of the earthquake Ground-Motion (GM) were considered. In this case, the soil parameters were modelled by random fields and the earthquake GM was modelled by a random process. Given the scarcity of studies involving the probabilistic seismic responses, a free field soil medium subjected to a seismic loading was firstly considered. The aim is to investigate the effect of the soil spatial variability and/or the time variability of the earthquake GM using a simple model. Then, a SSI problem was investigated in the second part of this chapter.

The study ends by a general conclusion of the principal results obtained from the analyses.

CHAPTER I. LITERATURE REVIEW

I.1 INTRODUCTION

Traditionally, the analysis and design of geotechnical structures are based on deterministic approaches. In these approaches, constant conservative values of the soil and/or the loading parameters are considered with no attempt to characterize and model the uncertainties related to these parameters.

Many sources of uncertainties may be encountered in geotechnical engineering problems. Some of these uncertainties result from natural variation and thus are considered as inherent (or aleatory). Others (called epistemic) arise from a lack of knowledge or ignorance. The aleatory sources of uncertainty cannot be reduced or resolved through the collection of additional information or from expert knowledge. Examples of aleatory uncertainty include the natural spatial variability of the soil properties as a result of depositional and post-depositional processes and the time variability of the earthquake ground-motion. As for the epistemic sources of uncertainty, they may be reduced through more careful measurement or additional data collection. In this thesis, only the aleatory uncertainties and more precisely the spatial variability of the soil properties and the time variability of the earthquake ground-motion (when a seismic loading is involved) are considered.

It should be mentioned here that in any probabilistic analysis, there are two tasks that must be performed. First, it is necessary to identify and quantify the sources of uncertainty (i.e. the soil spatial variability and the time variability of the earthquake ground motion in our study). This task is usually carried out through experimental investigations and expert judgment. Although this first step is extremely important, it will not be considered throughout this work. Instead, the values of the soil and loading uncertainties used in the analysis are taken from the literature. After the input uncertainties have been appropriately quantified, the task remains to quantify the influence of these uncertainties on the output of the model. This task is referred to as the uncertainty propagation. In other words, the uncertainty propagation aims to study the impact of the input uncertainty on the variation of a model output (response).

During the recent years, different approaches (especially the meta-modeling techniques) were developed for the uncertainty propagation. These approaches are detailed later in this chapter. Of particular interest are the Polynomial Chaos Expansion (PCE) methodology and its extension the

Sparse Polynomial Chaos Expansion (SPCE) methodology which are used in the framework of this thesis to perform the probabilistic analysis.

The aim of this thesis is to investigate the effect of the soil spatial variability and the time variability of the seismic loading (when a seismic loading is considered) on the response of geotechnical structures. More specifically, the probabilistic analyses were performed in the case of a strip footing resting on a spatially varying soil or rock medium and subjected to a static or a seismic load.

This chapter aims at first presenting the different sources of uncertainties. Then, the soil spatial variability and the time variability of the earthquake ground-motion are explained in some detail. This is followed by a brief presentation of the different meta-modeling techniques. Finally, the PCE and the SPCE methodologies which are the methods used in this thesis are presented in some detail.

I.2 SOURCES OF UNCERTAINTIES

While many sources of uncertainties may exist, they are generally categorized as either aleatory or epistemic [Der Kiureghian and Ditlevsen (2009)]. Uncertainties are characterized as epistemic if the modeler sees a possibility to reduce them by gathering more data or by refining the transformation models as explained later. Uncertainties are categorized as aleatory if the modeler does not foresee the possibility of reducing them through the collection of additional information.

In geotechnical engineering, two types of epistemic uncertainties can be faced: The measurements and the transformation uncertainties. The first one is due to the sampling error that results from limited amount of information. This uncertainty can be minimized by considering more samples. The second one is introduced when field or laboratory measurements are transformed into design soil properties using empirical or other correlation models. This uncertainty can be reduced by considering more refined mathematical or empirical models.

As for the aleatory (inherent) uncertainties, the soil material itself is spatially variable and the earthquake is temporally variable. The inherent soil variability primarily results from the natural geologic processes which modify the in-situ soil mass. As for the seismic loading, the time variability results from the fact that the values of the acceleration at the different time steps are random.

In this thesis, only two aleatory uncertainties which are the spatial variability of the soil properties and the time variability of the earthquake ground-motion are considered. The next two sections aim at presenting both the soil spatial variability and the time variability of the ground motion.

I.3 SPATIAL VARIABILITY OF THE SOIL PROPERTIES

In this section, one presents (i) the statistical characterization of the soil spatial variability, (ii) the method used to model (i.e. calculate at unsampled points) this spatial variability, (iii) an overview of the random fields discretization methods and finally (iv) the expansion optimal linear estimation (EOLE) method which is the method of random field discretization used in this thesis to perform the probabilistic analysis.

I.3.1 Statistical characterization of the soil spatial variability

In order to statistically characterize the spatial variability of a soil property, VanMarcke (1977) stated that three statistical parameters are needed: (i) the mean; (ii) the variance (or standard deviation or coefficient of variation); and (iii) the autocorrelation distance (a) (or more generally the autocorrelation function).

The coefficient of variation and the autocorrelation distance are measures of the randomness of the uncertain soil property. An almost homogenous soil will have a large value of (a), whereas one whose property exhibits strong variation over small distances has a low value of (a). In other words, the autocorrelation distance is the distance over which the values of the soil parameter exhibit strong correlation and beyond which, they may be treated as independent random variables [Jaksa (1995)].

When performing probabilistic studies in geotechnical engineering (e.g. determining the probabilistic ultimate bearing capacity or the probabilistic settlement of foundations), it is important to use realistic values of the mean, the standard deviation and the autocorrelation distance (a) of the uncertain soil property. For that purpose, several investigations should be undertaken to quantify these quantities. This is done by performing geotechnical or geophysical tests. In general, the geotechnical tests involve a small area. They are performed to obtain direct information on the soil property at different locations. In general, one needs to perform a large number of tests in order to characterize the variability of the soil property. As for the geophysical tests, they are an efficient alternative to the geotechnical investigations since they allow one to explore a large area with a smaller number of tests. They are performed to obtain indirect measures of the soil property and mainly comprise interpretation of signals (e.g. electrical conductivity, dielectric constant, density, elastic properties, thermal properties, and radioactivity) to characterize a site. For more details on the site investigation methods, the reader may refer to Breysse and Kastner (2003) among others.

After the collection of different values of a given soil property, the determination of the mean and standard deviation of this property is performed using the conventional statistical analysis. This analysis provides the variability of the soil property; however, it does not provide the spatial trend. Thus; to characterize the spatial variation of the soil property, one needs to characterize the autocorrelation distance (*a*). For this purpose, two mathematical techniques can be found in literature to identify the autocorrelation structure of a soil property. These are the random field theory and the geostatistics tools. In this thesis, the random field theory is the method used when performing the probabilistic analysis.

I.3.1.1 Random field theory

The random field theory is commonly used in literature to describe the soil spatial variability. According to VanMarcke (1983), the random field theory should incorporate the observed behavior that values at adjacent locations are more related than those separated by some distance. For this purpose, a fundamental statistical property which is the autocorrelation function (ACF) is introduced in addition to the classical statistical parameters (i.e. the mean and standard deviation or coefficient of variation). The ACF is a plot of the correlation coefficient versus the distance. This ACF may be used to identify (i) the autocorrelation distance (*a*) or (ii) the scale of fluctuation (δ). If the soil property of interest is denoted by *Z*, the correlation coefficient ρ between the values of that property at two different locations is defined as follows:

$$\rho(\Delta h)=\frac{C\left[Z\left(X_{i}\right),Z\left(X_{i+\Delta h}\right)\right]}{\sigma_{Z}^{2}}=\frac{1}{\sigma_{Z}^{2}}E\left\{\left[Z\left(X_{i}\right)-\mu_{Z}\right]\left[Z\left(X_{i+\Delta h}\right)-\mu_{Z}\right]\right\} \tag{I.1}$$

Where *X* is the vector which represents the location. It is given by $X=(x)$ in the case of a one-dimensional random field, $X=(x,y)$ in the case of a two-dimensional (2D) random field and $X=(x,y,z)$ in the case of a three-dimensional (3D) random field. On the other hand, $Z(X_i)$ is the value of the property *Z* at location X_i; $Z(X_{i+\Delta h})$ is the value of the property *Z* at location, $X_{i+\Delta h}$; Δh is the separation distance between the data pairs; E[.] is the expected value; *C* is the covariance and μ_Z and σ_Z are respectively the mean and standard deviation of the property *Z*. It should be emphasized here that it is not possible to know the value of ρ between any two arbitrary points. Thus; in practice, one needs to determine the ACF which allows one to calculate the value of the correlation coefficient between any two arbitrary points. This can be done by collecting some values of the property Z (also known as the data samples) at equally separation distance Δh. These values are gathered in the vector $\chi=\{Z(X_1),...,Z(X_s)\}$ where s is the number of these data samples and $X_{i+1}=X_i+\Delta h$. These data samples are then used to determine the sample ACF as follows:

$$\rho_k=\rho(k\Delta h)=\frac{\sum_{i=1}^{s-k}\left[Z(X_i)-\mu_Z\right]\left[Z(X_{i+k})-\mu_Z\right]}{\sum_{i=1}^{N}\left[Z(X_i)-\mu_Z\right]^2} \qquad k=0, 1, \dots, K \qquad \text{(I.2)}$$

The sample ACF is the graph of ρ_k for $k=0, 1, 2, ..., K$, where K is the maximum allowable number of lags (data intervals). Generally, $K=s/4$ (Box and Jenkins 1970), where s is the total number of data samples.

The ACF is often used to determine the distance over which a property exhibits strong correlation. Two measures of this quantity which are the autocorrelation distance (a) or the scale of fluctuation (δ) may be evaluated. The autocorrelation distance (a) is defined as the distance required for the autocorrelation function to decay from 1 to e^{-1} (0.3679). On the other hand, the scale of fluctuation is defined as the area under the ACF [Fenton (1999)]. The determination of the autocorrelation distance (a) is done by fitting the sample ACF to one of the models given in Table I.1 where $k\Delta h$ is the lag distance and (a) is the autocorrelation distance.

Model	Autocorrelation function	Scale of fluctuation (δ)
Single exponential	$\rho_k=\exp\left(\frac{-\lvert k\Delta h\rvert}{a}\right)$	$\delta=2a$
Square exponential	$\rho_k=\exp\left(-\left[\frac{\lvert k\Delta h\rvert}{a}\right]^2\right)$	$\delta=\sqrt{\pi}a$
Cosine exponential	$\rho_k=\exp(-a\lvert k\Delta h\rvert)\cos(ak\Delta h)$	$\delta=\frac{1}{a}$
Second-order Markov	$\rho_k=(1+a\lvert k\Delta h\rvert)\exp(-a\lvert k\Delta h\rvert)$	$\delta=\frac{4}{a}$

Table I.1. Theoretical ACF used to determine the autocorrelation distance (*a*) [Vanmarcke (1983)]

Finally, it should be mentioned that the modeling of the spatial variability is greatly facilitated by the data being stationary [Uzielli et al. (2005)]. Stationarity is insured if (i) the mean is constant with distance (i.e. no trend exists in the data); (ii) the variance is constant with distance; (iii) there are no seasonal variations; and (iv) there are no irregular fluctuations. In random field theory, it is a common practice to transform a non-stationary data set to a stationary one by removing a low-order polynomial trend (i.e. a first or a second order polynomial) using the ordinary least square method.

I.3.1.2 Geostatistics

Geostatistics was firstly developed by Krige and Matheron in the early 1960s and has since been applied to many disciplines including: groundwater hydrology and hydrogeology; surface hydrology; earthquake engineering and seismology; pollution control; geochemical exploration; and geotechnical engineering. In fact, geostatistics can be applied to any natural phenomena that vary spatially or temporally [Journel and Huijbregts (1978)]. Just as random field theory makes use of the ACF, geostatistics utilizes the 'semivariogram'. The semivariogram is a plot of semivariances versus the distance. This semivariogram may be used to identify the range of influence (*a*) which is analogue to the autocorrelation distance in the random field theory. If the soil property of interest is denoted by *Z*, the semivariance is defined as follows:

$$\gamma(\Delta h) = \frac{1}{2} E\left\{\left[Z\left(X_{i+\Delta h}\right) - Z\left(X_i\right)\right]^2\right\} \qquad \text{(I.3)}$$

where $Z(X_i)$ is the value of the property *Z* at location X_i; $Z(X_{i+\Delta h})$ is its value at location, $X_{i+\Delta h}$; Δh is the separation distance between the data pairs; and *E*[.] is the expectation operator. Thus, the semivariance is defined as half the expectation value (or the mean) of the squared difference between $Z(X_i)$ and $Z(X_{i+\Delta h})$. Like the ACF, one needs to determine the semivariogram which allows one to calculate the value of the semivariance between any two arbitrary points. This can be done by collecting some values of the property *Z* (also known as the data samples) at equally separation distance Δh. These values are gathered in the vector $\chi = \left\{Z\left(X_1\right), ..., Z\left(X_s\right)\right\}$ where *s* is the number of these data samples and $X_{i+1}.=X_i + \Delta h$. These data samples are then used to determine the sample semivariogram as follows:

$$\gamma_k = \gamma\left(k\,\Delta h\right) = \frac{1}{2N\left(k\right)} \sum_{i=1}^{s} \left[Z\left(X_{i+k}\right) - Z\left(X_i\right)\right]^2 \qquad k=0, 1, \ldots, K \qquad \text{(I.4)}$$

The samples semivariogram is thus the graph of γ_k for *k=0, 1, 2, ..., K*, where *K* is the maximum allowable number of lags (data intervals) and *N(k)* is the number of data pairs corresponding to a given value of *k*.

As the experimental semivariogram is a discrete function, it is desirable in geostatistics to adopt a continuous semivariogram. Hence, analytical models are generally fitted to the experimental semivariogram [Journel and Huijbregts (1978)]. The most common theoretical models of semivariograms are summarized in Table I.2, where the range of influence (a) is analogue to the autocorrelation distance in the random field theory.

Model	Semivariogram	Scale of fluctuation (δ)
Spherical	$\gamma_k = \begin{cases} 1.5\dfrac{k\Delta h}{a} - 0.5\left(\dfrac{k\Delta h}{a}\right)^3 & if \quad k\Delta h < a \\ 1 & otherwise \end{cases}$	$\delta = a$
Exponential	$\gamma_k = 1 - \exp\left(-\dfrac{k\,\Delta h}{a}\right)$	$\delta = 3a$
Gaussian	$\gamma_k = 1 - \exp\left(-\dfrac{(k\,\Delta h)^2}{a^2}\right)$	$\delta = \sqrt{3a}$

Table I.2. Theoretical semivariograms used to determine the range of influence (*a*) [Goovaerts (1998, 1999)]

It should be mentioned here that if the data samples are stationary and normalised to have a mean of zero and a variance of 1.0, the semivariogram is the mirror image of the ACF. The semivariogram and the ACF are related *via* the following relationship given by Fenton (1999):

$$\gamma_k = \sigma^2 (1 - \rho_k) \qquad \text{(I.5)}$$

where σ is the standard deviation of the data samples.

I.3.1.3 Values of the statistical parameters of some geotechnical properties

This section aims at providing the commonly used values of (i) the coefficients of variation *COV*s of some soil/rock properties, (ii) the coefficients of correlation between these parameters, and (iii) the autocorrelation distance (a).

<u>Values of the coefficients of variation COVs</u>

The aim of this section is to provide the different values of the coefficients of variation as given in literature for the soil shear strength parameters (cohesion c, angle of internal friction φ), the soil elastic properties (Young modulus E, Poisson ratio υ) and the rock mass parameters (Geological Strength Index *GSI*, uniaxial compressive strength σ_c) used in this thesis.

Concerning the type of the PDF of the different uncertain parameters; unfortunately, there is no sufficient data to give a comprehensive and complete description of the type of the PDF to be used in the numerical simulations. The existing literature [e.g. Griffiths and Fenton (2001), Griffiths et al. (2002), Fenton and Griffiths (2002, 2003, 2005), Fenton et al. (2003)] tends to recommend the use of a lognormal PDF for the Young's modulus *E*, Poisson's ratio *ν* and cohesion *c*. This recommendation is motivated by the fact that the values of these parameters are strictly positive. Concerning the internal friction angle *φ*, it is recommended to adopt a beta distribution for this parameter to limit its variation in the range of practical values. Finally, concerning the parameters *GSI* and σ_c, Hoek (1998) has recommended the use of a lognormal PDF for these parameters.

Soil cohesion c

For the undrained cohesion c_u of a clay, Cherubini et al. (1993) found that the coefficient of variation of this property decreases with the increase in its mean value. They recommended a range of 12% to 45% for moderate to stiff soil.

Author	COV_{c_u} (%)
Lumb (1972)	30 - 50 (UC test) 60 - 85 (highly variable clay)
Morse (1972)	30 - 50 (UC test)
Fredlund and Dahlman (1972)	30 - 50 (UC test)
Lee et al. (1983)	20 - 50 (clay) 25 - 30 (sand)
Ejezie and Harrop-Williams (1984)	28 – 96
Cherubini et al. (1993)	12 - 145 12 - 45 (medium to stiff clay)
Lacasse and Nadim (1996)	5 - 20 (clay – triaxial test) 10 - 30 (clay loam)
Zimbone et al. (1996)	43 – 46 (sandy loam) 58 – 77 (silty loam) 10 – 28 (clay)
Duncan (2000)	13 – 40

Table I.3. Coefficient of variation of the undrained soil cohesion

Phoon et al. (1995) stated that the variability of the undrained soil cohesion depends on the quality of the measurements. Low variability corresponds to good quality and direct laboratory or field tests. In this case, COV_{c_u} ranges between 10% and 30%. Medium variability corresponds to indirect tests. In this case, COV_{c_u} lies in a range from 30% to 50%. Finally, high variability corresponds to empirical correlations between the measured property and the uncertain parameter. In this case, COV_{c_u} ranges between 50% and 70%. The values of COV_{c_u} as proposed by other authors in literature are summarized in Table I.3.

Angle of internal friction φ of a soil

For the soil internal friction angle *φ*, smaller values of the coefficient of variation as compared to those of the soil cohesion have been proposed in literature. Based on the results presented by Phoon et al. (1995), the coefficient of variation of the internal friction angle ranges between 5% and 20% depending on the quality of the measurements. For good quality and direct measurements, COV_{φ} ranges between 5% and 10%. For indirect measurements, COV_{φ} lies in a range from 10% to 15%. Finally, for the empirical correlations, COV_{φ} ranges between 15% and 20%. Table I.4 provides the values of the coefficient of variation of the soil internal friction angle φ as proposed by several authors.

Author	COV_{φ} (%)	Type of soil
Lumb (1966)	9	Different soil types
Baecher et al. (1983)	5 – 20	Tailings
Harr (1987)	7 12	Gravel Sand
Wolff (1996)	16	Silt
Lacasse and Nadim (1996)	2 – 5	Sand
Phoon and Kulhawy (1999)	5 – 11 4 – 12	Sand Clay, Silt

Table I.4. Values of the coefficient of variation of the soil internal friction angle

Young's modulus E and Poisson's ratio v of a soil

It has been shown in the literature that soils with small values of the elastic Young modulus exhibit significant variability (Bauer and Pula 2000). Table I.5 presents some values of the coefficient of variation of the Young's modulus *E* used in literature. Concerning the Poisson's ratio *v*, there is no sufficient information about its coefficient of variation. Some authors suggest that the variability of this parameter can be neglected while others proposed a very limited range of variability.

Author	COV_E (%)
Baecher and Christian (2003)	2 – 42
Nour et al. (2002)	40 – 50
Bauer and Pula (2000)	15
Phoon and Kulhawy (1999)	30

Table I.5. Values of the coefficient of variation of the Young's modulus

Geological Strength Index (GSI) and uniaxial compressive strength (σ_c) of a rock mass

For the rock mass parameters, there is no sufficient infomation about their coefficients of variation. Hoek (1998) stated that the coefficient of variation of the Geological Strength Index *GSI* of a blocky/disturbed or disintegrated and poor rock mass (which is used in this thesis) is about 10%. As for the uniaxial compressive strength σ_c, relatively large values of its coefficient of variation have been proposed in literature. Gunsallus and Kulhawy (1984) stated that the coefficient of variation of the uniaxial compressive strength of intact rock ranges between 7% and 59% with an average value of about 27%. On the other hand, Hoek (1998) has proposed a value of 25%.

Coefficient of correlation r

The coefficient of correlation between two soil parameters represents the degree of dependence between these parameters. For the soil shear strength parameters c and φ, Lumb (1970) stated that the correlation coefficient $r(c, \varphi)$ ranges from -0.7 to -0.37. Yucemen et al. (1973) proposed values in a range between -0.49 and -0.24, while Wolff (1985) reported that $r(c, \varphi)$=-0.47. Finally, Cherubini (2000) proposed that $r(c, \varphi)$=-0.61. Concerning the correlation coefficient between the soil elastic properties E and v, this coefficient has received a little attention in literature. Bauer and Pula (2000) reported that there is a negative correlation between these parameters.

Autocorrelation distance (a)

A literature review on the values of the autocorrelation distances of different soil types and for different soil properties was given by El-Ramly (2003) and is presented in Table I.6. It should be emphasized here that the autocorrelation function and the autocorrelation distance (a) are generally site specific, and often challenging due to insufficient site data and high cost of site investigations.

Test type	Soil property	Soil type	Autocorrelation distance a(m)	
			vertical	horizontal
VST	c_u(VST)	Organic soft clay	1.2	-
VST	c_u(VST)	Organic soft clay	3.1	-
VST	c_u(VST)	Sensitive clay	3.0	30.0
VST	c_u(VST)	Very soft clay	1.1	22.1
VST	c_u(VST)	Sensitive clay	2.0	-
Q_u	$c_u(Q_u)$	Chicago clay	0.4	-
Q_u	$c_u(Q_u)$	Soft clay	2.0	40.0
UU	$c_u(UU)_N$	Offshore soil	3.6	-
DSS	$c_u(DSS)_N$	Offshore soil	1.4	-
CPT	q_c	North see clay	-	30.0
CPT	q_c	Clean sand	1.6	-
CPT	q_c	North sea soil	-	13.9
CPT	q_c	North sea soil	-	37.5
CPT	q_c	Silty clay	1.0	-
CPT	q_c	Sensitive clay	2.0	-
CPT	q_c	Laminated clay	-	9.6
CPT	q_c	Dense sand	-	37.5
DMT	P_o	Varved clay	1.0	-

Table I.6. Values of the autocorrelation distances of some soil properties as given by several authors (El-Ramly 2003)

[a]VST, vane shear test; Q_u, unconfined compressive strength test; UU, unconfined undrained triaxial test; DSS, direct shear test; CPT, cone penetration test; DMT, dilatometer test;
[b]c_u(VST), undrained shear strength from VST; $c_u(Q_u)$, undrained shear strength from Q_u; $c_u(UU)_N$, normalized undrained shear strength from UU; $c_u(DSS)_N$, normalized undrained shear strength from DSS; q_c, CPT trip resistance; P_o, DMT lift-off pressure.

I.3.2 Practical modeling of the soil spatial variability using the Optimal Linear Estimation (OLE) method

After the characterization of the spatially varying soil property Z using the random field theory or the geostatistics tools, the mean μ_Z, the standard deviation σ_Z, and the autocorrelation distance (a) are known quantities. The fact of knowing the values of the soil property Z at some given points may allow one to approximate the value of Z at an arbitrary point X using the optimal linear estimation method OLE. Indeed, OLE makes use of the experimental data samples to estimate the values of a soil property at unsampled locations. This section is devoted to the presentation of the OLE method used to simulate the soil spatial variability (i.e. the method that can estimate the value of a spatially varying soil property at an arbitrary point using an analytical equation). It should be noted that the concepts used in OLE method will be employed for the discretization of a random field by the expansion optimal linear estimation EOLE method as will be seen later in this chapter.

OLE method was presented by Li and Der Kiureghian (1993). It is sometimes referred to as the Kriging method. It is a special case of the regression method on a linear function [Ditlevsen (1996)]. In this method, the approximated field $\tilde{Z}$ is defined by a linear function of the experimental data samples $\chi=\{Z(X_1),...,Z(X_s)\}$ as follows:

$$\tilde{Z}(X)=a(X)+\sum_{i=1}^{s}b_i(X)Z(X_i)=a(X)+b^T(X)\chi \qquad \text{(I.6)}$$

where *s* is the number of experimental data samples involved in the approximation. The functions $a(X)$ and $b_i(X)$ are determined by minimizing the variance of the error $Var\left[Z(X)-\tilde{Z}(X)\right]$ at each point *X* subjected to $E\left[Z(X)-\tilde{Z}(X)\right]=0$.

The resolution of the minimization problem allows one to obtain the unknown functions $a(X)$ and $b_i(X)$ and thus the approximated field $\tilde{Z}(X)$ as follows:

$$\tilde{Z}(X)=\mu_Z+\sigma_Z\sum\nolimits_{Z(X);\chi}^{T}\sum\nolimits_{\chi;\chi}^{-1}(\chi-\mu_Z) \qquad \text{(I.7)}$$

where μ_Z and σ_Z are respectively the mean and the standard deviation of the random field *Z*, $\Sigma_{\chi;\chi}^{-1}$ and $\Sigma_{Z(X);\chi}^{T}$ are respectively the inverse of the autocorrelation matrix $\Sigma_{\chi;\chi}$ and the transpose of the correlation vector $\Sigma_{Z(X);\chi}$. The autocorrelation matrix $\Sigma_{\chi;\chi}$ provides the correlation between each element in the vector $\chi=\{Z(X_i),...,Z(X_s)\}$ and all the other elements of the same vector. Thus, it is a square matrix of dimension *sxs*. As for the correlation vector $\Sigma_{Z(X);\chi}$, it provides the correlation between each element in the vector $\chi=\{Z(X_i),...,Z(X_s)\}$ and the value of the field at an arbitrary unsampeled point *X*. Thus, it is a vector of dimension *s*. The autocorrelation matrix $\Sigma_{\chi;\chi}$ and the correlation vector $\Sigma_{Z(X);\chi}$ are evaluated using the fitted autocorrelation function (ACF) determined after the characterization of the spatially varying soil property *Z*. It should be mentioned here that the exponential form of the ACF is the one that is the most commonly used in geotechnical engineering as stated by Popescu et al. (2005). It is given as follows:

$$\rho_X\left[(X),(X')\right]=\exp\left(-\left(\frac{|X-X'|}{a}\right)^n\right) \quad (I.8)$$

Where a is a vector that contains the values of the autocorrelation distances as follows; $a=(a_x)$ in the case of a one-dimensional random field, $a=(a_x,a_y)$ in the case of a two-dimensional (2D) random field and $a=(a_x,a_y,a_z)$ in the case of a three-dimensional (3D) random field. For n=1, the autocorrelation function is said to be exponential of order 1; however, for n=2, it is said to be square exponential.

Each element $\left(\Sigma_{\chi;\chi}\right)_{i,j}$ of the autocorrelation matrix $\Sigma_{\chi;\chi}$ and each element $\left(\Sigma_{Z(X);\chi}\right)_i$ of the correlation vector $\Sigma_{Z(X);\chi}$ are calculated using Equation (I.8) as follows:

$$\left(\Sigma_{\chi;\chi}\right)_{i,j}=\rho_Z\left[X_i,X_j\right] \quad (I.9)$$

$$\left(\Sigma_{Z(X);\chi}\right)_i=\rho_Z\left[X_i,X\right] \quad (I.10)$$

where *i=1, …,* s, *j=1, …,* s and X is the arbitrary unsampled point.

Finally, one can see that in Equation (I.7), the approximated random field $\tilde{Z}(X)$ is only a function of the location X because all the other terms in this equation are known. As a result, one needs to introduce a value for the location X to obtain an approximated value of the corresponding property $\tilde{Z}(X)$.

I.3.3 Brief overview of the numerical random fields discretization methods

For computational purposes, the real random field Z which may be represented by an infinite set of random variables has to be discretized in order to yield a finite set of random variables $\{\chi_j, j=1,...,s\}$, which are assigned to discrete locations. If the finite element/finite difference method is the method used in the mechanical analysis, it is convenient to evaluate the random field values in the same way as the finite element/finite difference model (i.e. at the nodes of the deterministic mesh or at the element mid points of this deterministic mesh). The discretization methods can be divided into three main groups [Sudret and Der Kiureghian (2000)]. Each group involves a number of discretization methods as may be seen below. After a brief presentation of the different methods of the three groups, the EOLE method used in this thesis will be presented in more detail.

I.3.3.1 Point discretization methods

In these methods, the random variables χ_j used in the analysis are selected values of Z at some given points X_j. This group involves the following methods:

a) Midpoint (MP) method

This method was introduced by Der Kiureghian and Ke (1998). In this method, the random field is discretized by associating to each element of the finite element/finite difference mesh, a single random variable defined as the value of the field at the centroid of that element.

b) Shape function (SF) method

This method was presented by Liu et al. (1986a,b). It is similar to the MP method with the difference that the random field is discretized by associating a single random variable to each node of the finite element/finite difference mesh. Thus, the value of the random field within an element is described in term of these nodal values and the corresponding shape functions.

c) Integration point (IP) method

In this method, the random field is discretized by associating a single random variable to each of the integration points appearing in the finite element resolution scheme.

I.3.3.2 Average discretization methods

a) Spatial average (SA) method

This method was proposed by VanMarcke and Grigoriu (1983). It consists in approximating the random field in each element of the finite element/finite difference mesh by a constant computed as the average of the original field over that element. This method was extensively used in geotechnical engineering for the study of the effect of the soil spatial variability.

I.3.3.3 Series expansion methods

In the series expansion discretization methods, the random field is approximated by an expansion that involves deterministic and stochastic functions. The deterministic functions depend on the coordinates of the point at which the value of the random field is to be calculated. This group involves the following methods:

a) Karhunen-Loeve (KL) expansion method

This method was presented by Spanos and Ghanem (1989). In this method, the random field is expressed as follows:

$$\tilde{Z}(X) = \mu_Z + \sigma_Z \sum_{j=1}^{N} \sqrt{\lambda_j} \xi_j \phi_j(X) \tag{I.11}$$

Where μ_Z and σ_Z are the mean and standard deviation of the random field Z, (λ_j, ϕ_j) are the eigenvalues and eigenfunctions of the autocorrelation function ρ_Z of the random field Z, ξ_j is a vector of uncorrelated standard normal random variables and N is the number of terms retained in the KL expansion. It should be noticed here that ξ_j are stochastic variables that represent the random nature of the uncertain soil parameter. However, the eigenfunctions $\phi_j(X)$ are the deterministic functions of the KL expansion. They can be evaluated as the solution of the following integral equation:

$$\int_{\Omega} \rho_Z(X, X') f_j(X') dX' = \lambda_j f_j(X) \tag{I.12}$$

This integral can be solved analytically only for few types of the autocorrelation functions (triangular and first order exponential functions) and for simple geometries. Otherwise, it has to be solved numerically.

b) Orthogonal series expansion (OSE) method

This method was proposed by Zhang and Ellingwood (1994). It was introduced to avoid solving the eigenvalue integral of Equation (I.12) using a complete set of orthogonal functions $h_j(X)$ (i.e. Legendre or Hermite polynomials). Thus, in this method, the random field is expressed as follows:

$$\tilde{Z}(X) = \mu_Z + \sigma_Z \sum_{j=1}^{N} \chi_j h_j(X) \tag{I.13}$$

where χ_j are zero mean random variables with unit variance and N is the number of terms retained in the expansion.

c) Expansion optimal linear estimation (EOLE) method

This method was introduced by Li and Der Kiureghian (1993). It makes use of the (OLE) or the kriging method concept in the special case of a Gaussian random field. This method uses a spectral representation of the autocorrelation matrix of the Gaussian random field and it is used in this thesis. Thus, it will be presented in more detail hereafter.

I.3.3.4 Conclusions

As stated by Sudret and Der Kiureghian (2000), in the MP, SF, IP, and SA methods, the discretized random field can be expressed as a finite summation as follows:

$$\tilde{Z}(X) = \sum_{j=1}^{N} \chi_j \phi_j (X) \tag{I.14}$$

where N is the number of terms retained in the discretization procedure, $\phi_j(X)$ are deterministic functions and χ_j are random variables obtained from the discretization procedure. They can be expressed as weighed integrals of the real random field Z over the volume Ω of the system as follows:

$$\chi_j = \int_{\Omega} Z(X)\omega(X)\, d\Omega \tag{I.15}$$

where $\omega(X)$ is the weight function. The values of the weight functions and the deterministic functions for all the above mentioned methods are given in Sudret and Der Kiureghian (2000) and they are reported in Appendix A of this thesis.

Sudret and Der Kiureghian (2000) have stated that the deterministic functions ϕ_j given in Equation (I.14) are not optimal in the case of mid point (MP), spatial average (SA), shape function (SF) and integration point (IP) methods. This means that the number of random variables involved in the discretization scheme is not minimal. Thus, of particular interest are the series expansion methods. In all these methods, the number of the deterministic functions ϕ_j is optimal and thus, the number of random variables involved is minimal.

As a conclusion, all the discretization methods presented in the first two groups provide non optimal solution which makes them unattractive tools for random field discretization. This is because the number of random variables needed to discretize the random fields using these methods is mesh depending. Thus, one obtains a large number of random variables for large finite element/finite difference models. The series expansion methods solve this problem. They provide the optimal number of random variables needed to accurately discretize the random field which makes them powerful tools for random field discretization. From this group, the eigenvalue problem of the KL method given in Equation (I.12) can be solved analytically only for few types of autocorrelation functions and geometries. As for the OSE method, it avoids solving the eigenvalue problem of the KL method given in Equation (I.12). On the other hand, this method is less attractive in terms of accuracy when compared to the KL and the EOLE method [cf. Sudret and Der Kiureghian (2000)]. For this reason, the EOLE method which uses the concept of OLE method is selected herein to perform the random field discretization. This method is described in some details in the following section.

I.3.4 The expansion optimal linear estimation (EOLE) method for random field discretization

The expansion optimal linear estimation method (EOLE) was proposed by Li and Der Kiureghian (1993). It makes use of the concepts employed in OLE (or the kriging method) which was presented in a previous section. This method only deals with uncorrelated Gaussian random fields because it uses a spectral representation of the vector $\chi = \{Z(X_1), ..., Z(X_s)\}$. To overcome the inconvenience of modeling only uncorrelated Gaussian random fields, Vořechovsky (2008) has extended this method to cover the general case of cross-correlated non-Gaussian random fields.

In this section one first presents EOLE method proposed by Li and Der Kiureghian (1993) to model uncorrelated Gaussian random fields. Then, the extension by Vořechovsky (2008) to cover the general case of two cross-correlated non-Gaussian random fields is presented.

In EOLE method, the fact that the spatially varying soil property is assumed to be Gaussian allows one to spectrally decompose its autocorrelation matrix $\Sigma_{\chi;\chi}$ that includes the correlation between each element of the vector $\chi = \{Z(X_1), ..., Z(X_s)\}$ with all the elements of this same vector. Thus $\chi = \{Z(X_1), ..., Z(X_s)\}$ can be written as follows:

$$\chi = \mu_Z + \sigma_Z \sum_{j=1}^{s} \sqrt{\lambda_j} \xi_j \phi_j \tag{I.16}$$

where ξ_j (*j=1, …, s*) are independent standard normal random variables and (λ_j, ϕ_j) are the eigenvalues and eigenvectors of the autocorrelation matrix $\Sigma_{\chi;\chi}$ verifying $\Sigma_{\chi;\chi}\phi_j = \lambda_j \phi_j$.

Substituting Equation (I.16) in to Equation (I.6) and solving the OLE problem leads to the following representation of the approximated random field $\tilde{Z}(X)$:

$$\tilde{Z}(X) = \mu_Z + \sigma_Z \sum_{j=1}^{s} \frac{\xi_j}{\sqrt{\lambda_j}} . (\phi_j)^T . \Sigma_{Z(X);\chi} \tag{I.17}$$

where μ_Z and σ_Z are respectively the mean and the standard deviation of the Gaussian random field *Z*, $\Sigma_{Z(x,y);\chi}$ is the correlation vector between each element in the vector χ and the value of the field at an arbitrary point X, ξ_j is a standard normal random variable, and s is the total number of point samples.

It should be mentioned that the series expansion given in Equation (I.17) can be truncated after N<s terms. This can be done by sorting the eigenvalues λ_j in a descending order. This number N should assure that the variance of the error is smaller than a prescribed tolerance $\varepsilon \approx 10\%$. Notice that the variance of the error for EOLE is given by Sudret and Der Kiureghian (2000) as follows:

$$Var\left[Z(X) - \tilde{Z}(X) \right] = \sigma_Z^2 \left\{ 1 - \sum_{j=1}^{N} \frac{1}{\lambda_j} \left(\left(\phi_j \right)^T \Sigma_{Z(X);\chi} \right)^2 \right\} \tag{I.18}$$

where $Z(X)$ and $\tilde{Z}(X)$ are respectively the exact and the approximate values of the random field at a given point X and $\left(\phi_j \right)^T$ is the transpose of the eigenvector ϕ_j.

I.3.4.1 Extension of EOLE for the generation of two cross-correlated non-Gaussian random fields

Let us consider two cross-correlated non-Gaussian random fields $Z_i^{NG}(X)$ $(i=1,2)$ described by: (i) constant means and standard deviations (μ_{Zi}, σ_{Zi}; $i=1,2$), (ii) non-Gaussian marginal cumulative density functions G_i $(i=1,2)$, (iii) a target cross-correlation matrix $C^{NG} = \begin{pmatrix} r_{1,1} & r_{1,2} \\ r_{2.1} & r_{2,2} \end{pmatrix}$ and (iv) a common autocorrelation function ρ_Z^{NG} [(X), (X')].

Since EOLE only deals with uncorrelated Gaussian random fields, the common non-Gaussian autocorrelation matrix $\Sigma_{\chi;\chi}^{NG}$ evaluated using Equation (I.9) (where ρ_Z in this equation is the non-Gaussian autocorrelation function ρ_Z^{NG}) and the target non-Gaussian cross-correlation matrix C^{NG} should be transformed into the Gaussian space using the Nataf correction functions proposed by Nataf (1962). This can be done by applying the following formulas:

$$\left(\Sigma_{\chi;\chi}^{k} \right)_{i,j} = \omega_{i,j} \left(\Sigma_{\chi;\chi}^{NG} \right)_{i,j}; \qquad i=1,\ldots,s; \qquad j=1,\ldots,s \qquad \text{and} \qquad k=1,2 \tag{I.19}$$

$$C_{i,j} = \omega_{i,j} C_{i,j}^{NG} \qquad ; \qquad i=1,2 \ \text{ and } \ j=1,2. \tag{I.20}$$

where $\omega_{i,j}$ is the correction factor.

As a result, one obtains two Gaussian autocorrelation matrices $\Sigma^1_{\chi;\chi}$ and $\Sigma^2_{\chi;\chi}$, and a Gaussian cross-correlation matrix C that can be used to discretize the two Gaussian random fields (of zero mean and unit variance) using EOLE as follows:

$$\tilde{Z}_i^G(X) = \sum_{j=1}^{N} \frac{\kappa^D_{i,j}}{\sqrt{\lambda^i_j}} \cdot \left(\phi^i_j\right)^T \cdot \Sigma^i_{Z(X);\chi} \; ; \qquad i=1,\,2 \tag{I.21}$$

where (λ^i_j, ϕ^i_j ; $i=1, 2$) are the eigenvalues and eigenvectors of the two Gaussian autocorrelation matrices ($\Sigma^i_{\chi;\chi}$; $i=1, 2$) respectively, $\Sigma_{Z(X);\chi}$ is the correlation vector between the random vector χ and the value of the field at an arbitrary point X as obtained using Equation (I.10), and finally N is the number of terms (expansion order) retained in the EOLE method. Notice finally that ($\kappa^D_{i,j}$; $i=1, 2$) are two cross-correlated blocks of independent standard normal random variables obtained using the Gaussian cross-correlation matrix C between the two fields as follows: (i) one should compute the diagonal eigenvalues matrix Λ^C with its corresponding eigenvectors matrix Φ^C of the Gaussian cross-correlation matrix C using the spectral decomposition of the cross-correlation matrix C, and (ii) generate the block sample vector κ^D which contains the two cross-correlated blocks ($\kappa^D_{i,j}$; $i=1, 2$) of independent standard random variables using the following formula:

$$\left(\kappa^D\right)^T = \Phi^D (\Lambda^D)^{1/2} \xi^T \tag{I.22}$$

where Φ^D is a ($2N$x$2N$) block matrix resulting from the multiplication of each element in the matrix Φ^C by the unit matrix of order N (the expansion order), Λ^D is a ($2N$x$2N$) block matrix resulting from the multiplication of each element in the matrix Λ^C by the unit matrix of order N and $\xi = \left\{\xi^1 = \left(\xi^1_1, \ldots, \xi^1_N\right), \xi^2 = \left(\xi^2_1, \ldots, \xi^2_N\right)\right\}$ is a block vector which contains two blocks (ξ^i ; $i=1, 2$) of N standard Gaussian independent random variables for each one.

Once the two Gaussian cross-correlated random fields are obtained, they should be transformed to the non-Gaussian space by applying the following formula:

$$\tilde{Z}_i^{NG}(X) = G_i^{-1}\left\{\Phi\left[\tilde{Z}_i^G(X)\right]\right\} \qquad i = 1,\, 2 \tag{I.23}$$

where $\Phi(.)$ is the standard normal cumulative density function. It should be mentioned here that the series given by Equation (I.21) are truncated for a number of terms N (expansion order) smaller than the number of grid points s, after sorting the eigenvalues (λ^i_j ; $j=1, \ldots, N$) in a descending order. This number should assure that the variance of the error given in Equation (I.18) is smaller than a prescribed tolerance as previously mentioned. In order to clarify the EOLE method and its extension by Vořechovsky (2008), a detailed numerical example is presented in Appendix B to illustrate the different steps for generating cross-correlated non-Gaussian random fields.

I.4 TIME VARIABILITY OF THE SEISMIC LOADING

An earthquake is usually initiated by a series of irregular slippages along faults, followed by a large number of random reflections, refractions, dispersions and attenuations of the seismic waves within the complex ground formations through which they travel. Consequently, an earthquake Ground-Motion (GM) exhibits nonstationarity in both time and frequency domains [Rezaeian and Der Kiureghian (2008)]. The temporal nonstationarity is due to the variation of the intensity of the earthquake GM over time. This intensity evolves with time from zero to a roughly constant value representing the phase of strong motion, and then decreases gradually to zero. The frequency (or spectral) nonstationarity is the change of the frequency content of the earthquake GM over time. Typically, high-frequency compressional (P) waves tend to dominate the initial few seconds of the motion. These are followed by moderate-frequency shear (S) waves, which tend to dominate the strong-motion phase of the ground-motion. Finally, low-frequency surface waves tend to dominate the end of the motion.

The growing interest to perform probabilistic dynamic analysis in recent years has further increased the need for stochastic modeling of earthquake GMs. This is because in such analysis, one needs a large number of recorded ground motions. However, for many regions, the database of recorded motions is not sufficient. As a result, there is an increasing interest in methods for generation of synthetic GMs.

For many years, stochastic processes and more precisely the zero-mean Gaussian process have been used to model earthquake GMs [cf. Shinozuka and Sato (1967), Liu (1970), Ahmadi (1979), Kozin (1988), Shinozuka and Deodatis (1988), Zerva (1988), Papadimitriou (1990), Conte and Peng (1997), Rezaeian and Der Kiureghian (2008) and Rezaeian and Der Kiureghian (2010)]. In order to establish a valid model to simulate stochastic earthquake GMs, statistical characterization of existing earthquake GM is necessary to correctly model the corresponding nonstationarities [cf. Liu (1970), Ahmadi (1979), Zerva (2009) and Rezaeian and Der Kiureghian (2008)].

I.4.1 Statistical characterization of the time variability of earthquake GMs

An earthquake GM is nonstationary in both the time and the frequency domains. Thus, it is statistically characterized by a time-varying standard deviation (i.e. the standard deviation changes as a function of time) and a time-varying autocorrelation function (or the corresponding power spectral density (PSD) function [cf. Figure I.1]). It should be mentioned here that the PSD function represents the autocorrelation function in the frequency domain and it is obtained by applying the Fourier transform on the autocorrelation function. The PSD function is thus used to statistically characterize the GM in the frequency domain. In particular, the PSD function provides the time-varying (i) predominant frequency which gives a measure of where the spectral density is concentrated along the frequency axis, and (ii) frequency bandwidth, corresponding to the dispersion of the spectral density around the predominant frequency [cf. Figure I.2].

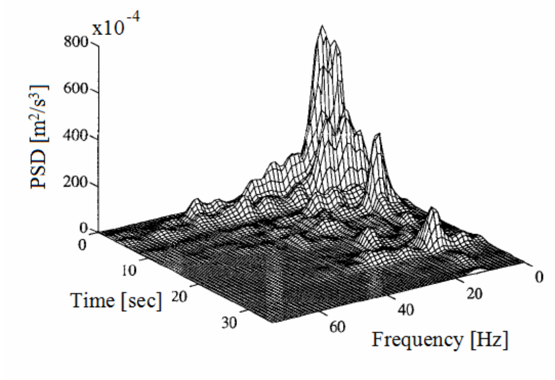

Figure I.1. Time-varying PSD function

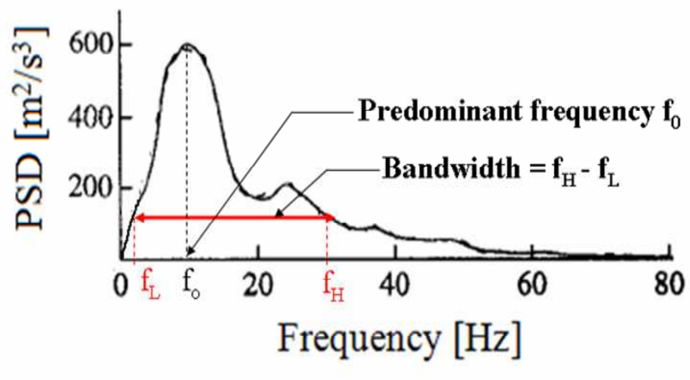

Figure I.2. Predominant frequency and bandwidth

I.4.2 Modeling of the stochastic earthquake GMs

A large number of stochastic models that describe the earthquake GM for a specific site by fitting to a recorded motion with known earthquake and site characteristics have been developed. Formal reviews are presented by Liu (1970), Ahmadi (1979), Shinozuka and Deodatis (1988) and Kozin (1988). The existing stochastic models can be classified into four categories [Rezaeian and Der Kiureghian (2008)]: (i) random processes which are obtained by passing a white noise through a filter and then multiply it by a time-modulation function to ensure the temporal nonstationarity. These models ignore the nonstationarity in the frequency domain [Shinozuka and Sato (1967)]. (ii) Random processes which are obtained by passing a Poisson pulse train through a linear filter [Cornel (1960)]. Through modulation in time of these processes, the two types of nonstationarity can be taken into account. The major difficulty remains to link these processes to target recorded acceleration time-histories. (iii) Random processes which are obtained using the

ARMA models (Auto-Regressive Moving Average) [Conte et al. (1992)] in which the variation of the model parameters over time allows to take into account both types of nonstationarity. However, it is difficult to relate the model parameters to the physical aspects of the earthquake GM. (iv) Random processes which are obtained by various forms of spectral representation [Der Kiureghian and Crempien (1989)]. These models require extensive treatment of the target recorded acceleration time history.

The stochastic model used in this thesis is the one developed by Rezaeian and Der Kiureghian (2008, 2010). It consists in passing a Gaussian white noise through a linear filter. However, unlike previous models, the filter has time-varying parameters, which allows the variation of the spectral content with time. Temporal nonstationarity is achieved by modulation in time.

The next subsections are organized as follows: First, a brief description of the stochastic model used in this thesis is presented. It is followed by a presentation of the different parameters related to this model.

I.4.2.1 The stochastic model description

For the generation of the stochastic synthetic earthquake GMs, the model given by Rezaeian and Der Kiureghian (2008, 2010) is used herein. In its continuous form, it is given as follows:

$$\tilde{x}(t) = q(t,\alpha)\left\{\frac{1}{\sigma_h(t)}\int_{-\infty}^{t} h\left[t-\tau,\lambda(\tau)\right]w(\tau)d\tau\right\} \quad \text{(I.24)}$$

In this expression, $q(t,\alpha)$ is a deterministic, positive, time-modulating function with parameters α controlling the shape and the intensity of the GM; $w(\tau)$ is a white-noise process; the integral inside the brackets is a filtered white-noise process with $h\left[t-\tau,\lambda(\tau)\right]$ denoting the Impulse-Response Function (IRF) of the filter with time-varying parameters $\lambda(\tau)$; and $\sigma_h^2(t) = \int_{-\infty}^{t} h^2\left[t-\tau,\lambda(\tau)\right]d\tau$ is the variance of the integral process. Because of the normalization by $\sigma_h(t)$, the process inside the curved brackets has unit standard deviation. As a result, $q(t,\alpha)$ equals the standard deviation of the resulting process $\tilde{x}(t)$. It should be noted that the modulating function $q(t,\alpha)$ completely defines the time-varying standard deviation of the presented stochastic model, whereas the form of the filter IRF and its time-varying parameters define its time-varying power spectral density function (PSD). In other words, simulating a stochastic synthetic earthquake GM consists in passing a Gaussian (white-noise) process (which is the source of stochasticity) through a linear filter with time-varying parameters. The obtained filtered white noise (which represents the time-varying PSD function of the model) is then normalized it by dividing it by its standard deviation. Thus, one obtains a normalized filtered white-noise with nonstationarity in the frequency domain. Finally, the temporal nonstationarity is insured by multiplying the normalized filtered white-noise by a time-modulation function (which represents the time-varying standard deviation of the model).

In order to facilitate digital simulation, the stochastic model given in Equation (I.24) is discretized in the time domain as follows [cf. Rezaeian and Der Kiureghian (2008)]:

$$\hat{x}(t) = q(t,\ \alpha) \left[\frac{\sum_{i=1}^{N} h\ \left[t - t_i\ ,\ \omega_f\ (t_i),\ \zeta_f\ (t_i) \right] u_i}{\sqrt{\sum_{i=1}^{N} h^2\ \left[t - t_i\ ,\ \omega_f\ (t_i),\ \zeta_f\ (t_i) \right]}} \right] \tag{I.25}$$

where $t_i = i \times \Delta t$ for *i=0, 1, …, N,* Δt is a small time step and $N = \frac{T}{\Delta t} + 1$ with T being the total duration of the motion. In most earthquake engineering applications, $\Delta t = 0.01s$. Finally, u_i are a set of standard normal random variables representing random pulses at the discrete time points t_i. Thus, these random variables u_i may be regarded as a train of random pulses that represent intermittent ruptures at the fault. The filter $h\ \left[t - \tau,\ \lambda(\tau) \right]$ may represent the medium through which the seismic waves travel (i.e. the soil medium). Thus, the obtained earthquake GM is the superposition of the filter response to those random pulses.

For a given modulating function and filter IRF, a realization of the process in Equation (I.25) is obtained by simulating at set of standard normal random variables u_i. for *i=1, …, N*.

I.4.2.2 The model parameters

In the current work, a 'Gamma' modulating function was selected. This choice was justified by the fact that this type of function captures the time-evolution of the intensity using a small number of parameters [Rezaeian (2010)]. It is given as follows:

$$q(t,\ \alpha) = \alpha_1 t^{\alpha_2 - 1}\ \exp(-\alpha_3 t) \tag{I.26}$$

where $\alpha = (\alpha_1 > 0,\ \alpha_2 > 1,\ \alpha_3 > 0)$. Of the three parameters, α_1 controls the intensity of the process, α_2 controls the shape of the modulating function and α_3 controls the duration of the motion. These parameters $\alpha = (\alpha_1,\ \alpha_2,\ \alpha_3)$ are related to three physically based parameters

$(\overline{I}_a,\, D_{5-95},\, t_{mid})$ which describe the real recorded GM in the time domain. The first variable, $\overline{I}_a$ is the so-called Arias Intensity ($\overline{I}_a$) given by: $\overline{I}_a = \dfrac{\pi}{2g}\int_0^{t_n}\left[a(t)\right]^2 dt$ [Kramer (1996)]. The second variable D_{5-95} represents the effective duration of the motion. It is defined as the time interval between the instants at which 5% and 95% of the expected $\overline{I}_a$ are reached respectively. Finally, the third variable t_{mid} is the time at the middle of the strong-shaking phase. It is selected as the time at which 45% level of the expected $\overline{I}_a$ is reached. The relationships between $\alpha = (\alpha_1,\, \alpha_2,\, \alpha_3)$ and $(\overline{I}_a,\, D_{5-95},\, t_{mid})$ are given in Appendix C.

For the filter IRF, a form that corresponds to the pseudo-acceleration response of a single-degree-of-freedom linear oscillator was selected. For more details on the pseudo-acceleration response of a single-degree-of-freedom linear oscillator, the reader may refer to Appendix D. It is given by:

$$
\begin{aligned}
h\left[t-\tau,\, \lambda(\tau)\right] &= \frac{\omega_f(\tau)}{\sqrt{1-\zeta_f^2(\tau)}}\exp\left[-\zeta_f(\tau)\omega_f(\tau)(t-\tau)\right]\times\sin\left[\omega_f(\tau)\sqrt{1-\zeta_f^2(\tau)}(t-\tau)\right] \qquad t \le \tau \\
&= 0 \qquad \text{otherwise}
\end{aligned}
\tag{I.27}
$$

where $\lambda(\tau) = (\omega_f(\tau),\, \zeta_f(\tau))$ is the set of time-varying parameters of the IRF with $\omega_f(\tau)$ denoting the frequency of the filter and $\zeta_f(\tau)$ denoting its damping ratio. Of these two parameters, $\omega_f(\tau)$ controls the predominant frequency of the process and $\zeta_f(\tau)$ controls its bandwidth. These two parameters $\omega_f(\tau)$ and $\zeta_f(\tau)$ are related to two physical parameters that describe the recorded GM in the frequency domain and which are respectively the predominant frequency and the bandwidth of the GM. As a measure of the evolving predominant frequency of the recorded GM, the rate of zero-level up-crossings is considered, and as a measure of its bandwidth, the rate of negative maxima (peaks) and positive minima (valleys) is considered. In Rezaeian and Der Kiureghian (2008), the evolution of the predominant frequency was determined by minimizing the difference between the cumulative mean number of zero-level up-crossings of the process in time with the cumulative count of the zero-level up-crossings of the recorded accelerogram. The mean number of zero-level up-crossings being the mean number of time per unit time that the process crosses the level zero from below. The bandwidth parameter $\zeta_f(\tau)$, was determined by minimizing the difference between the mean rate of negative maxima and positive minima with the observed rate of the same quantity in the recorded accelerogram. Details on the chosen filter IRF which has a form that corresponds to the pseudo-acceleration response of a single-degree-of-freedom linear oscillator, in addition to the procedure used to determine the parameters $\lambda(\tau)=(\omega_f(\tau),\ \zeta_f(\tau))$ of this filter are given in Appendix C.

I.5 PROBABILISTIC METHODS FOR UNCERTAINTY PROPAGATION

Development of efficient methods for uncertainty propagation in order to perform the probabilistic analyses has gained much attention in recent years due to the importance of introducing uncertainties in the model parameters. The uncertainty propagation aims to study the impact of input uncertainty on the variation of a model output (response). This can be done by first defining the analytical/numerical deterministic model. It should be mentioned here that the chosen deterministic model can be complex and/or computationally-expensive (Step B in Figure I.3). The second step consists in identifying the uncertain input parameters and modeling them by random variables or random fields (Step A in Figure I.3). The final step consists in propagating the uncertainty in the input parameters through the deterministic model (Step C in Figure I.3). In the probabilistic framework, all of the relevant information regarding the uncertainty of the model output is contained in its PDF. Thus, determining the PDF of the system response is the main goal in all uncertainty propagation methods. However, the fact that we are considering numerical models implies that the relation between the model uncertain inputs and the system response can not be represented by an analytical expression. Consequently, it is impossible to obtain a simple analytical expression of the PDF of the system response. However, for design purposes, all the information contained in the PDF are not necessary. Thus, depending on the type of study that is carried out, only a set of probabilistic outputs can be used. These probabilistic outputs may be the statistical moments (mean and standard deviation) or the probability of failure (or the probability of exceeding a given threshold value). The different probabilistic outputs may be computed as follows:

Consider M input random variables ($X_1, \ldots, X_M$) gathered in a vector X, and let $f_X(X)$ denote the joint PDF of the set X. Furthermore, we note that the system output $\Gamma=g(X)$. is a function of the input vector X. The expressions of the first two statistical moments of the system response are given by:

$$\mu_\Gamma = \int g(X) f_X(X) dX \tag{I.28}$$

$$\sigma_\Gamma = \int \left[g(X) - \mu_\Gamma \right]^2 f_X(X) dX \tag{I.29}$$

As for the probability of exceeding a threshold Γ_{max}, its expression is given as follows:

$$P_f = \int_{G \le 0} f_X(X)dX \tag{I.30}$$

where G is the performance function given as $G = \Gamma_{max} - \Gamma$

From these equations, one can notice that the statistical measures are expressed as an integral and can be seen as a numerical integration problem. Thus, variety of methods exists for their computation. These methods can be divided into two main categories which are the simulation methods and the metamodeling methods.

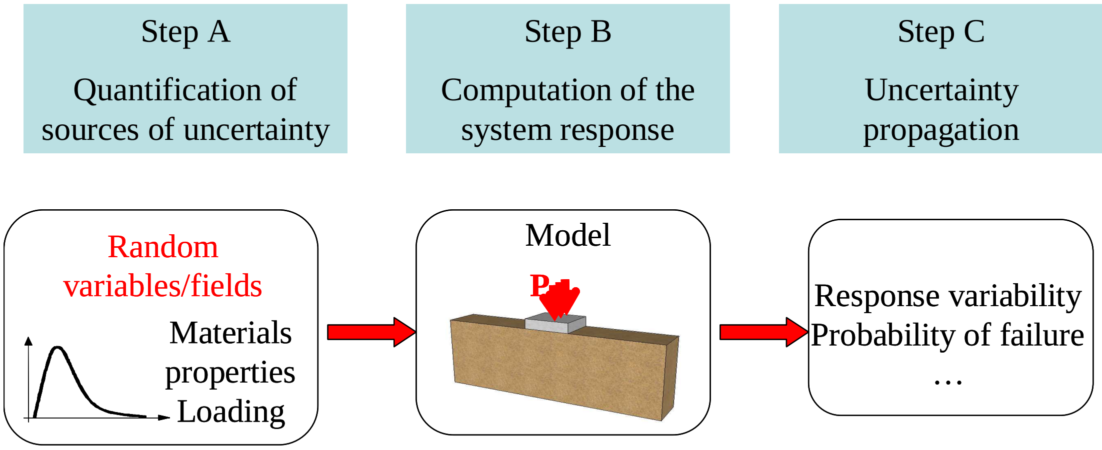

Figure I.3. General sketch for the probabilistic analyses

I.5.1 The simulation methods

This section is devoted to the presentation of the simulation methods used for the uncertainty propagation. This category regroups the universal Monte Carlo simulation (MCS) methodology and other more advanced simulation techniques (i.e. the Importance sampling (IS) and the Subset simulation (SS)). In spite of being rigorous and robust, the simulation methods are well-known to be very time-expensive especially when dealing with finite element or finite difference models which do not offer an analytical solution of the involved problem. The time cost is due to the fact that these methods require a great number of calls of the deterministic model to rigorously determine the PDF of the system response. The advanced simulation techniques (i.e. the IS and the SS) are all based on the modification of the MCS method in order to simulate more points in a particular zone of interest and thus they are very attractive when the probabilistic output of interest is the probability of failure. Thus, the MCS methodology remains the origin of all the advanced simulation techniques and deserves to be firstly presented. This is followed by a brief presentation of the SS method which is the most used advanced simulation method for the computation of the probability of failure.

I.5.1.1 Monte Carlo Simulation (MCS) methodology

The Monte Carlo simulation is a universal method to evaluate complex integrals. It consists in generating K samples which respect the joint probability density function $f_X(X)$ of the M random variables ($X_1, \ldots, X_M$) gathered in a vector X. For each sample, the system response is calculated. Thus; for the K samples, one obtains K values of the system response gathered in a vector $\Gamma = \left\{ \Gamma\left(X^{(1)}\right), \ldots, \Gamma\left(X^{(K)}\right) \right\}$ which may be used to determine the estimators of the first two statistical moments of the system response (i.e. the mean and the standard deviation). These two estimators of the first two statistical moments ($\tilde{\mu}_\Gamma, \tilde{\sigma}_\Gamma$) are given as follows:

$$\tilde{\mu}_\Gamma = \frac{1}{K} \sum_{i=1}^{K} \Gamma\left(X^{(i)}\right) \tag{I.31}$$

$$\tilde{\sigma}_\Gamma = \frac{1}{K-1} \sum_{i=1}^{K} \left[\Gamma\left(X^{(i)}\right) - \tilde{\mu}_\Gamma \right]^2 \tag{I.32}$$

It should be mentioned here that MCS methodology is applicable whatever the complexity of the system is. However, a very large number of realizations is required to obtain a rigorous PDF of the system response. Thus, MCS methodology is not practically applicable when the deterministic model is computationally-expensive and especially when computing small failure probabilities.

I.5.1.2 Subset Simulation (SS) methodology

The basic idea of subset simulation is that the small failure probability can be expressed as a product of larger conditional failure probabilities. Consider a failure region F defined by the condition $G<0$ where G is the performance function and let $\left(X^{(1)}, \ldots, X^{(K)}\right)$ be a sample of K realizations of the vector X composed of M random variables ($X_1, \ldots, X_M$). It is possible to define a sequence of nested failure regions $F_1, \ldots, F_j, \ldots, F_m$ of decreasing size where $F_1 \supset \ldots \supset F_j \supset \ldots \supset F_m = F$ (Figure I.4). An intermediate failure region F_j can be defined by $G<C_j$ where C_j is an intermediate failure threshold whose value is larger than zero. Thus, there is a decreasing sequence of positive failure thresholds $C_1, \ldots, C_j, \ldots, C_m$ corresponding respectively to $F_1, \ldots, F_j, \ldots, F_m$ where $C_1 > \ldots > C_j > \ldots > C_m = 0$. In the SS approach, the space of uncertain parameters is divided into a number m of levels with equal number K_s of realizations $\left(X^{(1)}, \ldots, X^{(K_s)}\right)$. An intermediate level j contains a safe region and a failure region defined with respect to a given failure threshold C_j. The failure probability corresponding to this intermediate level j is calculated as follows:

$$P(F_j \mid F_{j-1}) = \frac{1}{K_s} \sum_{k=1}^{K_s} I_{F_j}\left(X^{(k)}\right) \tag{I.33}$$

where $I_{F_j}\left(X^{(k)}\right)=1$ if $X^{(k)} \in F_j$ and $I_{F_j}\left(X^{(k)}\right)=0$ otherwise. Notice that in the SS approach, the first K_s realizations are generated using MCS methodology according a target joint probability density function $f_X(X)$. The next K_s realizations of each subsequent level are obtained using Markov chain method based on Metropolis-Hastings (M-H) algorithm.

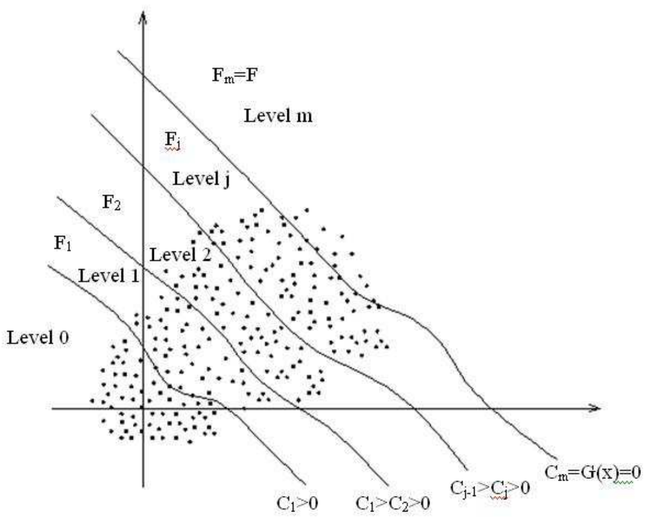

Figure I.4. Nested Failure domain

The failure probability $P(F) = P(F_m)$ of the failure region F can be calculated from the sequence of conditional failure probabilities as follows [Au and Beck (2001)]:

$$P(F) = P(F_m) = P(F_1)\prod_{j=2}^{m} P(F_j \mid F_{j-1}) \tag{I.34}$$

For more details on the SS approach and its extension to the case of spatially varying soil properties, the reader may refer to Ahmed and Soubra (2012) and Ahmed (2012).

I.5.2 The metamodeling techniques

To overcome the inconvenience of the simulation methods, the metamodeling techniques are proposed in this regard. The aim of these techniques is to replace the original computationally-expensive deterministic model by a meta-model (i.e. an analytical equation). A variety of metamodeling techniques exist. The Response Surface Methodology (RSM) [Box et al. (1978), Bucher and Bourgund (1990), Myers and Montgomery (1995)] is a well known approach for constructing simple approximation of complex numerical model using polynomial regression. Another interesting metamodeling technique is the Kriging method [Sacks et al. (1989), Booker et al. (1999)] which is based on interpolation. Finally, the Polynomial Chaos Expansion (PCE) [Spanos and Ghanem (1989), Isukapalli et al. (1998), Xiu and Karniadakis (2002), Berveiller et al. (2006), Sudret et al. (2006), Sudret and Berveiller (2008), Huang et al. (2009), Blatman and Sudret (2010)] provides a rigorous approximation of complex numerical models with reasonable computation effort. This method has gained large attention due to its efficiency. The next subsections aim to briefly present the RSM and the Kriging method. They are followed by a more detailed presentation of the PCE methodology which is the metamodeling technique employed in this thesis.

I.5.2.1 The Response Surface Methodology (RSM)

The Response Surface Methodology (RSM) aims at approximating the system response *Γ(X)* by an explicit function of the random variables. The most popular form of this function is a second order polynomial model, which can be expressed as:

$$\Gamma_{RSM}\left(X\right)=a_0+\sum_{i=1}^{M}a_i X_i+\sum_{i=1}^{M}b_i X_i^2 \qquad \text{(I.35)}$$

where X_i are the random variables, M is the number of random variables and $\left(a_i, b_i\right)$ are coefficients obtained by the least squares method, which minimizes the sum of the squares between the predicted values $\Gamma_{RSM}\left(X^{(i)}\right)$ and the model values $\Gamma=\left\{\Gamma\left(X^{(1)}\right),\ldots,\Gamma\left(X^{(K)}\right)\right\}$ where K is the number of samples points. It should be emphasized here that the second order polynomial used in the RSM method has limited capability to accurately model highly nonlinear response surfaces. Higher-order polynomial models can be used to model a highly nonlinear response surfaces; however, instabilities may arise [cf. Barton (1992)]. Furthermore, this requires a large number of sample points. This enormously increases the computation time and make the RSM solution inadequate in this case.

I.5.2.2 The Kriging Method

This method was presented and detailed in section I.3.2 for the approximation of a random field at unsampled points using the values of this field at sampled points. This method is used herein to approximate the system response *Γ(X)* at any point *X* where the sample points are obtained in this case using a simulation technique (e.g. the Monte Carlo simulation). Thus, for *K* sample points, one obtains *K* values of the system response gathered in a vector $\Gamma = \left\{ \Gamma\left(X^{(1)}\right), ..., \Gamma\left(X^{(K)}\right) \right\}$ which may be used to obtain the approximated system response using the Kriging method as follows [Jin (2005)]:

$$\Gamma_{Kriging}\left(X\right) = a_0 + b_0 \sum\nolimits_{\Gamma(X);\Gamma}^{T} \sum\nolimits_{\Gamma;\Gamma}^{-1} \left(\Gamma - a_0\right) \tag{I.36}$$

where a_0 and b_0 are respectively the mean the standard deviation of the system responses $\Gamma = \left\{ \Gamma\left(X^{(1)}\right), ..., \Gamma\left(X^{(K)}\right) \right\}$, $\Sigma_{\Gamma;\Gamma}^{-1}$ and $\Sigma_{\Gamma(X);\Gamma}^{T}$ are respectively the inverse of the autocorrelation matrix $\sum_{\Gamma;\Gamma}$ and the transpose of the correlation vector $\Sigma_{\Gamma(X);\Gamma}$. It should be mentioned that a row *i* of the autocorrelation matrix gives the values of the correlation between the value of the response at the sampled point $\Gamma\left(X^{(i)}\right)$ and all the values of the response at the sampled points $\Gamma = \left\{ \Gamma\left(X^{(1)}\right), ..., \Gamma\left(X^{(K)}\right) \right\}$ and $\Sigma_{\Gamma(X);\Gamma}$ is a vector whose elements provide the correlation between the value of the response at the unsampled point *Γ(X)* and the values of the response at the sampled points gathered in the vector $\Gamma = \left\{ \Gamma\left(X^{(1)}\right), ..., \Gamma\left(X^{(K)}\right) \right\}$. Notice however that the ACF used to determine the autocorrelation matrix $\sum_{\Gamma;\Gamma}$ and the correlation vector $\Sigma_{\Gamma(X);\Gamma}$ is obtained by fitting one of the analytical ACF given in Table I.1 to the sample ACF obtained using the available system responses $\Gamma = \left\{ \Gamma\left(X^{(1)}\right), ..., \Gamma\left(X^{(K)}\right) \right\}$.

I.5.2.3 The Polynomial chaos expansion PCE methodology - the classical truncation scheme

The polynomial chaos expansion (PCE) aims at replacing a complex deterministic model (i.e. finite element/finite difference numerical model) by a meta-model. This allows one to calculate the system response (when performing MCS) using an approximate simple analytical equation [Spanos and Ghanem (1989), Isukapalli et al. (1998, 1999), Xiu and Karniadakis (2002), Berveiller et al. (2006), Huang et al. (2009), Blatman and Sudret (2010), Li et al (2011), Mollon et al. (2011), Houmadi et al. (2011), Mao et al. (2012), Al-Bittar and Soubra (2012)]. Thus, the metamodel may be used to perform the probabilistic analysis with a significant reduction in the computation time.

The PCE makes use of multivariate polynomials which are orthogonal with respect to the joint probability density function of the input random vector. The different types of the joint probability density functions and their corresponding multivariate polynomials are given in Table I.7.

probability density functions	Polynomials
Gaussian	Hermite
Gamma	Laguerre
Beta	Jacobi
Uniform	Legendre

Table I.7. Usual probability density functions and their corresponding families of orthogonal polynomials [Xiu and Karniadakis (2002)].

In this work, the Gaussian joint probability density function and its corresponding multivariate Hermite polynomials are used. Notice that the coefficients of the PCE may be efficiently computed using a non-intrusive technique where the deterministic calculations are done using for example a finite element or a finite difference software treated as a black box. The most used non-intrusive method is the regression approach [Isukapalli et al. (1998, 1999), Sudret et al. (2006), Huang et al. (2009), Blatman and Sudret (2010), Li et al (2011), Mollon et al. (2011), Houmadi et al. (2011), Mao et al. (2012), Al-Bittar and Soubra (2012)]. It is used in this thesis. The PCE methodology can be described as follows:

Consider a mechanical model with M input uncertain parameters gathered in a vector $X = \{X_1, \ ..., \ X_M\}$. The different elements of this vector can have different types of the probability density function. In order to represent our mechanical system response by a PCE, all the uncertain parameters should be represented by a unique chosen PDF. Table I.7 presents the usual probability density functions and their corresponding families of orthogonal polynomials. Based on the Gaussian PDF chosen in this work, the system response can be expanded onto an orthogonal polynomial basis as follows:

$$\Gamma_{PCE}(\xi) = \sum_{\beta=0}^{\infty} a_\beta \Psi_\beta(\xi) \cong \sum_{\beta=0}^{P-1} a_\beta \Psi_\beta(\xi) \qquad \text{(I.37)}$$

where ξ is the vector resulting from the transformation of the random vector X into an independent standard normal space, P is the number of terms retained in the truncation scheme,

a_β are the unknown PCE coefficients to be computed and Ψ_β are multivariate (or multidimensional) Hermite polynomials which are orthogonal with respect to the joint probability density function of the standard normal random vector ξ. These multivariate Hermite polynomials can be obtained from the product of one-dimensional Hermite polynomials of the different random variables as follows:

$$\Psi_\beta = \prod_{i=1}^{M} H_{\alpha_i}(\xi) \tag{I.38}$$

Where $H_{\alpha_i}(.)$ is the α_i-th one-dimensional Hermite polynomial and α_i are a sequence of M non-negative integers $\{\alpha_1, \ldots, \alpha_M\}$. The expressions of the one-dimensional Hermite polynomials are given in Appendix E. In practice, one should truncate the PCE representation by retaining only the multivariate polynomials of degree less than or equal to the PCE order p (i.e. the classical truncation scheme). Notice that the classical truncation scheme suggests that the first order norm $\|.\|_1$ of any multivariate polynomial Ψ_β should be less than or equal to the order p of the PCE as follows [Blatman (2009)]:

$$\|\alpha\|_1 = \sum_{i=1}^{M} \alpha_i \leq p \tag{I.39}$$

Using this method of truncation, the number P of unknown PCE coefficients is given by:

$$P = \frac{(M+p)!}{M!\,p!} \tag{I.40}$$

As may be seen from Equation (I.40), the number P of the PCE coefficients which is the number of terms retained in Equation (I.37) dramatically increases with the number M of random variables and the order p of the PCE. This number becomes very high in the case of random fields where the number of random variables is significant.

Once the coefficients a_β of the PCE given by Equation (I.37) have been computed, the statistical moments (mean, standard deviation, skewness, and kurtosis) can be calculated with no additional cost. This can be done by performing Monte Carlo simulations on the meta-model and not on the original computationally-expensive finite element/finite difference numerical model. This significantly reduces the cost of the probabilistic analysis since a large number of Monte Carlo simulations (say 1,000,000) can be performed in a negligible time when using the metamodel. The next subsection is devoted to the method used for the computation of the coefficients a_β of the PCE using the regression approach.

Computation of the PCE coefficients by the regression approach

Consider a set of K realizations $\{\xi^{(1)} = (\xi_1,...,\xi_M),...,\xi^{(K)} = (\xi_1,...,\xi_M)\}$ of the standard normal random vector ξ. These realizations are called experimental design (ED) and can be obtained from Monte Carlo (MC) simulations or any other sampling scheme (e.g. Latin Hypercube (LH) sampling or Sobol set). We note $\Gamma = \left\{\Gamma\left(\xi^{(1)}\right),...,\Gamma\left(\xi^{(K)}\right)\right\}$, the corresponding values of the response determined by deterministic calculations. The computation of the PCE coefficients using the regression approach is performed using the following equation:

$$\hat{a} = (\eta^T \eta)^{-1} \eta^T \Gamma \tag{I.41}$$

where the data matrix η is defined by:

$$\eta_{i\beta} = \Psi_\beta(\xi^{(i)}), \qquad i = 1,...,K, \quad \beta = 0,...,P-1 \tag{I.42}$$

In order to ensure the numerical stability of the treated problem in Equation (I.41), the size K of the ED must be selected in such a way that the matrix $(\eta^T \eta)^{-1}$ is well-conditioned. This implies that the rank of this matrix should be larger than or equal to the number of unknown coefficients. This test was systematically performed while solving the linear system of equations of the regression approach.

Computation of the PCE coefficient of determination

The quality of the output approximation *via* a PCE closely depends on the PCE order p. To ensure a good fit between the meta-model and the true deterministic model (i.e. to obtain the optimal PCE order), one successively increases the PCE order until a prescribed accuracy was obtained. The simplest indicator of the fit quality is the well-known coefficient of determination R^2 given by:

$$R^2 = 1 - \frac{\frac{1}{K}\sum_{i=1}^{K}\left[\Gamma\left(\xi^{(i)}\right) - \Gamma_{SPCE}\left(\xi^{(i)}\right)\right]^2}{\frac{1}{K-1}\sum_{i=1}^{K}\left[\Gamma\left(\xi^{(i)}\right) - \overline{\Gamma}\right]^2} \tag{I.43}$$

where

$$\overline{\Gamma} = \frac{1}{K}\sum_{i=1}^{K}\Gamma\left(\xi^{(i)}\right) \tag{I.44}$$

The value $R^2 = 1$ indicates a perfect fit of the true model response Γ, whereas $R^2 = 0$ indicates a nonlinear relationship between the true model response Γ and the PCE model response Γ_{PCE}. The coefficient R^2 may be a biased estimate since it does not take into account the robustness of the meta-model (i.e. its capability of correctly predicting the model response at any point which does not belong to the experimental design). As a consequence, one makes use of a more reliable and rigorous coefficient of determination denoted Q^2 [Blatman (2009)]. In order to compute this coefficient of determination Q^2, one needs to sequentially remove a point from the experiment design composed of K points. Let $\Gamma_{\xi \backslash i}$ be the meta-model that has been built from the experiment design after removing the i^{th} observation and let $\Delta^i = \Gamma(\xi^{(i)}) - \Gamma_{\xi \backslash i}(\xi^{(i)})$ be the predicted residual between the model evaluation at point $\xi^{(i)}$ and its prediction based on $\Gamma_{\xi \backslash i}$. Thus, the corresponding coefficient of determination Q^2 is obtained as follows:

$$Q^2 = 1 - \frac{\frac{1}{K}\sum_{i=1}^{K}\left(\Delta^i\right)^2}{\frac{1}{K-1}\sum_{i=1}^{K}\left[\Gamma\left(\xi^{(i)}\right) - \overline{\Gamma}\right]^2} \tag{I.45}$$

The two coefficients R^2 and Q^2 will be used in this thesis to check the accuracy of the fit.

Global sensitivity analysis (GSA)

Once the PCE coefficients are determined, a global sensitivity analysis (GSA) based on Sobol indices can be easily performed. Notice that the first order Sobol index of a given random variable ξ_i ($i=1,\ldots, M$) gives the contribution of this variable in the variability of the system response. The first order Sobol index is given by Salteli (2000) and Sobol (2001) as follows:

$$S(\xi_i) = \frac{Var\left[E\left(Y \mid \xi_i\right)\right]}{Var\left(Y\right)} \tag{I.46}$$

where Y is the system response, $E\left(Y \mid \xi_i\right)$ is the expectation of Y conditional on a fixed value of ξ_i, and Var denotes the variance. In the present work, the system response is represented by a PCE. Thus, by replacing Y in Equation (I.46) with the PCE expression, one obtains the Sobol index formula as a function of the different terms of the PCE [Sudret (2008)]. This formula is given by:

$$S(\xi_i) = \frac{\sum_{\beta \in I_i}\left(a_\beta\right)^2 E\left[\left(\Psi_\beta\right)^2\right]}{D_{PCE}} \tag{I.47}$$

where a_β are the obtained PCE coefficients, Ψ_β are the multivariate Hermite polynomials, $E[.]$ is the expectation operator, and D_{PCE} is the variance of the response approximated by the PCE.

The response variance D_{PCE} is given by Sudret (2008) as follows:

$$D_{PCE} = \sum_{\beta=0}^{P-1} \left(a_\beta\right)^2 E\left[\left(\Psi_\beta\right)^2\right] \tag{I.48}$$

Notice that the term $E\left[\left(\Psi_\beta\right)^2\right]$ that appears in both Equation (I.47) and Equation (I.48) is given by Sudret (2008) as follows:

$$E\left(\Psi_\beta^2\right) = \prod_{i=1}^{M} \alpha_i\,! \tag{I.49}$$

where the α_i are the same sequence of M non-negative integers $\{\alpha_1, \ldots, \alpha_M\}$ used in Equation (I.38). Notice that I_i in Equation (I.47) denotes the set of indices β for which the corresponding Ψ_β terms are only functions of the random variable ξ_i (i.e. they only contain the variable ξ_i). It should be emphasized that Equation (I.47) used to compute the Sobol indices can only be used when uncorrelated random variables are involved. Notice however that this equation was used in this thesis to determine the contribution of correlated random fields. For both uncorrelated or correlated variables, it was assumed that a direct relationship exist between each physical variable and its corresponding standard variable. Although this assumption is exact in the case of uncorrelated variables, it is not true in the case of correlated variables. This means that the computed Sobol indices using this assumption should be handled with care in the case of correlated variables. An ongoing research on this topic is necessary to lead to rigorous values of the Sobol indices in this case. Some interesting and recent papers on this subject may be found in Kucherenko et al. (2012), Li et al. (2010), Da Veiga et al. (2009) and Caniou et al. (2012).

In order to illustrate the construction of a PCE and the derivation of the equations providing Sobol indices, an illustrative example of a PCE of order p=3 using only M=2 random variables (ξ_1 and ξ_2) is presented in Appendix E.

I.6 CONCLUSION

In this chapter, a literature review on the spatial variability of the soil properties and the time variability of the seismic loading was presented. The characterization and modeling of the soil spatial variability were firstly presented. This was followed by the characterization and the modeling of the time variability of seismic loading. In this thesis, the soil spatial variability will be modeled by random fields characterized by their probability density functions PDFs and their autocorrelation functions. As for the time variability of seismic loading, it was modeled by a parameterized stochastic model that is based on a modulated, filtered white-noise process which should be fitted to a real target acceleration time history. Finally, the different methods of uncertainties propagation used to perform the probabilistic analyses were presented. These methods were divided into two main categories which are the simulation methods and the metamodeling techniques. The simulation methods involve the Monte Carlo simulation (MCS) methodology which is known to be the most rigorous and robust probabilistic method and other more advanced simulation techniques (i.e. the Importance sampling (IS) and the Subset simulation (SS)). As for the metamodeling techniques, three well known methods were presented which are (i) the Response Surface Methodology (RSM), (ii) the Kriging method and finally (iii) the Polynomial Chaos Expansion (PCE). This last method is of particular interest. It is the method used in the present work. In this method, the meta-model is obtained by expanding the system response on a suitable basis, which is a series of multivariate polynomials that are orthogonal with respect to the joint probability density function of the input random variables. Consequently, the characterization of the PDF of the system response is equivalent to the evaluation of the PCE coefficients. In addition to the PDF, this method allows the computation of the PCE-based Sobol indices. These indices provide the contribution of each uncertain parameter in the variability of the system response.

CHAPTER II. PROBABILISTIC ANALYSIS OF STRIP FOOTINGS RESTING ON 2D SPATIALLY VARYING SOILS/ROCKS USING SPARSE POLYNOMIAL CHAOS EXPANSION

II.1 INTRODUCTION

The spatial variability of the soil/rock properties affects the behavior of geotechnical structures (bearing capacity, foundation settlement, slope stability, etc.). Several probabilistic analyses on foundations have considered the effect of the spatial variability of the soil properties [Griffiths and Fenton (2001), Griffiths et al. (2002), Fenton and Griffiths (2002), Nour et al. (2002), Fenton and Griffiths (2003), Popescu et al. (2005), Breysse et al. (2005), Breysse et al. (2007), Niandou and Breysse (2007), Youssef Abdel Massih (2007), Soubra et al. (2008), Jimenez and Sitar (2009), Cho and Park (2010) and Breysse (2011)]. As for the probabilistic analyses of foundations resting on a spatially varying rock mass, only few studies may be found in literature [Ching et al. (2011)].

It should be mentioned that when dealing with probabilistic studies that involve spatially varying soil/rock properties, the classical Monte Carlo Simulation (MCS) methodology is generally used to determine the probability density function (PDF) of the system response. It is well known that this method is a very time-expensive approach. This is because (i) it generally makes use of finite element or finite difference models which are generally time-expensive and (ii) it requires a great number of calls of the deterministic model.

To overcome the inconvenience of the time cost, the Sparse Polynomial Chaos Expansion (SPCE) methodology was proposed in this regard. Notice that the sparse polynomial chaos expansion is an extension of the Polynomial Chaos Expansion (PCE). A PCE or a SPCE methodology aims at replacing the finite element/finite difference deterministic model by a meta-model (i.e. a simple analytical equation).

Within the framework of the PCE or the SPCE methodology, the PDF of the system response can be easily obtained. This is because MCS is no longer applied on the original computationally-expensive deterministic model, but on the meta-model. This consists in performing a great number of simulations on the meta-model. The other significant advantage of the present SPCE methodology with respect to the classical crude MCS method is that it allows one to easily perform a global sensitivity analysis based on Sobol indices using the SPCE coefficients. These indices give the contribution of each random field to the variability of the system response.

In this chapter, the SPCE methodology was used to perform a probabilistic analysis at both ultimate limit state (ULS) and serviceability limit state (SLS) of strip footings. Two case studies were considered in this chapter. The first one involves the case of strip footings resting on a spatially varying soil mass obeying the Mohr-Coulomb (MC) failure criterion [Al-Bittar and Soubra (2011), Al-Bittar and Soubra (2012a, 2012b) and Al-Bittar (2012)] and the second one considers the case of strip footings resting on a spatially varying rock mass obeying the Hoek-Brown (HB) failure criterion [Al-Bittar and Soubra (2012c)].

In the case of the spatially varying soil mass, a probabilistic analysis at both ULS and SLS of vertically loaded strip footings was performed. The soil shear strength parameters (c and φ) were considered as anisotropic cross-correlated non-Gaussian random fields at ULS and the soil elastic parameters (E and υ) were considered as anisotropic uncorrelated non-Gaussian random fields at SLS. Notice that the system response used at ULS was the ultimate bearing capacity (q_{ult}); however, the footing vertical displacement (v) was considered as the system response at SLS.

Concerning the case of the spatially varying rock mass obeying the Hoek-Brown (HB) failure criterion, only the ULS case of vertically loaded footings was considered. The uniaxial compressive strength of the intact rock (σ_c) was modeled as a non-Gaussian random field and the Geological Strength Index (GSI) was modeled as a random variable. Notice that the system response considered was the ultimate bearing capacity (q_{ult}) of the footing.

Finally, it should be mentioned that the deterministic models used to calculate the different system responses were based on numerical simulations using FLAC^{3D} software. The adaptive algorithm by Blatman and Sudret (2010) to build up a SPCE was used to obtain an analytical equation of the system response.

This chapter is organized as follows: The next section aims at presenting the SPCE methodology. It is followed by the presentation of the probabilistic analysis and the corresponding numerical results (PDF of the system response and the corresponding statistical moments) for both cases of (i) strip footings resting on a spatially varying soil mass obeying MC failure criterion and (ii) strip footings resting on a spatially varying rock mass obeying HB failure criterion. Then, a brief discussion on the validity of the SPCE methodology for the computation of the probability of failure is presented. The chapter ends by a conclusion of the main findings.

II.2 ADAPTIVE SPARSE POLYNOMIAL CHAOS EXPANSION SPCE – THE HYPERBOLIC (Q-NORM) TRUNCATION SCHEME

The sparse polynomial chaos expansion (SPCE) which is an extension of the PCE methodology (cf. section I.5.2.3) was proposed by Blatman and Sudret (2009, 2010) to deal with high dimensional stochastic problems (i.e. when a large number of random variables is involved). The idea behind the SPCE came from the fact that the number of significant terms in a PCE is relatively small [see Blatman (2009)] since the multidimensional polynomials Ψ_β corresponding to high-order interaction (i.e. those resulting from the multiplication of the H_{α_i} with increasing α_i values) are associated with very small values of coefficients a_β. Blatman (2009) also stated that the term resulting from the multiplication of the H_{α_i} with all α_i=0 (i=1, …, M) leads to a significant coefficient a_0 in the PCE. This coefficient represents the probabilistic mean value of the system response. Based on these observations, a new truncation strategy was proposed by Blatman and Sudret (2009, 2010) in which the multidimensional polynomials Ψ_β corresponding to high-order interaction were penalized. This was performed by considering that the q-norm (not the first ordre norm) should be smaller than the PCE order p as follows [Blatman (2009)]:

$$\left\|\alpha\right\|_q = \left(\sum_{i=1}^{M}(\alpha_i)^q\right)^{1/q} \leq p \qquad \text{(II.1)}$$

where q is a coefficient (0<q<1). In this formula, q can be chosen arbitrarily. Blatman and Sudret (2010) have shown that sufficient accuracy is obtained when using $q \geq 0.5$.

The proposed SPCE methodology leads to a sparse polynomial chaos expansion that contains a small number of unknown coefficients. These coefficients can be calculated from a reduced number of calls of the deterministic model with respect to the classical PCE methodology. This is of particular interest in the present case of random fields which involve a significant number of random variables. Notice that the SPCE methodology as proposed by Blatman and Sudret (2010) is based on an iterative procedure to arrive to a minimal number for the SPCE coefficients. This procedure is briefly described as follows:

1. Prescribe a target accuracy Q^2_{TARGET}, a q value that satisfies $q \geq 0.5$, and a maximal value of the SPCE order p. In this chapter, a target accuracy $Q^2_{TARGET} = 0.999$, a coefficient q=0.7, and a maximal SPCE order p=5 were used.

2. Consider a set of K realizations of the standard normal random vector ξ (called experimental design ED) and collect the corresponding model evaluations in the vector Γ. Consider also an empty matrix η. It should be noted here that the random vector ξ describes the soil spatial variability within a given realization. As it will be shown later, the dimension of this vector increases for smaller values of the autocorrelation distances.

3. Initialization (p=0): add to η (in the first column) the vector $\eta_{i0} = \Psi_0(\xi^{(i)})$ for i=1, …, K (see Equation (I.42) where $\xi^{(i)}$ is the vector of independent standard normal random variables corresponding to the i^{th} realization and η_{i0} is a vector that includes the multidimensional Hermite Polynomial of order 0 (i.e. Ψ_0) for the different K realizations. Notice that the Ψ_0 term results from the multiplication of the $H_{\alpha i}$ where all the α_i ($i=0, 1, \ldots, M$) are equal to zero.

4. Enrichment of the SPCE basis (p=p+1): Two sub steps are performed within this step as follows:

- Forward step: Add to η (in the subsequent columns) the different vectors $\eta_{i\beta} = \Psi_\beta(\xi^{(i)})$ corresponding to increasing β values (β>0) for which the Ψ_β terms have a q-norm satisfying $p-1 \leq \|\alpha\|_q \leq p$. Then, use the obtained η matrix to solve the regression problem using Equation (I.41). Save only the vectors $\eta_{i\beta} = \Psi_\beta(\xi^{(i)})$ for which a significant increase in the coefficient of determination Q^2 is obtained.

- Backward step: Discard from η the vectors $\eta_{i\beta} = \Psi_\beta(\xi^{(i)})$ for which the Ψ_β terms having a q-norm strictly less than p (i.e. $\|\alpha\|_q < p$) lead to a negligible decrease in the coefficient of determination Q^2.

5. Go to step 4 to perform an enrichment of the (ED) by adding K' realizations of the vector ξ if the regression problem is ill-posed. Otherwise go to step 6.

6. Stop if either the target accuracy Q^2_{TARGET} is achieved or if p reached the order fixed by the user, otherwise go to step 4.

One should remember that the coefficient of determination Q^2 used to check the goodness of the fit of the SPCE was presented in section I.5.2.3. Blatman and Sudret (2010) have stated that a value of Q^2_{TARGET} =0.99 provides accurate estimates of the two first statistical moments (i.e. mean and standard deviation). However, the estimates of the third and fourth moments need a larger

Q^2_{TARGET} value (i.e. Q^2_{TARGET} =0.999). This value is the one used in this thesis. Concerning the number of realizations K and K' employed in the above procedure, relatively high values of K and K' (say K=200 and K'=100) were used in case where the deterministic models are relatively non-expensive as the ULS analysis of strip footings resting on a weightless soil/rock mass (see sections II.3.1 and II.4). In this case, one may avoid the successive post-treatment which may be computationally-expensive. On the contrary, smaller values of K and K' (say K=100 and K'=20) were used in case of more computationally-expensive deterministic models as the case of the square footings resting on a purely cohesive soil (see chapter III).

Once the unknown coefficients of the SPCE are determined, the PDF of the system response and its corresponding statistical moments (i.e. mean μ, standard deviation σ, skewness δ_u, and kurtosis κ_u) can be easily estimated. This can be done by simulating a large number of realizations (using Monte Carlo technique) of the independent standard normal random variables. Simulating a large number of realizations and their corresponding responses using the meta-model dramatically reduces the computation time.

II.3 PROBABILISTIC ANALYSIS OF STRIP FOOTINGS RESTING ON A SPATIALLY VARYING SOIL MASS OBEYING MOHR-COULOMB (MC) FAILURE CRITERION

The aim of this section is to present the probabilistic numerical results in the case of strip footings resting on a spatially varying soil mass and subjected to a vertical loading. Both the ultimate and the serviceability limit states (i.e. ULS and SLS) are considered herein.

II.3.1 The ultimate limit state ULS case

In this section, the probabilistic numerical results obtained from the ULS analysis are presented and discussed. This analysis involves the computation of the ultimate bearing capacity (q_{ult}) of a strip footing resting on a weightless spatially varying soil mass. The soil shear strength parameters (c and φ) were considered as anisotropic cross-correlated non-Gaussian random fields. The soil dilation angle ψ was considered to be related to the soil friction angle φ by $\psi = 2\varphi/3$. This means that the soil dilation angle was implicitly assumed as a random field that is perfectly correlated to the soil friction angle random field.

Notice that the same autocorrelation function (square exponential) was used for both c and φ. As for the autocorrelation distances a_x and a_y of the two random fields c and φ, both cases of isotropic (i.e. a_x=a_y) and anisotropic (i.e. a_x#a_y) random fields will be treated although the soil is rarely isotropic in reality. For the isotropic case, a range of 1.5-100m was considered. For the anisotropic case, El-Ramly et al. (2003) have shown that a_x is within a range of 10-40m, while a_y ranges from 1 to 3m. These values are in accordance with those given by Phoon and Kulhawy (1999). In our study, the reference values adopted for a_x and a_y were a_x=10m and a_y=1m while the wide ranges of 2-50m and 0.5-50m were considered respectively for a_x and a_y when performing the parametric study in order to explore the possible existence of a minimum value for the probabilistic mean.

The soil cohesion c was assumed to be lognormally distributed. Its mean value and coefficient of variation (referred to as reference values) were taken as follows: $\mu_c = 20kPa, Cov_c = 25\%$. On the other hand, the soil friction angle φ was assumed to be bounded (i.e. $0 \le \varphi \le 45^o$). A beta distribution was selected for this parameter with a mean value and a coefficient of variation given as follows: $\mu_\varphi = 30^0, Cov_\varphi = 10\%$. In order to incorporate the dependence between the soil shear strength parameters, the cross-correlation coefficient $r(c, \varphi)$ is needed. Yucemen et al. (1973) reported values that are in a range of $-0.49 \le r \le -0.24$, while Lumb (1970) suggested values of $-0.7 \le r \le -0.37$. In this study, a value of -0.5 was taken as the reference value, and the range of $-0.5 \le r \le 0$ was considered in the parametric study. The reference cross-correlation matrix between the two random fields (c, φ) is thus given by $C^{NG} = \begin{pmatrix} 1 & -0.5 \\ -0.5 & 1 \end{pmatrix}$.

The deterministic model was based on numerical simulations using the finite difference code FLAC^{3D}. The soil behavior was modeled using a conventional elastic-perfectly plastic model based on Mohr-Coulomb (MC) failure criterion. Notice that the Young modulus E and the Poisson ratio υ were assumed to be deterministic since the ultimate bearing capacity is not sensitive to these parameters. Their corresponding values were respectively $E = 60MPa$ and $\nu = 0.3$. Concerning the footing, a weightless strip foundation of 2m width and 0.5m height was used. It was assumed to follow an elastic linear model ($E = 25GPa$, $\nu = 0.4$). Finally, the connection between the footing and the soil mass was modeled by interface elements having the same mean values of the soil shear strength parameters in order to simulate a perfectly rough soil-footing interface. These parameters have been considered as deterministic in this study. Concerning the elastic properties of the interface, they also have been considered as deterministic and their values were as follows: $K_s = 1GPa, K_n = 1GPa$ where K_s and K_n are respectively the shear and normal stiffnesses of the interface.

As shown in Figure II.1, the adopted soil domain considered in the analysis is 15m wide by 6m deep. It should be noted that the size of a given element in the deterministic mesh depends on the autocorrelation distances of the soil properties. Der Kiureghian and Ke (1988) have suggested that the length of the largest element of the deterministic mesh in a given direction (horizontal or vertical) should not exceed 0.5 times the autocorrelation distance in that direction. In order to respect this criterion for the different autocorrelation distances, two different deterministic meshes were considered in FLAC^{3D}. The first one is devoted to the case of moderate to large values of the autocorrelation distances (i.e. when $a_x \geq 10m$ and $a_y \geq 1m$) [see Figure II.1(a)] and the second one for the small values of the autocorrelation distances (i.e. when $1.5m \leq a_x < 10m$ or $0.5m \leq a_y < 1m$) [see Figure II.1(b)]. For the boundary conditions, the horizontal movement on the vertical boundaries of the grid was restrained, while the base of the grid was not allowed to move in both the horizontal and the vertical directions.

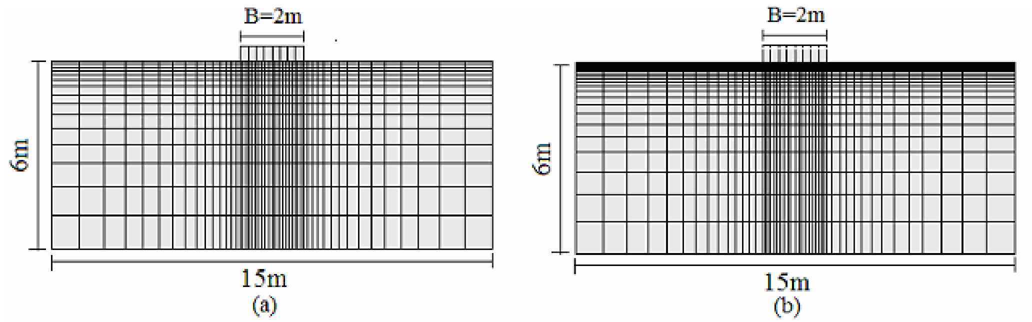

Figure II.1. Mesh used for the computation of the ultimate bearing capacity: (a) for moderate to great values of the autocorrelation distances ($a_x \geq 10m$ and $a_y \geq 1m$), (b) for small values of the autocorrelation distances ($a_x < 10m$ or $a_y < 1m$)

The following sections are organized as follows: First, a step-by-step procedure used to obtain the probabilistic results is presented. It is followed by the presentation of some realizations of the random fields and the PDFs of the system responses. Finally, the effect of the different probabilistic governing parameters on the PDF of the ultimate bearing capacity (q_{ult}) is presented and discussed.

II.3.1.1 Step-by-step procedure used for the computation of the probabilistic results

A Matlab 7.0 code was implemented to obtain the probabilistic results. The different steps of this code in the general case of two anisotropic cross-correlated non-Gaussian random fields are as follows:

(a) Introduce the input statistical parameters described in the preceding section.

(b) Discretize the two random fields c and φ using EOLE method and its extensions by Vořechovsky (2008) as presented in the first chapter using the following steps:

- Define the stochastic grid: Li and Der Kiureghian (1993) have shown that the variance of the error [Equation (I.18)] is large at the boundaries of the stochastic domain. This problem can be solved by using a stochastic domain Ω_{RF} that extends beyond the boundaries of the physical domain Ω. In this work, a uniform stochastic grid of dimensions Ω_{RF}=[16m, 7m] was used while the size of the physical domain was Ω=[15m, 6m] (see Figure II.1). On the other hand, Li and Der Kiureghian (1993) have shown that the number of grid-points in the stochastic grid strongly depends on the autocorrelation distances. These authors have shown that a ratio of about $\frac{l_{RF}}{a}=\frac{1}{5}$ provides a sufficient accuracy in terms of the variance of the error where l_{RF} is the typical element size in the stochastic grid, and a is the autocorrelation distance. In this work, the number of grid points in the stochastic grid was chosen as follows: 6 grid-points were considered within each autocorrelation distance (horizontal or vertical) with a minimum of 6 grid-points in that direction when the autocorrelation distance is larger than the size of the stochastic domain. Thus, a fine stochastic mesh was used for a highly heterogeneous soil and a coarse stochastic mesh was used for a slightly heterogeneous soil.

- Calculate the common autocorrelation matrix $\Sigma^{NG}_{\chi;\chi}$ using Equation (I.9) (remember here that the dimension of this matrix depends on the values of the autocorrelation distances a_x and a_y). Then, compute the corresponding autocorrelation matrices $\Sigma^{c}_{\chi;\chi}$ and $\Sigma^{\varphi}_{\chi;\chi}$ in the Gaussian space using Nataf model [Equation (I.19)]. Finally, compute for each random field (c and φ) its N largest eigenmodes λ^i_j and φ^i_j (where i=c, φ and j=1,…, N), for which the variance of the error is smaller than a threshold of say $\varepsilon \approx 10\%$. It should be mentioned here that both matrices $\Sigma^{c}_{\chi;\chi}$ and $\Sigma^{\varphi}_{\chi;\chi}$ were quasi-similar to $\Sigma^{NG}_{\chi;\chi}$ and thus the number of eigenmodes (or the number of random variables) which is necessary to discretize each one of the two random fields was similar. As may be seen from Figure II.2, for smaller values of the autocorrelation distance (a_x, a_y or a_x=a_y), the number N of eigenmodes increases. The total number of random variables retained for different cases (where two random fields were considered) is presented in Table II.1. This number is equal to the number of eigenmodes N of a single random field multiplied by 2 since two random fields were considered in the analysis. It should be noticed that the cases where a significant number of random variables (>88) are needed correspond to very small autocorrelation distances (i.e. a_y<1m and a_x<2m). These autocorrelation distances are not of practical interest [see El-Ramly et al. (2003)], and can thus be neglected in this study.

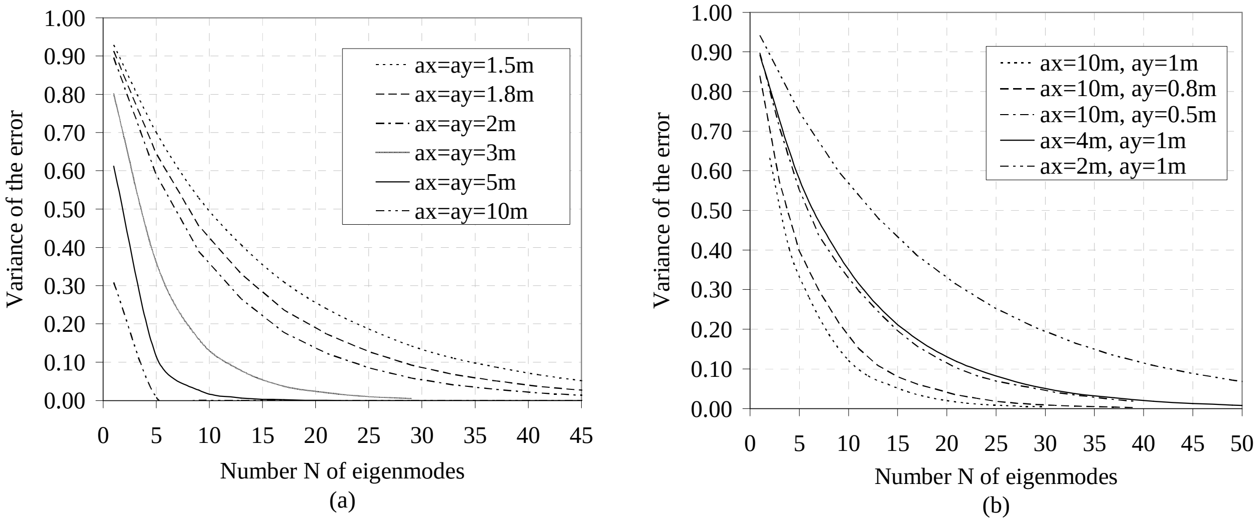

Figure II.2. Number *N* of eigenmodes needed in the EOLE method: (a) isotropic case, (b) anisotropic case

		Total number of random variables used to discretize the two random fields (c, φ)
Isotropic case	$a_x = a_y = 1.5m$	70
	$a_x = a_y = 1.8m$	60
	$a_x = a_y = 2m$	50
	$a_x = a_y = 3m$	24
	$a_x = a_y = 5m$	20
	$a_x = a_y = 10m$	10
Anisotropic case	$a_x = 10m, a_y = 1m$	24
	$a_x = 10m, a_y = 0.8m$	30
	$a_x = 10m, a_y = 0.5m$	44
	$a_x = 4m, a_y = 1m$	48
	$a_x = 2m, a_y = 1m$	88

Table II.1. Number of random variables used to discretize the two random fields *c* and *φ* for both cases of isotropic and anisotropic autocorrelation distances

- Calculate the Gaussian cross-correlated matrix C by applying the Nataf model on the original non-Gaussian cross-correlation matrix C^{NG}. This was performed using Equation (I.20).

- Discretize the two anisotropic cross-correlated Gaussian fields c and φ using Equation (I.21) where κ^D was computed using Equation (I.22); the transformation to the non-Gaussian space being done by applying Equation (I.23).

(c) Use the adaptive SPCE methodology by Blatman and Sudret (2010) to determine the meta-model as follows: First, it should be noted that for each realization, the values of the two random fields (c and φ) were determined at the centroid of each element of the deterministic mesh using Equations (I.21) and (I.23). Once the different elements of the mesh are filed with values of c and φ, the ultimate bearing capacity (q_{ult}) for this specific realization can be determined. The experimental design (ED) was obtained by first simulating the initial number of realizations K=200 of the two random fields (c and φ) using MCS technique. The relatively large number of additional simulations K' =100 is used each time the regression problem is ill-posed (i.e. when the rank of the matrix used in the regression approach is smaller than the number of unknown coefficients). The algorithm stops if either the target accuracy Q^2_{TARGET} is achieved or if p reached the maximal order fixed by the user. In this work, a target accuracy $Q^2_{TARGET} = 0.999$, a coefficient q=0.7, and a maximal order p=5 were used. Notice that for the reference case [a_x=10m, a_y=1m, $r(c, \varphi)$ =-0.5], the algorithm have stopped when the target accuracy was reached. The corresponding order of the SPCE was equal to 4. In this case, where 24 random variables were needed (see Table II.1), the PCE in its "full" truncation schemes leads to P=20,475 unknown coefficients. This means that a minimum of 20,475 collocation points (i.e. a minimum of 20,475 calls of the deterministic model) were needed to accurately represent the ultimate bearing capacity by a meta-model. Using the SPCE methodology, only P=186 unknown coefficients were retained and only 800 calls of the deterministic model were found to be largely sufficient to construct the meta-model. Consequently, an important reduction in the number of calls of the deterministic model can be obtained using the SPCE. This greatly facilitates the solution of the problem of random fields.

(d) Use the meta-model to perform the post-treatment. This consists in determining: (i) the PDF of the ultimate bearing capacity and the corresponding statistical moments (mean, variance, skewness, and kurtosis) and (ii) the Sobol indices for each random field (c and φ).

Finally, it should be mentioned that a link between Matlab and FLAC^{3D} was performed in order to automatically exchange the data in both directions and thus to decrease the computation time.

II.3.1.2 Random fields' realizations and PDFs of the system responses

It should be remembered here that the computation time required for the generation of a single realization is strongly related to the number of eigenmodes N used in the discretization scheme. For very small values of the autocorrelation distances, the number of eigenmodes significantly increases leading to a significant computation time (more than an hour for a single realization). Figure II.3 presents six realizations for three different configurations. As may be seen from this figure, the anisotropy and the negative cross-correlation are well reflected by the obtained random fields realizations.

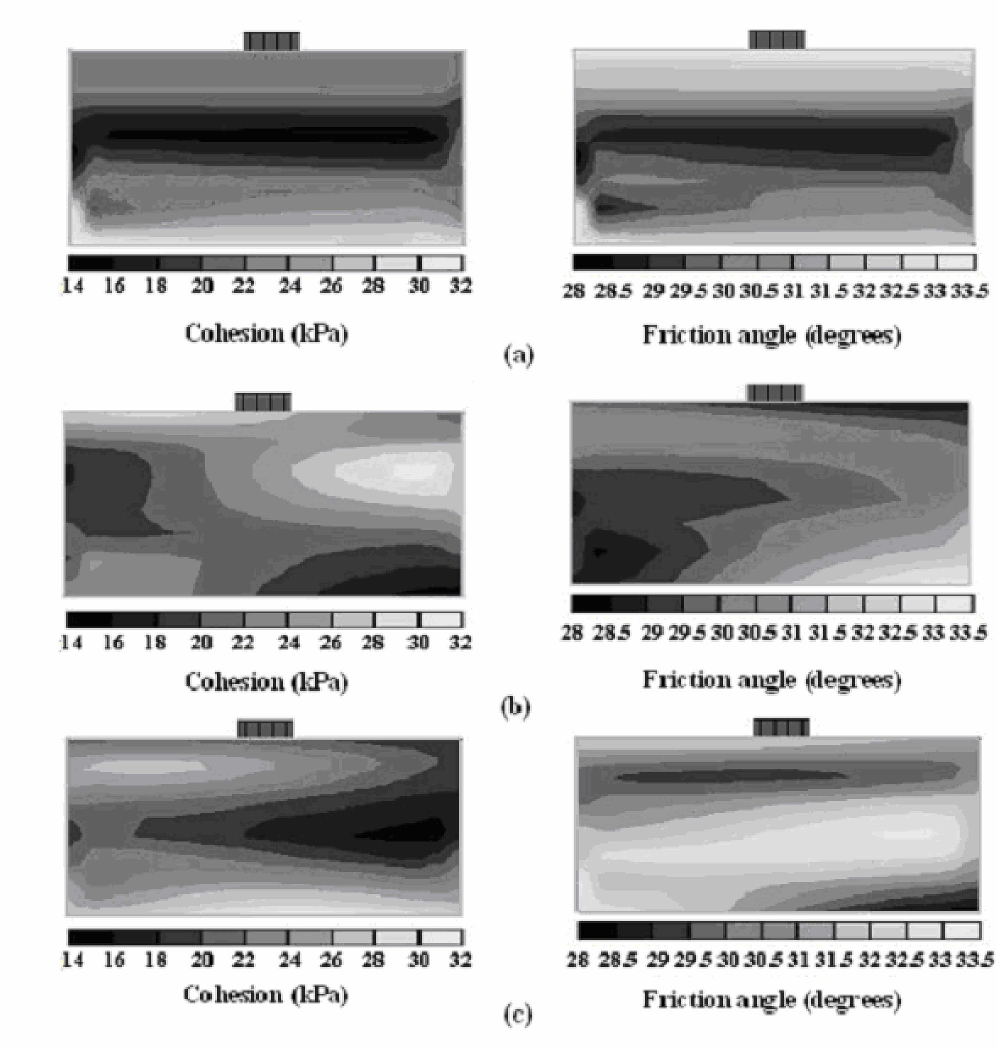

Figure II.3. Typical realizations of the random fields :(a) [a_x=100m, a_y=1m, $r(c, \varphi)$=-0.5]; (b) [a_x=10m, a_y=1m, $r(c, \varphi)$=-0.5]; (c) [a_x=10m, a_y=1m, $r(c, \varphi)$=-0.9]

Figure II.4 presents the PDFs of the footing ultimate bearing capacity and the footing rotation for the reference case where a_x=10m, a_y=1m, and $r(c, \varphi)$=-0.5. Figure II.5 presents the velocity field for one single simulation (i.e. a single realization of the two random fields c and φ). As may be seen from this figure, the spatial variability of the soil properties can produce a non-symmetrical mechanism even though the footing is subjected to a symmetrical vertical load. Although the footing rotation of a single realization is not null as may be seen from Figure II.5, the mean value of the rotation for the whole number of realizations is null [see Figure II.4(b)], and the standard deviation of this rotation was found equal to 1.6×10^{-4} radians. Concerning the ultimate bearing capacity, its mean and standard deviation values are equal to 658.2*kPa* and 93.57*kPa* respectively.

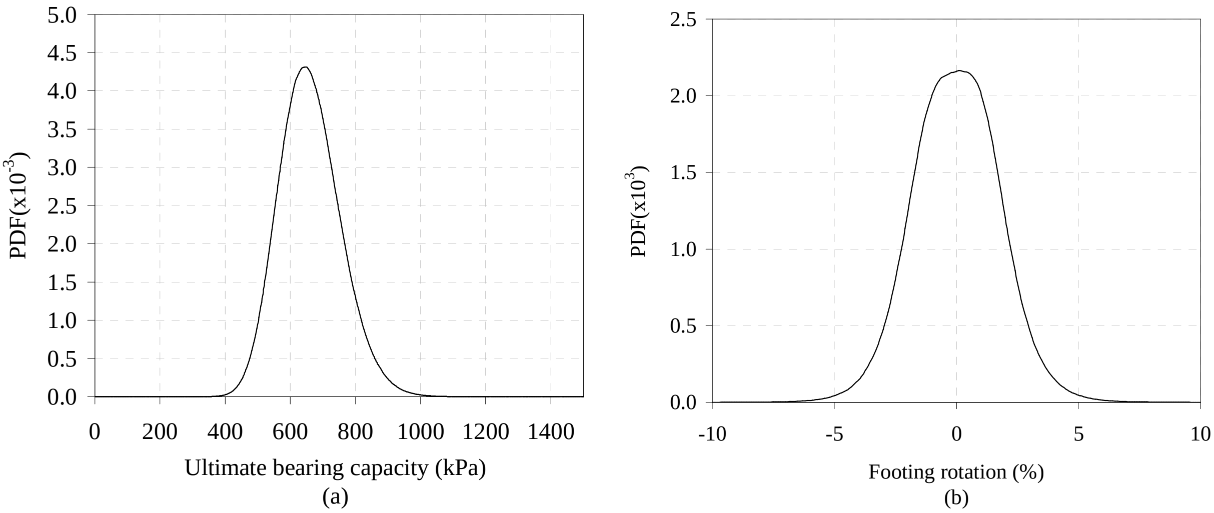

Figure II.4. Bearing capacity and footing rotation for the reference case where a_x=10m, a_y=1m, and $r(c, \varphi)$=-0.5: (a) PDF of the ultimate bearing capacity; and (b) PDF of the footing rotation

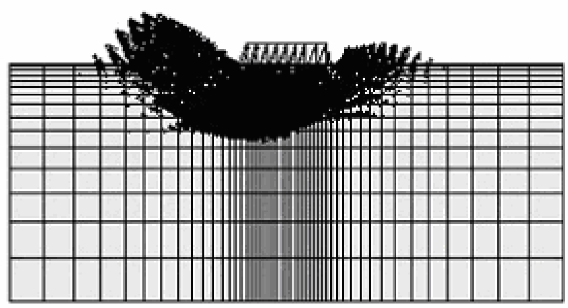

Figure II.5. Velocity field for a typical realization of the two random fields for the reference case where a_x=10m, a_y=1m and $r(c, \varphi)$ =-0.5

II.3.1.3 Probabilistic parametric study

The aim of this section is to study the effect of the different probabilistic governing parameters (autocorrelation distances, coefficients of variation) of the two random fields and the correlation between both fields on the PDF of the ultimate bearing capacity of the foundation.

<u>Effect of the autocorrelation distance: The isotropic case</u>

Figure II.6 provides the PDFs of the ultimate bearing capacity (i) for different values of the isotropic autocorrelation distance $a_x=a_y$ (1.5, 1.8, 2, 3, 5, 10, 50, 100m) when $r(c, \varphi)$=-0.5 and (ii) for the case of random variables with $r(c, \varphi)$=-0.5. Table II.2 presents the four statistical moments for the cases presented in Figure II.6.

As expected, the PDF and the statistical moments corresponding to a great value of the autocorrelation distance ($a_x=a_y$=100m) are close to those given by the case of random variables. This is because the case of random variables can be considered as the limiting case of random fields with an infinite value of the autocorrelation distance.

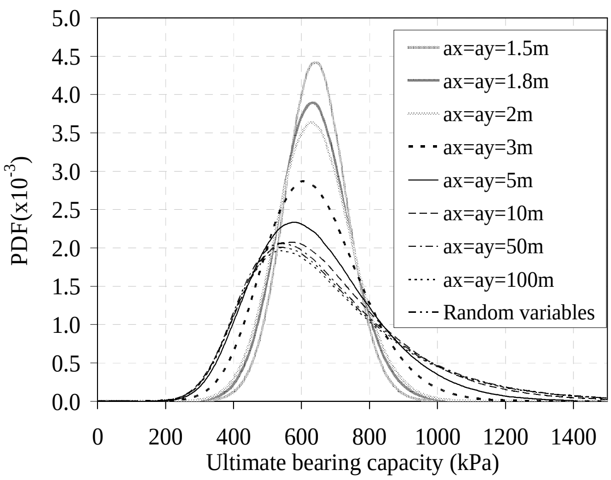

Figure II.6. Influence of the isotropic autocorrelation distance $a_x=a_y$ on the PDF of the ultimate bearing capacity in the case where $r(c, \varphi)$=-0.5

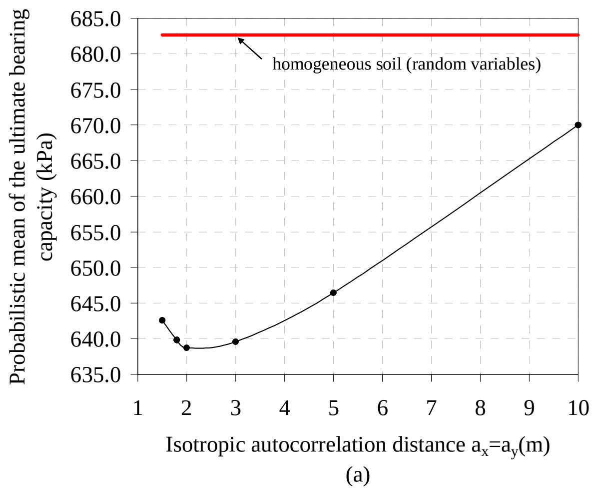

Figure II.7. Influence of the isotropic autocorrelation distance $a_x=a_y$ on the probabilistic mean of the ultimate bearing capacity in the case where $r(c, \varphi)$=-0.5

Figure II.6 shows that the PDF is less spread out when the autocorrelation distance decreases. For the very large values of the isotropic autocorrelation distance $a_x=a_y$=100m, the coefficient of variation of the ultimate bearing capacity tends to a constant maximal value (see Table II.2) which is the value corresponding to the case of random variables as mentioned above. In this case, the different values of a shear strength parameter (c or φ) of a given realization are perfectly correlated. This means that for a given simulation, a single value of c and a single value of φ are affected to the entire soil domain. These values are chosen according to the prescribed PDFs of c

and φ and thus they may vary in the range of values imposed by these PDFs. This leads to a large variability of the ultimate bearing capacity. It should be emphasized here that the large value of the variability is due to the fact that one obtains a large variety of homogenous soils with low, intermediate and high values of the soil shear strength parameters c and φ. The decrease in the autocorrelation distance from infinity to a finite value (moderate or small where $a_x = a_y \leq 10m$) limits the correlation (in a given simulation) to a finite zone which leads to several zones with different values of the shear strength parameters c and φ over the entire soil domain. This means that in a single simulation, one obtains a set of weak and strong zones for which the position may change from simulation to another one. The case of moderate to small values of $a_x = a_y$ leads to a decrease in the variability of the ultimate bearing capacity since (i) the cases of very high or very small values of the bearing capacity are now absent and (ii) the presence of the soil heterogeneity (zones of weak and strong soil) will produce a somewhat close global behavior of the footing because of the averaging phenomenon over the possible failure mechanism. Notice finally that the decrease in the variability of the ultimate bearing capacity becomes the most significant for the case of a very small value of the autocorrelation distance because the rapid change in the values of the shear strength parameters from element to another neighboring one leads to quasi-similar values of the ultimate bearing capacity for all the realizations. The soil can be considered as a homogeneous medium in this case.

$a_x = a_y$ (m)	$\mu_{q_{ult}}$ (kPa)	$\sigma_{q_{ult}}$ (kPa)	COV_{qult} (%)	δ_u (-)	κ_u (-)
1.5	642.6	88.8	13.8	0.06	0.08
1.8	639.8	101.4	15.8	0.19	0.13
2	638.7	108.9	17.0	0.20	0.13
3	639.6	138.8	21.7	0.40	0.30
5	646.4	175.8	27.2	0.67	0.66
10	670.0	217.7	32.5	0.92	1.48
50	676.5	227.4	33.6	1.07	1.93
100	680.7	229.9	33.8	1.08	2.03
Random variables	682.7	232.8	34.1	1.09	2.47

Table II.2. Effect of the isotropic autocorrelation distance a_x=a_y on the statistical moments of the ultimate bearing capacity

Figure II.7 and Table II.2 show that the probabilistic mean value of the ultimate bearing capacity presents a minimum when the autocorrelation distance a_x=a_y is nearly equal to the footing breadth B (i.e. in our case when a_x=a_y=2m). Notice that the minimal probabilistic mean was also observed by Fenton and Griffiths (2003) and Soubra et al. (2008). For very large values of the autocorrelation distance (a_x=a_y=100m), the probabilistic mean tends to the one of the homogenous soil (case of random variables) as may be seen from Table II.2. On the other hand, for very small values of the autocorrelation distance, the probabilistic mean becomes greater than the minimal value because the weakest path becomes increasingly tortuous and its length is also longer. As a result, the failure mechanism will start to look for shorter path cutting through higher values of the shear strength parameters.

Table II.2 shows the impact of the autocorrelation distance a_x=a_y on both the skewness and the kurtosis of the PDF. For small values of a_x=a_y, the skewness and kurtosis of the response are small which means that the PDF of the response is not far from a Gaussian one in these cases. Notice however that these moments increase when a_x=a_y increases which means that for great values of a_x=a_y, the shape of the PDF of the output becomes far from a Gaussian one (the point of maximum density of probability, i.e. the mode moves to smaller values).

Finally, Table II.3 shows the effect of the autocorrelation distance a_x=a_y on the Sobol indices *S(c)* and *S(φ)* of the two random fields *c* and *φ* when *r(c, φ)*=-0.5. This table shows that both indices are quasi-constant regardless of the autocorrelation distance values. The increase in a_x=a_y has no significant impact on the Sobol indices since we increase a_x=a_y in both fields by the same amount. Table II.3 also shows that the variability of the ultimate bearing capacity is mainly due to the cohesion random field which has a Sobol index of about 71%. This result is logical in our case where a weightless soil was considered; the *Nγ* term which is very sensitive to *φ* being absent in this case.

$a_x = a_y$ (m)	$S(c)$	$S(\varphi)$
1.5	0.70	0.30
1.8	0.71	0.29
2	0.72	0.28
3	0.73	0.27
5	0.71	0.29
10	0.73	0.27
50	0.70	0.30
100	0.71	0.29
Random variables	0.69	0.31

Table II.3. Effect of the isotropic autocorrelation distance a_x=a_y on the Sobol indices of the two random fields *c* and *φ*

Effect of the autocorrelation distances: The anisotropic case

Figure II.8 presents the PDFs of the ultimate bearing capacity (i) for different values of a_y (a_y=0.5, 0.8, 1, 2, 5, 8, 50m) when a_x=10m and $r(c, \varphi)$=-0.5 and (ii) for the case of a one-dimensional random field with a horizontally varying soil mass where a_x=10m and $r(c, \varphi)$=-0.5. Table II.4 presents the corresponding four statistical moments. Similarly, Figure II.9 presents the PDFs of the ultimate bearing capacity (i) for different values of a_x (a_x=2, 4, 10, 20, 30, 50m) when a_y=1m and $r(c, \varphi)$=-0.5 and (ii) for the case of a one-dimensional random field with a vertically varying soil mass where a_y=1m and $r(c, \varphi)$=-0.5. Table II.5 presents the corresponding four statistical moments.

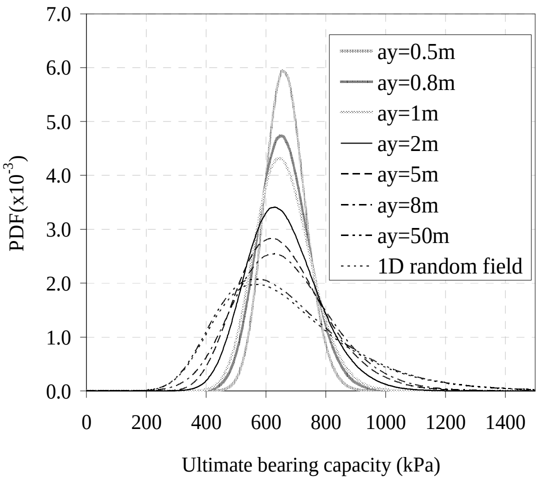

Figure II.8. Influence of the vertical autocorrelation distance a_y on the PDF of the ultimate bearing capacity in the case where $r(c, \varphi)$=-0.5 and a_x=10m

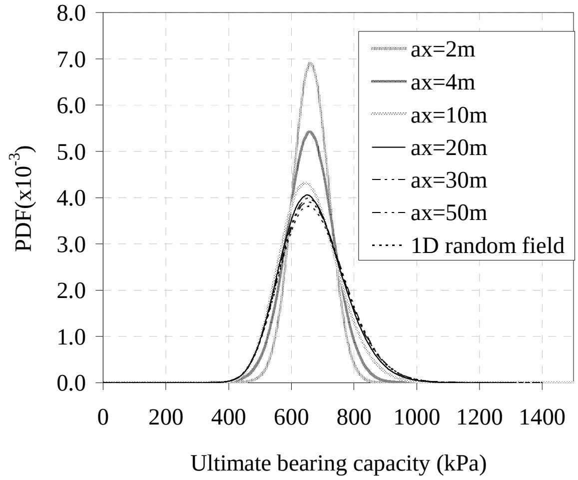

Figure II.9. Influence of the horizontal autocorrelation distance a_x on the PDF of the ultimate bearing capacity in the case where $r(c, \varphi)$=-0.5 and a_y=1m

For the very large values of the autocorrelation distance (a_x or a_y), the coefficient of variation of the ultimate bearing capacity tends to a constant maximal value which corresponds to the value obtained in the case of a one-dimensional random field as may be seen from Tables II.4 and II.5. In this case, the values of c (and also those of φ) are perfectly correlated in a single direction (vertical or horizontal); however, the other direction is allowed to exhibit variations in the values of c (and φ) according to the value of the autocorrelation distance fixed for that direction. This leads to a horizontal or a vertical multilayer. The values of 32.7 and 15.4 (see Tables II.4 and II.5) concerning the variability of the one-dimensional random fields are smaller than the value of 34.1 (see Table II.2) corresponding to the case of random variables. This is because contrarily to the random variables case where the shear strength parameters c and φ of each simulation are chosen from their PDFs where small, high and intermediate values of these parameters lead to a large variability; in the present case of one-dimensional random field, the horizontal or vertical strong layers prevent a large failure mechanism and lead to quasi similar smaller values of the ultimate bearing capacity and thus to a smaller variability of this bearing capacity. Finally, the decrease in the autocorrelation distance from infinity (i.e. from the case of a 1D random field) to a finite value recreates variation in the values of the shear strength parameters which reduces the values of the ultimate bearing capacity and the variability of this bearing capacity.

a_y (m)	$\mu_{q_{ult}}$ (kPa)	$\sigma_{q_{ult}}$ (kPa)	COV_{qult} (%)	δ_u (-)	κ_u (-)
0.5	665.5	67.6	10.2	0.20	0.09
0.8	662.1	83.7	12.6	0.27	0.14
1	658.2	93.6	14.2	0.29	0.16
2	660.6	120.7	18.3	0.42	0.26
5	661.0	147.3	22.3	0.55	0.45
8	662.2	148.7	26.8	0.61	0.54
50	672.1	219.2	32.6	0.95	1.51
1D horizontal random field	672.4	219.6	32.7	0.94	1.50

Table II.4. Effect of the vertical autocorrelation distance a_y on the statistical moments of the ultimate bearing capacity

a_x (m)	$\mu_{q_{ult}}$ (kPa)	$\sigma_{q_{ult}}$ (kPa)	COV_{qult} (%)	δ_u (-)	κ_u (-)
2	662.7	55.7	8.4	0.02	0.05
4	660.2	72.1	10.9	0.03	0.11
10	658.2	93.6	14.2	0.29	0.16
20	669.8	100.2	15.0	0.38	0.23
30	673.3	102.6	15.2	0.39	0.27
50	675.2	103.7	15.4	0.40	0.24
1D vertical random field	676.0	104.1	15.4	0.45	0.25

Table II.5. Effect of the horizontal autocorrelation distance a_x on the statistical moments of the ultimate bearing capacity

Figures II.10 and II.11 and Tables II.4 and II.5 show that the probabilistic mean of the ultimate bearing capacity presents a minimum value of 658.2*kPa* at a certain value of the ratio a_x/a_y (in our work this value is equal to 10 for the prescribed values of the soil and footing characteristics). The presence of a minimum value can be explained as follows:

For a prescribed value of the horizontal autocorrelation distance a_x [see Figure II.10 and Table II.4], the very small value of the vertical autocorrelation distance a_y (i.e. corresponding to a_x/a_y>>1) creates a horizontal multilayer composed of very thin sublayers for which each sublayer may have a large or a small value of the shear strength parameters [see Figure II.12(a)]. On the other hand, the very large value of the vertical autocorrelation distance a_y (i.e. corresponding to a_x/a_y<<1) leads to a vertical multilayer (case of a one-dimensional random field with a horizontally varying soil mass) composed of a finite number of sublayers for which each sublayer may have a large or a small value of the shear strength parameters [see Figure II.12(b)].

For both cases of very small and very large values of a_y, the variety of sublayers with large and small values of the shear strength parameters leads to a greater value of the ultimate bearing capacity. This large value occurs because the sublayers having large values of the shear strength parameters play the role of an obstacle. Therefore, the failure mechanism will cut these sublayers having large values of the soil shear strength parameters. Finally, for medium values of the autocorrelation distances [see Figure II.12(e)], the soil contains a number of stiff zones adjacent to a number of soft zones whose areas are less extended in both the vertical and the horizontal directions compared to the two previous cases. This allows the development of the failure mechanism through the soft soil zones and thus, this leads to smaller values of the ultimate bearing capacity.

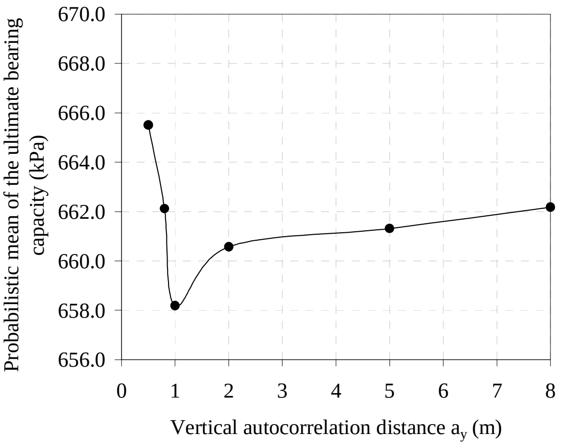

(a)

Figure II.10. Influence of the vertical autocorrelation distance a_y on the probabilistic mean value of the ultimate bearing capacity in the case where $r(c, \varphi)$=-0.5 and a_x=10m

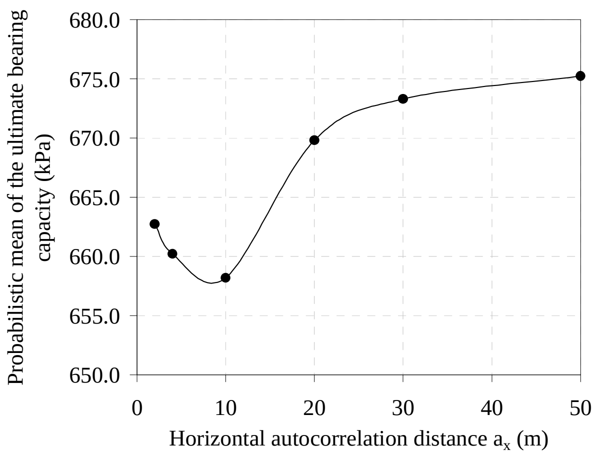

(b)

Figure II.11. Influence of the horizontal autocorrelation distance a_x on the probabilistic mean value of the ultimate bearing capacity in the case where $r(c, \varphi)$=-0.5 and a_y=1m

Similarly to Figure II.10, Figure II.11 shows that for a prescribed value of the vertical autocorrelation distance a_y, the very small value of the horizontal autocorrelation distance a_x leads to a vertical multilayer composed of a large number of thin sublayers for which each sublayer may have a large or a small value of the shear strength parameters [see Figure II.12(c)]. On the other hand, a horizontal multilayer is obtained in the case of a very large value of a_x [see

Figure II.12(d)]. Finally, a soil composed of several soft and stiff zones of finite dimensions is obtained for intermediate values of the autocorrelation distances [see Figure II.12(e)]. For all the three cases corresponding to small, intermediate and high values of the horizontal autocorrelation distance, the explanation given for Figure II.10 remains valid herein.

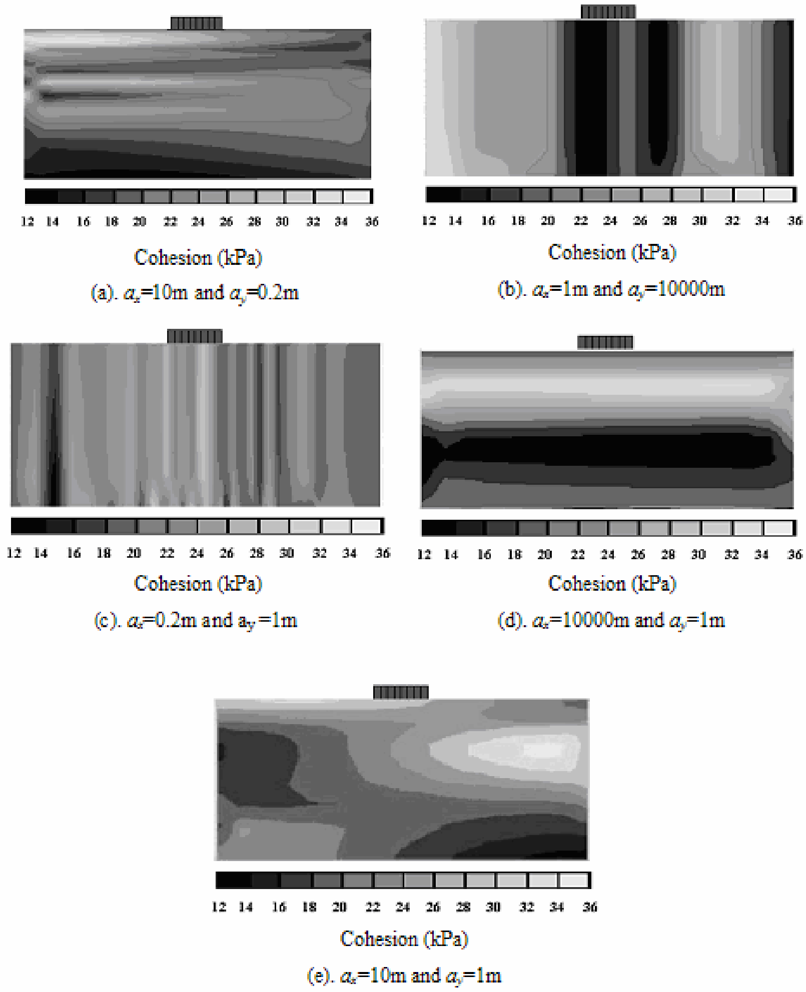

Figure II.12. Cohesion random field for different values of the autocorrelation distances

As a conclusion, one may observe that the increase in the vertical autocorrelation distance in Figure II.10 from very small to very large values leads to a soil configuration that varies from a horizontal to a vertical multilayer. This situation is reversed in Figure II.11 where the soil configuration varies from a vertical to a horizontal multilayer. The ultimate bearing capacity was found to be the smallest for an intermediate value of the autocorrelation distance (a_x or a_y) where the failure mechanism can easily develop in the soil mass.

Tables II.4 and II.5 show the impact of the increase in a_y and a_x on both the skewness and the kurtosis of the PDF. As in the case of the isotropic autocorrelation distance, the PDF of the response is not far from a Gaussian one for small values of a_y or a_x.

Finally, Tables II.6 and II.7 show the effect of the increase in a_y and a_x on the Sobol indices $S(c)$ and $S(\varphi)$ of the two random fields when $r(c, \varphi)$=-0.5. These tables show, as in the isotropic case, that the variability of the ultimate bearing capacity is mainly due to the cohesion random field which has a Sobol index of about 71%.

a_y(m)	$S(c)$	$S(\varphi)$
0.5	0.71	0.29
0.8	0.71	0.29
1	0.72	0.28
2	0.71	0.29
5	0.72	0.28
8	0.74	0.26
50	0.69	0.31
1D random field	0.72	0.28

Table II.6. Effect of the vertical autocorrelation distance a_y on the Sobol indices of c and φ

a_x(m)	$S(c)$	$S(\varphi)$
2	0.68	0.32
4	0.71	0.29
10	0.72	0.28
20	0.72	0.28
30	0.73	0.27
50	0.73	0.27
1D random field	0.71	0.29

Table II.7. Effect of the horizontal autocorrelation distance a_x on the Sobol indices of c and φ

Effect of the cross-correlation coefficient

Figure II.13 presents the PDFs of the ultimate bearing capacity for negatively cross-correlated $r(c, \varphi)$=-0.5 and non-correlated $r(c, \varphi)$=0 random fields when a_x=10m and a_y=1m, and Table II.8 presents the corresponding four statistical moments.

Figure II.13 and Table II.8 show that the variability of the ultimate bearing capacity decreases when considering a negative correlation between the two random fields. This is because the increase of one parameter value implies a decrease in the other parameter. Thus, the total shear strength slightly varies. This leads to a reduced variation in the ultimate bearing capacity. It should be mentioned that the probabilistic mean value of the ultimate bearing capacity slightly increases when a negative correlation between the two random fields exists.

Finally, the Sobol indices presented in Table II.9 (in the case where a_x=10m and a_y=1m) show the same behavior detected in the previous sections.

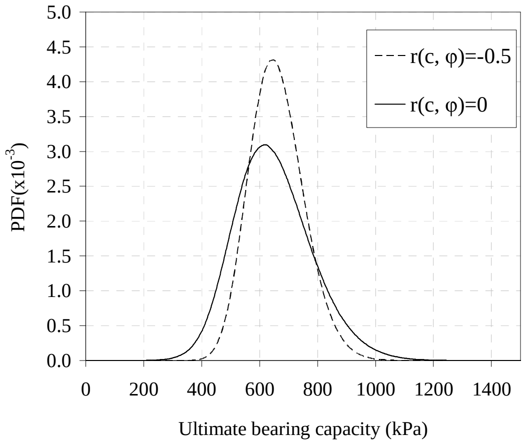

Figure II.13. Influence of the cross-correlation coefficient on the PDF of the ultimate bearing capacity in the case where a_x=10m and a_y=1m

$r(c,\varphi)$	$\mu_{q_{ult}}$ (kPa)	$\sigma_{q_{ult}}$ (kPa)	COV_{qult} (%)	δ_u (-)	κ_u (-)
-0.5	658.2	93.6	14.2	0.29	0.16
0	648.3	133.4	20.6	0.42	0.34

Table II.8. Effect of the cross-correlation coefficient between the random fields of *c* and *φ* on the statistical moments of the ultimate bearing capacity

$r(c,\varphi)$	$S(c)$	$S(\varphi)$
-0.5	0.72	0.28
0	0.72	0.28

Table II.9. Effect of the coefficient of correlation on the Sobol indices of the two random fields *c* and *φ*

Effect of the coefficients of variation of the random fields

Figure II.14 presents the PDFs of the ultimate bearing capacity for three different configurations of the coefficients of variation of the random fields. Notice that for the three configurations, $r(c, \varphi)$=-0.5, a_x=10m and a_y=1m. Tables II.10 and II.11 present (for the three configurations) the four statistical moments of the ultimate bearing capacity and the Sobol indices of the two fields (c, φ).

Figure II.14 and Table II.10 show (as expected) that the variability of the ultimate bearing capacity increases when the coefficients of variation of the random fields increase; the increase being more significant for the cohesion parameter.

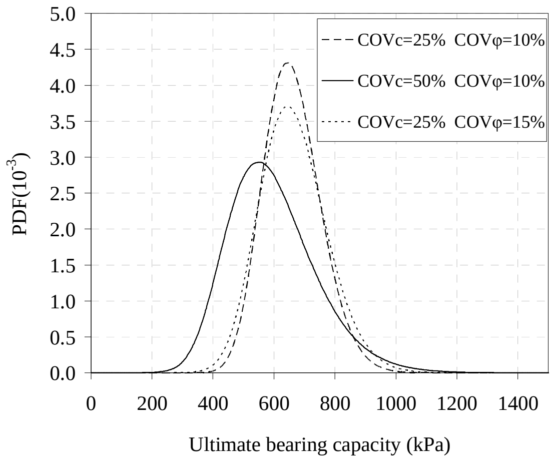

Figure II.14. Effect of the coefficients of variation of the random fields on the PDF of the ultimate bearing capacity in the case where a_x=10m, a_y=1m and $r(c, \varphi)$=-0.5

		$\mu_{q_{ult}}$ (kPa)	$\sigma_{q_{ult}}$ (kPa)	COV_{qult} (%)	δ_u (-)	κ_u (-)
$COVc = 25\%$	$COV\ \varphi = 10\%$	658.2	93.6	14.2	0.35	0.20
$COVc = 50\%$	$COV\ \varphi = 10\%$	595.7	141.0	23.7	0.57	0.57
$COVc = 25\%$	$COV\ \varphi = 15\%$	664.2	108.3	16.3	0.33	0.19

Table II.10. Effect of the coefficients of variation of the random fields *c* and *φ* on the statistical moments of the ultimate bearing capacity

		$S(c)$	$S(\varphi)$
$COVc = 25\%$	$COV\ \varphi = 10\%$	0.68	0.32
$COVc = 50\%$	$COV\ \varphi = 10\%$	0.91	0.09
$COVc = 25\%$	$COV\ \varphi = 15\%$	0.51	0.49

Table II.11. Effect of the coefficients of variation of the random fields *c* and *φ* on the Sobol indices of the two random fields *c* and *φ*

From Table II.11, one can see that an increase in the coefficient of variation of a soil parameter increases its Sobol index and thus its weight in the variability of the ultimate bearing capacity. This automatically reduces the contribution of the other uncertain parameter. This increase is more significant for the soil friction angle. This is because an increase by 100% in the coefficient of variation of the cohesion parameter increases its Sobol index by about 35%, while increasing the coefficient of variation of the friction angle by only 50% increases its Sobol index by about 50%.

II.3.2 The serviceability limit state SLS case

The aim of this section is to present the probabilistic numerical results obtained from the analysis at the serviceability limit state (SLS) of strip footings resting on a spatially varying soil and subjected to a central vertical load (P_v). It involves the computation of the central vertical footing displacement (v).

Both the soil Young modulus E and the soil Poisson ratio υ were firstly considered as random fields in order to determine the weight of each random field in the variability of the system response. In a second stage, only the uncertain parameter with a significant weight in the variability of the system response will be considered as a random field. Notice that the same autocorrelation function (square exponential) was used for both random fields. Both cases of isotropic (i.e. a_x=a_y) and anisotropic (i.e. a_x#a_y) random fields will be treated and the same values of the autocorrelation distances employed in the ULS case are used herein.

The soil Young modulus E was assumed to be lognormally distributed. Its mean value and coefficient of variation (referred to as reference values) were taken as follows: $\mu_E = 60MPa, Cov_E = 15\%$. Similarly, the soil Poisson ratio υ was assumed to be lognormally distributed with a mean value and a coefficient of variation given as follows: $\mu_v = 0.3, Cov_v = 5\%$.

The deterministic model was based on numerical simulations using the finite difference code FLAC^{3D}. Even though a serviceability limit state is considered, the soil behavior was modeled using a conventional elastic-perfectly plastic model based on Mohr-Coulomb failure criterion in order to consider the plasticity that may occur at the footing edges even under the service loads. Notice that the soil cohesion c, the soil angle of internal friction φ and the soil dilation angle ψ were assumed to be deterministic since the footing vertical displacement is not sensitive to these variables. Their corresponding values were respectively $c = 20kPa$, $\varphi = 30^o$ and $\psi = 20^o$. Concerning the footing and the interface properties, they were considered as deterministic. The same mean values used for these properties in the ULS case were employed herein. Moreover, the soil domain and mesh used in the ULS analysis (cf. Figure II.1) were also utilized in this case. Finally, notice that the footing was subjected to a vertical applied pressure q_a=500kPa.

The following sections are organized as follows: First, a global sensitivity analysis is performed considering both the soil Young modulus E and the soil Poisson ratio υ as random fields. This is followed by a presentation of the parametric study considering only the most influential random field that has a significant weight in the variability of the system response.

II.3.2.1 Global sensitivity analysis

The aim of this section is to perform a global sensitivity analysis which enables one to keep in the probabilistic parametric study that follows only the random field that has a significant weight in the variability of the system response. This greatly facilitates the probabilistic analysis since it reduces by half the computation time.

The different steps to perform the probabilistic analysis were presented in section II.3.1.1 and are not repeated herein. The global sensitivity analysis was presented for the reference case study (i.e. when a_x=10m and a_y=1m) considering both the Young modulus E and the Poisson ratio υ as two uncorrelated random fields. For this case, 24 random variables were needed in order to discretize the two random fields (cf. Table II.1).

Figure II.15 depicts the values of Sobol indices for the 24 random variables, as given by the obtained SPCE. The first 12 random variables [i.e. ξ_i for i=1, …, 12] correspond to the Young modulus random field and the last 12 random variables [i.e. ξ_i for i=13, …, 24] are those corresponding to the Poisson ratio random field.

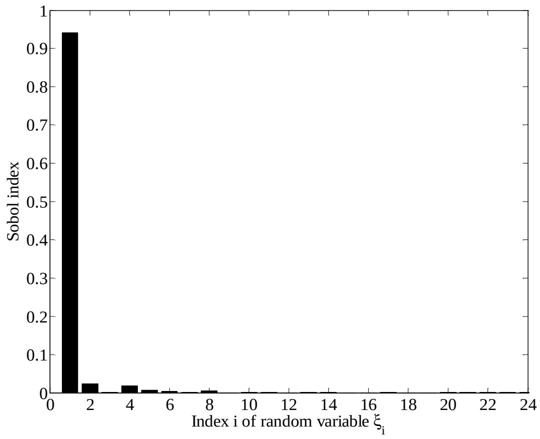

Figure II.15. Sobol indices of the two random fields [the Young modulus for ξ_i (i=1, …, 12) and the Poisson ratio for ξ_i (i=13, …, 24)]

Figure II.15 shows that only three random variables (ξ_1, ξ_2 , ξ_4) of the Young modulus random field are the most influential (they involve 98.4% of the response variance). Notice that the first random variable ξ_1 provides alone 94% of the response variance. The Poisson ratio random field has a quasi-negligible weight in the variability of the system response (0.14% of the system variance). For this reason, it can be considered as deterministic in the following section.

II.3.2.2 Probabilistic parametric study

The aim of this section is to study the effect of the different statistical governing parameters (autocorrelation distances and coefficient of variation of the random field *E*) on the PDF of the footing vertical displacement (*v*).

<u>*Effect of the autocorrelation distances: The isotropic and anisotropic cases*</u>

Figures II.16, II.17 and II.18 provide the PDFs of the footing vertical displacement (*v*) for (i) the isotropic case for different values of $a_x=a_y$, (ii) the anisotropic case for different values of a_y and (iii) the anisotropic case for different values of a_x. Tables II.12, II.13 and II.14 present the four statistical moments for the cases presented in those figures.

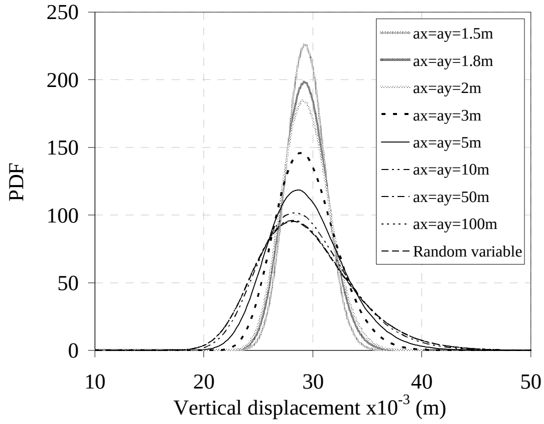

Figure II.16. Influence of the isotropic autocorrelation distance $a_x= a_y$ on the PDF of the footing vertical displacement

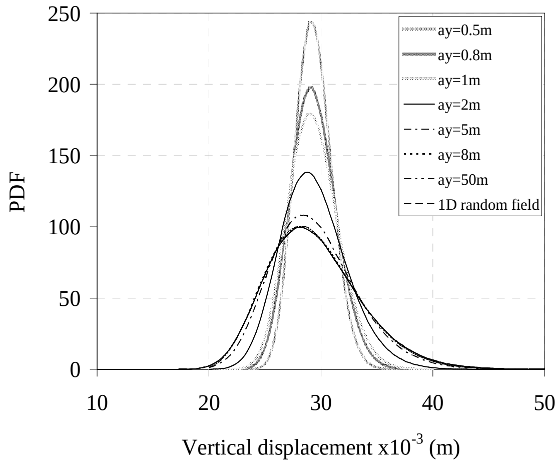

Figure II.17. Influence of the vertical autocorrelation distance a_y on the PDF of the footing vertical displacement in the case where a_x=10m

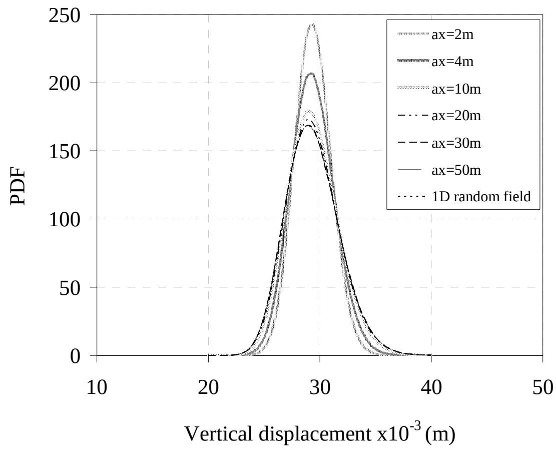

Figure II.18. Influence of the horizontal autocorrelation distance a_x on the PDF of the footing vertical displacement in the case where a_y=1m

Concerning the variability of the footing vertical displacement (v), similar trends as those obtained in the ULS analysis are obtained herein. One can see that the PDFs are less spread out when the autocorrelation distance decreases. Thus, the same explanations done in the ULS analysis remain valid herein.

On the other hand, Tables II.12, II.13 and II.14 show that the probabilistic mean value of the footing vertical displacement does not exhibit a minimum and it remains constant regardless of the value of the autocorrelation distance (this mean value is found to be slightly greater than the deterministic value of 28.8mm which makes it more critical). The non-presence of a minimum is contrary to the ULS probabilistic results (as obtained by the present analysis, by Fenton and Griffiths (2003) and by Soubra et al. (2008)) where a minimum exists for a given value of the autocorrelation distance. This phenomenon can be explained by the fact that at SLS, the applied footing pressure q_a=500kPa is not sufficiently high to induce or initiate a failure mechanism which may pass through the weakest zones for a given value of the autocorrelation distance. Thus; in the SLS analysis, there is no particular value of the autocorrelation distance for which the soil exhibits some weakness with respect to the other values of the autocorrelation distance.

$a_x = a_y$ (m)	μ_v x10^{-3} (m)	σ_v x10^{-3} (m)	COV_v (%)	δ_u (-)	κ_u (-)
1.5	29.4	1.8	6.1	0.09	0.01
1.8	29.4	2.0	6.8	0.19	0.05
2	29.4	2.2	7.5	0.23	0.07
3	29.4	2.8	9.5	0.33	0.15
5	29.5	3.5	11.9	0.39	0.28
10	29.5	4.1	13.9	0.43	0.33
50	29.5	4.4	14.9	0.47	0.41
100	29.5	4.4	14.9	0.47	0.41
Random variable	29.5	4.4	14.9	0.47	0.41

Table II.12. Effect of the isotropic autocorrelation distance a_x=a_y on the statistical moments of the footing vertical displacement

Tables II.12, II.13 and II.14 also show the impact of the autocorrelation distance on both the skewness and the kurtosis of the PDF. For small values of the autocorrelation distance, the skewness and kurtosis of the response are close to zero which means that the PDF of the response is not far from a Gaussian one in these cases. Notice however that these moments increase when the autocorrelation distance increases which means that for great values of the autocorrelation distance, the shape of the PDF of the output becomes far from a Gaussian one.

a_y (m)	μ_v x10^{-3} (m)	σ_v x10^{-3} (m)	COV_v (%)	δ_u (-)	κ_u (-)
0.5	29.3	1.6	5.5	0.17	0.03
0.8	29.4	2.0	6.8	0.21	0.06
1	29.4	2.2	7.5	0.24	0.08
2	29.4	3.0	10.2	0.33	0.21
5	29.5	3.8	12.9	0.41	0.31
8	29.4	4.1	13.9	0.42	0.32
50	29.5	4.2	14.2	0.45	0.34
1D random field	29.5	4.2	14.2	0.45	0.34

Table II.13. Effect of the vertical autocorrelation distance a_y on the statistical moments of the footing vertical displacement when a_x=10m

a_x (m)	μ_v x10^{-3} (m)	σ_v x10^{-3} (m)	COV_v (%)	δ_u (-)	κ_u (-)
2	29.4	1.6	5.4	0.09	0.02
4	29.4	1.9	6.5	0.16	0.05
10	29.4	2.2	7.5	0.24	0.08
20	29.4	2.4	8.2	0.25	0.10
30	29.4	2.4	8.2	0.26	0.15
50	29.4	2.4	8.2	0.26	0.15
1D random field	29.4	2.4	8.2	0.26	0.15

Table II.14. Effect of the horizontal autocorrelation distance a_x on the statistical moments of the footing vertical displacement when a_y=1m

Effect of the coefficient of variation of the random field

Figure II.19 presents the PDFs of the footing vertical displacement (v) for four different values of the coefficient of variation of the Young modulus random field. Notice that for these four configurations, a_x=10m, and a_y=1m. Table II.15 presents (for the four configurations) the four statistical moments of the footing vertical displacement.

As expected, Figure II.19 and Table II.15 show that the variability of the footing vertical displacement increases when the coefficient of variation of the Young modulus random field increases. On the other hand, the mean value of the footing vertical displacement was found to significantly increase when the coefficient of variation of the Young modulus increases. This is of particular interest since the probabilistic mean value (29.4mm) obtained for the reference case where $Cov_E = 15\%$ becomes unconservative and no longer valid when the variability of the input random field significantly increases.

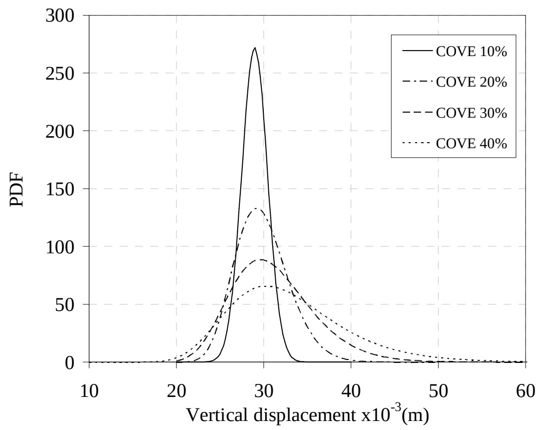

Figure II.19. Influence of the coefficient of variation COV_E on the PDF of the footing vertical displacement in the case where a_x=10 and a_y=1m

COV_E (%)	μ_v x10^{-3} (m)	σ_v x10^{-3} (m)	COV_v (%)	δ_u (-)	κ_u (-)
10	29.0	1.5	5.2	0	0
20	29.8	3.0	10.1	0.32	0.15
30	31.1	4.7	15.1	0.49	0.41
40	32.9	6.6	20.1	0.65	0.78

Table II.15. Effect of the coefficient of variation (COV_E) of the random field *E* on the statistical moments of the footing vertical displacement when a_x=10m, a_y=1m

Table II.15 also shows that for the smallest value of Cov_E (i.e. $Cov_E = 10\%$), the skewness and kurtosis of the response are equal to zero which means that the PDF of the response is Gaussian in this case. Notice however that when Cov_E increases, the shape of the PDF of the output becomes far from a Gaussian one.

II.4 PROBABILISTIC ANALYSIS OF STRIP FOOTINGS RESTING A SPATIALLY VARYING ROCK MASS OBEYING HOEK-BROWN (HB) FAILURE CRITERION

The aim of this section is to present the probabilistic numerical results in the case of vertically loaded strip footings resting on a spatially varying rock mass obeying Hoek-Brown (HB) failure criterion. Only the ultimate limit state ULS is considered herein. It involves the computation of the ultimate bearing capacity (q_{ult}).

The rock mass follows the generalized HB failure criterion [Hoek and Brown (1980), Hoek et al. (2002), Hoek and Marinos (2007) and Brown (2008)]. In this criterion, only intact rocks or heavily jointed rock masses (i.e. with sufficiently dense and randomly distributed joints) can be considered. The HB failure criterion is characterized by four parameters:

(i) the geological strength index (*GSI*)

(ii) the uniaxial compressive strength of the intact rock (σ_c)

(iii) the intact rock material constant (m_i)

(iv) (iv) the disturbance coefficient (*D*).

Mao et al. (2011, 2012) have modeled these four parameters as random variables and have performed a probabilistic analysis of the ultimate bearing capacity (q_{ult}) of foundations. These authors have shown that the variability of the ultimate bearing capacity is mainly due to the uniaxial compressive strength of the intact rock (σ_c) and the geological strength index (*GSI*). Based on this study, only these two parameters were considered herein as uncertain. The rock uniaxial compressive strength of the intact rock (σ_c) was considered as a non-Gaussian (log-normally distributed) random field characterized by a square exponential autocorrelation function. Its mean value and coefficient of variation (referred to as reference values) were taken as follows: $\mu_{\sigma_c} = 10MPa, COV_{\sigma_c} = 25\%$. As for *GSI*, Ching et al. (2011) have stated that this parameter is based on engineering judgment. It characterizes the overall rock mass condition and it does not represent a precise physical parameter varying in space. Thus, this parameter cannot be modeled as a random field and will be treated herein as a log-normally distributed random variable with a mean value and a coefficient of variation given as follows: $\mu_{GSI} = 25, COV_{GSI} = 10\%$ [Brown (2008)]. Finally, it should be mentioned that the intact rock material constant (m_i) and the disturbance coefficient (*D*) were assumed to be deterministic since the probabilistic ultimate bearing capacity was found not sensitive to the variability of these parameters [Mao et al. (2012)]. Their corresponding values were respectively $m_i = 8$ and $D = 0.3$.

The deterministic model was based on numerical simulations using FLAC^{3D} software. A footing of breadth B=1m was considered in the analysis. For this calculation, a rock mass of 20m wide by 6m deep was found necessary (Figure II.20). The rock behavior was modeled by an elastic perfectly plastic model obeying the generalized HB failure criterion. It should be emphasized here that an associated flow rule was considered in this study in order to be able to compare the obtained results to those given in literature using the limit analysis theory [Mao et al. (2012) and Merifield et al. (2006)]. For this purpose, the confining stress at constant volume σ_3^{cv} must be properly selected. In fact, beyond the value of σ_3^{cv}, no volume changes are expected to appear.

This means that when σ_3^{cv}/σ_c is very small, the case of a deformation at constant volume is rapidly reached and the model can be considered to follow a non-associated flow rule with a zero dilation angle. On the contrary, the case of a large value of σ_3^{cv}/σ_c means that the deformation at the constant volume can not be reached easily and thus the model can be considered to follow an associated flow rule. In the present chapter, a value of $\sigma_3^{cv}/\sigma_c = 2$ was selected. This value was chosen since greater values have not significantly decrease the value of the ultimate bearing capacity.

The present deterministic model was validated by comparison of its results with those provided by Mao et al. (2012) and Merifield et al. (2006) for different configurations of the rock parameters. The results are presented for the case of a weightless material. The value of the Poisson ratio adopted in this section is 0.3. As for the modulus of deformation of the HB rock mass, Hoek et al. (2002) have proposed the following relationship between this parameter and the HB failure criterion parameters:

$$E_m = \left(1 - \frac{D}{2}\right)\sqrt{\frac{\sigma_c}{100}}.10^{\left((GSI-10)/40\right)} \quad \text{(II.2)}$$

where E_m in this equation is given in GPa.

Table II.16 presents a comparison between the results obtained from the present deterministic model and those given by Mao et al. (2012) and Merifield et al. (2006). It should be mentioned here that the results given by Merifield et al. (2006) present the average values between the upper and lower bound solutions of the limit analysis theory. On the other hand, Mao et al. (2012) presents only an upper bound solution of the ultimate bearing capacity. Table II.16 shows that the present numerical model provides slightly more critical values of the ultimate bearing capacity. This model will be used to perform the probabilistic analysis.

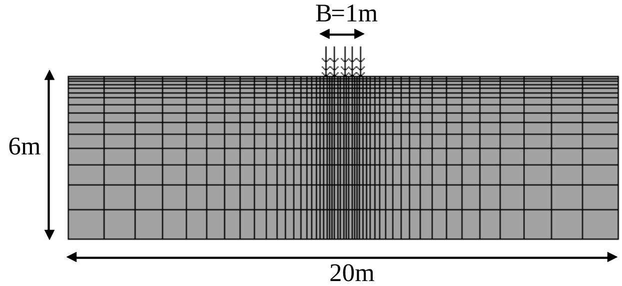

Figure II.20. Mesh used for the computation of the ultimate bearing capacity

GSI (-)	σ_c (*MPa*)	m_i (*MPa*)	FLAC^{3D}	Mao et al. (2012)	Merifield et al. (2006)
20	7.5	10	1.460	1.600	1.568
20	10	10	1.960	2.130	2.090
20	12.5	10	2.450	2.670	2.613
20	15	10	2.930	3.200	3.135
20	20	10	3.920	4.270	4.180
30	7.5	10	2.784	3.040	2. 978
30	10	10	3.710	4.060	3.970
30	12.5	10	4.660	5.070	4.963
30	15	10	5.605	6.120	5.955
30	20	10	7.498	8.080	7.940

Table II.16. Values of q_{ult} (*MPa*) as given by FLAC^{3D}, by Merifield et al. (2006) and by Mao et al. (2012) when D=0

As for the autocorrelation distances a_x and a_y of the random field (σ_c), it was assumed here that $a=a_x=a_y$. Notice that the adopted reference value of the autocorrelation distance (a) is 2m; however, a range of 0.5-100m was considered for the parametric study. For the different values of the autocorrelation distance (a), the total number N of random variables (or eigenmodes) that should be used to discretize the random field of σ_c within a prescribed value of 10% for the variance of the error is presented in Table II.17. Notice that the numbers given in Table II.17 are those corresponding to the rock domain [20m, 6m] presented in Figure II.20.

Autocorrelation distance a(m)	Total number of random variables used to discretize the uniaxial compression strength random field
0.5	120
1	99
2	35
5	8
10	5
50	5
100	5

Table II.17. Number of random variables needed to discretize the random field σ_c

The following subsections are organized as follows: First, a global sensitivity analysis is performed. This is followed by a presentation of the parametric study. The aim of this parametric study is to show the effect of the different governing statistical parameters (autocorrelation distance, coefficient of variation) on both the PDF of the ultimate bearing capacity and the Sobol indices of the uncertain parameters (i.e. σ_c and *GSI*).

II.4.1 Global sensitivity analysis

The aim of this section is to perform a global sensitivity analysis for the reference case (i.e. when *a*=2m). Figure II.21 depicts the values of Sobol indices as given by the obtained SPCE for (i) the random variable *GSI* and (ii) the 35 random variables representing the random field σ_c. The first random variable ξ_1 corresponds to *GSI* and its Sobol index was found to be equal to 0.66. However, the last 35 random variables [i.e. ξ_i for i=2, …, 36] are those corresponding to the σ_c random field. The sum of their Sobol indices gives the weight of the random field σ_c in the variability of the ultimate bearing capacity. This sum was found to be equal to 0.34.

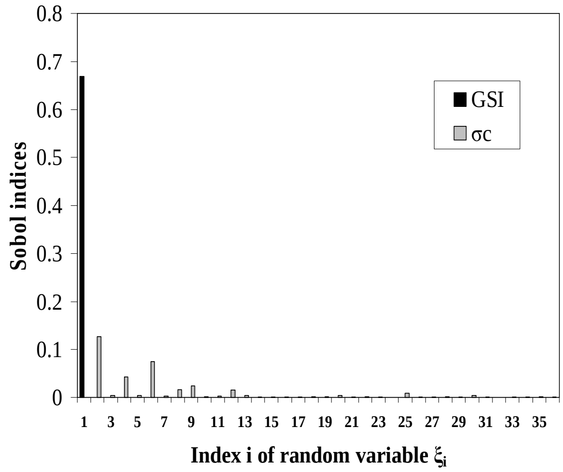

Figure II.21. Sobol indices of the random variable *GSI* [i.e. ξ_i(i=1)] and the random field σ_c [i.e. ξ_i(i=2, …, 36)]

Figure II.21 shows that only six random variables (ξ_2, ξ_4, ξ_6, ξ_8, ξ_9, ξ_{12}) of the σ_c random field are the most influential (they involve 89% of the variance of σ_c). This can be explained by the fact that the system response (i.e. the ultimate bearing capacity) is a quantity that depends on the average distribution of the spatially-varying rock property over the entire domain and it is therefore quite insensitive to small-scale fluctuations of σ_c. In addition, one can notice that the Sobol indices of the random variables corresponding to the eigenmodes which are symmetric with respect to the vertical axis [cf. Blatman and Sudret (2011)] present the most significant values. This can be explained by the fact that the bearing capacity is more sensitive to the values of the rock property situated at the central axis of the footing. Along this axis, the values of the calculated random field σ_c results from the summation of the maximal values of the different symmetrical eigenmodes; the non-symmetrical eigenmodes being equal to zero at these locations. This explains the fact that only the symmetrical eigenmodes significantly contribute to the variability of q_{ult}. Notice finally that a similar result was obtained by Blatman and Sudret (2011) when considering the sttelement problem of foundations.

II.4.2 Probabilistic parametric study

The aim of this section is to study the effect of the different statistical governing parameters (autocorrelation distance of σ_c and coefficient of variation of both σ_c and *GSI*) (i) on the PDF of the ultimate bearing capacity and (ii) on Sobol indices.

II.4.2.1 Effect of the isotropic autocorrelation distance (a)

Figure II.22 provides the PDFs of the ultimate bearing capacity for different values of the isotropic autocorrelation distance of σ_c (a =0.5, 1, 2, 5, 10, 50, 100m) and for the case where σ_c is modeled as a random variable (case of a homogenous rock mass). Table II.18 presents the four statistical moments for the cases presented in this figure.

As expected, the PDF and the statistical moments corresponding to a great value of the autocorrelation distance (a=100m) are similar to those given by the case of a random variable. Concerning the effect of the autocorrelation distance on the variability of the ultimate bearing capacity, one obtains similar trends as the case of strip footings resting on spatially varying soil mass. Thus, the same explanations done before remain valid herein.

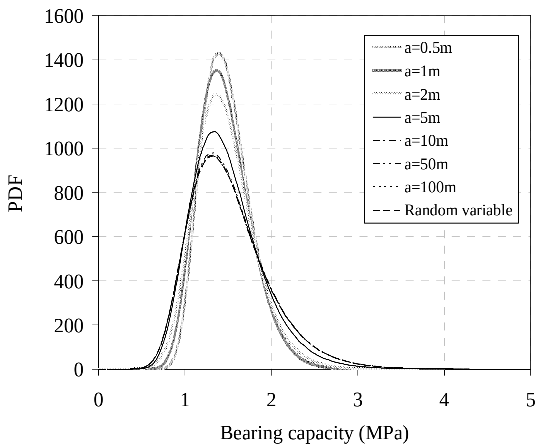

Figure II.22. Influence of the isotropic autocorrelation distance *a* on the PDF of the ultimate bearing capacity

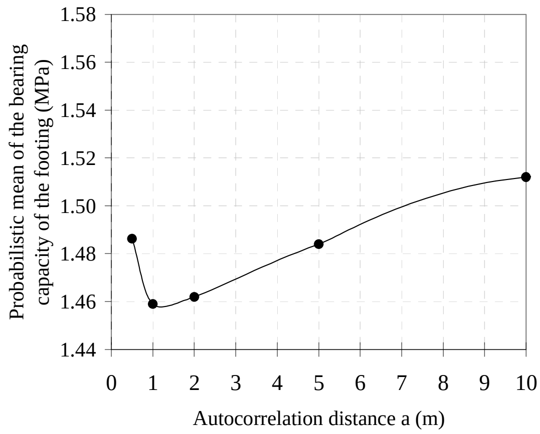

Figure II.23. Influence of the isotropic autocorrelation distance *a* on the probabilistic mean of the ultimate bearing capacity

Figure II.23 and Table II.18 show that the probabilistic mean value of the ultimate bearing capacity presents a minimum when the autocorrelation distance is nearly equal to the footing breadth B (i.e. in our case when a =1m). Notice that this minimal probabilistic mean was also observed when considering the bearing capacity of foundations resting on a soil mass. Thus, the same explanation which was done before remains valid herein.

Autocorrelation distance a(m)	$\mu_{q_{ult}}$ (MPa)	$\sigma_{q_{ult}}$ (MPa)	$COV_{q_{ult}}$ (%)	δ_u (-)	κ_u (-)
0.5	1.486	0.288	19.4	0.46	0.31
1	1.459	0.301	20.9	0.45	0.32
2	1.462	0.342	23.4	0.52	0.54
5	1.484	0.408	27.5	0.79	1.10
10	1.512	0.450	29.8	0.88	1.29
50	1.557	0.486	31.4	0.97	1.69
100	1.560	0.488	31.4	0.98	1.73
Random variable	1.560	0.488	31.4	1.02	1.72

Table II.18. Effect of the autocorrelation distance *a* on the statistical moments of the ultimate bearing capacity

Table II.18 also shows the impact of the autocorrelation distance on both the skewness and the kurtosis of the PDF. For small values of the autocorrelation distance, the skewness and kurtosis of the response are small which means that the PDF of the response is not far from a Gaussian one in these cases.

Finally, Figure II.24 and Table II.19 show the effect of the autocorrelation distance on the Sobol indices of the random field σ_c and the random variable *GSI*. The results show that for very large values of the autocorrelation distance (i.e. a =100m), the variability of the ultimate bearing capacity is mainly due to σ_c. Similar results were obtained by Mao et al. (2012) where the uncertain parameters were modeled by random variables. It should be emphasized here that σ_c is the most weighted parameter in the variability of the ultimate bearing capacity only in the case of very large values of the autocorrelation distance or in the case of random variables. Indeed, Figure II.24 shows that the decrease in the autocorrelation distance of σ_c reduces its weight in the variability of the ultimate bearing capacity and increases the weight of *GSI*. Although this result was impossible to be detected when a simplified modeling (i.e. random variables) of the uncertain rock parameters was used, it can be explained by the fact that the small values of the autocorrelation distance increase the rock mass heterogeneity (i.e. one obtains a set of weak and strong zones) which will produce a somewhat close global behavior of the footing from simulation to another one because of the averaging phenomenon over the zone of possible failure mechanism. The expected decrease in the variability of the ultimate bearing capacity with the decrease in the autocorrelation distance of σ_c is reflected herein by a decrease in the weight of σ_c

in the variability of this response. For the limiting case of a very small value of the autocorrelation distance, σ_c can be seen as a deterministic value which implies that in this case the variability of the ultimate bearing capacity is only due to *GSI* (i.e. S(*GSI*) tends to one).

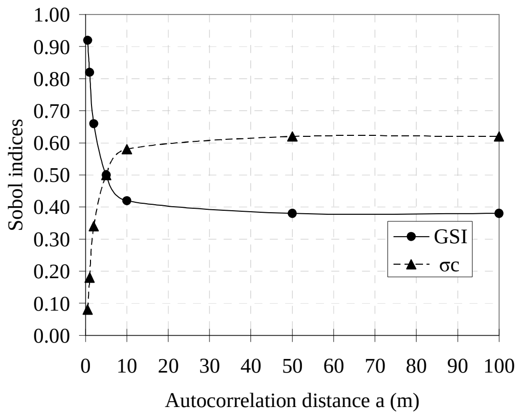

Figure II.24. Influence of the autocorrelation distance *a* on the Sobol indices of *GSI* and σ_c

Autocorrelation distance *a*(m)	*S(GSI)*	$S(\sigma_c)$
0.5	0.92	0.08
1	0.82	0.18
2	0.66	0.34
5	0.50	0.50
10	0.42	0.58
50	0.38	0.62
100	0.38	0.62
Random variable	0.38	0.62

Table II.19. Influence of the autocorrelation distance *a* on the Sobol indices of *GSI* and σ_c

II.4.2.2 Effect of the coefficient of variation

The effect of the coefficients of variation (*COV*s) of the random field σ_c and the random variable *GSI* is studied and presented in Figure II.25, Table II.20 and Table II.21. Notice that in this study, the adopted value of the autocorrelation distance of the random field σ_c is the reference value (i.e. *a*=2m).

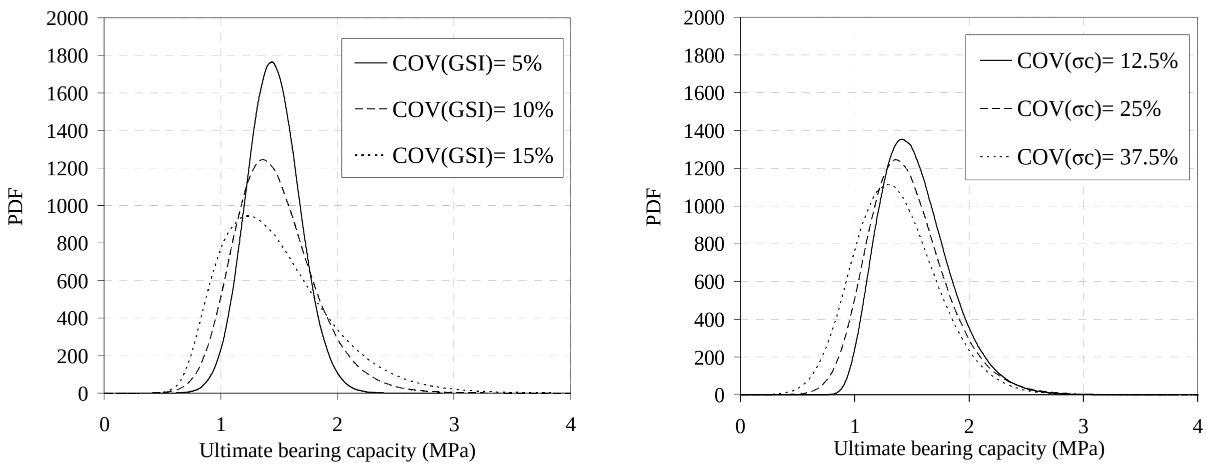

(a) (b)

Figure II.25. Influence of the coefficients of variation *COV*s of the random variable *GSI* and the random field σ_c on the PDF of the ultimate bearing capacity: (a) influence of COV_{GSI}; (b) influence of $COV_{\sigma c}$

COV_{GSI}	COV_{σ_c}	$\mu_{q_{ult}}$ (MPa)	$\sigma_{q_{ult}}$ (MPa)	$COV_{q_{ult}}$ (%)	δ_u (-)	κ_u (-)
10%	12.5%	1.530	0.307	20.1	0.48	0.46
10%	25%	1.462	0.342	23.4	0.52	0.54
10%	37.5%	1.366	0.364	26.7	0.53	0.58
5%	25%	1.470	0.226	15.4	0.13	0.05
10%	25%	1.462	0.342	23.4	0.52	0.54
15%	25%	1.451	0.458	31.6	0.73	0.77

Table II.20. Effect of the coefficients of variation (*COV*s) of the random field σ_c and the random variable *GSI* on the statistical moments (μ, σ, δ_u, κ_u) of the ultimate bearing capacity when *a*=2m

Figure II.25 and Table II.20 show that the variability of the ultimate bearing capacity increases (as expected) when the coefficient of variation of either the random field σ_c or the random variable *GSI* increases; the increase being more significant for the *GSI* parameter (see Table II.20). This is because an increase in the coefficient of variation of σ_c by 50% (with respect to its reference value) increases the *COV* of the ultimate bearing capacity by only about 13.9%, while increasing the coefficient of variation of *GSI* by 50% (with respect to its reference value) increases the *COV* of the ultimate bearing capacity by about 34.9%. Table II.20 also shows that the probabilistic mean value of the ultimate bearing capacity slightly decreases when the coefficients of variation increase.

COV_{GSI}	COV_{σ_c}	S(*GSI*)	S(σ_c)
10%	12.5%	0.88	0.12
10%	25%	0.66	0.34
10%	37.5%	0.49	0.51
5%	25%	0.32	0.68
10%	25%	0.66	0.34
15%	25%	0.82	0.18

Table II.21. Effect of the coefficients of variation (*COV*s) of the random field σ_c and the random variable *GSI* on the Sobol indices of *GSI* and σ_c when *a*=2m

From Table II.21, one can see that an increase in the coefficient of variation of a rock parameter increases its Sobol index and thus its weight in the variability of the ultimate bearing capacity; this automatically reduces the contribution of the other uncertain parameter. This increase is more significant for σ_c. This is because an increase in the coefficient of variation of *GSI* by 50% (with respect to its reference value) increases its Sobol index by only about 24.3%, while increasing the coefficient of variation of σ_c by 50% (with respect to its reference value) increases its Sobol index by about 50%.

II.5 DISCUSSION

Although the focus of this chapter involves the computation of the statistical moments of the different system responses, the aim of this section is to briefly discuss the validity of the present SPCE methodology for the computation of the probability of failure P_f. For this purpose, a comparison between the results obtained using the Subset Simulation (SS) method by Ahmed and Soubra (2012) (see section I.5.1.2) and those obtained with the proposed SPCE methodology are presented herein. The comparison was performed in the ULS case of a strip footing resting on a weightless c-φ soil for the reference case where a_x=10m, a_y=1m, and $r(c, \varphi)$=-0.5. (cf. section II.3.1.2). The footing is subjected to a vertical load P_s=400kN/m. The performance function used to calculate the failure probability is $G = \frac{P_u}{P_s} - 1$ where P_u is the ultimate footing load.

In order to calculate the failure probability P_f by SS method, an optimal number K_s of simulations per level should be selected. This number should be greater than 100 to provide a small bias in the calculated P_f value [Honjo 2008]. In this case study, a number of simulation per level K_s=200 was chosen. The obtained P_f value was equal to $3.5\text{x}10^{-4}$. Notice that four levels of SS were required to calculate this P_f value. The total number of simulations K is equal to 740. The P_f value obtained by SS is to be compared to the P_f value of $4.72\text{x}10^{-4}$ obtained using the SPCE methodology. One can observe a small difference between the two methods. It should be emphasized that this is a preliminary validation of the SPCE methodology for the computation of the failure probability. Further tests are necessary to confirm the agreement between the results of the two methods.

II.6 CONCLUSIONS

In this chapter, a probabilistic analysis at both ultimate limit state (ULS) and serviceability limit state (SLS) of strip footings was performed. Two case studies were considered in this chapter. The first one involves the case of strip footings resting on a 2D spatially varying soil mass obeying the Mohr-Coulomb (MC) failure criterion and the second one considers the case of strip footings resting on a 2D spatially varying rock mass obeying the Hoek-Brown (HB) failure criterion.

In the case of the spatially varying soil mass, a probabilistic analysis at both ULS and SLS of vertically loaded strip footings was performed. The soil shear strength parameters (c and φ) were considered as anisotropic cross-correlated non-Gaussian random fields at ULS and the soil elastic parameters (E and υ) were considered as anisotropic uncorrelated non-Gaussian random fields at SLS. Notice that the system response used at ULS was the ultimate bearing capacity (q_{ult}); however, the footing vertical displacement (v) was considered as the system response at SLS. Concerning the case of the spatially varying rock mass, only the ULS case was considered. The methodology proposed by Vořechovsky (2008) was used to generate the two random fields. The sparse polynomial chaos expansion (SPCE) methodology was employed for the probabilistic analysis. The adaptive algorithm suggested by Blatman and Sudret (2010) to build up a SPCE was adopted to obtain a meta-model (i.e. an approximate analytical expression) of the system responses. These meta-models were employed to perform the probabilistic analysis using Monte Carlo simulation technique. Notice finally; that at the ULS analysis, only weightless soil and weightless rock masses were considered. This is because introducing the soil/rock weight in the deterministic model increases the computation time from 5 to 10 min per simulation. Although this difference may not seem to be significant for a single simulation, it becomes dramatically important during the probabilistic analyses where a large number of simulations is needed for each probabilistic analysis.

The numerical results have shown the interest of the SPCE methodology with respect to the classical PCE method in the case of random fields where a significant number of random variables were used in the analysis. The numerical results have also shown that the variability of the system responses (i.e. the ultimate bearing capacity in the ULS analysis and the vertical displacement of the footing in the SLS analysis) increases (as expected) with the increase in the coefficients of variation of the random fields. It was also shown that an increase in the coefficient of variation of a random field increases its Sobol index and thus its weight in the variability of the system response and decreases the weight of the other parameter. The negative correlation between the random fields decreases the response variability.

With a decrease in the autocorrelation distances (a_x or a_y or a_x=a_y), a less spread out PDF of the system response was obtained. The probabilistic mean value of the ultimate bearing capacity (in both cases of soil and rock masses) presents a minimum. This minimum was obtained in the isotropic case when the autocorrelation distance is nearly equal to the footing breadth B; while for the anisotropic case (presented only when a soil mass is considered), this minimum was obtained (for prescribed footing and soil characteristics) at a given value of the ratio between the horizontal and the vertical autocorrelation distances. Small values of the autocorrelation distances lead to small values of the skewness and kurtosis of the system responses. Thus, a PDF of the system response that is not far from a Gaussian one was obtained in these cases. Finally, the obtained results show the importance of considering the spatial variability of the soil/rock properties in the probabilistic studies since some observed phenomena (such as the non-symmetrical soil failure and the variation in the weight of parameters with the autocorrelation distance) can not be seen when homogenous soils are considered.

CHAPTER III. EFFECT OF THE SOIL SPATIAL VARIABILITY IN THREE DIMENSIONS ON THE ULTIMATE BEARING CAPACITY OF FOUNDATIONS

III.1 INTRODUCTION

The effect of the spatial variability of a soil/rock property was extensively investigated in the previous chapter using a two-dimensional (2D) analysis. In this case, the soil/rock mass exhibits spatial variability in a given plane and remains uniform in the direction normal to this plane where the autocorrelation distance is implicitly taken as infinite.

Few authors have investigated the effect of the 3D soil spatial variability. One may cite among others Fenton and Griffiths (2005) for the foundation settlement problem, Griffiths et al. (2009) for the slope stability analysis and Popescu et al. (2005) for the seismic liquefaction problem. To the best of the authors' knowledge, there are no investigations on the effect of the 3D soil spatial variability on the ultimate bearing capacity of foundations. This chapter fills this gap.

The effect of the soil spatial variability in three dimensions is investigated in this chapter through the study of the ultimate bearing capacity of strip and square foundations resting on a purely cohesive soil with a spatially varying cohesion in the three dimensions [Al-Bittar and Soubra (2012d)]. For this purpose, the soil cohesion was modeled as a 3D random field. Both cases of isotropic and anisotropic random fields were considered.

In order to investigate the effect of the spatial variability in the third direction, the results of the ultimate bearing capacity of foundations obtained using a 3D random field were compared to those corresponding to a 2D random field for two cases of a strip and a square footing. The objective is to check the validity of considering a 2D random field in both cases of plane strain and three-dimensional problems.

III.2 PROBABILISTIC ANALYSIS OF STRIP AND SQUARE FOOTINGS RESTING ON A 3D SPATIALLY VARYING SOIL MASS

The aim of this section is to perform a probabilistic analysis of shallow foundations taking into account the soil spatial variability in three dimensions. More specifically, the analysis involves the computation of the ultimate bearing capacity (q_{ult}) of square and strip footings resting on a purely cohesive soil that exhibits spatial variability in three dimensions. Notice that for both the square and strip footings considered in the analysis, the cases of 2D and 3D anisotropic non-

Gaussian cohesion random fields were investigated. The objective is to check the validity of the commonly used assumption of a 2D random field in both cases of plane strain and 3D problems.

As for the random field discretization method of the 3D random field, a straightforward extension to the 3D case of the Expansion Optimal Linear Estimation (EOLE) methodology proposed by Li and Der Kiureghian (1993) and extended by Vořechovsky (2008) (see details in section I.3.4.1) was used in this chapter. It should be emphasized here that this extension of EOLE method to the 3D case is straightforward because the autocorrelation matrix $\Sigma_{\chi;\chi}$ calculated using Equation (I.9) provides the correlation between each node of the stochastic mesh and all the nodes of this mesh. Thus, $\Sigma_{\chi;\chi}$ is always a square matrix of dimensions *sxs* regardless of the random field dimension.

Concerning the probabilistic method of analysis, the Sparse Polynomial Chaos Expansion (SPCE) presented in the previous chapter is used herein. It aims at replacing the FLAC^{3D} deterministic model by a meta-model (i.e. a simple analytical equation). This allows one to easily calculate the system response (when performing the probabilistic analysis by MCS) using a simple analytical equation.

The deterministic model was based on numerical simulations using the finite difference code FLAC^{3D}. The undrained soil behavior was modeled using a conventional elastic-perfectly plastic model based on Tresca failure criterion. On the other hand, an associative flow rule was considered in this study. This assumption is justified by the fact that for purely cohesive materials no volume changes are expected to appear during plastic deformation. Notice that the soil Young modulus E and Poisson ratio υ were assumed to be deterministic since the ultimate bearing capacity is not sensitive to these variables. Their corresponding values were respectively $E = 60MPa$ and $\nu = 0.49$. Concerning the footing, a weightless rigid foundation was used. It was assumed to follow an elastic linear model ($E = 25GPa$, $\nu = 0.4$). The connection between the footing and the soil mass was modeled by interface elements having the same mean values of the soil shear strength parameters in order to simulate a perfectly rough soil-footing interface. These parameters have been considered as deterministic in this study. Concerning the elastic properties of the interface, they also have been considered as deterministic and their values were as follows: $K_s = 1GPa$, $K_n = 1GPa$ where K_s and K_n are respectively the shear and normal stiffnesses of the interface.

Figure III.1(a) shows the adopted soil domain considered in the analysis of the square footing case. It is 5mx5m wide by 2m deep. A 'relatively fine' mesh was considered for the analysis. On the other hand, the soil domain and the corresponding mesh for the strip footing case (in the 2D plane) are similar to those obtained with the cross-section of the square footing soil domain at Y=2.5m or at X=2.5m (cf. Figure III.1(b)).

It should be noted that the size of a given element in the deterministic mesh depends on the autocorrelation distances of the soil properties. Der Kiureghian and Ke (1988) have suggested that the length of the largest element of the deterministic mesh in a given direction (horizontal or vertical) should not exceed 0.5 times the autocorrelation distance in that direction. In order to respect this criterion for the different autocorrelation distances, a refinement of the deterministic mesh was performed in FLAC^{3D} for the very small values of the autocorrelation distances (<1m). This mesh will be called hereafter 'very fine' mesh.

For the boundary conditions of the square footing case, the horizontal movement on the vertical boundaries of the grid was restrained, while the base of the grid was not allowed to move in both the horizontal and the vertical directions. The same boundary conditions were adopted for the strip footing case together with another condition related to the plane strain.

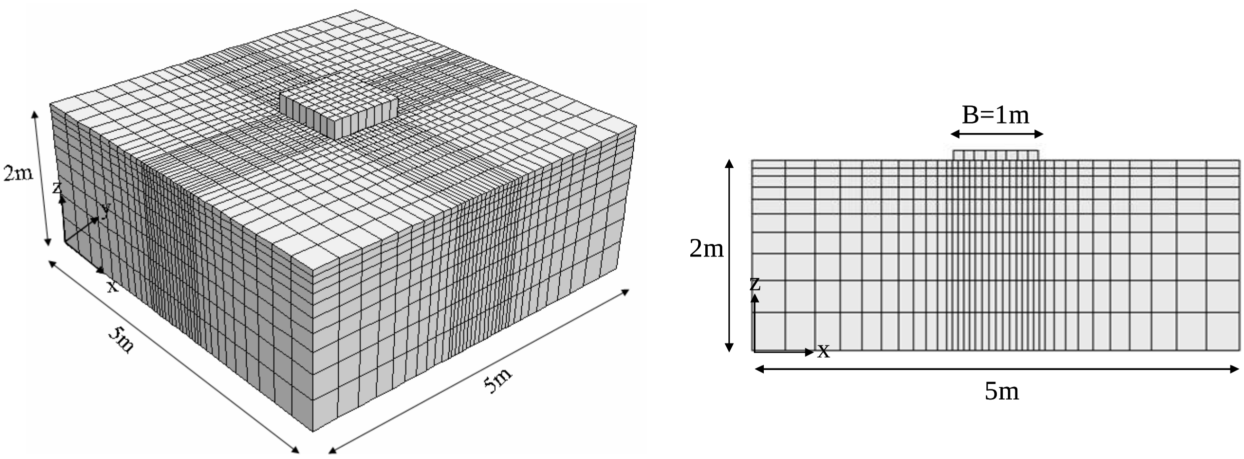

(a) (b)

Figure III.1. Mesh used for the computation of the ultimate bearing capacity of (a) square footing and (b) strip footing

III.3 NUMERICAL RESULTS

In this section, one firstly presents the obtained deterministic numerical results. This is followed by a presentation of the probabilistic numerical results.

III.3.1 Deterministic numerical results

The aim of this section is to present the deterministic numerical results for both the square and the strip footings considered in the analysis.

The three-dimensional 'relatively fine' mesh has led to a deterministic value of ultimate bearing capacity coefficient N_c=6.54 for the square footing case. The difference with the recent finite element solution (N_c=5.91) by Gourvenec et al. (2006) and the recent upper-bound solution (N_c=6.41) by Gourvenec et al. (2006) was respectively about 9% and 2%. It should be emphasized here that a 'very fine' mesh has led to a value of N_c=6.15 which is only 5% smaller (i.e. better) than the value of 6.54 obtained using the 'relatively fine' mesh. Notice however that this solution requires an increase in the computation time by 2 hours and thus, this 'very fine' mesh was not retained in the present probabilistic analysis. A similar procedure that makes use of a 'relatively fine' (not 'very fine') mesh was advocated by Griffiths et al. (2002) when performing a probabilistic analysis. It should be emphasized herein that when dealing with probabilistic studies based on three-dimensional finite element/finite difference deterministic models, the time cost is very important especially when the soil spatial variability (and more specifically the variability of the soil property in three dimensions) is introduced. The reasons are:

(i) The computation time of a single deterministic solution significantly increases with the increase in the density of the three-dimensional deterministic mesh.

(ii) The fact of providing (for each simulation of a single probabilistic analysis) different values of the soil cohesion to the different elements of the mesh, will add a dramatic computation time especially for very fine meshes.

(iii) The large number of simulations required for each probabilistic analysis.

Thus, in order to enable the investigation of the effect of the soil spatial variability in the three dimensions for the present three-dimensional mechanical problem, a 'relatively fine' (not 'very fine') mesh was considered in the square footing case. This is a compromise between the computation time and the accuracy of the probabilistic solution.

Concerning the strip footing case, it should be remembered that the same 'relatively fine' mesh used in the central plane of the square footing was adopted for the values of the autocorrelation distances greater than 1m (cf. Figure III.1(b)), although a finer mesh would be possible because of the relatively small computation time in this case. This choice was adopted in order to maintain a similarity with the mesh employed for the square footing. Notice that a 'very fine' mesh has led in this case to a value of N_c=5.43 which is about 5% larger that the closed form solution N_c=5.14 and it is about 2% larger than the recent finite element solution N_c=5.31 by Gourvenec et al. (2006). The adopted ‘relatively fine' mesh has led to a value N_c=5.74 which is about 10% higher than the closed form solution N_c=5.14 and is only 5% higher than the solution given by the 'very fine' mesh.

III.3.2 Probabilistic numerical results

In this section, the probabilistic numerical results of both the square and strip footings resting on a purely cohesive spatially varying soil are presented. The soil cohesion parameter was modeled as anisotropic non-Gaussian (log-normal) random field using a square exponential autocorrelation function. Its mean value and coefficient of variation (referred to as reference values) were taken as follows: $\mu_c = 20kPa, COV_c = 25\%$.

It should be emphasized here that for both the square and strip footings considered in the analysis, the cases of 2D and 3D cohesion random fields were investigated. As for the autocorrelation distances a_x, a_y and a_z of the cohesion random field, both cases of isotropic random fields (i.e. a_x=a_y=a_z for the 3D random field case and a_x=a_z for the 2D random field case) and anisotropic random fields (i.e. a_x=a_y#a_z for the 3D random field case and a_x#a_z for the 2D random field case) will be treated although the soil is rarely isotropic in reality.

When isotropic random fields are used, the autocorrelation distance for both the 2D and the 3D random fields will be denoted by (a) later on in this chapter (i.e. a=a_x=a_y=a_z for the 3D random field case and a=a_x=a_z for the 2D random field case). Also, when referring to anisotropic random fields, the horizontal autocorrelation distance for both the 2D and the 3D random fields will be denoted by a_h (i.e. a_h=a_x=a_y for the 3D random field case and a_h=a_x for the 2D random field case). Furthermore, the vertical autocorrelation distance for both the 2D and the 3D random fields will be denoted by a_v (i.e. a_v=a_z for both the 3D and 2D random fields cases).

For the isotropic case, a range of 0.5-10m was considered (cf. Table III.1). For the anisotropic case, the reference values adopted for the horizontal and the vertical autocorrelation distances were 10m and 1m while the wide ranges of 0.5-10m and 0.15-10m were considered respectively for the horizontal and the vertical autocorrelation distances when performing the parametric study for both the square and the strip footings (cf. Table III.1).

For the considered soil domain and for the different values of the autocorrelation distances (a, a_h or a_v) used in the analysis, the total number N of random variables (or eigenmodes) that should be used to discretize the cohesion random field within a value of the variance of the error $\leq 10\%$ is presented in Table III.1. It should be emphasized here, that for the very small values of the autocorrelation distance where a large number of random variables (≥ 500) was needed to discretize the random field, a maximum number of random variables N=300 was employed. This is because beyond this value, numerical difficulties may occur. The use of this number may lead to relatively large values of the variance of the error (>10%) but this will not affect the accuracy of the obtained system response. This is because of the very fast decay of the importance of random variables in the variability of the system response as was shown in the previous chapter.

		3D random field	2D random field
Isotropic case with varying values of a (m)	0.5	2000	150
	1	500	50
	2	20	10
	5	10	5
	10	5	5
Anisotropic case with varying values of a_v (m) when a_h=10m	0.15	20	12
	0.25	12	8
	0.5	8	5
	1	5	5
	2	5	5
	5	5	5
	10	5	5
Anisotropic case with varying values of a_h (m) when a_v=1m	0.5	1500	100
	1	500	50
	2	30	8
	5	10	5
	10	5	5

Table III.1. Number of random variables needed to discretize the 3D and 2D cohesion random fields in the case of the square footing

Figure III.2(a) presents, for the case of the square footing, a typical realization of the 3D cohesion random field in the isotropic case where a=0.5m. Only one half of the soil domain is presented in this figure in order to show the variation of the cohesion in the plane X=2.5m (i.e. the central plan under the footing). As may be seen from this figure, dark regions correspond to small values of the cohesion c while light regions refer to lager values.

Figure III.2(b) presents a 3D view of the failure mechanism (for the random field realization shown in Figure III.2(a)) using the contours of the strain rate. This view clearly shows the influence of the 3D spatial variability on the obtained failure mechanism in both the central vertical plane (X=2.5m) and the top horizontal plane representing the ground surface. From this figure, one can see that the failure mechanism is more developed through the weaker zones and is limited when strong zones are encountered. Contrarily to the case of a homogeneous soil, a non-symmetrical mechanism is obtained herein, although the footing is subjected to a symmetrical vertical load.

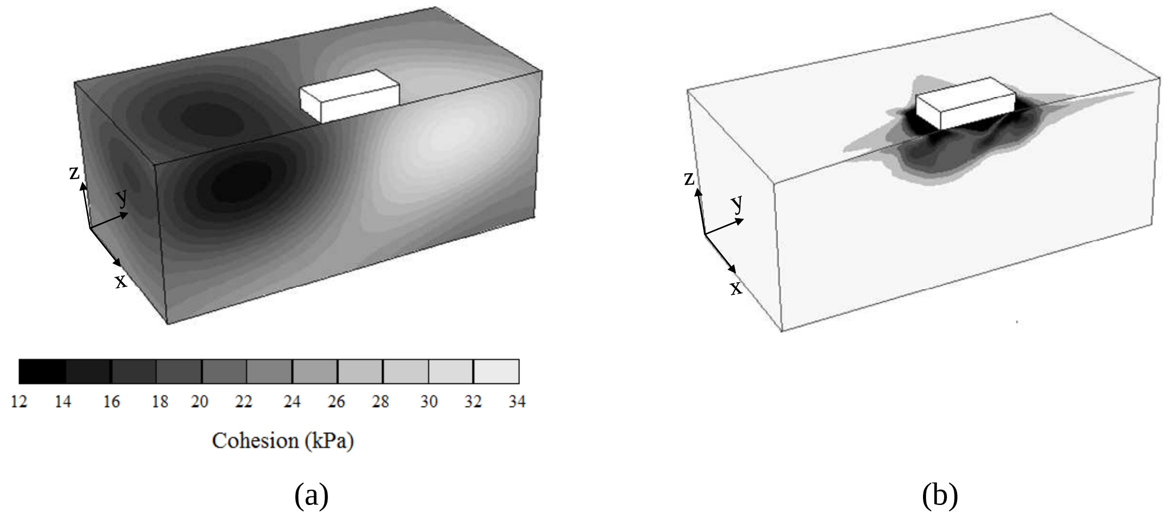

Figure III.2. Perspective view of half of the soil domain showing (a) a random field realization (the contour lines provide the distribution of the soil cohesion on the envelope of this domain) and (b) the contours of the strain rate

On the other hand, the probabilistic numerical results have shown that for the particular case of a purely cohesive soil, the probabilistic ultimate bearing capacity can be written as follows: $q_{ult} = \mu_c N_c$ where μ_c is the mean value of the random field *c* and N_c is the probabilistic ultimate bearing capacity coefficient. This is because a change in the mean value of the random field *c* (for the same value of the coefficient of variation $COV_c = 25\%$) have led to the same PDF of N_c as may be seen from Figure III.3. Thus, in this chapter, the non-dimensional coefficient N_c will be used (instead of q_{ult}) to represent the ultimate bearing capacity in a probabilistic framework. This coefficient depends on the statistical parameters of the random field (i.e. autocorrelation distances and coefficient of variation). Furthermore, this coefficient (as in the deterministic analysis) is independent of the values of the soil cohesion c and the footing breadth B. It should be noted that all the probabilistic results presented in this chapter are provided for the practical value of the coefficient of variation $COV_c = 25\%$.

Finally, it should be mentioned here that for the reference case where a_h=10m and a_v=1m, the computation time is about 45 min per simulation for the square footing case and about 5 min per simulation for the strip footing case. This time includes the computation of the values of the cohesion random field at the different elements centroids of the mesh and their introduction in the deterministic mesh together with the time required for the deterministic calculation. This computation time significantly increases for the very small values of the autocorrelation distances. This is because the large number of random variables in these cases will induce additional computation time to calculate the values of the cohesion random field for the different elements centroids of the deterministic mesh. Notice finally, that for the reference case, 300 calls of the deterministic model were found to be sufficient to construct the meta-model within the prescribed target accuracy Q^2_{TARGET} =0.999.

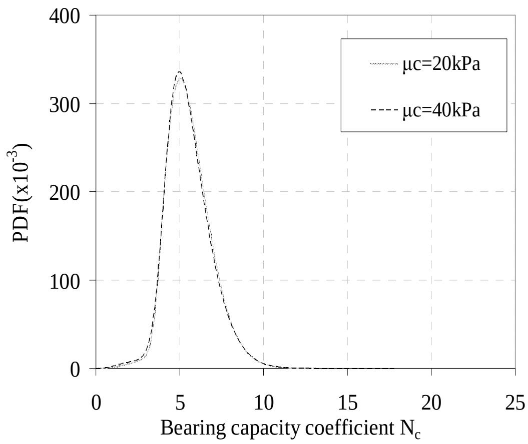

Figure III.3. Influence of the mean value of the cohesion on the PDF of the bearing capacity coefficient N_c of a strip footing when using 3D random field for a_h=10m, a_v=1m and COV_c=25%

III.3.2.1 Effect of the autocorrelation distance: The isotropic case

Table III.2 presents the effect of the isotropic autocorrelation distance (*a*) on the statistical moments of the bearing capacity coefficient N_c for both the square and strip footings using a 3D random field and a 2D random field.

Table III.2 table shows that for a small value of the autocorrelation distance (*a*=0.5m), the variability of the bearing capacity coefficient (expressed by the non-dimensional parameter COV_{N_c}) is smaller when a 3D random field in considered. However, for the large values of the autocorrelation distance (*a*=10m), quasi-similar values of the response variability were obtained in both cases of 3D and 2D random fields. These observations are valid for both the strip and the square footings. Figure III.4 confirms these observations.

Table III.2 also shows that for both the square and strip footings, the variability of N_c decreases when the autocorrelation distance decreases. For the very large values of the autocorrelation distance, the 3D and 2D random fields are superimposed because they tend to their limiting case of random variable for which the autocorrelation distance is infinite. The decrease in the autocorrelation distance from infinity to a finite value (moderate or small where $a \leq 5m$) limits the correlation (in a given simulation) to a finite zone which leads to a smaller variability in the system response. It should be emphasized here that because the case of 2D random field exhibits soil spatial variability in a given plane and shows a non-varying soil in the direction normal to this plane (because the cohesion random field is perfectly correlated in that third direction), the variability of N_c was found to be larger in that case as compared to the case of a 3D random field. This observation may be explained by the fact that in the case of a 3D random field, the soil exhibits spatial variability in three directions and thus, in a single simulation, one obtains a set of weak and strong zones in the 3D space for which the position may change from simulation to another one. This case leads to a decrease in the variability of N_c since the soil heterogeneity (zones of weak and strong soil) is now present in the three directions and it will produce a somewhat close global behavior of the footing from simulation to another one because of the averaging phenomenon over the possible three-dimensional failure mechanism. This averaging phenomenon is more limited in the 2D random field case because of the perfect correlation in the third direction.

		Square footing			Strip footing		
3D random field	a (m)	μ_{N_c}	σ_{N_c}	COV_{N_c} (%)	μ_{N_c}	σ_{N_c}	COV_{N_c} (%)
	0.5	6.34	0.51	8.0	5.38	0.47	8.7
	1	6.39	1.02	15.9	5.49	0.86	15.7
	2	6.46	1.38	21.3	5.55	1.15	20.8
	5	6.51	1.53	23.5	5.69	1.36	24.0
	10	6.52	1.58	24.2	5.72	1.40	24.5
2D random field	a (m)	μ_{N_c}	σ_{N_c}	COV_{N_c} (%)	μ_{N_c}	σ_{N_c}	COV_{N_c} (%)
	0.5	6.34	0.94	14.8	5.41	0.60	11.0
	1	6.41	1.27	19.9	5.51	0.91	16.6
	2	6.48	1.46	22.6	5.58	1.20	21.4
	5	6.52	1.57	24.1	5.70	1.37	24.1
	10	6.52	1.58	24.2	5.73	1.40	24.5

Table III.2. Effect of the isotropic autocorrelation distance (*a*) on the statistical moments μ_{N_c} and σ_{N_c} of the bearing capacity coefficient N_c of square and strip footings using both 3D and 2D random fields

Finally, Table III.2 shows that for both the square and strip footings, the probabilistic mean value of N_c is slightly smaller when considering a 3D random field, but this difference is not significant and can thus be neglected. The probabilistic mean in both 3D and 2D random field cases is found to be slightly smaller than the deterministic value (6.54 for the square footing and 5.74 for the strip footing) which makes it slightly more critical.

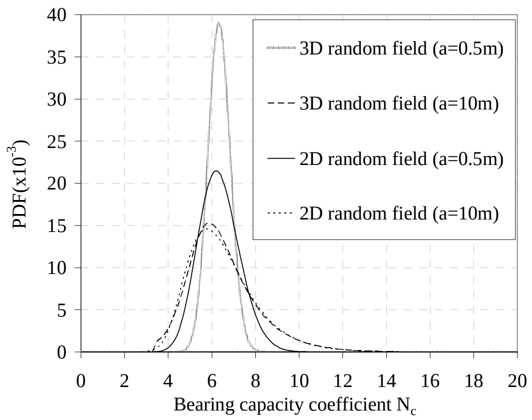

Figure III.4. Comparison between the PDFs of the bearing capacity coefficient N_c of a square footing when using 3D and 2D isotropic random fields

III.3.2.2 Effect of the autocorrelation distance: The anisotropic case

Table III.3 presents the effect of the vertical autocorrelation distance a_v on the statistical moments of the bearing capacity coefficient N_c for the square and strip footings using both 3D and 2D random fields when a_h=10m. Similarly, Table III.4 present the effect of the horizontal autocorrelation distance a_h on the statistical moments of the bearing capacity coefficient N_c for the square and strip footings using 3D and 2D random fields when a_v=1m.

Tables III.3 and III.4 show that for the very small values of the horizontal or vertical autocorrelation distance, the variability of N_c (expressed by the non-dimensional parameter COV_{N_c}) is smaller when a 3D random field is considered (this difference is negligible when investigating the effect of the vertical autocorrelation distance because the chosen horizontal autocorrelation distance, i.e. a_h=10m is relatively large and thus the 2D and the 3D random fields tend to the same one-dimensional vertically varying soil mass). However, for the large values of the horizontal or vertical autocorrelation distance (i.e. a_h=10m or a_v=10m), quasi-similar values of the response variability are obtained in both cases of 3D and 2D random fields. These observations are valid for both the strip and the square footings. Figure III.5 and Figure III.6 confirm these observations.

		Square footing			Strip footing		
	a_v (m)	μ_{N_c}	σ_{N_c}	COV_{N_c} (%)	μ_{N_c}	σ_{N_c}	COV_{N_c} (%)
3D random field	0.15	6.24	0.96	15.3	5.38	0.66	12.2
	0.25	6.27	1.15	18.3	5.39	0.82	15.3
	0.5	6.38	1.38	21.7	5.45	1.04	19.2
	1	6.48	1.52	23.5	5.58	1.24	22.3
	2	6.51	1.57	24.1	5.67	1.36	23.9
	5	6.51	1.58	24.2	5.71	1.39	24.4
	10	6.52	1.58	24.2	5.72	1.40	24.5
	a_v (m)	μ_{N_c}	σ_{N_c}	COV_{N_c} (%)	μ_{N_c}	σ_{N_c}	COV_{N_c} (%)
2D random field	0.15	6.24	0.97	15.5	5.39	0.67	12.5
	0.25	6.27	1.16	18.5	5.41	0.84	15.5
	0.5	6.38	1.39	21.8	5.47	1.06	19.3
	1	6.48	1.53	23.5	5.59	1.25	22.4
	2	6.51	1.57	24.1	5.69	1.36	24.0
	5	6.51	1.58	24.2	5.72	1.40	24.4
	10	6.52	1.58	24.2	5.73	1.40	24.5

Table III.3. Effect of the vertical autocorrelation distance (a_v) on the statistical moments μ_{N_c} and σ_{N_c} of the bearing capacity coefficient N_c of square and strip footings using both 3D and 2D random fields

		Square footing			Strip footing		
	a_h (m)	μ_{N_c}	σ_{N_c}	COV_{N_c} (%)	μ_{N_c}	σ_{N_c}	COV_{N_c} (%)
3D random field	0.5	6.34	0.48	7.6	5.41	0.50	9.3
	1	6.39	1.02	15.9	5.49	0.86	15.7
	2	6.44	1.32	20.4	5.51	1.07	19.5
	5	6.46	1.48	22.9	5.56	1.20	21.6
	10	6.48	1.52	23.5	5.58	1.24	22.3
	a_h (m)	μ_{N_c}	σ_{N_c}	COV_{N_c} (%)	μ_{N_c}	σ_{N_c}	COV_{N_c} (%)
2D random field	0.5	6.35	1.01	15.9	5.43	0.70	12.8
	1	6.41	1.27	19.9	5.51	0.91	16.6
	2	6.47	1.39	21.5	5.53	1.10	19.9
	5	6.47	1.48	22.8	5.57	1.21	21.7
	10	6.48	1.53	23.5	5.59	1.25	22.4

Table III.4. Effect of the horizontal autocorrelation distance (a_h) on the statistical moments μ_{N_c} and σ_{N_c} of the bearing capacity coefficient N_c of square and strip footings using both 3D and 2D random fields

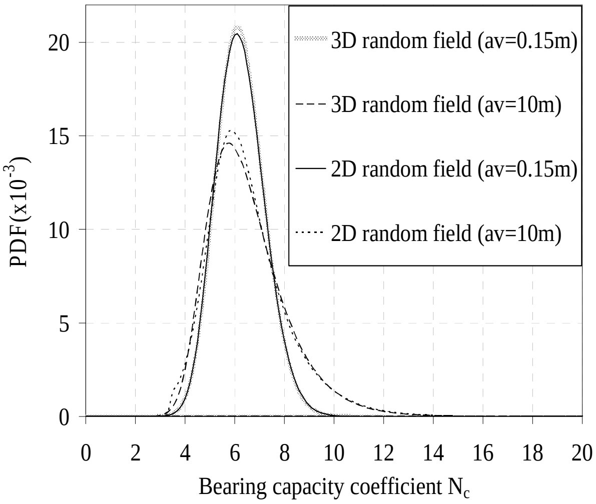

Figure III.5. Comparison between the PDFs of the bearing capacity coefficient N_c of a square footing when using 3D and 2D anisotropic random fields and for a_h=10m

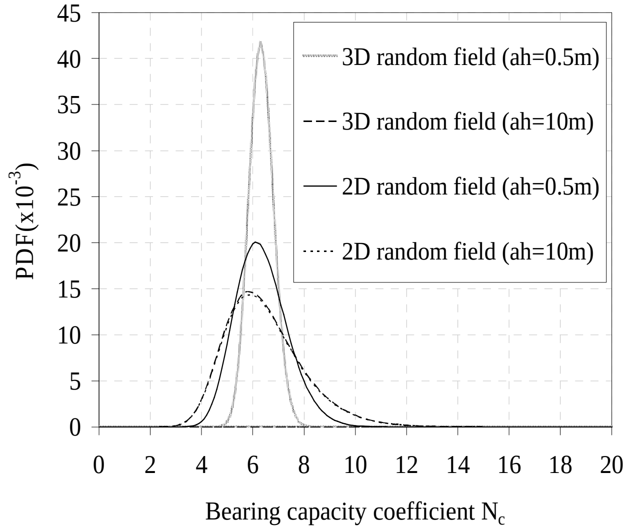

Figure III.6. Comparison between the PDFs of the bearing capacity coefficient N_c of a square footing when using 3D and 2D anisotropic random fields and for a_v=1m

Table III.3 and Table III.4 also show that for both the square and strip footings, the variability of N_c decreases when the autocorrelation distance decreases. This can be explained by the fact that for the very large values of the horizontal autocorrelation distance a_h (a_h=10m), the 3D and 2D random fields tend to their limiting case of a one-dimensional random field with a vertically varying soil mass. Similarly, for the very large values of the vertical autocorrelation distance a_v (a_v=10m), the 2D and 3D random fields tend respectively to their limiting cases of one- and two-dimensional random fields with a horizontally varying soil masses. In all these cases, the cohesion random field is perfectly correlated in a prescribed direction (horizontal or vertical); however, the other direction (vertical or horizontal) is allowed to exhibit variations in the value of the cohesion according to the value of the autocorrelation distance fixed for that direction. This induces a reduction in the variability of N_c with respect to the case where $a_h=a_v$=10m. The decrease in the autocorrelation distance from the case of a horizontally varying soil mass (where $a_v=\infty$) or a vertically varying soil mass (where $a_h=\infty$) to the case where the infinite value of the autocorrelation distance decreases to a finite value, re-create further variations in the value of the cohesion. This reduces once again the variability of N_c with respect to the case where $a_h=a_v$=10m.

Finally, as in Table III.2, Table III.3 and Table III.4 show that the probabilistic mean in both 3D and 2D random field cases is found to be slightly smaller than the deterministic value but the difference is negligible.

III.3.3 Discussion

A comparison between the values of the coefficients of variation of N_c (obtained using 3D and 2D random fields) for both the isotropic and anisotropic cases and for both the strip and square footings is provided in Table III.5. This comparison is presented in the form of a ratio between the values of the coefficients of variation of the 3D and 2D random fields.

Table III.5 shows that for both the square and strip footings, the ratio $COV_{N_c}^{3D} \big/ COV_{N_c}^{2D}$ is the smaller for the very small values of the autocorrelation distance. This ratio tends to the value of unity for the very large values of the autocorrelation distances. Thus, the third dimension is important to be considered only when small values of the autocorrelation distances are encountered.

On the other hand, the numerical results have shown that the non-dimensional parameters a/B, a_h/B and a_v/B can be adopted in the probabilistic analysis of foundations. This is because changing both the values of the autocorrelations distances a_h and a_v (or a) and the footing breadth B in a way to preserve the same ratio a_h/B and a_v/B (or a/B) have led to the same PDF of N_c. Therefore, N_c is a function of only a/B or (a_h/B and a_v/B) and the coefficient of variation of the cohesion random field. The autocorrelation distances a, a_h and a_v used in all the tables and figures of this chapter can be replaced by a/B, a_h/B and a_v/B respectively since the footing breadth B was taken equal to 1m in all the above analyses. This makes all the tables of this chapter non-dimentional and can be used for any value of a_h/B and a_v/B (or a/B) when COV_c=25%.

Autocorrelation distance (m)	Values of $COV_{N_c}^{3D} \big/ COV_{N_c}^{2D}$ for different values of the isotropic autocorrelation distance		Values of $COV_{N_c}^{3D} \big/ COV_{N_c}^{2D}$ for different values of the vertical autocorrelation distance a_v when a_h=10m		Values of $COV_{N_c}^{3D} \big/ COV_{N_c}^{2D}$ for different values of the horizontal autocorrelation distance a_h when a_v=1m	
	Square	Strip	Square	Strip	Square	Strip
0.15	-	-	0.987	0.981	-	-
0.25	-	-	0.991	0.987	-	-
0.5	0.540	0.794	0.995	0.992	0.477	0.724
1	0.803	0.946	0.997	0.994	0.802	0.946
2	0.942	0.969	0.998	0.998	0.948	0.981
5	0.974	0.998	0.999	1.000	0.999	0.991
10	0.998	1.000	0.999	1.000	1.000	0.994

Table III.5. Ratios between the coefficients of variation values of N_c (obtained using 3D and 2D random fields) for both the square and strip footings

III.4 CONCLUSIONS

A probabilistic analysis that considers the effect of the spatial variability in three dimensions was investigated through the study of the ultimate bearing capacity of strip and square foundations resting on a purely cohesive soil with a spatially varying cohesion in the three dimensions. The main reason for which a purely cohesive soil was used is to investigate the effect of the spatial variability in the third direction with the use of a relatively non-expensive deterministic model.

In order to investigate the effect of the spatial variability in the third direction on the ultimate bearing capacity of foundations, the results obtained using a 3D random field were compared to those corresponding to a 2D random field for the two cases of strip and square footings. The objective is to check the validity of a 2D random field in both cases of plane strain and three-dimensional problems.

The soil cohesion parameter was modeled as anisotropic non-Gaussian (log-normal) random field with a square exponential autocorrelation function. A straightforward extension to the 3D case of the Expansion Optimal Linear Estimation (EOLE) methodology proposed by Li and Der Kiureghian (1993) and extended by Vořechovsky (2008) was used in this chapter. The deterministic model was based on 3D numerical simulations using $FLAC^{3D}$ software. An efficient uncertainty propagation methodology that makes use of a non-intrusive approach to build up a sparse polynomial chaos expansion for the system response was employed.

The probabilistic numerical results have shown that for small values of the autocorrelation distances, the variability of the ultimate bearing capacity computed by considering a 3D random field is smaller than the one obtained with the 2D random field for both cases of square and strip footings. The ratio $COV_{N_c}^{3D} \big/ COV_{N_c}^{2D}$ between the values of the coefficients of variation of N_c using the 3D and 2D random fields is the smaller for the very small values of the autocorrelation distance. This ratio tends to the value of unity for the very large values of the autocorrelation distances. Thus, the third dimension is important to be considered when small autocorrelation distances are encountered. As for the probabilistic mean values, slightly smaller values were obtained in the case of the 3D random field but the difference is negligible.

CHAPTER IV. COMBINED USE OF THE SPARSE POLYNOMIAL CHAOS EXPANSION METHODOLOGY AND THE GLOBAL SENSITIVITY ANALYSIS FOR HIGH-DIMENSIONAL STOCHASTIC PROBLEMS

IV.1 INTRODUCTION

In the previous two chapters, an efficient approach to deal with uncertainty propagation in the case of high-dimensional problems (i.e. when a large number of random variables is involved) was presented. This approach is based on the sparse polynomial chaos expansion (SPCE) for the system response and leads to a reduced computational cost as compared to the classical polynomial chaos expansion (PCE) methodology. Notice that both, the PCE and the SPCE methodologies, aim at replacing the original complex deterministic model which may be an analytical model or a finite element/finite difference model by a meta-model. This allows one to easily calculate the system response (when performing MCS) using a simple analytical equation.

When dealing with high-dimensional stochastic problems making use of computationally-expensive deterministic models (e.g. three-dimensional analysis of shallow rectangular or circular footings resting on 3D spatially varying ponderable soils), the time cost remains important even with the use of the SPCE. Consequently, a method that can reduce once again the cost of the probabilistic analysis (i.e. the number of calls of the deterministic model) is needed.

In this chapter, an efficient combined use of the SPCE methodology and the Global Sensitivity Analysis (GSA) is proposed [Al-Bittar and Soubra (2012e, 2012f, 2012g)]. The basic idea of this combination is that, for a given discretized random field, the obtained random variables do not have the same weight in the variability of the system response. The variables with a very small contribution in the variability of the system response can be discarded which significantly reduces the dimensionality of the treated problem. This allows one to perform a probabilistic analysis using a reduced Experiment Design (ED) and thus a smaller number of calls of the computationally-expensive deterministic model. The main challenge remains in detecting the most influential random variables in order to reduce the dimensionality of the problem. For this purpose, a procedure that makes use of both the SPCE and the GSA (denoted hereafter by SPCE/GSA) is proposed in this regard.

The proposed methodology was firstly validated using a relatively non-expensive model. This model was extensively investigated in the second chapter of this thesis using the SPCE methodology. It involves the computation of the ultimate bearing capacity of a strip footing resting on a weightless spatially varying soil where the soil cohesion and angle of internal friction (c and φ) were modeled by two anisotropic non-Gaussian cross-correlated random fields. Secondly, the SPCE/GSA procedure was applied to two computationally-expensive deterministic models that involve the computation of the PDF of the ultimate bearing capacity of a strip footing resting on a ponderable soil in both cases of (i) 2D random fields and (ii) 3D random fields. While an extensive parametric study was undertaken in the case of the 2D spatially varying soil, only a single soil configuration was considered in the case of the 3D spatially varying soil. The study of the case of rectangular or circular footings resting on a ponderable 3D spatially varying soil will be the subject of future studies.

This chapter is organized as follows: The proposed SPCE/GSA procedure is firstly presented. It is followed by the numerical results. The chapter ends by a conclusion of the main findings

IV.2 EFFICIENT COMBINED USE OF THE SPCE METHODOLOGY AND THE GLOBAL SENSITIVITY ANALYSIS GSA

As mentioned previously, the time cost of the probabilistic analysis remains important even with the use of the SPCE when dealing with computationally-expensive deterministic models. Consequently, a procedure that can reduce once again this time cost is needed.

An efficient combined use of the SPCE methodology and the GSA is proposed in this section. In this method, a small SPCE order is firstly selected to approximate the system response by a meta-model. It should be noted that the random variables involved in the system response are those that result from the discretization of the random fields into a finite number of random variables. A GSA based on Sobol indices is then performed on this small SPCE order to determine the weight of each random variable in the variability of the system response. As a result, the variables with very small values of their Sobol indices (i.e. those that have a small weight in the variability of the system response) can be discarded. Consequently, a response which only depends on a smaller number of random variables is obtained. In other words, one obtains a response with an 'effective dimension'. This dimension is smaller than the initial dimension where the total number of random variables was considered. As it will be shown later, the use of a small SPCE order to perform the GSA is not a concern since higher SPCE orders lead to the same influential random variables. Once the 'effective dimension' was determined, a higher SPCE order that makes use of only the most influential random variables can be used. This significantly reduces the computation time. The use of a higher SPCE order is necessary in order to lead to an improved fit of the SPCE. The SPCE/GSA procedure can be described in more details by the following steps:

- Discretize the random field(s): This step may be made using EOLE method and its extensions by Vořechovsky (2008) (see section I.3.4). After the discretization procedure, a random field is represented by N independent standard normal random variables. If the total number of random fields involved in the analysis is equal to $N_{RF,}$ the total number of random variables is thus given by $N_T= N_{RF}xN$ which can be relatively large especially for small values of the autocorrelation distances as was seen in the previous chapters. Notice that the equation $N_T=N_{RF}xN$ is only applicable if all the random fields share the same autocorrelation function.

- Select a preliminary small order of the sparse polynomial chaos expansion (e.g. p=2) to approximate the system response by a meta-model. The main reason for selecting a small order is the exploration of the most influential random variables (i.e. those that have a significant weight in the variability of the system response) using a small Experiment Design (ED). It should be emphasized here that the small value of the SPCE order leads to a significant decrease in the size of the experiment design, i.e. in the number of calls of the deterministic model.

- Perform a GSA based on Sobol indices (using the obtained second order SPCE) to determine the weight of each random variable (of the different random fields) in the variability of the system response. The variables with very small values of their Sobol indices have no significant weight in the variability of the system response and can thus be discarded. Consequently, a response that only depends on a smaller number of random variables is obtained. In other words, one obtains a response with an 'effective dimension' N_e that is smaller than the initial dimension where the total number N_T of random variables was considered. It should be mentioned here that the small SPCE order (i.e. p=2) used firstly to perform the GSA is sufficient to provide the weight of each random variable in the variability of the system response since higher SPCE orders lead to the same influential random variables as will be seen later in the numerical results.

- Use the same Experiment Design (ED) which was employed before but this time by only keeping the most influential random variables. By reducing the number of random variables from N_T to N_e (where $N_e<N_T$), one has the possibility to use a higher SPCE order (i.e. p>2). The use of a higher SPCE order is necessary to lead to an improved fit of the SPCE since the coefficient of determination Q^2 given in Equation (I.45) increases when the SPCE order increases as it will be shown in the numerical results.

As a conclusion, the use of the SPCE/GSA procedure is expected to provide a good fit of the deterministic model with a reduced number of model evaluations as compared to the classical SPCE approach.

IV.3 NUMERICAL RESULTS

The aim of this section is to make use of the SPCE/GSA approach for the determination of the probabilistic numerical results of two computationally-expensive deterministic models. More specifically, one focuses on the computation of the probability density function (PDF) of the ultimate bearing capacity (q_{ult}) of a strip footing resting on a ponderable soil in both cases of (i) 2D random fields and (ii) 3D random fields. It should be mentioned here that a somewhat similar problem was considered in chapter II using the SPCE approach: Since the SPCE approach was unable to consider the case of a ponderable soil because of the significant computational cost, only the case of a weightless soil was considered. Also, only 2D random fields were investigated.

The soil cohesion c and friction angle φ were modeled by two anisotropic cross-correlated non-Gaussian random fields. The deterministic model was based on numerical simulations using FLAC^{3D}. The inputs of the deterministic and probabilistic models are the same as those considered in chapter II and more precisely in section II.3.1 where a probabilistic analysis of a strip footing resting on a weightless 2D spatially varying (c, φ) soil mass was undertaken. The only additional parameter used herein is the soil unit weight γ whose value is considered to be equal to 18 kN/m^3.

Before the presentation of the probabilistic results of a ponderable soil for both cases of 2D and 3D random fields, it seems necessary to validate the present SPCE/GSA procedure by comparison of its results with those obtained by the use of the classical SPCE (in the case of a weightless soil). This is the aim of the next subsection.

IV.3.1 Validation of the SPCE/GSA procedure

The aim of this section is the validation of the present SPCE/GSA approach. For this purpose, a comparison between the results obtained using the classical SPCE method and those obtained with the proposed SPCE/GSA procedure is presented in the case of a weightless soil (which is a relatively non-expensive deterministic model). It should be mentioned here that when neglecting the soil weight γ, the computation time decreases from 10 to 5 min per simulation. Although this difference may not seem to be significant for a single simulation, it becomes dramatically important during the probabilistic analyses where a large number of simulations is needed for each probabilistic analysis.

The validation of the SPCE/GSA procedure is done for the illustrative case [a_x=10m, a_y=1m, $r(c, \varphi)$=-0.5] referred to hereafter as the reference case. For this configuration, the discretization of the two random fields c and φ has led to a total number of random variables N_T equal to 24 (12 random variables for each random field as was shown in Table II.1 of chapter II). By using the total number of random variables N_T, a fourth order SPCE was necessary to reach the target accuracy Q^2_{TARGET} =0.999. An ED involving 800 points was needed to solve the regression problem given in Equation (I.41) (i.e. to obtain a well-conditioned regression problem for which the rank of the matrix $(\eta^T \eta)^{-1}$ is larger than or equal to the number of unknown coefficients). On the other hand, by using the present SPCE/GSA procedure, a GSA was performed to detect the most influential random variables. Different SPCE orders (i.e. orders 2, 3, and 4) were considered in order to check if the SPCE order has an impact on the determination of the most influential random variables.

Figure IV.1 depicts the values of Sobol indices for the 24 random variables, as given by the SPCEs of orders 2, 3 and 4. The first 12 random variables [i.e. ξ_i for i=1, …, 12] correspond to the cohesion random field and the last 12 random variables [i.e. ξ_i for i=13, …, 24] are those corresponding to the friction angle random field. Figure IV.1 shows that whatever the SPCE order is, the two first random variables of both fields (i.e. ξ_1, ξ_2, ξ_{13}, ξ_{14}) are the most influential. For the two random fields, a very fast decay in the weight of the random variables is noticed with quasi negligible values beyond the first two random variables. In fact, the first two random variables of the two random fields, which correspond to the first two eigenmodes of both fields involve 95% of the response variability as may be seen from Table IV.1. This is logical since the system response (i.e. the ultimate bearing capacity q_{ult}) is a quantity that depends on the average distribution of the soil properties (c, φ) which is therefore quite insensitive to small-scale fluctuations of the spatially varying shear strength parameters c and φ. Notice that the first eigenmodes provide the average distribution of the shear strength parameters over the soil domain; however, the remaining eigenmodes give the small scale fluctuations around this average distribution.

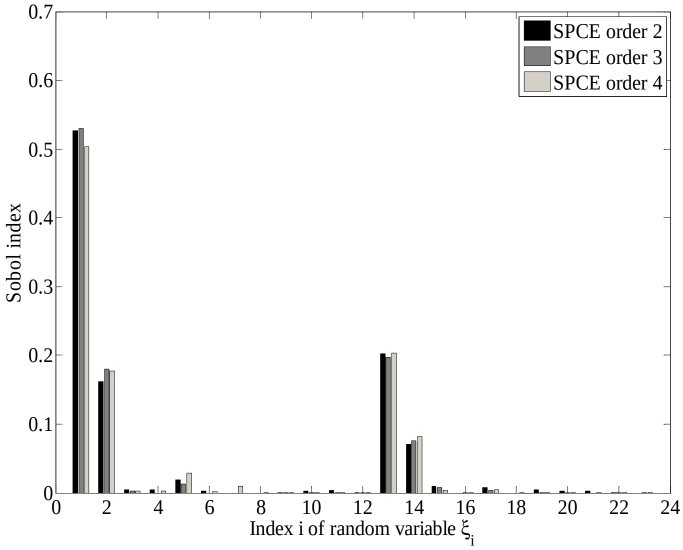

Figure IV.1. Sobol indices for SPCEs of orders 2, 3, and 4 using the total number of eigenmodes ξ_i (i=1, ..., 24)

	ξ_i (i=1, ..., 12) for the cohesion random field											
	ξ_1	ξ_2	ξ_3	ξ_4	ξ_5	ξ_6	ξ_7	ξ_8	ξ_9	ξ_{10}	ξ_{11}	ξ_{12}
Sobol index	0.500	0.170	0.002	0.002	0.030	0.002	0.009	2 x10^{-4}	2 x10^{-4}	9 x10^{-5}	2x10^{-4}	7 x10^{-5}
	ξ_i (i=13, ..., 24) for the friction angle random field											
	ξ_{13}	ξ_{14}	ξ_{15}	ξ_{16}	ξ_{17}	ξ_{18}	ξ_{19}	ξ_{20}	ξ_{21}	ξ_{22}	ξ_{23}	ξ_{24}
Sobol index	0.200	0.080	0.001	8x10^{-4}	0.002	5x10^{-4}	6x10^{-4}	3x10^{-4}	1x10^{-4}	4 x10^{-5}	4 x10^{-5}	5 x10^{-5}

Table IV.1. Sobol indices for the reference case where a_x=10m, a_y=1m, and $r(c,\varphi)$=-0.5

Figure IV.1 clearly shows that the Sobol indices of the different random variables do not significantly change with the SPCE order. Thus, a second order SPCE is sufficient to identify the influential random variables (i.e. those that have a significant weight in the variability of the ultimate bearing capacity). Increasing the SPCE order has led to the same influential random variables which justify the small SPCE order chosen to perform the preliminary investigations. The main advantage of a small SPCE order is that a small ED is sufficient to solve the regression problem. As shown in Table IV.2, 150 calls of the deterministic model are needed to solve the regression problem for a second order SPCE. This number attains 800 for a fourth order SPCE. This significant increase is because the number of unknown coefficients significantly increases from 29 to 144 when one chooses a fourth order SPCE instead of a second order SPCE. It should be emphasized here that the number of coefficients that appear in Table IV.2 is that retained by the iterative SPCE procedure suggested by Blatman and Sudret (2010). Notice finally that the number of coefficients of the full PCEs of order 2, 3 and 4 are respectively 325, 2925 and 20475. This clearly shows that the use of the PCE in the case of random fields would not be feasible.

SPCE order	2	3	4
Number of unknown coefficients *P*	29	35	144
Number of model evaluations	150	350	800

Table IV.2. Number of unknown coefficients and model evaluations for different SPCE orders

To choose the number of random variables which will be retained hereafter within the SPCE/GSA procedure, the different random variables of the two random fields are firstly sorted in a descending order according to the values of their Sobol indices (cf. the first three columns in Table IV.3). A threshold of acceptance t_a is then fixed as a percentage of the most influential (weighted) random variable. In the present work, the most influential random variable is ξ_1 and it has a Sobol index S_1=0.5. Different values of the threshold were tested (cf. first line in Table IV.3). The random variables having a Sobol index smaller than the prescribed threshold t_a are discarded (marked with the symbol (-) in the table). In this work, a threshold of 2% of the Sobol index of the most weighed random variable is considered as sufficient; the corresponding retained random variables provide 98% of the total variance of the system response as may be seen from the last line of the 7th column in Table IV.3. For this threshold, an 'effective dimension' N_e=5 is obtained (i.e. five random variables are considered to be the most weighed). The five retained random variables (ξ_1, ξ_{13}, ξ_2, ξ_{14}, ξ_5) will now be used with the already existing 150 model evaluations which were firstly employed to approximate the second order SPCE (using the total number of random variables N_T=24).

The reduction in the number of random variables from N_T=24 to N_e=5 provides the possibility to use higher SPCE orders (i.e. p>2) with the same ED (i.e. the 150 model evaluations). The use of a higher SPCE order is necessary to lead to an improved fit of the SPCE since the coefficients R^2 and Q^2 increase when the SPCE order increases as shown in Table IV.4 for both the classical SPCE approach (using the total number of random variables N_T=24 and the number of model evaluations of Table IV.2) and the present SPCE/GSA procedure (where the effective dimension is equal to 5, i.e. N_e=5 and the number of model evaluations is fixed to 150). By using the SPCE/GSA procedure, an SPCE up to p=8 was reached using only 150 model evaluations. This order is to be compared to the fourth order SPCE which was used in the SPCE methodology.

Index i of random variable ξ_i	Random variable ξ_i (i=1, ..., 24)	Sobol index S_i (i=1, ..., 24)	t_a=0.5% x S_1 =0.0025	t_a=1% x S_1 =0.005	t_a=1.5% x S_1 =0.0075	t_a=2% x S_1 =0.01	t_a=2.5% x S_1 =0.0125
1	ξ_1	S_1=0.500	0.500	0.500	0.500	0.500	0.500
13	ξ_{13}	S_{13}=0.200	0.200	0.200	0.200	0.200	0.200
2	ξ_2	S_2=0.170	0.170	0.170	0.170	0.170	0.170
14	ξ_{14}	S_{14}=0.080	0.080	0.080	0.080	0.080	0.080
5	ξ_5	S_5=0.030	0.030	0.030	0.030	0.030	0.030
7	ξ_7	S_7=0.009	0.009	0.009	0.009	-	-
6	ξ_6	S_6=0.002	0.002	-	-	-	-
17	ξ_{17}	S_{17}=0.002	0.002	-	-	-	-
3	ξ_3	S_3=0.002	0.002	-	-	-	-
4	ξ_4	S_4=0.002	0.002	-	-	-	-
15	ξ_{15}	S_{15}=0.001	-	-	-	-	-
16	ξ_{16}	S_{16}=8.0 x10^{-4}	-	-	-	-	-
19	ξ_{19}	S_{19}=6.0 x10^{-4}	-	-	-	-	-
18	ξ_{18}	S_{18}=5.0 x10^{-4}	-	-	-	-	-
20	ξ_{20}	S_{20}=3.0 x10^{-4}	-	-	-	-	-
8	ξ_8	S_8=2.0 x10^{-4}	-	-	-	-	-
9	ξ_9	S_9=2.0 x10^{-4}	-	-	-	-	-
11	ξ_{11}	S_{11}=2.0 x10^{-4}	-	-	-	-	-
21	ξ_{21}	S_{21}=1.0 x10^{-4}	-	-	-	-	-
10	ξ_{10}	S_{10}=9.0 x10^{-5}	-	-	-	-	-
12	ξ_{12}	S_{12}=7.0 x10^{-5}	-	-	-	-	-
24	ξ_{24}	S_{24}=5.0 x10^{-5}	-	-	-	-	-
22	ξ_{22}	S_{22}=4.0 x10^{-5}	-	-	-	-	-
23	ξ_{23}	S_{23}=4.0 x10^{-5}	-	-	-	-	-
	Sum of Sobol indices	1.001	0.997	0.989	0.989	0.98	0.98

Table IV.3. Sobol indices S_i of the different random variables ξ_i and the retained random variables for the different values of the threshold of acceptance t_a

From Table IV.4, one can notice that with the use of the SPCE/GSA procedure, the Q^2 and R^2 coefficients increase with the increase of the SPCE order and stabilize beyond the order 5. This means that there is a need to increase the SPCE order to improve the fit; however, there is no improvement in the fit beyond the fifth order. On the other hand, the values of Q^2 and R^2 (0.963 and 0.972) given by the present approach for a sixth SPCE order are smaller than those of the classical SPCE approach with a fourth order (i.e. 0.994 and 0.999). This is because 19 random variables were discarded which slightly affect the goodness of the fit. It should be mentioned that although the values of both Q^2 and R^2 are provided, the values of only Q^2 could be sufficient for the analysis because this coefficient is more rigorous than R^2.

	SPCE order	2	3	4	5	6	7	8
Total number of random variables N_T	Coefficient of determination R^2	0.998	0.999	0.999	-	-	-	-
	Coefficient of determination Q^2	0.824	0.932	0.994	-	-	-	-
Reduced number of random variables N_e	Coefficient of determination R^2	0.961	0.963	0.968	0.970	0.972	0.972	0.972
	Coefficient of determination Q^2	0.791	0.883	0.957	0.961	0.963	0.963	0.963

Table IV.4. Coefficients of determination R^2 and Q^2 for different SPCE orders when using the total and the reduced number of random variables

Figure IV.2 shows the PDF of the ultimate bearing capacity as obtained by both the classical SPCE approach (with the total number of random variables N_T=24) and the proposed SPCE/GSA procedure (using only five random variables). Table IV.5 provides the corresponding statistical moments and coefficients of determination R^2 and Q^2. Notice that the results of the present SPCE/GSA approach are given in Table IV.5 for different values of the number of model evaluations (from 150 to 800) and for a fifth order SPCE. From this table, one can see that the coefficients R^2 and Q^2 of the SPCE/GSA procedure are quasi constant with the increase in the number of model evaluations. This means that 150 model evaluations are sufficient and there is no need for more model evaluations to improve the accuracy of the fit. On the other hand, one can observe (see Figure IV.2 and Table IV.5) that the first two statistical moments (μ and σ) are well estimated with the present SPCE/GSA approach using the 150 model evaluations. However, the third and fourth statistical moments (δ_u and κ_u) need more model evaluations (800 model evaluations) in order to converge to their reference values given by the SPCE approach (cf. Table IV.5). This demonstrates the efficiency of the present SPCE/GSA procedure to compute only the first two statistical moments with a much reduced number of the model evaluations (150 model evaluations) with respect to the classical SPCE approach (with 800 model evaluations).

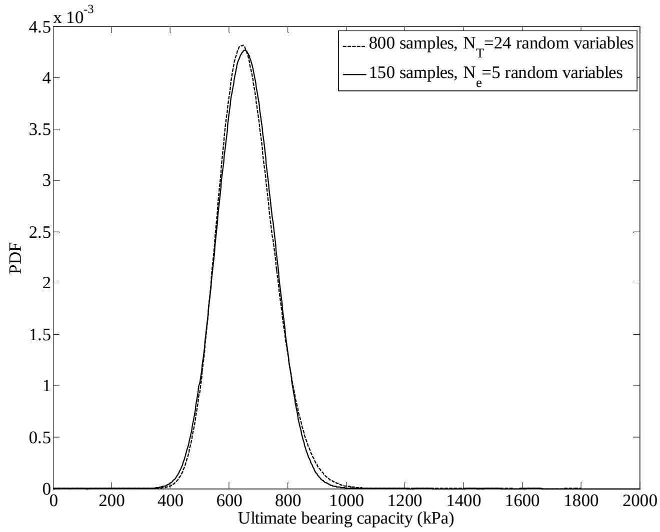

Figure IV.2. PDF of the ultimate bearing capacity for both the classical SPCE method with the total number of random variables N_T =24 and the proposed SPCE/GSA procedure with only five random variables N_e =5 when a_x=10m, a_y=1m and $r(c, \varphi)$= -0.5

	Number of model evaluations	Mean μ (kPa)	Standard deviation σ (kPa)	Skewness δ_u (-)	Kurtosis κ_u (-)	R^2	Q^2
With the total number of random variables N_T=24	800	658.2	93.57	0.287	0.163	0.999	0.995
With the reduced number of random variables N_e=5	150	657.84	90.80	0.105	0.013	0.968	0.950
	200	658.98	91.53	0.168	0.056	0.972	0.951
	250	659.90	92.10	0.188	0.063	0.964	0.953
	300	659.73	92.15	0.202	0.060	0.962	0.963
	400	660.05	90.95	0.291	0.050	0.969	0.960
	500	659.50	90.81	0.296	0.043	0.970	0.963
	600	659.75	90.99	0.272	0.116	0.968	0.963
	700	659.50	90.85	0.280	0.164	0.968	0.963
	800	659.85	91.20	0.300	0.160	0.970	0.967

Table IV.5. Coefficients of determination R^2 and Q^2 of the SPCE and statistical moments (μ, σ, δ_u and κ_u) of the ultimate bearing capacity as given by the classical SPCE approach and by the present SPCE/GSA procedure

As for the Sobol indices of the two random fields *c* and φ, Table IV.6 shows that the SPCE/GSA procedure with only 150 model evaluations gives the same results obtained by the classical SPCE approach using 800 model evaluations which demonstrates once again the efficiency of the present SPCE/GSA procedure.

	Number of model evaluations	i	S_i (i=1, ..., 12)	i	S_i (i=13, ..., 24)	$S\,(c)=\sum_{i=1}^{12} S_i$	$S\,(\varphi)=\sum_{i=13}^{24} S_i$
With the total number of random variables N_T=24	800	1	0.500	13	0.200	0.715	0.285
		2	0.170	14	0.080		
		3	0.002	15	0.001		
		4	0.002	16	8.0×10^{-4}		
		5	0.030	17	0.002		
		6	0.002	18	5.0×10^{-4}		
		7	0.009	19	6.0×10^{-4}		
		8	2.0×10^{-4}	20	3.0×10^{-4}		
		9	2.0×10^{-4}	21	1.0×10^{-4}		
		10	9.0×10^{-5}	22	4.0×10^{-5}		
		11	2.0×10^{-4}	23	4.0×10^{-5}		
		12	7.0×10^{-5}	24	5.0×10^{-5}		

	Number of model evaluations	i	S_i (i=1, 2, 3)	i	S_i (i=4, 5)	$S\,(c)=\sum_{i=1}^{3} S_i$	$S\,(\varphi)=\sum_{i=4}^{5} S_i$
With the reduced number of random variables N_e=5	150	1	0.510	4	0.076	0.721	0.279
		2	0.200	5	0.190		
		3	0.010				

Table IV.6. Sobol indices as computed from the classical SPCE approach (with N_T=24) and the present SPCE/GSA procedure (with N_e=5).

IV.3.2 Probabilistic results of a ponderable soil for the two cases of 2D and 3D random fields

The aim of this section is to present the probabilistic numerical results in the case of a ponderable soil mass. The objective is to compute the PDF of the ultimate bearing capacity of a shallow strip foundation resting on a 2D and a 3D spatially varying (c, φ) soil where the soil shear strength parameters are modeled as two anisotropic cross-correlated non-Gaussian random fields. It should be emphasized here that the case of a ponderable soil significantly increases the computation time with respect to the case of a weightless soil.

As shown in Figure IV.3, the adopted soil domain considered in the analysis is 13m wide by 5m deep. The footing breadth is equal to 1m. For the boundary conditions, the horizontal movement on the vertical boundaries of the grid is restrained, while the base of the grid is not allowed to move in both the horizontal and the vertical directions.

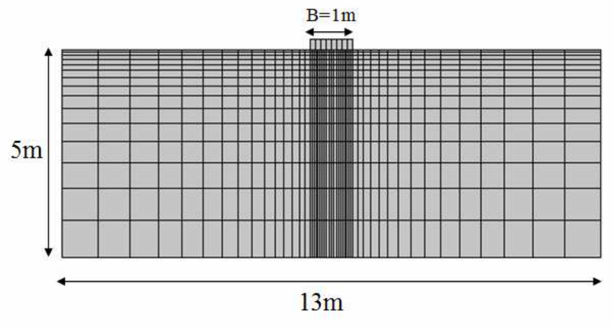

Figure IV.3. Adopted soil domain and the corresponding deterministic mesh

In this section, one first presents an extensive parametric probabilistic study using the SPCE/GSA procedure to investigate the effect of the different probabilistic governing parameters of the two random fields (autocorrelation distances, coefficients of variation) and the correlation between both fields on the PDF of the ultimate bearing capacity of a strip foundation resting on a ponderable soil with 2D spatially varying shear strength parameters. This is followed by a presentation of the probabilistic results obtained in the case of a ponderable soil and 3D spatially varying shear strength parameters. It should be noticed here that when investigating the effect of 3D random fields, only the reference case [i.e. a_h=a_x=a_y=10m, a_v=a_z=1m and $r(c, \varphi)$=-0.5] was considered. The aim behind considering a ponderable soil with 3D random fields is to introduce an additional computational cost due to the generation of 3D random fields. Another additional cost could be introduced by considering the case of a rectangular or a circular footing with 3D spatially varying shear strength parameters.

In both cases of 2D and 3D random fields, c and φ are discretized into a finite number of random variables. As was shown in the previous two chapters, this number is small for the very large values of the autocorrelation distances and significantly increases for the small values of the autocorrelation distances.

Table IV.7 provides the total number N_T of random variables needed to discretize the two random fields c and φ within a prescribed variance of the error of 10% for both the 2D and 3D random fields. This table also provides the number N_e of the retained random variables as obtained using the SPCE/GSA procedure. One can observe an important reduction in the dimensionality of the treated problem with the use of the proposed SPCE/GSA procedure. For instance, the reduced number N_e of random variables is equal to 21 when a_x=a_y=0.25m. This number is to be compared to the total number N_T=1760 which shows once again that the ultimate bearing capacity is not sensitive to the very small fluctuations of the two random fields.

			N_T: Total number of random variables used to discretize the two random fields (c, φ)	N_e: Number of most influent random variables used to construct the SPCE when t_a =2%xS_1
2D random fields (c, φ)	Isotropic case with varying values of a_x=a_y (m)	0.25	1760	21
		0.5	460	21
		1	120	20
		1.5	70	20
		2	50	20
		3	24	12
		5	20	8
		10	10	6
	Anisotropic case with varying values of a_y (m) when a_x=10m	0.15	140	22
		0.25	84	21
		0.5	44	13
		0.8	30	9
		1	24	5
		2	24	5
		5	24	5
		8	24	5
	Anisotropic case with varying values of a_x (m) when a_y=1m	0.5	200	22
		1	120	20
		2	88	20
		4	48	16
		20	24	12
		30	24	8
		50	24	8
3D random fields (c, φ)	Reference case [a_h=a_x=a_y=10m, a_v=a_z=1m]		50	14

Table IV.7. Number of random variables used to discretize the two random fields c and φ for both cases of 2D and 3D random fields

In the following two sections, the extensive parametric study concerning the case of the 2D spatially varying soil is first presented. This is followed by a presentation of the probabilistic results when investigating the 3D spatially varying soil.

IV.3.2.1 Probabilistic parametric study in the case of a ponderable soil and 2D random fields

In the following subsections, the effect of the different statistical governing parameters of the two random fields (autocorrelation distances, coefficients of variation) and the correlation between these random fields on the PDF of the ultimate bearing capacity was investigated in the particular case of 2D random fields. Furthermore, a global sensitivity analysis based on Sobol indices was also performed.

<u>Effect of the autocorrelation distances</u>

Figure IV.4 shows the PDFs of the ultimate bearing capacity for different values of the isotropic autocorrelation distance $a_x=a_y$ and Figures IV.5 and IV.6 show the PDFs of the ultimate bearing capacity for different configurations with anisotropic autocorrelation distances. Tables IV.8, IV.9 and IV.10 present the first two statistical moments of all these PDFs together with those corresponding to great values of the autocorrelation distances.

Figures IV.4, IV.5 and IV.6 and Tables IV.8, IV.9 and IV.10 show that the variability of the ultimate bearing capacity decreases when the autocorrelation distance $a_x=a_y$, a_y or a_x decreases. Similar observation was provided in chapter II in the case of a weightless soil mass. The variability of the ultimate bearing capacity decreases with the increase in the soil heterogeneity since the zone involved by the possible failure mechanism will have (for the very small values of the autocorrelation distances) somewhat uniform values of the shear strength parameters over this zone because of the large number of high and small values of the shear strength parameters. This leads to close values of the ultimate bearing capacity from simulation to another one and thus to a smaller variability in this bearing capacity.

Figure IV.7 and Table IV.8 show that the probabilistic mean value of the ultimate bearing capacity presents a minimum when the isotropic autocorrelation distance $a_x=a_y$ is nearly equal to the footing breadth B (i.e. in our case when $a_x=a_y$=1m). Notice that the minimal probabilistic mean was also observed in chapter II in the ULS analysis when isotropic random fields were studied. Thus, the same explanation which had done before remains valid herein.

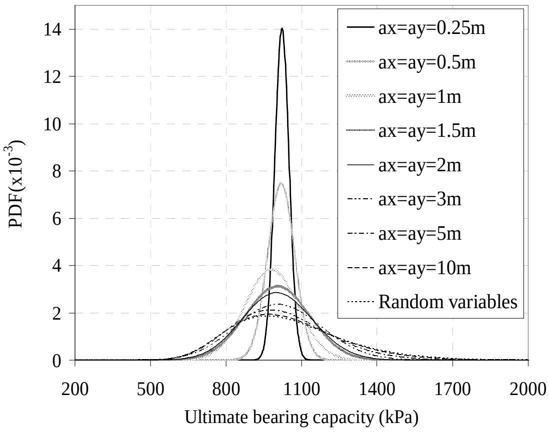

Figure IV.4. Influence of the isotropic autocorrelation distance a_x=a_y on the PDF of the ultimate bearing capacity in the case where *r(c, φ)*=-0.5

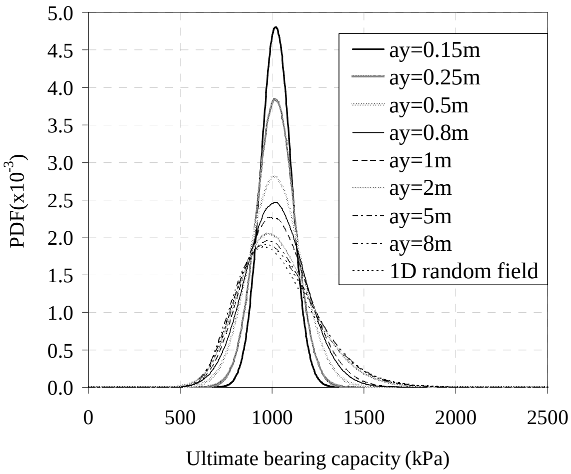

Figure IV.5. Influence of the vertical autocorrelation distance a_y on the PDF of the ultimate bearing capacity in the case where *r(c, φ)*=-0.5 and a_x=10m

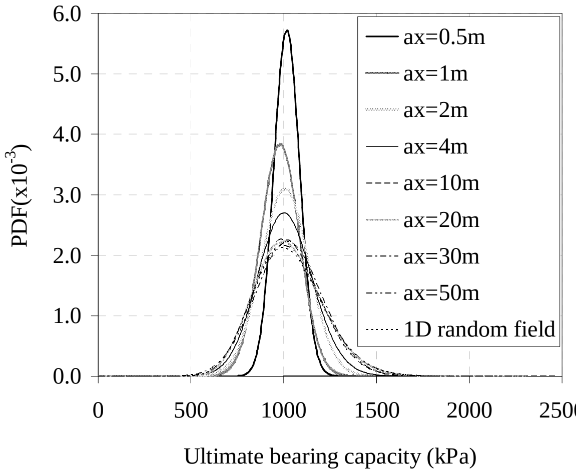

Figure IV.6. Influence of the horizontal autocorrelation distance a_x on the PDF of the ultimate bearing capacity in the case where *r(c, φ)*=-0.5 and a_y=1m

As for the anisotropic soil, Figures IV.8 and IV.9 and Tables IV.9 and IV.10 show that the probabilistic mean value of the ultimate bearing capacity presents a minimum at a certain value of a_y (or a_x) for a prescribed value of a_x (or a_y). Thus, one may expect that there is a given soil configuration (corresponding to given values of a_x and a_y) for which one obtains an absolute minimal mean value for the ultimate bearing capacity q_{ult}. It should be mentioned here that the increase in the autocorrelation distance a_y in Figure IV.8 leads to a soil configuration that varies from a horizontal to a vertical multilayer with a succession of layers with high and small values of the shear strength parameters. This situation is reversed in Figure IV.9 (in which a_x increases) where the soil configuration varies from a vertical to a horizontal multilayer. The ultimate bearing capacity was found to be the smallest for an intermediate value of the autocorrelation distance a_y (or a_x) for a prescribed value of a_x (or a_y) where the failure mechanism can easily develop in the soil mass.

$a_x = a_y (m)$	$\mu_{q_{ult}}$ (kPa)	$\sigma_{q_{ult}}$ (kPa)	$COV_{q_{ult}}$ (%)
0.25	1022.3	28.5	2.8
0.5	1019.3	53.2	5.2
1	980.2	103.3	10.5
1.5	1001.4	127.0	12.6
2	1005.1	136.9	13.6
3	1012.7	169.2	16.7
5	1021.7	195.1	19.1
10	1040.0	216.9	20.9
50	1051.5	230.1	21.9
100	1052.0	230.9	21.9
Random variables	1052.2	230.9	21.9

Table IV.8. Effect of the isotropic autocorrelation distance a_x=a_y on the statistical moments (μ, σ) of the ultimate bearing capacity

a_y (m)	$\mu_{q_{ult}}$ (kPa)	$\sigma_{q_{ult}}$ (kPa)	$COV_{q_{ult}}$ (%)
0.15	1021.5	82.8	8.1
0.25	1018.5	103.7	10.2
0.5	1018.0	133.1	13.1
0.8	1020.4	161.8	15.8
1	1022.7	172.0	16.8
2	1032.9	203.2	19.7
5	1038.6	212.2	20.4
8	1039.4	216.3	20.8
50	1041.0	217.5	20.9
1D random field	1041.1	217.6	20.9

Table IV.9. Effect of the vertical autocorrelation distance a_y on the statistical moments (μ, σ) of the ultimate bearing capacity when a_x=10m

$a_x (m)$	$\mu_{q_{ult}}$ (kPa)	$\sigma_{q_{ult}}$ (kPa)	$COV_{q_{ult}}$ (%)
0.5	1017.0	69.7	6.7
1	980.2	103.3	10.5
2	1004.0	121.1	12.1
4	1010.4	150.4	14.9
10	1022.7	172.0	16.8
20	1029.2	179.9	17.5
30	1030.4	184.2	17.9
50	1030.5	185.5	18.0
1D random field	1030.6	185.7	18.0

Table IV.10. Effect of the horizontal autocorrelation distance a_x on the statistical moments (μ, σ) of the ultimate bearing capacity when a_y=1m

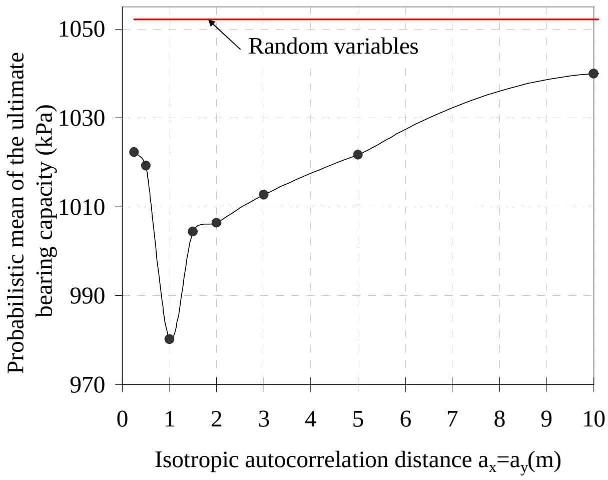

Figure IV.7. Influence of the isotropic autocorrelation distance a_x=a_y on the probabilistic mean of the ultimate bearing capacity in the case where *r(c, φ)*=-0.5.

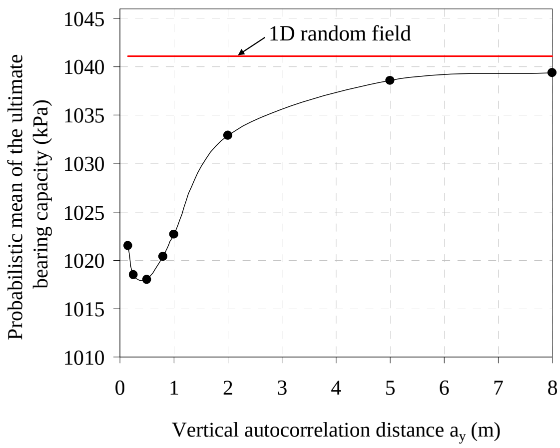

Figure IV.8. Influence of the vertical autocorrelation distance a_y on the probabilistic mean value of the ultimate bearing capacity in the case where a_x=10m and *r(c, φ)*=-0.5

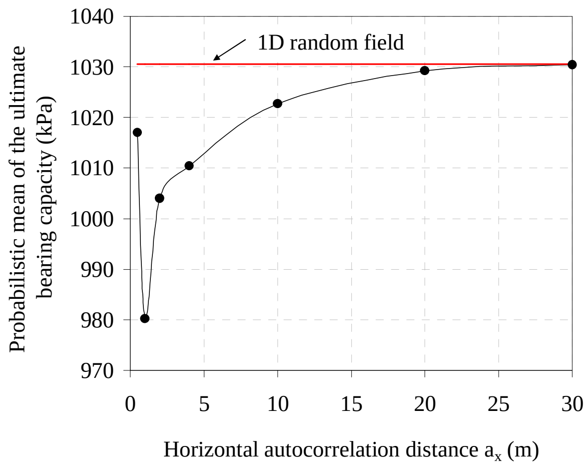

Figure IV.9. Influence of the horizontal autocorrelation distance a_x on the probabilistic mean value of the ultimate bearing capacity in the case where a_y =1m and *r(c, φ)*=-0.5

Finally, Tables IV.11, IV.12, and IV.13 show the effect of the autocorrelation distances a_x=a_y, a_y and a_x on the Sobol indices *S(c)* and *S(φ)* of the two random fields *c* and *φ*. These tables show that both indices are quasi-constant with the increase of a_x=a_y, a_y or a_x. This is because we increase the autocorrelation distances in both fields by the same amount. These tables also show that the random fields of *c* and *φ* have almost the same weight in the variability of the ultimate bearing capacity (*S(c)*=0.48 and *S(φ)*=0.52). These results are to be compared to those obtained by Al-Bittar and Soubra (2012a) in the case of a weightless soil where *S(c)*=0.71 and *S(φ)*=0.29. The large value of *S(c)* in the case of a weightless soil is due to the absence of the term responsible of the soil weight in the bearing capacity equation.

$a_x = a_y (m)$	$S(c)$	$S(\varphi)$
0.25	0.48	0.52
0.5	0.49	0.51
1	0.48	0.52
1.5	0.48	0.52
2	0.48	0.52
3	0.49	0.51
5	0.47	0.53
10	0.48	0.52
50	0.49	0.51
100	0.49	0.51
Random variables	0.49	0.51

Table IV.11. Effect of the isotropic autocorrelation distance a_x=a_y on the Sobol indices of the two random fields *c* and *φ*

a_y (m)	$S(c)$	$S(\varphi)$
0.15	0.48	0.52
0.25	0.48	0.52
0.5	0.49	0.51
0.8	0.48	0.52
1	0.49	0.51
2	0.47	0.53
5	0.47	0.53
8	0.48	0.52
50	0.48	0.52
1D random field	0.49	0.51

Table IV.12. Effect of the vertical autocorrelation distance a_y on the Sobol indices of the two random fields *c* and *φ* when a_x=10m

$a_x (m)$	$S(c)$	$S(\varphi)$
0.5	0.48	0.52
1	0.48	0.52
2	0.48	0.52
4	0.47	0.53
10	0.49	0.51
20	0.48	0.52
30	0.48	0.52
50	0.48	0.52
1D random field	0.49	0.51

Table IV.13. Effect of the horizontal autocorrelation distance a_x on the Sobol indices of the two random fields *c* and *φ* when a_y=1m

Effect of the cross-correlation coefficient

Figure IV.10 presents the PDFs of the ultimate bearing capacity for negatively cross-correlated $r(c, \varphi)$=-0.5 and non-correlated $r(c, \varphi)$=0 random fields when a_x=10m and a_y=1m, and Table IV.14 presents the two corresponding statistical moments (μ, σ).

Figure IV.10 and Table IV.14 show that the variability of the ultimate bearing capacity decreases when considering a negative correlation between the two random fields. This is because the increase of one parameter value implies a decrease in the other parameter. Thus, the total shear strength slightly varies. This leads to a reduced variation in the ultimate bearing capacity. It should be mentioned that the probabilistic mean value of the ultimate bearing capacity slightly increases when a negative correlation between the two random fields exists. Finally, the Sobol indices presented in Table IV.15 show that the negative correlation slightly increases the weight of the soil cohesion in the variability of the ultimate bearing capacity.

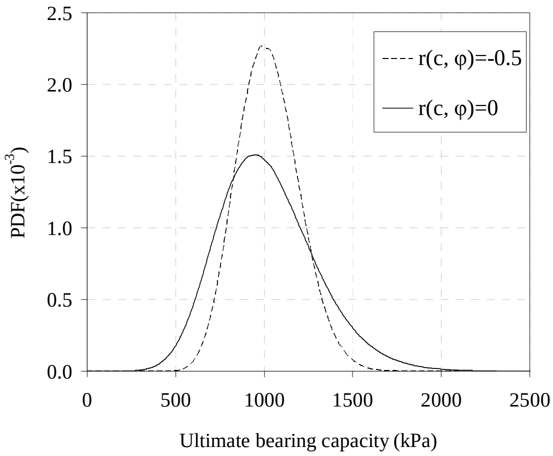

Figure IV.10. Influence of the cross-correlation coefficient r(c, φ) on the PDF of the ultimate bearing capacity in the case where a_x=10m and a_y=1m

$r(c,\varphi)$	$\mu_{q_{ult}}$ (kPa)	$\sigma_{q_{ult}}$ (kPa)	$COV_{q_{ult}}$ (%)
-0.5	1022.7	172.1	16.8
0	1019.7	275.1	27.0

Table IV.14. Effect of the cross-correlation coefficient *r(c, φ)* between the random fields of *c* and *φ* on the statistical moments (*μ*, *σ*) of the ultimate bearing capacity when a_x=10m and a_y=1m

$r(c,\varphi)$	$S(c)$	$S(\varphi)$
-0.5	0.49	0.51
0	0.45	0.55

Table IV.15. Effect of the coefficient of correlation on the Sobol indices of the two random fields *c* and *φ* when a_x=10m and a_y=1m

Effect of the coefficients of variation of the random fields

Tables IV.16 and IV.17 present for five different configurations of the coefficients of variation of the random fields, the two statistical moments (μ, σ) of the ultimate bearing capacity and the Sobol indices of the two fields (c, φ).

Table IV.16 shows that the variability of the ultimate bearing capacity increases (as expected) when the coefficient of variation of either random field increases. From Table IV.17, one can see that an increase in the coefficient of variation of a soil parameter increases its Sobol index and thus its weight in the variability of the ultimate bearing capacity. This automatically reduces the contribution of the other uncertain parameter.

		$\mu_{q_{ult}}$ (kPa)	$\sigma_{q_{ult}}$ (kPa)	$COV_{q_{ult}}$ (%)
$COVc = 50\%$	$COV\varphi = 10\%$	970.8	241.7	24.9
$COVc = 37.5\%$	$COV\varphi = 10\%$	998.5	205.9	20.6
$COVc = 25\%$	$COV\varphi = 10\%$	1022.7	172.0	16.8
$COVc = 25\%$	$COV\varphi = 15\%$	1036.0	224.5	21.7
$COVc = 25\%$	$COV\varphi = 20\%$	1053.7	284.2	27.0

Table IV.16. Effect of the coefficients of variation (*COVc*, *COVφ*) of the random fields *c* and *φ* on the statistical moments (*μ*, *σ*) of the ultimate bearing capacity when a_x=10m, a_y=1m and *r(c, φ)*= -0.5

		$S(c)$	$S(\varphi)$
$COVc = 50\%$	$COV\varphi = 10\%$	0.79	0.21
$COVc = 37.5\%$	$COV\varphi = 10\%$	0.68	0.32
$COVc = 25\%$	$COV\varphi = 10\%$	0.49	0.51
$COVc = 25\%$	$COV\varphi = 15\%$	0.28	0.72
$COVc = 25\%$	$COV\varphi = 20\%$	0.17	0.83

Table IV.17. Effect of the coefficients of variation (*COVc*, *COVφ*) of the random fields *c* and *φ* on the Sobol indices of the two random fields *c* and *φ* when a_x=10m, a_y=1m and *r(c, φ)*= -0.5

IV.3.2.2 Probabilistic results in the case of a ponderable soil and 3D random fields

In this section, one presents the probabilistic results obtained in the case of a ponderable soil and 3D random fields. Only the reference case [i.e. a_h=10m, a_v=1m and *r(c, φ)*=-0.5] was considered in the analysis. This is because the effect of introducing the spatial variability in the third direction was extensively investigated in chapter III. The only reason for which the three-dimensional case was considered herein is to present the capability of the SPCE/GSA procedure in solving the computationally-expensive problems which were impossible to be considered before.

The PDF obtained when 3D random fields were considered is compared to that obtained with the use of 2D random fields in Figure IV.11. From this figure, one can see that the variability of the ultimate bearing capacity is slightly smaller when 3D random fields were considered. Table IV.18 confirms this observation. Similar results were obtained in the previous chapter when considering a purely cohesive soil. Finally, the Sobol indices presented in Table IV.19 show that the random fields of *c* and *φ* have almost the same weight in the variability of the ultimate bearing capacity for both 2D and 3D random fields cases.

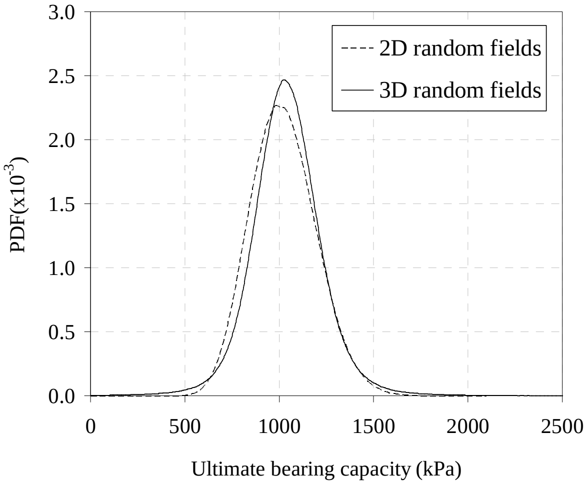

Figure IV.11. PDFs of the ultimate bearing capacity for both the 2D and the 3D random fields for the reference case where a_h=10m, a_v=1m and $r(c, \varphi)$=-0.5

	$\mu_{q_{ult}}$ (kPa)	$\sigma_{q_{ult}}$ (kPa)	$COV_{q_{ult}}$ (%)
2D random fields	1022.7	172.1	16.8
3D random fields	1020.9	167.0	16.3

Table IV.18. Statistical moments (μ, σ) of the ultimate bearing capacity using both 2D and 3D random fields for the reference case where a_h=10m, a_v=1m and $r(c, \varphi)$=-0.5

	$S(c)$	$S(\varphi)$
2D random fields	0.49	0.51
3D random fields	0.47	0.53

Table IV.19. Sobol indices of the two random fields c and φ in both the 2D and the 3D cases for the reference case where a_h=10m, a_v=1m and $r(c, \varphi)$=-0.5

IV.4 CONCLUSIONS

An efficient combined use of the SPCE methodology and the global sensitivity analysis (GSA) has been proposed in this chapter. The aim is to reduce the cost of the probabilistic analysis of high-dimensional stochastic problems making use of computationally-expensive deterministic models. This methodology was firstly validated in this work using a relatively non-expensive deterministic model (case of a strip footing resting on a weightless soil mass with 2D random fields). Then it was applied to two computationally-expensive deterministic models (case of a strip footing resting on a ponderable soil mass with 2D and 3D random fields).

The validation consists in comparing both the classical SPCE method that uses the total number of random variables and the proposed combination between the SPCE and the GSA that makes use of a reduced number of random variables. Satisfactory results were obtained using a smaller number of model evaluations with the proposed methodology. The first two statistical moments and the Sobol indices show good agreement between the two methods. On the other hand, the third and fourth statistical moments need more model evaluations in order to converge to their reference values obtained using the classical SPCE approach.

The application of the proposed methodology to two expensive deterministic models that involve the computation of the PDF of the ultimate bearing capacity in the cases of a ponderable soil with 2D and 3D random fields (which were impossible to be considered before) have shown that (i) the variability of the ultimate bearing capacity increases with the increase in the coefficients of variation of the random fields; (ii) the cohesion and the friction angle random fields have almost the same weight in the variability of the ultimate bearing; (iii) the increase in the coefficient of variation of a soil parameter (c or φ) increases its Sobol index and thus its weight in the variability of the system response and decreases the weight of the other parameter; (iv) the negative correlation between the soil shear strength parameters decreases the response variability; (v) the decrease in the autocorrelation distances (a_x or a_y or a_x=a_y), leads to a less spread out (PDF) of the ultimate bearing capacity; (vi) the probabilistic mean value of the ultimate bearing capacity presents a minimum which was obtained in the isotropic case when the autocorrelation distance is nearly equal to the footing breadth B; while for the anisotropic case, this minimum was obtained (for prescribed footing and soil characteristics) at a given value of the ratio between the horizontal and the vertical autocorrelation distances; and finally, (vii) a comparison between the results obtained using 2D and 3D random fields have shown that the variability of the ultimate bearing capacity is smaller when 3D random fields were considered. As a future work, one may consider the case of a rectangular or a circular footing resting on a ponderable soil with 3D spatially varying shear strength parameters.

CHAPTER V. EFFECT OF THE SOIL SPATIAL VARIABILITY AND/OR THE TIME VARIABILITY OF THE SEISMIC LOADING ON THE DYNAMIC RESPONSES OF GEOTECHNICAL STRUCTURES

V.1 INTRODUCTION

This chapter focuses on the dynamic responses induced by an earthquake Ground-Motion (GM) taking into account the soil spatial variability and/or the time variability of the seismic loading.

Contrarily to the case of the static loading considered in the previous chapters where only the soil and the footing were considered in the analysis (because the system response was mainly the ultimate bearing capacity of the footing), the case of a seismic loading should consider the soil, the footing and the superstructure since the seismic energy will be dissipated in both the soil and the superstructure [Sadek (2012)]. Thus, a proper modeling of the entire soil-footing-structure system including the interaction between the soil and the footing should be considered in order to lead to reliable solutions.

The response of a soil-footing-structure system subjected to seismic loading has been extensively investigated in literature using deterministic approaches where average values of the soil properties (shear modulus, angle of internal friction, cohesion, etc.) and deterministic recorded acceleration time-histories were used [Chen and Sawada (1983), Leshchinsky and San (1994), You and Michalowski (1999), Michalowski (2002), Loukidis et al. (2003), Sadek and Shahrour (2004) and Grange et al. (2009a, 2009b) among others].

It should be mentioned here that when dealing with seismic loads, an aleatory uncertainty related to the earthquake Ground-Motion (GM) appears in addition to the soil spatial variability and the variability of the superstructure. This additional source of aleatory uncertainty is the time variability of the earthquake Ground-Motion (GM). Consequently, reliable responses of the superstructure cannot be predicted using a deterministic approach; a probabilistic technique seems to be necessary. The probabilistic techniques enable the rigourous propagation of the different uncertainties from the input parameters to the system responses.

In this chapter, the effect of the soil spatial variability and/or the time variability of the earthquake GM on the seismic responses of geotechnical structures is investigated. The variability of the superstructure was not considered in the analysis. Given the scarcity of studies involving the probabilistic seismic responses, a free field soil medium subjected to a seismic loading was firstly considered. The aim is to investigate the effect of the soil spatial variability and/or the time variability of the earthquake GM using a simple model. Then, a soil-structure interaction SSI problem was investigated in the second part of this chapter.

It should be emphasized here that few authors have worked on the analysis of the seismic responses using probabilistic approaches [Koutsourelakis et al. (2002), Wang and Hao (2002), Nour et al. (2003), Popescu et al. (2005, 2006) and Lopez-Caballero and Modaressi-Farahmand-Rasavi (2010)]. In all these works, the classical Monte Carlo Simulation (MCS) methodology with a very small number of realizations was used to determine the probability density function (PDF) of the seismic response [e.g. only 50 simulations were used in Koutsourelakis et al (2002)]. This is because of the significant computation time required per simulation when using finite element/finite difference dynamic models.

As for the probabilistic methods used in this chapter, two methods were employed. The first one is the classical Monte Carlo Simulation (MCS) methodology and the second one is the Sparse Polynomial Chaos Expansion (SPCE) methodology which consists in substituting the system response by a meta-model.

This chapter is organized as follows: First, the case of an elastic free field soil mass is investigated. This is followed by the SSI problem. The chapter ends by a conclusion of the main findings.

V.2 CASE OF AN ELASTIC FREE FIELD SOIL MASS

In this section, the effect of the soil spatial variability and/or the time variability of the earthquake GM was firstly investigated through the study of an elastic free field soil mass.

The soil shear modulus *G* was modeled as a non-Gaussian random field and the earthquake GM was modeled as a random process. The EOLE methodology presented in chapter I was used to discretize the shear modulus random field. As for the earthquake GM, the method proposed by Rezaeian and Der Kiureghian (2010) which consists in fitting a parameterized stochastic model to the real recorded earthquake GM was utilized. The deterministic model was based on numerical simulations using the dynamic option of the finite difference code FLAC^{3D}. The dynamic response considered in the analysis was the amplification of the maximum acceleration at the soil surface.

The following subsections are organized as follows: one first presents the deterministic numerical modeling of the dynamic problem and the corresponding results. Then, the probabilistic analyses and the corresponding probabilistic results are presented and discussed.

V.2.1 Numerical modeling

The deterministic dynamic model is based on numerical simulations using the finite difference software FLAC^{3D}. Two types of modeling were considered in this thesis (see Figure V.1). The first one considers a two-dimensional soil mass of 30m width and 24m depth. As for the second model (called hereafter 'column' model), it considers a soil column of 1m width and 24m depth. The objective of these two types of modeling is to verify that the 'column' model is sufficient to simulate the propagation of the seismic waves in the soil mass and to deduce the distribution of the peak accelerations as a function of depth. Thus, replacing the 2D model with the 'column' model may significantly reduce the probabilistic computational time.

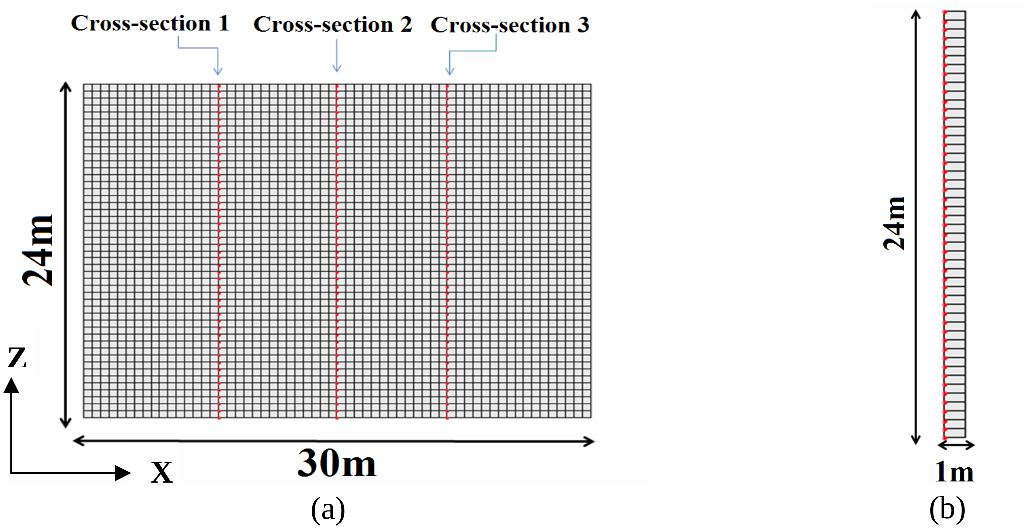

Figure V.1. The two considered numerical models (a) 2D model and (b) 'column' model

The numerical modeling of a mechanical problem in the presence of dynamic loading requires the definition of (i) the soil domain and the corresponding mesh, (ii) the soil constitutive model, (iii) the boundary conditions, (iv) the mechanical damping and (v) the used dynamic (seismic) signal. These parameters are presented in the following subsections.

V.2.1.1 Definition of the soil domain and the corresponding mesh

The first step in a numerical modeling is the definition the soil domain and the corresponding mesh. In the finite difference dynamic analysis by FLAC^{3D}, numerical distortions may occur during the propagation of the seismic waves if the elements size of the mesh is not convenient.

Thus, the size Δl of an element of the mesh should respect the following condition [Itasca (2000)]:

$$\Delta l \leq \frac{V_s}{10 * f_{\max}} \tag{V.1}$$

where V_s is the shear wave velocity, and f_{max} is the maximum frequency of the incident seismic signal [Kuhlemeyer and Lysmer, (1973)]. The shear wave velocity V_s in Equation (V.1) can be calculated using the values of the soil shear modulus G and the soil density ρ as follows:

$$V_s = \sqrt{\frac{G}{\rho}} \tag{V.2}$$

The mesh used in this study respects the condition given by Equation (V.1) and is presented in Figure V.1.

V.2.1.2 Definition of the soil constitutive model

FLAC^{3D} offers a variety of soil constitutive models. The most used ones in dynamic analysis are the elastic and the elasto-plastic models (perfect, softening or hardening). Even though an elasto-plastic model would be more convenient to model the soil behavior especially for the cases of medium and high earthquake GMs, an elastic model (which is characterized by reversible deformations) was used in this work. The aim is to investigate the effect of the soil spatial variability and/or the time variability of the earthquake GM using a simple model. This model is defined by two parameters which are (i) the shear modulus G, and (ii) the bulk modulus K. Other constitutive models which may take into account the nonlinearity of the soil will be employed in future works.

V.2.1.3 Definition of the boundary conditions

In dynamic analysis, assuming a null horizontal displacement on the two vertical boundaries of the soil domain as is the case in the static analysis may cause reflections of the seismic waves during their propagation in the model. To overcome such problem, FLAC^{3D} offers the option of applying absorbing boundary conditions of type "quiet Boundaries" or "free field" [Itasca, (2000)]. These boundary conditions absorb the energy of the wave approaching these limits which allows avoiding the reflection of these waves. In this thesis, the boundary conditions applied to the lateral vertical boundaries are of type "free field". This type of boundary conditions is suitable for vertical surfaces while the boundary conditions of type "quiet Boundaries" are generally convenient in the case of horizontal surfaces.

V.2.1.4 Definition of the mechanical damping

In the natural dynamic systems, the internal friction may lead to partial dissipation of the energy of vibration. The software FLAC^{3D} provides a damping of type "Rayleigh damping" (among other types of damping) which is based on two parameters: (i) the natural frequency of the system and (ii) the damping ratio (defined as a percentage of the critical damping). This type of damping is used in this chapter. The damping ratio used in the dynamic models presented in this work is equal to 5% of the critical damping [Bourdeau (2005)]. Notice that in most geological materials, the natural damping ratio is in the range of 2 to 5% of the critical damping.

V.2.1.5 Input seismic signal

The input seismic signal used in this work is the synthetic signal of Nice for which the corresponding accelerogram is presented in Figure V.2(a). This signal is used because it is representative of the French design spectrum [Grange (2008)]. It has a maximum acceleration equal to 0.33g. Its corresponding Fourier amplitude spectrum is shown in Figure V.2(b). It should be mentioned here that the use of a different seismic signal may lead to different results.

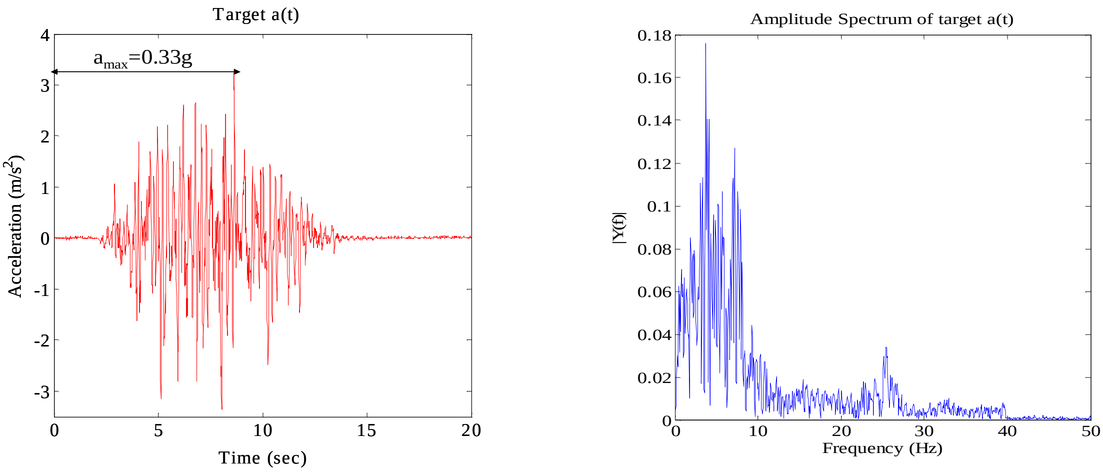

(a) (b)

Figure V.2. (a) Accelerogram of the synthetic signal of Nice and (b) the corresponding Fourier amplitude spectrum

V.2.2 Deterministic results

V.2.2.1 Validation of the 'column' model

The aim of this section is to check the validity of the 'column' model for its use in the probabilistic analyses. The main reason for which it is desirable to use the 'column' model instead of a two-dimensional (2D) soil domain is its reasonable computation time (40 min per simulation). This computation time enormously increases when a 2D model is used (24 hours per simulation). Remember that the 2D model involves a two-dimensional soil mass (see Figure V.1(a)) and the 'column' model involves a one-dimensional soil column (see Figure V.1(b)). For both models, the considered dynamic response was the distribution of the maximum acceleration along a vertical cross-section.

For the dynamic analyses, an elastic constitutive model was used to describe the soil behavior. The values of the shear modulus, bulk modulus and density of the soil were as follows: G=100MPa, K=250MPa, and ρ=1800 kg/m^3.

In order to avoid the numerical distortion that may occur during the propagation of the seismic waves in the model, the element size Δl must satisfy the condition given by Equation (V.1). Using Equation (V.2) which provides the value of the shear wave velocity as a function of the values of G and ρ, the shear wave velocity was found to be equal to 235.7m/s. From Figure V.2(b), one can see that the maximal frequency f_{max} is equal to 40Hz. Thus, the maximum element size must be less than or equal to 0.59m. In the studied model, the selected element size Δl was taken equal to 0.5m (see Figure V.1).

Concerning the boundary conditions, the lower horizontal boundary (along X) was subjected to the seismic load (i.e. the synthetic accelerogram of Nice). Boundary conditions of type "free field" were applied along the lateral vertical boundaries of the model [Bourdeau (2005)].

As for the mechanical damping, Rayleigh damping was used with a central frequency (natural frequency) f_c=2.5Hz and a damping ratio equal to 5% of the critical damping. Notice that the approximate formula of the natural frequency of a soil column given by Widmer (2003) (i.e. $f_o=V_s/4H$ where V_s is the shear wave velocity calculated using Equation (V.2) and H is the height of the soil column) was used to calculate the value of the central frequency f_c=2.5Hz. As for the damping ratio, the value of 5% used by Bourdeau (2005) was adopted in this thesis.

Figure V.3 shows the distribution of the maximum acceleration as a function of depth for the three cross-sections of the 2D soil mass and for the 1D soil column. This figure shows that the four distributions are superimposed, which makes valid the hypothesis of using a soil column instead of a 2D soil mass when performing the probabilistic analysis.

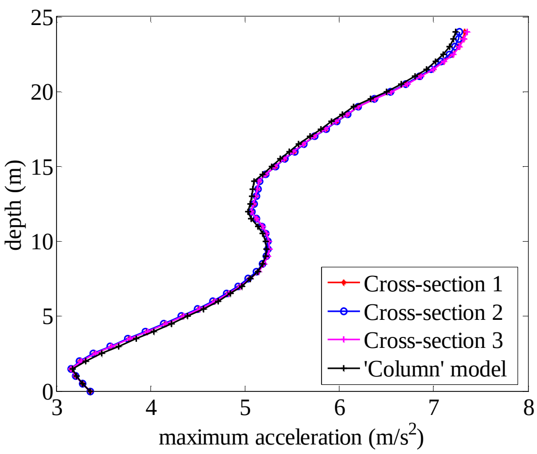

Figure V.3. Distribution of the maximum acceleration as a function of depth for the three cross-sections of the 2D model and for the 1D soil column

V.2.2.2 Distribution of the maximum acceleration for different values of the shear modulus G

The aim of this section is to study the effect of the variation of the shear modulus G on the dynamic response (distribution of the maximum acceleration A_{max}) using the 'column' model. For this purpose, a wide range of values of G was considered. The illustrative value of the bulk modulus K was taken equal to 250*MPa*. In most soils, the shear wave velocity V_s varies between 200*m/s* and 900*m/s* [Nour et al. (2003)]. In this thesis, this range of values was considered with a step of 50*m/s*. The corresponding values of the shear modulus G were calculated using Equation (V.2).

Figure V.4 shows the distribution of A_{max} for five values of the shear modulus G. This figure shows that for very low values of G, and very large values of G, the amplification (i.e. the ratio between the value of the maximum acceleration of the signal at a given depth and its maximum value at the base of the soil mass) is relatively small. For intermediate values of G, this amplification is more significant. For illustration, Figure V.5 shows the values of the maximum acceleration at the top of the soil column as a function of the values of the shear modulus G. From this figure, one can notice that large amplifications were obtained for the values of G between 162*MPa* and 1012.5*MPa*. This amplification decreases outside this range of values.

In order to explain the significant values of the amplifications, one should refer to the Fourier amplitude spectrum of the input seismic signal shown in Figure V.2(b). From this figure, one can see that the predominant frequency band is between 3*Hz* and 9*Hz*. By using the approximate formula of the natural frequency of a soil column given by Widmer (2003) ($f_o=V_s/4H$ where V_s is the shear wave velocity and H is the height of the soil column), one may show that for the values of G comprised between 162*MPa* and 1012.5*MPa*, the band of predominant frequencies of the soil column coincides with the predominant frequency band of the input seismic signal. This coincidence leads to the so-called 'phenomenon of resonance' which induces the significant amplification.

Finally, the influence of the bulk modulus K on the maximum acceleration is presented in Figure V.6 by considering three values of K (100*MPa*, 250*MPa* and 600*MPa*). This figure presents the values of the maximum acceleration on the top of the soil column as a function of the shear modulus values G for the three values of the bulk modulus K. It clearly shows that the bulk modulus K has no influence on the maximum acceleration at the top of the soil column. This indicates that for a seismic loading, the soil does not exhibit volumetric strains. This is perfectly acceptable since the seismic signal is composed of compressional P waves (which dominate the first short period of the seismic signal) followed by shear S waves that dominate the strong shaking phase, which make them more influent in the seismic signal.

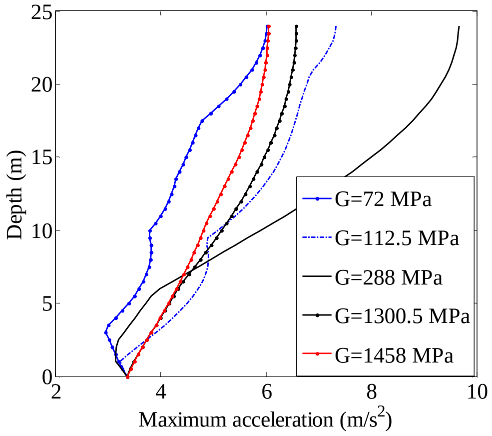

Figure V.4. Distribution of the maximum acceleration for different values of the shear modulus *G*

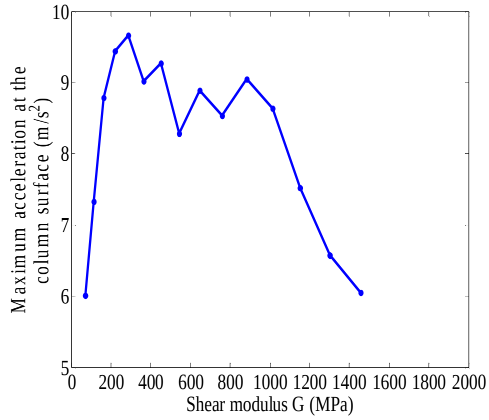

Figure V.5. Variation of the maximum acceleration at the top of the column as a function of the shear modulus *G*

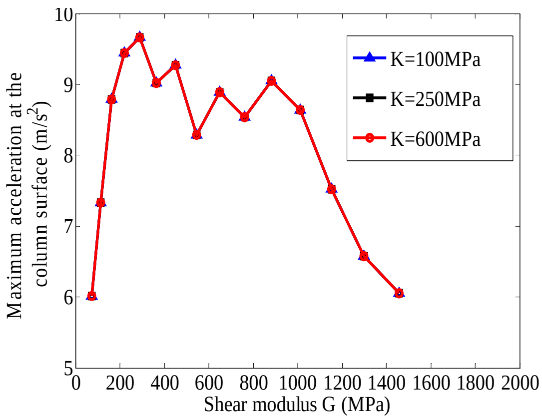

Figure V.6. Variation of the maximum acceleration at the top of the column as a function of the shear modulus *G* for three values of *K*

V.2.3 Probabilistic dynamic analysis

The aim of this section is to present the probabilistic dynamic analysis. It should be remembered here that the dynamic system response involves the maximum acceleration (A_{max}) at the top of the soil column. In this study, the effect of both the soil spatial variability and the time variability of the earthquake GM on the dynamic response were considered.

The soil shear modulus G was considered as a one-dimensional (1D) non-Gaussian random field varying in the vertical direction. It was described by a square exponential autocorrelation function and was assumed to be log-normally distributed. Two reference mean values of the shear modulus were considered. The first one is $\mu_{G_1} = 72MPa$ corresponding to a non resonant value (i.e. this value is located on the left hand part of the curve in Figure V.5) and the second one is $\mu_{G_2} = 288MPa$ corresponding to a resonant value. For both mean values ($\mu_{G_1} = 72MPa$ and $\mu_{G_2} = 288MPa$), a coefficient of variation equal to 30% was considered as the reference value. As for the vertical autocorrelation distance a_y, the adopted reference value was equal to 2m while the range of 0.5m-20m was considered when performing the parametric study. The computation time that was necessary for the generation of the random field increases when the autocorrelation distance decreases. Notice however that this time was relatively small in the case of the 1D random field for the range of autocorrelation distances considered in the analysis.

In order to simulate the stochastic synthetic earthquake GMs using the method given by Rezaeian and Der Kiureghian (2010), the synthetic signal of Nice (for which the corresponding accelerogram is presented in Figure V.2(a)) was used as a target accelerogram.

The deterministic model was based on numerical simulations using the dynamic option of the finite difference code FLAC^{3D}. It was presented and detailed in the previous section. It should be noted here that in dynamic analysis, the size of a given element in the mesh depends on both the autocorrelation distances of the soil properties and the wavelength λ associated with the highest frequency component f_{max} of the input seismic signal.

For the autocorrelation distances of the soil properties, Der Kiureghian and Ke (1988) have suggested that the length of the largest element in a given direction (horizontal or vertical) should not exceed 0.5 times the autocorrelation distance in that direction. As for the wavelength λ associated with the highest frequency component f_{max} of the input signal, Itasca (2000) has suggested that the element size should not exceed 1/10 to 1/8 this wavelength λ in order to avoid numerical distortion of the propagating waves (see Equation (V.1)). Figure V.2(b) shows that the value of the maximum frequency is f_{max}=40Hz. In order to respect the two mentioned criterions, two different deterministic meshes were considered in FLAC^{3D}. The first one was devoted to the case of moderate to great values of a_y and V_s where an element size of 0.5m was chosen to perform the dynamic analysis (i.e. when $V_s \geq 200m/s$ and $a_y \geq 1m$), and the second one for small values of a_y or V_s where the element size was adjusted in order to respect the previous two conditions.

The following subsections are organized as follows: First, a brief description of a step-by-step procedure used to generate the stochastic earthquake GM is presented. It is followed by a presentation of some realizations of this stochastic earthquake GM. Finally, one examines the effect of (i) the soil spatial variability considered alone with a deterministic earthquake GM, (ii) the time variability of the earthquake GM considered alone with a homogenous soil mass and (iii) both the soil spatial variability combined with the time variability of the earthquake GM.

V.2.3.1 Step-by-step procedure used to generate the stochastic earthquake GM

The different steps used to generate the stochastic earthquake GMs are summarized as follows:

(a) Introduce the target input seismic signal and the corresponding time step *Δt* and total duration *T*. In this work, the target input seismic signal is the synthetic Nice accelerogram presented in Figure V.2 which has a time step *Δt*=0.01*s* and a total duration *T*=20*s*.

(b) Determine the parameters $\alpha = (\alpha_1, \alpha_2, \alpha_3)$ of the time modulation function as follows:

First, calculate the three physically-based parameters $(\bar{I}_a, D_{5-95}, t_{mid})$ which describe the real recorded GM in the time domain. The first variable, $\bar{I}_a$ is calculated using Equation (C.1). The second variable D_{5-95} is the time interval between the instants at which 5% and 95% of $\bar{I}_a$ are reached respectively (cf. Figure C.1). Finally, the third variable t_{mid} is the time at which 45% of $\bar{I}_a$ is reached (cf. Figure C.1). Then, use these three physical parameters to deduce the values of the parameters $\alpha = (\alpha_1, \alpha_2, \alpha_3)$ of the time modulation function using Equations (C.2), (C.3) and (C.4). The values of the three physical parameters $(\bar{I}_a, D_{5-95}, t_{mid})$ and the corresponding values of the time modulation function parameters $\alpha = (\alpha_1, \alpha_2, \alpha_3)$ for the synthetic Nice accelerogram used in this thesis are presented in Table V.1.

The three physical parameters	$\bar{I}_a$=8.5$s.g$	$D_{5\text{-}95}$=6.78s	t_{mid}=4.728s
The time modulation function parameters	α_1=0.385	α_2=3.537	α_3=0.576

Table V.1. Values of the three physical parameters and the corresponding values of the time modulation function parameters for the synthetic Nice accelerogram

(c) Determine the filter IRF parameters $\lambda(\tau)=(\omega_f(\tau),\ \zeta_f(\tau))$ (with $\omega_f(\tau)=\omega_{mid}+\omega'(\tau-t_{mid})$ denoting the natural frequency and $\zeta_f(\tau)=\zeta_f$ denoting the damping ratio) as follows:

First, optimize the frequency parameters ω_{mid} and ω' as follows:

- Plot the cumulative count of zero-level up-crossings of the target earthquake GM (cf. Figure V.7(a)). The zero-level up-crossings are the number of times per unit time that the process crosses the level zero from below.
- Fit the obtained cumulative count of zero-level up-crossings by a second degree polynomial ($p=p_1x^2+p_2x+p_3$) (cf. Figure V.7(a)).
- Use the obtained second degree polynomial to deduce the frequency parameters ω_{mid} and ω' using Equation (C.7).

The fitted second order polynomial for the synthetic Nice accelerogram is presented in Figure V.7(a) and it is given by: $p=-0.05x^2+8.11x+36.96$. The corresponding frequency parameters are ω_{mid} =7.63Hz and ω'=-0.1.

Second, optimize the damping ratio ζ_f as follows:

- Plot the cumulative count of negative maxima (peaks) and positive minima (valleys) (cf. Figure V.7(b)) for the target earthquake GM.
- Generate filtered processes (Equation (I.25)) using the frequency parameters ω_{mid} and ω' (which were optimized at the previous step) with a series of constant damping ratio (i.e. $\zeta_f=0.1,\ 0.2,\ ...,\ 0.9$) and see for which value of the damping ratio the cumulative count of positive minima and negative maxima of the simulated and target motions fit the most.

- Compute the optimal value of the damping ratio ζ_f as follows: $\zeta_f = \zeta_p - e_p \left[\frac{(\zeta_p - \zeta_n)}{(e_p - e_n)} \right]$

  where ζ_p and ζ_n are the damping ratios that correspond to the smallest positive and negative errors respectively and e_p and e_n are the smallest positive and negative errors respectively. For the synthetic Nice accelerogram, Figure V.7(b) presents the target cumulative count of positive minima and negative maxima and the nine simulated filtered processes using the optimized values of frequency parameters ω_{mid} and $\omega^{'}$. The corresponding optimal value of the damping ratio is ζ_f =0.56.

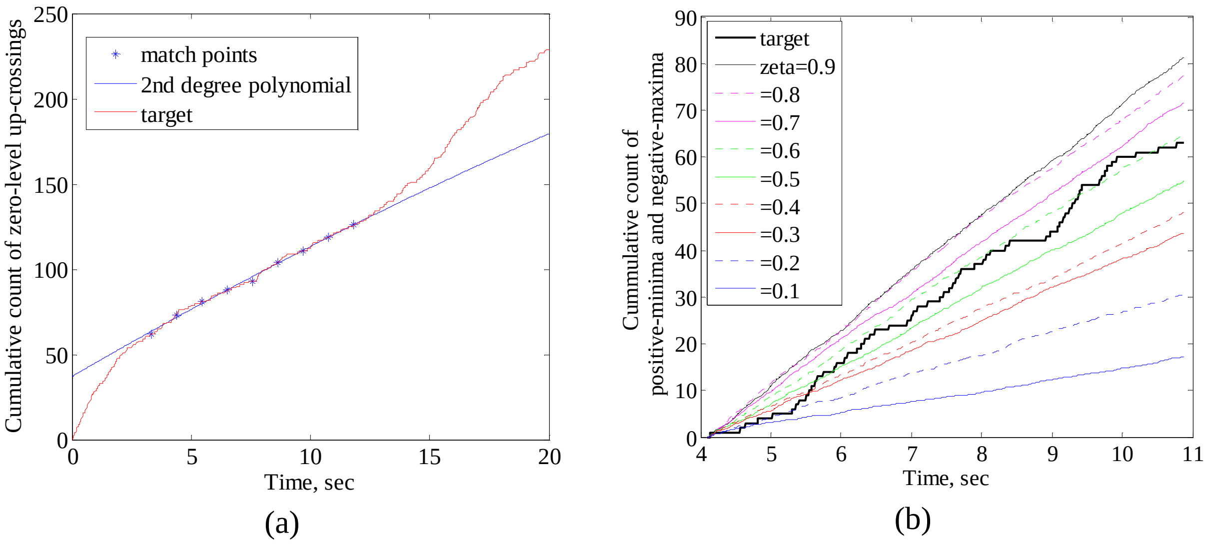

Figure V.7. Identification of filter parameters for the synthetic Nice accelerogram, (a) matching the cumulative number of zero level up-crossings (b) matching the cumulative count of negative maxima and positive minima

(d) Use Equation (I.25) to simulate a stochastic synthetic earthquake GM. A realization of the stochastic synthetic acceleration time history is obtained by simulating the vector of standard normal random variables u_i (i=1, …, $N = \frac{T}{\Delta t} + 1 = 2001$).

V.2.3.2 Realizations of the stochastic earthquake GM

The target acceleration time history used to generate stochastic earthquake GM is the Nice synthetic accelerogram shown in Figure V.2(a). This target acceleration time history was used to identify the parameters of the stochastic model given in Equation (I.25). These parameters were calculated in the previous section. Thus, realizations of the stochastic synthetic acceleration time histories can be performed by generating for each realisation a vector u_i (i=1, …, N) of standard normal random variables where $N = \frac{T}{\Delta t} + 1 = 2001$ and by applying Equation (I.25). Notice that the computation time that was necessary for the identification of the stochastic model parameters was negligible (about 2min). Also, the time that was needed to generate a realization of the stochastic synthetic acceleration time history was quasi-negligible (i.e. smaller than 1min for each realization).

Figure V.8 presents five realizations of the stochastic earthquake GM. This figure shows that the different simulated acceleration time histories have different maximum accelerations which will induce different dynamic system responses.

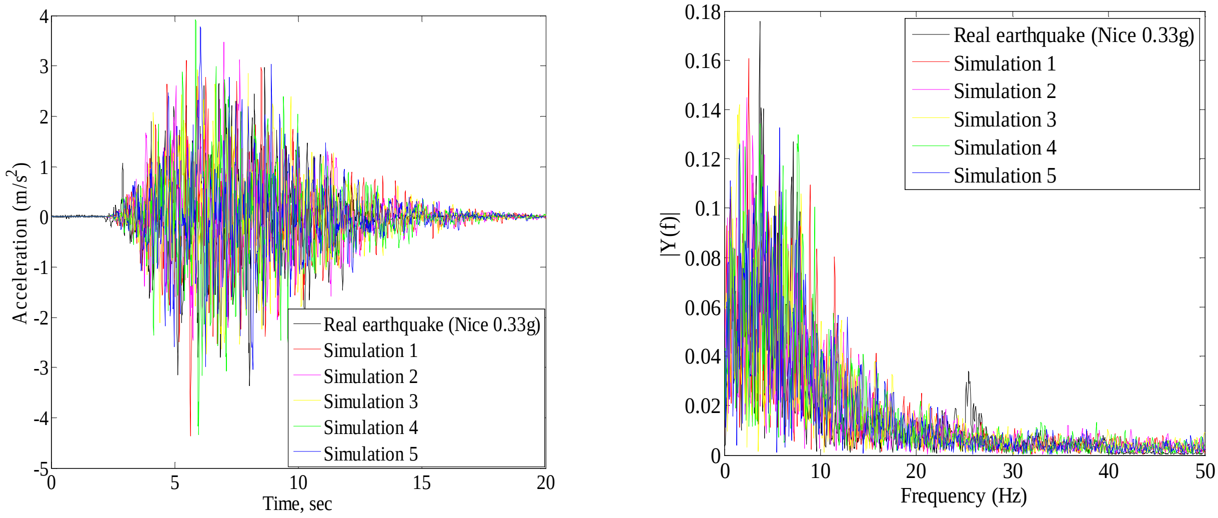

(a) (b)

Figure V.8. (a) Target and five simulated acceleration time-histories, and (b) their corresponding Fourier amplitude spectrum

V.2.4 Probabilistic results

The aim of this section is to study the effect of the soil spatial variability and/or the time variability of the earthquake GM on the statistical moments of A_{max} at the top of the soil column using both the MCS and the SPCE methodologies.

V.2.4.1 Monte-Carlo simulation results

In this section, the results obtained based on the Monte-Carlo simulation (MCS) methodology are presented and discussed. It should be mentioned here that the number of simulations K to be used should be sufficient to accurately calculate the first two statistical moments. This number should insure the convergence of the mean estimator of A_{max} at the top of the soil column and its corresponding coefficient of variation as a function of the number of simulations.

Figure V.9 presents the estimators of the mean and coefficient of variation of A_{max} at the top of the soil column as a function of the number of simulations. This figure shows that the convergence is reached for a number of simulations larger than 300. A number of simulation K=500 was used hereafter to perform the probabilistic analysis using the MCS method.

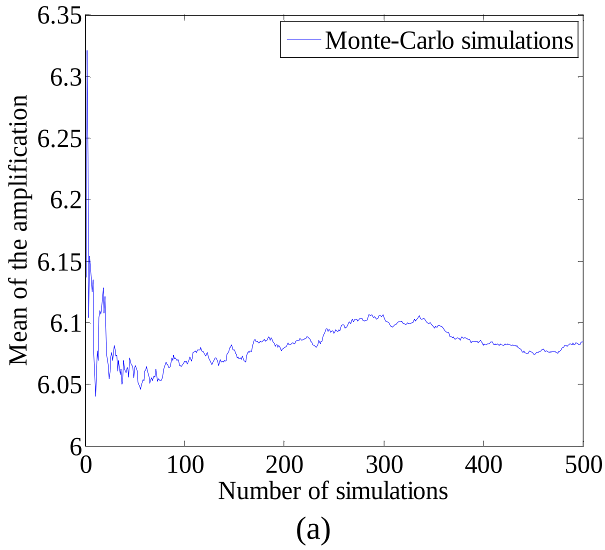

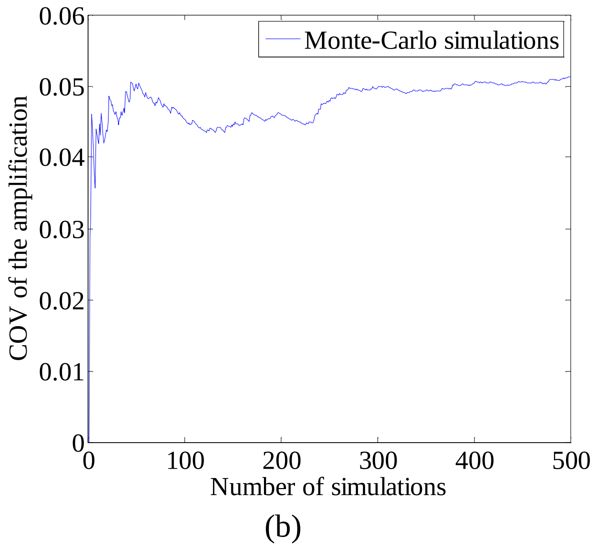

Figure V.9. (a) Mean and (b) coefficient of variation of A_{max} at the top of the soil column as a function of the number of simulations when a_y=0.5m

Effect of the mean value and the autocorrelation distance

The effect of the soil spatial variability and/or the time variability of the earthquake GM on A_{max} at the top of the soil column is studied and presented in Table V.2 for the two mean values of the shear modulus ($\mu_{G_1} = 72MPa$ and $\mu_{G_2} = 288MPa$) when COV_G=30%. Different values of the vertical autocorrelation distance (a_y=0.5, 2, 5, 10 and 20m) were considered in the analyses.

In the case where only the soil spatial variability was considered, Table V.2 shows (as in the deterministic analysis) that smaller mean values of A_{max} at the top of the soil column were obtained when a non resonant mean value of the shear modulus G was used (i.e. $\mu_{G_1} = 72MPa$) as compared to those obtained when a resonant mean value of the shear modulus G was utilized (i.e. $\mu_{G_2} = 288MPa$). Notice also that for the weak soil configuration (i.e. when $\mu_{G_1} = 72MPa$), the mean value of A_{max} decreases when the vertical autocorrelation distance a_y decreases. This is because the soil heterogeneity will introduce some strong zones which will limit the amplification of the acceleration at the top of the soil column. On the contrary, for the strong soil configuration (i.e. $\mu_{G_2} = 288MPa$), the mean value of A_{max} increases when the vertical autocorrelation distance

a_y decreases. This is because the soil heterogeneity will introduce some weakness zones which will increase the amplification of the acceleration at the top of the soil column.

On the other hand, Table V.2 shows that the variability of A_{max} is maximal for the very large values of the autocorrelation distance (a_y=20m). This variability decreases when the vertical autocorrelation distance a_y decreases. The same trend was obtained in the three previous chapters where static loading cases were considered. In these cases, the small values of the autocorrelation distances produce the so-called 'averaging phenomenon' for which the rapid change in the values of a soil property from element to another neighboring one leads to quasi-similar behavior for all the realizations. In the dynamic loading cases, this 'averaging phenomenon' is also produced but along the wave's path. Thus, the rapid change in the values of the shear modulus along the wave path leads to quasi-similar behavior for all the realizations. This leads to close values of A_{max} at the top of the soil column and thus to a smaller variability in this response. Notice that similar results were obtained by Al-Bittar et al. (2012a) when the dynamic behavior of a spatially varying slope subjected to stochastic GM was investigated (cf. Appendix F). From Table V.2, one can also observe that the variability of A_{max} is larger for the case of the weak soil corresponding to a small mean value of the shear modulus G (i.e. $\mu_{G_1} = 72MPa$).

The maximum variability obtained when only the soil spatial variability was considered is largely smaller than the one obtained when only the time variability of the earthquake GM was considered as may be seen from Table V.2. The values of the variability of A_{max} obtained when only the time variability of the earthquake GM was considered (i.e. 20.64% for $\mu_{G_1} = 72MPa$ and 18.70% for $\mu_{G_2} = 288MPa$) are about two times larger than those obtained when only the soil spatial variability was taken into account. Notice however that the obtained results may change in the case where a different seismic loading was considered.

Finally, when both the soil spatial variability and the time variability of the GM have been considered in the analysis, one obtains a variability of A_{max} which is far below the one obtained by superposition of the variabilities of A_{max} as obtained from the soil spatial variability and the time variability of the earthquake GM considered separately. Thus, if one applies the superposition method to obtain the variability of the dynamic responses, the obtained variability may be largely overestimated.

Case where only the spatial variability of the shear modulus was considered						
	$\mu_{G_1}=72MPa$			$\mu_{G_2}=288MPa$		
a_y(m)	$\mu_{A_{max}}$ (m/s^2)	$\sigma_{A_{max}}$ (m/s^2)	$COV_{A_{max}}$ (%)	$\mu_{A_{max}}$ (m/s^2)	$\sigma_{A_{max}}$ (m/s^2)	$COV_{A_{max}}$ (%)
0.5	6.08	0.31	5.12	9.82	0.19	1.92
2	6.19	0.43	6.96	9.76	0.30	3.95
5	6.29	0.54	8.52	9.65	0.49	5.03
10	6.35	0.66	10.34	9.60	0.55	5.75
20	6.38	0.66	10.34	9.53	0.55	5.80
Case where only the time variability of the earthquake GM was considered						
	$\mu_{G_1}=72MPa$			$\mu_{G_2}=288MPa$		
	7.01	1.45	20.64	8.75	1.63	18.70
Case where both the spatial variability of the shear modulus and time variability of the earthquake GM were considered						
	$\mu_{G_1}=72MPa$			$\mu_{G_2}=288MPa$		
a_y(m)	$\mu_{A_{max}}$ (m/s^2)	$\sigma_{A_{max}}$ (m/s^2)	$COV_{A_{max}}$ (%)	$\mu_{A_{max}}$ (m/s^2)	$\sigma_{A_{max}}$ (m/s^2)	$COV_{A_{max}}$ (%)
0.5	6.85	1.44	20.99	8.66	1.63	18.82
2	6.88	1.45	21.14	8.69	1.64	18.92
5	6.89	1.47	21.26	8.67	1.69	19.52
10	6.98	1.51	21.69	8.73	1.72	19.69
20	6.99	1.51	21.69	8.73	1.72	19.69

Table V.2. Effect of the soil spatial variability and/or the time variability of the earthquake GM on the maximum acceleration at the top of the soil column

<u>Effect of the coefficient of variation</u>

The aim of this section is to study the effect of the coefficient of variation of *G* on the statistical moments of A_{max} at the top of the soil column considering two cases of deterministic and stochastic earthquake GMs for the two mean values of *G* ($\mu_{G_1}=72MPa$ and $\mu_{G_2}=288MPa$). Three different values of the coefficient of variation (COV_G=15%, 30% and 45%) were considered in the analyses.

Table V.3 shows that the increase in the coefficient of variation of *G* has practically no influence on the mean value of A_{max}. On the other hand, the variability of A_{max} at the top of the column increases (as expected) when the coefficient of variation of *G* increases; this increase is more significant in the case of the stronger soil and when only the soil spatial variability is considered in the analysis. Finally, notice that the variability of A_{max} at the top of the column reaches the most significant values in the case of a weak soil ($\mu_{G_1} = 72MPa$) and when both the soil spatial variability and the time variability of the earthquake GM were considered.

Case where only the spatial variability of the shear modulus was considered						
	$\mu_{G_1} = 72MPa$			$\mu_{G_2} = 288MPa$		
COV_G (%)	$\mu_{A_{max}}$ (m/s^2)	$\sigma_{A_{max}}$ (m/s^2)	$COV_{A_{max}}$ (%)	$\mu_{A_{max}}$ (m/s^2)	$\sigma_{A_{max}}$ (m/s^2)	$COV_{A_{max}}$ (%)
15	6.13	0.41	6.61	9.74	0.17	1.78
30	6.19	0.43	6.96	9.65	0.49	5.03
45	6.16	0.52	8.42	9.60	0.64	6.70
Case where both the spatial variability of the shear modulus and time variability of the earthquake GM were considered						
	$\mu_{G_1} = 72MPa$			$\mu_{G_2} = 288MPa$		
COV_G (%)	$\mu_{A_{max}}$ (m/s^2)	$\sigma_{A_{max}}$ (m/s^2)	$COV_{A_{max}}$ (%)	$\mu_{A_{max}}$ (m/s^2)	$\sigma_{A_{max}}$ (m/s^2)	$COV_{A_{max}}$ (%)
15	6.95	1.45	20.87	8.67	1.61	18.59
30	6.88	1.45	21.14	8.70	1.65	18.92
45	6.65	1.50	22.47	8.72	1.70	19.50

Table V.3. Effect of the coefficient of variation of G on A_{max} at the top of the soil column considering deterministic and stochastic earthquake GM

V.2.4.2 Sparse polynomial chaos expansion results

In this section, the results obtained based on the Sparse Plynomial Chaos Expansion (SPCE) methodology are presented. It should be mentioned here that the 500 simulations which were used in the previous section to perform the analyses by the MCS methodology were employed herein in order to construct the SPCE. Additional simulations were performed for the cases where the regression problem was ill-posed. However, the number of simulations was not increased until reaching the target coefficient of determiniation Q^2_{TARGET} of 0.999. This is because of the high computational cost of each dynamic analysis. In this study, only the case of spatially varying soil column was considered. This is because introducing the time variability of the earthquake GM will add 2001 random variables to the problem. This very large number of random variables makes the SPCE methodology not feasible.

Table V.4 presents the total number *N* of random variables (or eigenmodes) that should be used to discretize the random field of *G* (within the prescribed value of 10% for the variance of the error) for the different values of the vertical autocorrelation distance a_y.

Vertical autocorrelation distance a_y(m)	Number of random variables
0.5	35
2	10
5	5
10	5
20	5

Table V.4. Number of random variables needed to discretize the random field *G*

<u>Effect of the mean value and the autocorrelation distance</u>

The effect of the soil spatial variability on the PDF of A_{max} at the top of the soil column for the two mean values of the shear modulus ($\mu_{G_1} = 72MPa$ and $\mu_{G_2} = 288MPa$) is studied and presented in Figure V.10. Different values of the vertical autocorrelation distance (a_y=0.5, 2, 5, 10 and 20m) were considered in the analyses.

Figure V.10 shows that the variability of A_{max} at the top of the soil column decreases when the vertical autocorrelation distance a_y decreases. Similar observation was provided in the previous section where MCS was employed. Even though these PDFs present logical trends (similar to what was obtained in the previous chapters where a static loading was studied), they can not be considered as rigorous. This is because relatively small values of the coefficient of determination Q^2 were obtained in this case where a seismic loading was considered.

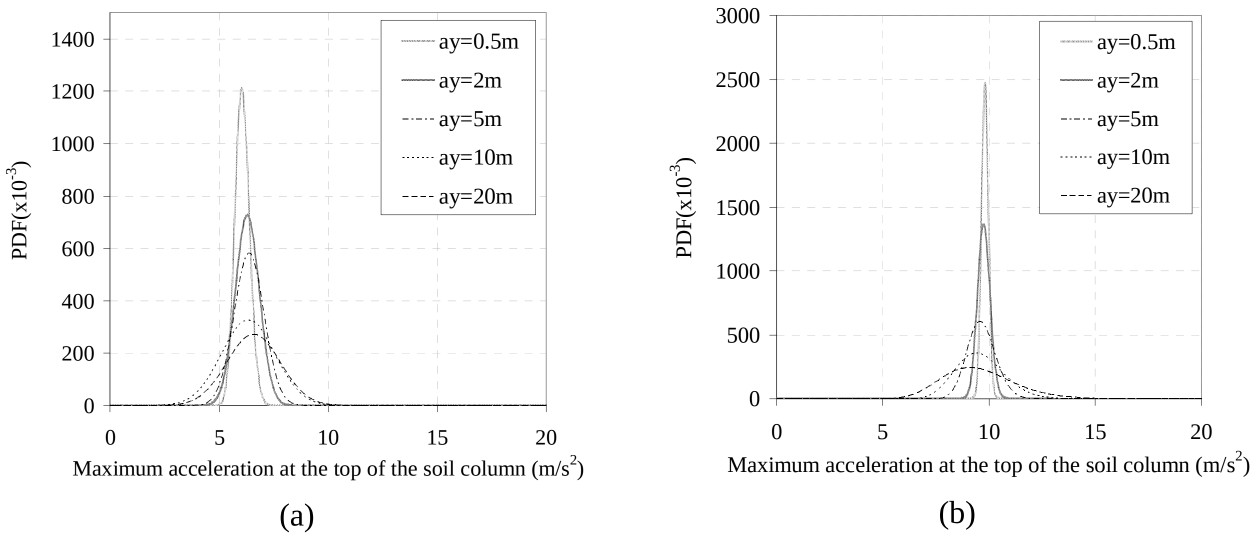

Figure V.10. Influence of the vertical autocorrelation distance a_y on the PDF of A_{max} at the top of the soil column when (a) $\mu_{G_1} = 72MPa$ and (b) $\mu_{G_2} = 288MPa$

Table V.5 presents a comparison between the statistical moments of A_{max} at the top of the soil column as obtained using both the MCS and the SPCE methodologies. This table also provides the values of Q^2 obtained when the SPCE methodology was used.

From Table V.5, one can observe a small difference between the two first statistical moments as given by both the MCS and the SPCE methodologies even though relatively small values of Q^2 were obtained with the use of the SPCE methodology. Thus, the relatively small values of Q^2 may not have a major influence on the two first statistical moments, but they certainly affect the third and fourth statistcal moments. This makes the obtained PDFs invalid at the distribution tails.

In fact, there are two possible reasons for which relatively small values of Q^2 may occur. The first one is the chosen system response A_{max} which may be obtained at different time steps from simulation to another one. As for the second reason, it may be the number of simulations which needs to be increased. In order to detect the main reason for which the relatively small values of Q^2 were obtained, a test on only the chosen system response A_{max} was performed. This test was not presented in this chapter but was provided in Appendix G. As for the number of simulations, the test was not performed because of the significant computation time of the dynamic deterministic model (40 min per simulation).

$\mu_{G_1} = 72MPa$							
	Monte-Carlo simulations			Sparse Polynomial Chaos Expansion			
a_y(m)	$\mu_{A_{\max}}$ (m/s^2)	$\sigma_{A_{\max}}$ (m/s^2)	$COV_{A_{\max}}$ (%)	$\mu_{A_{\max}}$ (m/s^2)	$\sigma_{A_{\max}}$ (m/s^2)	$COV_{A_{\max}}$ (%)	Q^2
0.5	6.08	0.31	5.12	6.07	0.23	3.97	0.535
2	6.19	0.43	6.96	6.18	0.37	6.00	0.587
5	6.29	0.53	8.52	6.29	0.42	6.68	0.686
10	6.35	0.65	10.34	6.33	0.54	8.53	0.788
20	6.38	0.66	10.34	6.37	0.56	8.80	0.790
$\mu_{G_2} = 288MPa$							
	Monte-Carlo simulations			Sparse Polynomial Chaos Expansion			
a_y(m)	$\mu_{A_{\max}}$ (m/s^2)	$\sigma_{A_{\max}}$ (m/s^2)	$COV_{A_{\max}}$ (%)	$\mu_{A_{\max}}$ (m/s^2)	$\sigma_{A_{\max}}$ (m/s^2)	$COV_{A_{\max}}$ (%)	Q^2
0.5	9.82	0.19	1.92	9.81	0.14	1.43	0.555
2	9.76	0.30	3.95	9.76	0.27	2.77	0.665
5	9.65	0.49	5.03	9.65	0.46	4.77	0.810
10	9.60	0.55	5.75	9.60	0.50	5.21	0.800
20	9.53	0.55	5.80	9.53	0.50	5.25	0.750

Table V.5. Comparison between the statistical moments (μ, σ) of A_{max} at the top of the soil column as obtained using both the MCS and the SPCE methodologies

V.3 CASE OF A SOIL-STRUCTURE INTERACTION (SSI) PROBLEM

In this section, the SSI problem was investigated through the analysis of a five storey building [Al-Bittar et al. (2012b)]. In order to study a SSI problem, three methods can be found in literature [Pecker (1984)]:

(i) The superposition method which subdivides the complex SSI problem into simpler problems (kinematics interaction and inertial interaction [Kausel et al. (1978)]), this method being valid only for linear problems.

(ii) The direct methods that use a classical finite element/finite difference approaches [Prevost (1999)], but these methods require good knowledge of the constitutive laws and are very computationally-expensive.

(iii) The hybrid methods that are a combination of the two previous methods and therefore they are more attractive because of their computational cost.

The macro-element approach belongs to the last category and it is used to model the present SSI problem. The macro-element concept developed by Nova and Montrasio (1991) consists in condensing the soil (material) and interface (geometric) nonlinearities into a representative point (the centre of the foundation) and it works with generalized variables (forces and displacements). It thus allows the simulation of the behaviour of shallow foundations in a simplified way.

The main reason for which the macro-element concept is chosen to perform the probabilistic analysis is that the time cost for a single deterministic calculation is relatively small (five minutes per simulation). Thus, this model is suitable for the probabilistic analysis which requires a great number of calls of the deterministic model. In this thesis, only the time variability of the seismic loading was considered in the analysis.

Finally, notice that the dynamic system responses retained for the probabilistic analysis are:

(i) The maximum horizontal displacement at the top of the building.

(ii) The three maximum displacements of the footing centre.

(iii) The three maximum reaction forces at the contact of the soil and the footing.

The probabilistic results are presented in the form of statistical moments and in the form of probability of exceeding of predefined thresholds.

The following subsections are organised as follows: one first presents the numerical modeling of the dynamic problem. Then, the obtained probabilistic numerical results are presented and discussed.

V.3.1 Numerical modeling

The SSI problem involves a five-storey building. The CAMUS IV structure [CAMUS (1997)] is the one chosen in this study. This structure is a 1/3 scaled mock-up. It is composed of (i) two parallel reinforced concrete walls without opening and (ii) six square floors that link these walls (Figure V.11(a)). The entire structure rests on two rectangular footings of 0.8mx2.1m (Figure V.11(a)). The total height of the model is 5.1m and the total mass is estimated to be equal to 36 tons. The wall of a given floor is 4m long, 1.70m high and 6cm thick [CAMUS (1997)]. The building and the footings rest on a high density sand. The container which contains the sand has a horizontal cross-section of 4.6mx4.6m and a depth of 4m.

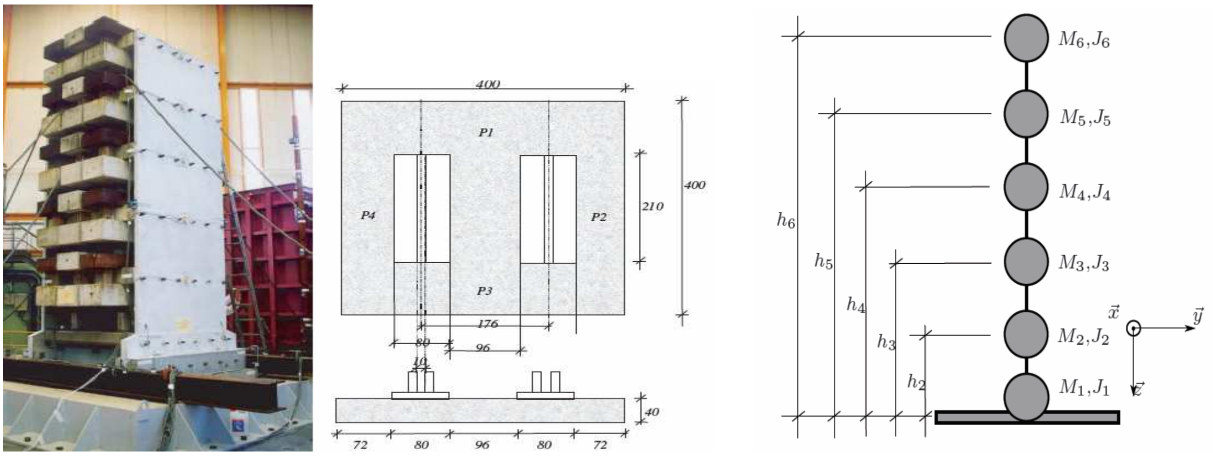

(a) (b)

Figure V.11. The five-storey building: (a) The CAMUS IV real model, and (b) the simplified numerical lumped mass system

For the numerical calculations, the CAMUS IV five-storey building was modelled using a simple lumped mass system (Figure V.11(b)). In this system, the building was simulated using beam elements and concentrated masses. Thus, each storey i was reduced to a single mass M_i that has an inertia equal to J_i. The values of the masses and the corresponding inertias for the different stories are given in Table V.6. The material behaviour of the beams was considered linear elastic. The soil-foundation system was modelled using the macro-element concept.

Several 2D macroelements exist in literature [Nova and Montrasio (1999), Cassidy et al. (2002) and Crémer et al. (2001)]. The 2D macro-element developed in Crémer et al. (2002) is adequate for static, cyclic and dynamic loadings (e.g. earthquake) and it considers both the plasticity of the soil and the uplift of the foundation. Grange et al. (2009a) have extended the macro-element of Crémer et al. (2002). Their macro-element can simulate the 3D behaviour of foundations having different shapes (circular, rectangular and strip). This recent version of the macro-element was adopted in this thesis to perform the probabilistic dynamic analysis. It should be mentioned here that the mathematical description of the macro-element is summarized in Appendix H. More details are given in Crémer et al. (2001), Crémer et al. (2002), Grange (2008), Grange et al. (2009a) and Grange et al. (2009b).

Height h_i (m) (see Figure 1)	Mass (Kg)	Inertia ($Kg.m^2$)
h_1=0.1	M_1=4786	J_1=1600
h_2=1.4	M_2=6825	J_2=3202
h_3=2.3	M_3=6825	J_3=3202
h_4=3.2	M_4=6825	J_4=3202
h_5=4.1	M_5=6825	J_5=3202
h_6=5	M_6=6388	J_6=3124

Table V.6. Parameters used to model the five-storey building

Elastic parameters	
$K_{\theta\theta}^{el}$=52MNm/rad	
K_{hh}^{el}=105MN/m	
K_{zz}^{el}=120MN/m	
Plastic parameters	
q_{ult}=0.58MPa	κ=1
a=0.93	ξ=1
b=0.8	a_1=1
c=1	a_2=1
d=1	a_3=1
e=1	a_4=1
f=1	a_5=1

Table V.7. Parameters used to model the soil-foundation (macro-element)

The macro-element considered in this study has two superposed nodes. The first node is considered fixed and the second node is connected to the structure. The dynamic loading is applied to the first node. For the used high density sand, Grange et al. (2009b) have identified the different parameters of the macro-element by fitting the model to the experimental results given by Grange (2008). These parameters are presented in Table V.7 where q_{ult} is the ultimate bearing capacity of the rectangular footing; a, b, c, d, e and f are the coefficients that appear in Equation (H.1); κ and ξ are the parameters of the flow rule; and finally a_1, a_2, a_3, a_4 and a_5 are the parameters used to calculate the variable γ as may be seen in Grange (2008). In the following sections, the obtained probabilistic results are presented and discussed.

V.3.2 Probabilistic numerical results

The aim of this section is to present the probabilistic numerical results. It should be remembered here that the dynamic responses considered in the analysis of the behavior of the five storey building involve (i) the maximum horizontal displacement at the top of the building, (ii) the three maximum displacements of the footing centre, and finally (iii) the three maximum reaction forces at the contact of the soil and the footing.

In this study, only the effect of the time variability of the earthquake GM on the dynamic responses was considered. This is because the macro-element concept consists in condensing the soil (material) and interface (geometric) nonlinearities into a representative point (the centre of the foundation), which make it impossible to model the soil spatial variability of the soil properties.

The aim of the next two subsections is to present respectively (i) the statistical moments of the dynamic responses and (ii) the fragility curves corresponding to three different damage levels. A number of 100,000 stochastic synthetic acceleration time histories was used in the analysis. This large number of samples is necessary to obtain accurate values of the failure probability.

V.3.2.1 Statistical moments of the dynamic responses

Table V.8 presents the two first statistical moments (i.e. the probabilistic mean and the standard deviation) together with the deterministic mean values for the following dynamic responses: (i) the maximum horizontal displacement at the top of the building, (ii) the three maximum displacements of the footing centre, and finally (iii) the force resultants (V_{max}, N_{max}, M_{max}) at the contact of the soil and the footing.

Table V.8 shows that the probabilistic mean value of the maximum horizontal displacement at the top of the building is almost 10 times larger that the one obtained at the footing centre. On the other hand, large values of the coefficient of variation *COV* are obtained for the different output parameters ($19.75<COV<41.5$). From a probabilistic point of view, large values of the coefficient of variation indicate that the responses are spread out over a large range of values. This is critical since in this case the mean values of these responses are not representative and can not be considered as reliable data for design procedure. For some output parameters (such as the maximum displacement at the top of the building and the maximum moment at the bottom), this phenomenon is amplified by the fact that the probabilistic mean value is significantly larger than the deterministic one.

Stochastic dynamic response	Deterministic mean	Probabilistic mean μx10^{-3}	Standard deviation σx10^{-3}	Coefficient of variation *COV* (%)
The maximum horizontal displacement at the top of the building (m)	22.7	31.5	9.7	30.80
The maximum horizontal displacement of the footing centre (m)	2.4	2.8	0.6	21.43
The maximum vertical displacement of the footing centre (m)	4.2	5.3	2.2	41.50
The maximum rotation of the footing centre (rad)	4.1	5.8	1.9	32.76
The maximum normal force at the contact of the soil and the footing (MN)	3.8	5.6	2.3	41.07
The maximum shear force at the contact of the soil and the footing (MN)	27.9	31.4	6.2	19.75
The maximum moment at the contact of the soil and the footing (MN)	34.3	37.3	7.7	20.64

Table V.8. Effect of stochastic Ground-Motion on the statistical moments (μ, σ) of the seven dynamic responses

Figure V.12 presents the PDFs of the maximum horizontal displacement at the footing centre and at the top of the building. This figure shows that the PDF of the maximum horizontal displacement at the top of the building is more spread out and thus more critical.

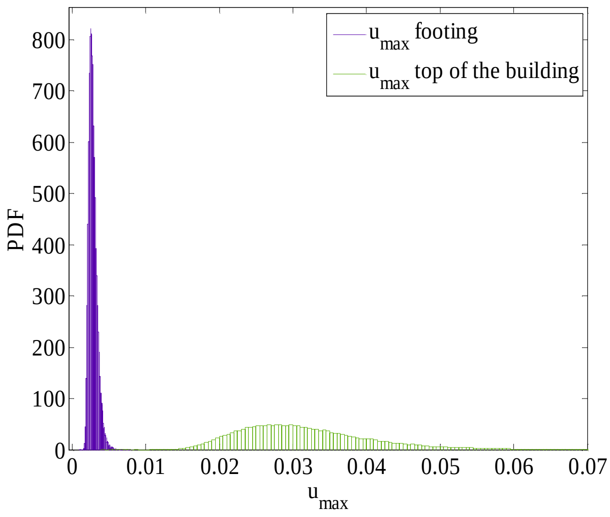

Figure V.12. PDF of the maximum horizontal displacement (a) at the centre of the footing, and (b) at the top of the building

V.3.2.2 Fragility curves

The probability that a certain level of damage (tolerable maximum horizontal displacement) will be exceeded at a specified peak ground acceleration *PGA* can be expressed in the form of fragility curves.

The fragility curves can be performed since the stochastic ground motions create variability in the PGA ($0.2g<PGA<0.7g$). In this section, fragility curves for the maximum horizontal displacement at the top of the building and for the maximum moment at the contact of the soil and the footing are computed.

Figure V.13(a) presents three fragility curves corresponding to the maximum horizontal displacement at the top of the building for three levels of damage [(i) minor damage for which u_{max}=0.01m, (ii) medium damage for which u_{max}=0.04m and (iii) major damage for which u_{max}=0.06m]. On the other hand, Figure V.13(b) presents three fragility curves corresponding the maximum moment at the contact of the soil and the footing for three levels of damage [(i) minor damage for which M_{max}=0.01*MNm*, (ii) medium damage for which M_{max}=0.04*MNm* and (iii) major damage for which M_{max}=0.06*MNm*]. These figures allow one to determine the probability of exceeding a tolerable value of the dynamic response corresponding to a given value of the peak ground acceleration (*PGA*).

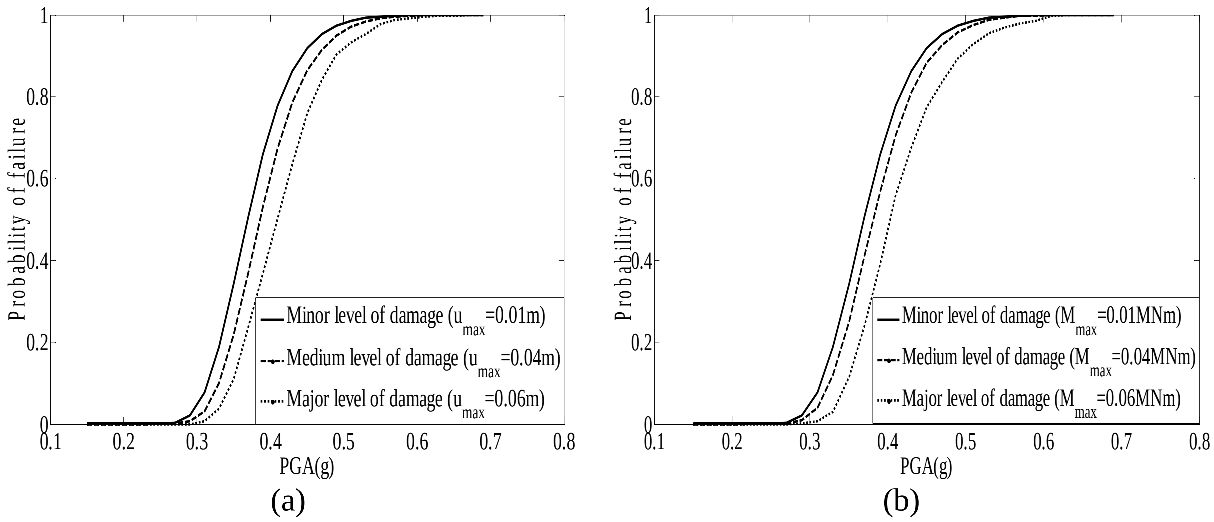

Figure V.13. Fragility curves for different levels of damage (a) maximum horizontal displacement at the top of the building, and (b) maximum moment at the contact of the soil and the footing

V.4 CONCLUSIONS

In this chapter, the dynamic responses induced by an earthquake Ground-Motion (GM) taking into account the soil spatial variability and/or the time variability of the seismic loading were investigated. It should be mentioned here that when dealing with seismic loads, an aleatory uncertainty which is the time variability of the earthquake GM appears in addition to the soil spatial variability and the variability of the superstructure. Given the scarcity of studies involving the probabilistic seismic responses, a free field soil medium subjected to a seismic loading was firstly considered. The aim is to investigate the effect of the soil spatial variability and/or the time variability of the earthquake GM using a simple model. Then, a SSI problem was investigated in the second part of this chapter.

In the case where a free field medium was considered, the effect of the soil spatial variability and/or the time variability of the earthquake GM was investigated through the study of an elastic free field soil mass. The soil shear modulus G was modeled as a non-Gaussian random field and the earthquake GM was modeled as a random process. The EOLE methodology was used to discretize the shear modulus random field. As for the earthquake GM, the method proposed by Rezaeian and Der Kiureghian (2010) which consists in fitting a parameterized stochastic model to the real recorded earthquake GM was utilized. The dynamic response considered in the analysis was the amplification of the maximum acceleration at the soil surface. The deterministic dynamic numerical model was based on numerical simulations using the finite difference software FLAC^{3D}. Two types of modeling were considered in this chapter. The first one considers a two-dimensional soil mass and the second model considers a soil column. The objective of these two types of modeling was to verify the validity of the 'column' model in simulating the propagation of the seismic waves in the soil mass. This permits to replace the 2D computationally-expensive model with the relatively non-expensive 'column' model which may significantly reduce the probabilistic computational time. As for the probabilistic methods used in this chapter, two methods were used. The first one is the classical Monte Carlo Simulation (MCS) methodology and the second one is the Sparse Polynomial Chaos Expansion (SPCE) methodology which consists in substituting the original deterministic model by a meta-model.

The deterministic numerical results of the free field case have shown that the 'column' model is sufficient to study the evolution of the maximum acceleration in the soil mass. This result is of particular interest for the probabilistic analyses which require a large number of calls to the deterministic model. On the other hand, the evolution of the maximum acceleration as a function of the shear modulus have shown that for a given range of the shear modulus values, an important increase in the maximum acceleration was obtained. For this range of values of *G*, the predominant frequency band of the soil 'column' corresponds to the predominant frequency band of the seismic loading, which leads to resonance phenomenon.

As for the probabilistic results of the free field case, the MCS methodology has shown that for the Nice accelerogram used in this thesis, the variability obtained when only the soil spatial variability was considered is largely smaller than the one obtained when only the time variability of the earthquake GM was considered. This result may change in the case where a different seismic signal is used. Considering both the soil spatial variability and the time variability of the GM has led to a variability of A_{max} which is far below from that obtained by superposition of the variabilities of A_{max} as obtained from the soil spatial variability and the time variability of the earthquake GM considered separately. As for the SPCE methodology results, the obtained statistical moments of A_{max} at the top of the soil column are close to those resulting from the MCS methodology, but the obtained PDFs can not be considered as rigorous because relatively small values of Q^2 were obtained in this case.

In the case where the SSI problem was considered, a probabilistic dynamic analysis of a five-storey building founded on two rigid rectangular footings was presented. The entire soil-structure system was considered in the analysis in which the soil and soil-footing interface were modelled by a macro-element. The main reason for which the macro-element concept was chosen to perform the probabilistic analysis is that the time cost for a single deterministic calculation is relatively small (five minutes per simulation). Only the time variability of the seismic loading was introduced in the computations; the soil spatial variability was not considered in the analysis. The probabilistic dynamic analyses were performed using the classical Monte Carlo Simulation (MCS) methodology.

The dynamic system responses retained for the probabilistic analysis of the SSI problem were (i) the maximum horizontal displacement at the top of the building, (ii) the three maximum displacements of the footing centre, and finally (iii) the three maximum reaction forces at the contact of the soil and the footing.

The probabilistic numerical results of the SSI problem have shown that (i) the probabilistic mean value of the maximum horizontal displacement at the top of the building was almost 10 times larger that the one obtained at the footing centre; (ii) large values of the coefficient of variation were obtained for the different output parameters; and finally (iii) stochastic ground motion time histories create variability in the PGA which allows one to perform fragility curves for the different dynamic responses.

GENERAL CONCLUSIONS

This study focuses on the probabilistic analysis of shallow foundations resting on spatially varying soils or rocks and subjected to either a static or a dynamic (seismic) loading. Two aleatory sources of uncertainty were considered. The first one is the soil (or rock) spatial variability which was modeled by random fields. The second one is the time variability of the earthquake GM (when seismic loads were considered) which was modeled by a random process. Both types of variabilities lead to high dimensional stochastic problems.

In this thesis, a literature review on the soil and the earthquake GM variabilities and the meta-modeling techniques was first presented. It was followed by two main parts.

The first part (which is composed of chapters II, III and IV) presents a probabilistic analysis of shallow foundations resting on spatially varying soils or rocks and subjected to a static loading. Both cases of strip and square footings were studied. Also, 2D and 3D random fields were considered in the analysis. In this part, the probabilistic method used to calculate the different probabilistic outputs was the Sparse Polynomial Chaos Expansion (SPCE) methodology and its extension the SPCE/GSA procedure.

In chapter II, a probabilistic analysis of shallow strip foundations resting on spatially varying soils or rocks was presented. Relatively non-expensive deterministic models were used in this chapter since the ULS analysis was performed in the case of a weightless material. The resulting ultimate bearing capacity is the one related to the N_c coefficient in the bearing capacity equation. In the case of spatially varying soil mass, a probabilistic analysis at both ULS and SLS of vertically loaded strip footings was performed. The soil shear strength parameters (c and φ) were considered as anisotropic cross-correlated non-Gaussian random fields at ULS and the soil elastic parameters (E and υ) were considered as anisotropic uncorrelated non-Gaussian random fields at SLS. Notice that the system response used at ULS was the ultimate bearing capacity; however, the footing vertical displacement was considered as the system response at SLS. Concerning the case of the spatially varying rock mass obeying the Hoek-Brown failure criterion, only the ULS case of vertically loaded footings was considered. The uniaxial compressive strength of the intact rock (σ_c) was considered as a non-Gaussian random field and the Geological Strength Index (GSI) was considered as a random variable. Notice that the system response considered was the ultimate bearing capacity of the footing in the case of a weightless rock mass. The methodology proposed by Vořechovsky (2008) was used to generate the random fields. The Sparse Polynomial Chaos Expansion (SPCE) methodology was used to perform the probabilistic analysis.

In chapter III, the effect of the spatial variability in three dimensions (3D) was investigated through the study of the ultimate bearing capacity of strip and square foundations resting on a purely cohesive soil with a spatially varying cohesion in the three dimensions. This case involves relatively non-expensive deterministic models although a 3D mechanical model (with a greater computation time with respect to the models of chapter II) was used. This is because of the use of a purely cohesive soil.

In chapter IV, an efficient combined use of the SPCE methodology and the Global Sensitivity Analysis (GSA) was proposed. The aim is to reduce the probabilistic computation time for high-dimensional stochastic problems involving expensive deterministic models. This procedure was illustrated through the probabilistic analysis at ULS of a strip footing resting on a ponderable soil with 2D and 3D random fields and subjected to a central vertical load.

The main findings of the first part can be summarized as follows:

- Chapters II and III have shown the superiority of the SPCE with respect to the classical MCS commonly used in geotechnical engineering problems involving spatially varying soils. The superiority comes from the small number of calls of the deterministic model. In addition to the determination of the PDF of the system response, the SPCE allows one to easily perform a global sensitivity analysis based on Sobol indices using the SPCE coefficients. These indices give the contribution of each random field in the variability of the system response.

- The classical SPCE methodology was found to be efficient when relatively non-expensive deterministic models are involved in the analysis (e.g. the ULS analysis of strip footings on a weightless material or the ULS analysis of 3D footings on a purely cohesive soil).

- The efficient combined use of the SPCE methodology and the Global Sensitivity Analysis (GSA) is needed when expensive deterministic models (e.g. strip, rectangular or circular footings resting on a ponderable soil with 2D/3D random fields) are involved in the analysis.

- The variability of the system responses (i.e. the ultimate bearing capacity in the ULS analysis and the vertical displacement of the footing in the SLS analysis) increases (as expected) with the increase in the coefficients of variation of the random fields. It was also shown that an increase in the coefficient of variation of a random field increases its

Sobol index and thus its weight in the variability of the system response and decreases the weight of the other random field.

- The negative correlation between the random fields decreases the response variability.
- The decrease in the autocorrelation distances (a_x or a_y or a_x=a_y), lead to a less spread out PDF of the system response
- The probabilistic mean value of the ultimate bearing capacity of strip footings (in both cases of soil and rock masses) presents a minimum. This minimum was obtained in the isotropic case when the autocorrelation distance is nearly equal to the footing breadth B; while for the anisotropic case (presented only when a soil mass is considered), this minimum was obtained (for prescribed footing and soil characteristics) at a given value of the ratio between the horizontal and the vertical autocorrelation distances.
- The small values of the autocorrelation distances lead to small values of the skewness and kurtosis of the system responses. Thus, a PDF of the system response that is not far from a Gaussian one is obtained in these cases.
- For small values of the autocorrelation distances, the variability of the ultimate bearing capacity computed by considering a 3D random field is smaller than the one obtained with the 2D random field for both cases of square and strip footings. Thus, the third dimension is important to be considered only when small autocorrelation distances are encountered.
- Some observed phenomena which can not be seen when homogenous soils are considered (such as the non-symmetrical soil failure and the variation in Sobol indices with the autocorrelation distance) are obtained when considering the spatial variability of the soil/rock properties in the probabilistic analysis.

The second part (which is composed of chapter V) presents a probabilistic analysis of the dynamic responses induced by a specific earthquake Ground-Motion (GM) (which is the Nice synthetic accelerogram), taking into account the soil spatial variability and/or the time variability of the seismic loading. Two cases involving (i) a free field and (ii) a SSI problem were considered in the analysis. In this part, the probabilistic methods used to calculate the probabilistic outputs were the classical Monte-Carlo simulation (MCS) method and the Sparse Polynomial Chaos Expansion (SPCE) methodology.

In the case where a free field medium was considered, the effect of the soil spatial variability and/or the time variability of the earthquake GM was investigated. The soil shear modulus *G* was modeled as a non-Gaussian random field and the earthquake GM was modeled as a random process. The dynamic response considered in the analysis was the amplification of the maximum acceleration at the soil surface. Two types of modeling were considered herein. The first one considers a two-dimensional soil mass and the second model considers a soil column. The objective of these two types of modeling was to verify the validity of the 'column' model in simulating the propagation of the seismic waves in the soil mass. As for the case where a SSI problem was considered, a probabilistic dynamic analysis of a five-storey building founded on two rigid rectangular footings was presented. The soil and soil-footing interface were modelled by a macro-element. The main reason for which the macro-element concept was used is the relatively small computation cost of the deterministic model. Only the time variability of the seismic loading was introduced in the computations; the soil spatial variability was not considered in the analysis. The dynamic system responses retained for the probabilistic analysis were: (i) the maximum horizontal displacement at the top of the building, (ii) the three maximum displacements of the footing centre, and finally (iii) the three maximum reaction forces at the contact of the soil and the footing. In this part, the main findings can be summarized as follows:

- The 'column' model was found sufficient to study the distribution of the maximum acceleration in the soil mass. This result is of particular interest for the probabilistic analyses which require a large number of calls to the deterministic model.
- The evolution of the maximum acceleration as a function of the shear modulus have shown that for a given range of the shear modulus values, an important increase in the maximum acceleration was obtained. For this range of values of *G*, the predominant frequency band of the soil 'column' corresponds to the predominant frequency band of the seismic loading, which leads to the resonance phenomenon.
- When using the Nice accelerogram, the variability obtained when only the soil spatial variability was considered was found largely smaller than the one obtained when only the time variability of the earthquake GM was considered.
- Considering both the soil spatial variability and the time variability of the earthquake GM has led to a variability of A_{max} which is far below from that obtained by superposition of the variabilities of A_{max} as obtained from the soil spatial variability and the time variability of the earthquake GM considered separately.

- The PDFs of A_{max} at the top of the soil column obtained using the SPCE methodology show similar trends as those obtained when static loading cases were considered, but these PDFs can not be considered as rigorous because relatively small values of Q^2 were obtained in this case.
- When considering the SSI problem involving the study of a five-storey building, large values of the coefficients of variation were obtained for the different system responses.
- The stochastic ground motion time histories create variability in the PGA which allows one to perform fragility curves for the different dynamic responses

Ongoing research topics may involve the following items:

For the static loading case:

- Consider the case of a rectangular or a circular footing resting on a ponderable soil with 3D spatially varying shear strength parameters using the SPCE/GSA procedure.
- Validate of the SPCE methodology for the computation of the failure probability.
- Use of a rigorous approach for the computation of Sobol indices in the case of correlated random variables.

For the seismic loading case:

- Investigate the effect of 2D random fields (instead of the 1D random fields) on the dynamic response in the case of the free field soil medium.
- Investigate the effect of changing the input seismic signal on the obtained probabilistic results.
- In the SSI problem, introduce the soil spatial variability in the macro-element. This can be done by first computing the PDF of the ultimate bearing capacity. Then, one may use the obtained PDF (instead of the deterministic value of q_{ult}) in the macro-element formulation.
- Explore new methodologies which may improve the meta-model in the case of highly nonlinear models.

REFERENCES

1. Ahmadi, G. (1979). "Generation of artificial time-histories compatible with given response spectra-a review." *Solid Mechanics Archives*, **4:** 207-239.

2. Ahmed, A., and Soubra, A.H. (2012). "Probabilistic analysis of strip footings resting on a spatially random soil using subset simulation approach." *Georisk: Assessment and Management of Risk for Engineered Systems and Geohazards*, **6(3):** 188-201.

3. Ahmed, A. (2012). "Simplified and Advanced Approaches for the Probabilistic Analysis of Shallow Foundations." *PhD. Thesis*, University of Nantes, France.

4. Al-Bittar, T., and Soubra, A.H. (2011). "Bearing capacity of strip footing on spatially random soils using sparse polynomial chaos expansion." *GeoRisk (GSP 224), ASCE*, Atlanta, USA, 26-28 June 2011.

5. Al-Bittar, T., and Soubra, A.H. (2012a). "Bearing capacity of strip footing on spatially random soils using sparse polynomial chaos expansion." *International Journal for Numerical and Analytical Methods in Geomechanics*, DOI: 10.1002/nag.2120.

6. Al-Bittar, T., and Soubra, A.H. (2012b). "Analysis at the serviceability limit state of strip footings resting on spatially varying soils using sparse polynomial chaos expansion." *Journal of Geotechnical and Geoenvironmental Engineering, ASCE*, under review.

7. Al-Bittar, T., and Soubra, A.H. (2012c). "Bearing capacity of spatially random rock masses obeying Hoek-Brown failure criterion." *International Journal of Rock Mechanics and Mining Sciences,* under review.

8. Al-Bittar, T., and Soubra, A.H. (2012d). "Effect of the soil spatial variability in three dimensions on the undrained bearing capacity of footings." *Géotechnique*, under revision.

9. Al-Bittar, T., and Soubra, A.H. (2012e). "Efficient sparse polynomial chaos expansion methodology for the probabilistic analysis of computationally-expensive deterministic models." *International Journal for Numerical and Analytical Methods in Geomechanics,* under review.

10. Al-Bittar, T., and Soubra, A.H. (2012f). "Efficient sparse polynomial chaos expansion methodology for computationally expensive deterministic models." *Proceedings of the 5th International Conference on Reliable Engineering Computing: Practical Applications and Practical Challenges,* Brno, Czech Republic, 13–15 June 2012.

11. Al-Bittar, T., and Soubra, A.H. (2012g). "Calcul probabiliste de la portance des fondations superficielles par l'utilisation du chaos polynomial creux et de l'analyse de sensibilité globale." *Compte-rendu des 7èmes Journées Nationales sur la Fiabilité*, Chambéry, France, 4-6 Juin 2012.

12. Al-Bittar, T. (2012). "Calcul de la capacité portante ultime des fondations superficielles filantes avec prise en compte de la variabilité spatiale." *Concours Jeunes Chercheurs, obtention du 4ème prix. XXXe Rencontres AUGC-IBPSA*, Chambéry, Savoie, 6-8 juin 2012.

13. Al-Bittar, T., Youssef Abdel-Massih, D., Soubra, A.H., and Hage-Chehade. F. (2012a). “Influence of soil spatial variability and stochastic ground-motion on the dynamic behavior of a slope.” *Geocongress, State of the Art and Practice in Geotechnical Engineering, ASCE,* Oakland, CA, USA, 25-29 March 2012.

14. Al-Bittar, T., Kotronis, P., Grange, S., and Soubra, A.H. (2012b). “Probabilistic dynamic analysis of a soil-structure system subjected to a stochastic earthquake Ground-Motion.” *Proceedings of the 10th World Congress on Computational Mechanics, WCCM*, São Paulo, Brazil, 8-13 July 2012.

15. Au, S.K., and Beck, J.L. (2001). “Estimation of small failure probabilities in high dimensions by subset simulation.” *Probabilistic Engineering Mechanics*, **16:** 263-277

16. Baecher, G.B., and Christian, J.T. (2003). “Reliability and statistics in geotechnical engineering.” *John Wiley & Sons Ltd, The Atrium, Southern Gate, Chichewter, West Sussex PO19 8SQ, England*, 205-242.

17. Baecher, G.B., Marr, W.A., Lin, J.S., and Consla, J. (1983). “Critical parameters of mine tailings embankments.” *Denver, CO, U.S.,* Bureau of Mines.

18. Barton, R.R. (1992). “Metamodels for Simulation Input-Output Relations.” *Proceedings of the 1992 Winter Simulation Conference*. Swain, J. J., et al. (eds.), Arlington, VA: 289-299.

19. Bauer, J. and Pula, W. (2000). “Reliability with respect to settlement limit-states of shallow foundations on linearly-deformable subsoil.” *Computers and Geotechnics,* **26:** 281-308.

20. Berveiller, M., Sudret, B., and Lemaire, M. (2006). "Stochastic finite element: a non intrusive approach by regression." *Revue Européenne de Mécanique Numérique,* **15(1-2-3):** 8-92.

21. Blatman, G., (2009). “Adaptive sparse polynomial chaos expansions for uncertainty propagation and sensitivity analysis.” *Ph.D thesis*, Université Blaise Pascal, Clermont-Ferrand.

22. Blatman, G., and Sudret, B. (2010). “An adaptive algorithm to build up sparse polynomial chaos expansions for stochastic finite element analysis.” *Probabilistic Engineering Mechanics,* **25:** 183–97.

23. Blatman, G., and Sudret, B. (2011). “Adaptive sparse polynomial chaos expansion based on least angle regression.” *Journal of Computational Physics,* **230:** 2345–2367.

24. Blatman, G., and Sudret, B. (2011). “Principal component analysis and Least Angle Regression in spectral stochastic finite element analysis.” *Applications of Statistics and Probability in Civil Engineering*. 669-676.

25. Booker, A.J., Dennis, J.E., Frank, P.D., Serafini, D.B., Torczon, V., and Trosset, M.W. (1999). “A rigorous framework For optimization of expensive functions by surrogates.” *Structural Optimization*, **17:** 1-13.

26. Bourdeau, C. (2005). “Effet de site et mouvements de versant en zones sismiques: apport de la modélisation numérique.” *Ph.D thesis,* Ecole de mines de Paris, 266 p.

27. Box, G.E.P., Hunter, W.G., and Hunter, J.S. (1978). “Statistics for experimenters.” *John Wiley and Sons.*

28. Box, G.E.P., and Jenkins, G.M. (1970). “Time series analysis: forecasting and control.” *Holden-Day, San Fransisco,* 553 p.

29. Breysse, D., and Kastner, R. (2003). “Sols urbains.” *Hermès Science Publications*, 462 pages.

30. Breysse, D., Niandou, H., Elchachi, S.M., and Houy, L. (2005). “Generic approach of soil-structure interaction considering the effects of soil heterogeneity.” Symposium in print "Risk and variability in geotechnical engineering", *Geotechnique,* **2:** 143-150.

31. Breysse, D., La Borderie, C., Elchachi, S.M., and Niandou, H. (2007). “Spatial variations in soil properties and their consequences on structural reliability.” *Civil Engineering and Environmental Systems,* **4(2):** 73-83.

32. Breysse, D. (2011). “Reliability of a shallow foundation footing.” Chap. 6, pp. 97-118, in Baroth, J., Breysse, D., Schoefs, F., Construction reliability: safety, variability and sustainability, ISTE Wiley.

33. Brown, E.T. (2008). “Estimating the mechanical properties of rock masses.” In: Potvin Y, Carter J, Dyskin A, Jeffrey R, editors. *Proceedings of the 1st southern hemisphere international rock mechanics symposium: SHIRMS 2008,* Perth, Western Australia, **1:** 3-21.

34. Bucher, C.G. and Bourgund, U. (1990). “A fast and e_cient response surface approach for structural reliability problems.” *Structural Safety,* **7:** 57-66.

35. CAMUS International Benchmark. (1997). “Mock-up and loading characteristics, specifications for the participants report.” *Report I, CEA and GEO*.

36. Caniou, Y.; Sudret, B. and Micol, A. (2012). “Analyse de sensibilité globale pour des variables corrélées -- Application aux modèles imbriqués et multiéchelles.” *Compte-rendu des 7èmes Journées Nationales sur la Fiabilité*, Chambéry, France, 4-6 Juin 2012.

37. Cassidy, M.J., Byrne, B.W,, Houlsby, G.T. (2002). “Modelling the behaviour of circular footings under combined loading on loose carbonate sand.” *Géotechnique*, **52(10):**705–712.

38. Chen, W.F., and Sawada, T. (1983). “Earthquake-induced slope failure in nonhomogeneous, anisotropic soils.” *Soils and Foundations*, **23(2):** 125-139.

39. Cherubini, C. (2000), “Reliability evaluation of shallow foundation bearing capacity on c', φ' soils.” *Canadian Geotechnical Journal,* **37:** 264-269.

40. Cherubini, C., Giasi, I., and Rethati, L. (1993). “The coefficient of variation of some geotechnical parameters.” *Probabilistic Methods in Geotechnical Engineering.* Edited by Li, K.S., and Lo, S-C.R., A.A. Balkema, Rotterdam, 179-183.

41. Ching, J., Hu, Y.G., Yang, Z.Y., Shiau, J.Q., Chen, J.C., and Li, Y.S. (2011). “Reliability-based design for allowable bearing capacity of footings on rock masses by considering

angle of distortion." *International Journal of Rock Mechanics and Mining Sciences,* **48:** 728-740.

42. Cho, S.E., and Park, H.C. (2010). "Effect of spatial variability of cross-correlated soil properties on bearing capacity of strip footing." *International Journal for Numerical and Analytical Methods in Geomechanics,* **34:** 1-26.

43. Conte, JP., Pister, KS., Mahin, SA. (1992). "Nonstationary ARMA modeling of seismic motions." *Soil Dynamics and Earthquake Engineering,* **11:** 411-426.

44. Conte, JP., and Peng, BF. (1997). "Fully nonstationary analytical earthquake ground-motion model." *Journal of Engineering Mechanics (ASCE)*, **12:** 15-24.

45. Cornell, CA. (1960). "Stochastic process models in structural engineering." *Technical Report No. 34,* Department of Civil Engineering, Stanford University, Stanford, CA.

46. Crémer, C., Pecker, A., and Davenne, L. (2001). "Cyclic macro-element for soil–structure interaction: material and geometrical non-linearities." *International Journal for Numerical and Analytical Methods in Geomechanics*, **25(13):** 1257–1284.

47. Crémer, C., Pecker, A., and Davenne, L. (2002). "Modelling of nonlinear dynamic behaviour of a shallow strip foundation with macro-element." *Journal of Earthquake Engineering*, **6(2):**175–211.

48. Da Veiga, S.; Wahl, F. and Gamboa, F. (2009). "Local polynomial estimation for sensitivity analysis on models with correlated inputs." *Technometrics,* **51:** 452-463

49. Der Kiureghian, A., and Ditlevsen, O. (2009). "Aleatory or epistemic? Does it matter?" *Structural Safety*, **31(2):** 105-112.

50. Der Kiureghian, A., and Ke, J.-B. (1988). "The stochastic finite element method in structural reliability." *Probabilistic Engineering Mechanics,* **3(2):** 83-91.

51. Der Kiureghian, A., and Crempien, J. (1989). "An evolutionary model for earthquake ground motion." *Structural Safety*; **6:** 235-246.

52. Ditlevsen, O. (1996). "Dimension reduction and discretization in stochastic problems by regression method." *in F. Casciati and B. Roberts, Editors, Mathematical models for structural reliability analysis,* CRC Mathematical Modelling Series, 2, 51-138.

53. Duncan, J.M. (2000). "Factors of safety and reliability in geotechnical engineering." *Journal of Geotechnical and Geoenvironmental Engineering, ASCE,* **126(4):** 307-316.

54. Ejezie, S., and Harrop-Williams, K. (1984). "Probabilistic characterization of Nigerian soils." *In Probabilistic Characterization of Soil Properties, Bridge Between Theory and Practice,* ASCE, 140-156.

55. El-Ramly, H., Morgenstern, N.R., and Cruden, D.M. (2003). "Probabilistic stability analysis of a tailings dyke on presheared clay-shale." *Canadian Geotechnical Journal,* **40:** 192-208.

56. Fenton, G.A., (1999). “Estimation for stochastic soil models.” *Journal of Geotechnical and Geoenvironmental Engineering, ASCE,* **125(6):** 470-485.

57. Fenton, G.A., and Griffiths, D.V. (2002), “Probabilistic foundation settlement on spatially random soil.” *Journal of Geotechnical and Geoenvironmental Engineering, ASCE,* **128(5):** 381-390.

58. Fenton, G.A., and Griffiths, D.V. (2003). "Bearing capacity prediction of spatially random c-φ soils." *Canadian Geotechnical Journal,* **40:** 54-65.

59. Fenton, G.A., and Griffiths, D.V. (2005). “Three-dimensional probabilistic foundation settlement.” *Journal of Geotechnical and Geoenvironmental Engineering, ASCE,* **131(2):** 232-239.

60. Fenton, G.A., Zhou, H., Jaksa, M.B., and Griffiths, D.V. (2003). “Reliability analysis of a strip footing designed against settlement.” *Applications of statistics and probability in civil engineering, Der Kiureghian, Madanat & Pestana (eds) © 2003 Millpress, Rotterdam.*

61. Fredlund, D.G., and Dahlman, A.E. (1972). “Statistical geotechnical properties of glacial lake Edmonton sediments.” *In Statistics and Probability in Civil Engineering,* Hong Kong University Press.

62. Ghanem, R., and Spanos, P. (1991). “Stochastic finite elements – A spectral approach.” *Springer, New York.*

63. Goovaerts, P. (1998). “Geostatistical tools for characterizing the spatial variability of microbiological and physico-chemical soil properties.” *Biol Fertil Soils*, **27:** 315–334.

64. Goovaerts, P. (1999). “Geostatistics in soil science: state-of-the-art and perspectives.” *Geoderma*, **89:** 1-45.

65. Gourvenec, S., Randolph, M. F., and Kingsnorth, O. (2006). “Undrained bearing capacity of square and rectangular footings.” *Internatinal Jounal of Geomechanics*, **6(3):** 147–157.

66. Grange, S., Kotronis, P., and Mazars, J. (2009a). “A macro-element to simulate 3D soil–structure interaction considering plasticity and uplift.” *International Journal of Solids and Structures*, **46:** 3651–3663.

67. Grange, S., Kotronis, P., and Mazars, J (2009b). “A macro-element to simulate dynamic Soil-Structure Interaction.” *Engineering Structures*, **31:** 3034–3046

68. Grange, S. (2008). “Risque sismique: stratégie de modélisation pour simuler la réponse des structures en béton et leurs interactions avec le sol.” *Ph.D thesis*, INPG.

69. Griffiths, D.V., and Fenton, G.A. (2001). “Bearing capacity of spatially random soil. The undrained clay Prandtl problem revisited.” *Géotechnique*, **51(4):** 351-359.

70. Griffiths, D.V., Fenton, G.A., and Manoharan, N. (2002). “Bearing capacity of rough rigid strip footing on cohesive soil: Probabilistic study.” *Journal of Geotechnical and Geoenvironmental Engineering, ASCE*, **128(9):** 743-755.

71. Griffiths, DV., Huang, J., and Fenton, GA. (2009). “On the reliability of earth slopes in three dimensions.” *Proceedings of the Royal Society A,* **465**: 3145-3164.

72. Gunsallus, KL., and Kulhawy, F.H. (1984) “A comparative evaluation of rock strength measures.” *International Journal of Rock Mechanics and Mining Sciences & Geomechanics Abstracts*, **21:** 233-248.

73. Harr, M.E. (1987). “Reliability-based design in civil engineering.” *McGraw-Hill Book Company*, New York, 290p.

74. Hoek, E. (1998). “Reliability of Hoek-Brown estimates of rock mass properties and their impact on design.” *International Journal of Rock Mechanics and Mining Sciences*, **35(1):** 63-68.

75. Hoek, E., and Brown, E. (1980). “Empirical strength criterion for rock masses.” *Journal of the Geotechnical Engineering Division*, **106:** 1013-35.

76. Hoek, E., Carranze-Torres, C., and Corkum, B. (2002). “Hoek-Brown failure criterion.” 2002 edition. In: Proceeding of the North American rock mechanics society meeting, Toronto, July,. 267-73.

77. Hoek, E., and Marinos, P. (2007). “A brief history of the development of the Hoek-Brown failure criterion.” *Soils Rocks*, **30(2):** 85-92.

78. Honjo, Y. (2008). “Monte Carlo Simulation in reliability analysis.” *In: Phoon, K.K., ed. Reliability-based design in Geotechnical Engineering:* Computations and applications. Taylor & Francis: 169-171.

79. Houmadi, Y., Ahmed, A., and Soubra, A.-H. (2012). “Probabilistic analysis of a one-dimensional soil consolidation problem.” *Georisk: Assessment and Management of Risk for Engineered Systems and Geohazards,* **6 (1):** 36-49.

80. Huang, S., Liang, B., and Phoon, K.K. (2009). "Geotechnical probabilistic analysis by collocation-based stochastic response surface method: An EXCEL add-in implementation." *Georisk: Assessment and Management of Risk for Engineered Systems and Geohazards,* **3(2):** 75-86.

81. Isukapalli, S.S. (1999). “Uncertainty analysis of transport-transformation models.” *Ph.D thesis*, the state university of New Jersey.

82. Isukapalli, S.S., Roy, A., and Georgopoulos, P.G. (1998). “Stochastic response surface methods (SRSMs) for uncertainty propagation: Application to environmental and biological systems.” *Risk Analysis,* **18(3):** 357-363.

83. Itasca. (2000). “FLAC 4.0 Manuals.” **–** Minnesota, ITASCA Consulting Group, Inc 2000.

84. Jaksa, M.B. (1995). “The influence of spatial variability on the geotechnical design properties of a stiff, overconsolidated clay.” *Ph.D. Thesis*, Faculty of Engineering, University of Adelaide.

85. Jimenez, R., and Sitar, N. (2009). “The importance of distributions types on finite element analyses of foundation settlement.” *Computers and Geotechnics*, **36:** 474-483.

86. Jin, Y. (2005). “A comprehensive survey of fitness approximation in evolutionary computation.” *Soft Computing - A Fusion of Foundations, Methodologies and Applications*, **9(1):** 3-12.

87. Journel, A.G., and Huijbregts, Ch J. (1978). “Mining Geostatistics.” *Academic Press*.

88. Kausel, E., Whitman, A., Murray, J., and Elsabee, F. (1978). “The spring method for embedded foundations.” *Nuclear Engineering and Design*, **48:** 377-392.

89. Koutsourelakis, S., Prevost, J.H., and Deodatis, G. “Risk assessement of an interacting structure-soil system due to liquefaction.” *Earthquake Engineering and Structural Dynamic*, **31:** 851-879.

90. Kozin, F. (1988). “Autoregressive moving average models of earthquake records.” *Probabilistic Engineering Mechanics*, **3:** 58-63.

91. Kramer, S. L. (1996). “Geothechnical earthquake engineering.” *Prentice Hall*, New Jersey.

92. Kucherenko, S., Tarantola, A. and Annoni, P. (2012). “Estimation of global sensitivity indices for models with dependent variables.” *Computer Physics Communications*, **183:** 937-946

93. Kuhlemeyer, R. L., and Lysmer, J. (1973). “Finite element method accuracy for wave propagation problems.” *Journal of Soil Mechanics & Foundations*, **99:** 421-427.

94. Lacasse, S., and Nadim, F. (1996). “Uncertainties in characterizing soil properties.” *Uncertainty in the Geologic Environment, ASCE*, Madison, 49-75.

95. Lee, I.K., White, W., and Ingles, O.G. (1983). “Geotechnical Engineering.” *Pitman, London, England.*

96. Leshchinsky, D., and San, K.C. (1994). “Pseudostatic seismic stability of slopes: Design charts.” *Journal of Geotechnical Engineering, ASCE*, **120(9):** 1514-1532.

97. Li, C.C., and Der Kiureghian, A. (1993). “Optimal discretization of random fields.” *Journal of Engineering Mechanics*, **119(6):** 1136-1154.

98. Li, D., Chen, Y., Lu, W., and Zhou, C. (2011). “Stochastic response surface method for reliability analysis of rock slopes involving correlated non-normal variables.” *Computers. and Geotechnics*, **38(1):** 58-68.

99. Li, G., Rabitz, H., Yelvington, P., Oluwole, O., Bacon, F.; Kolb, C. and Schoendorf, J. (2010). “Global sensitivity analysis for systems with independent and/or correlated inputs.” *The Journal of Physical Chemistry*, **114:** 6022-6032

100. Liu, S.C. (1970). “Synthesis of stochastic representations of ground motions.” *The Bell Systems Technical Journal*, **49:** 521-541.

101. Liu, W.-K., Belytschko, T., and Mani, A. (1986a). “Probabilistic finite elements for non linear structural dynamics.” *Computer Methods in Applied Mechanics and Engineering*, **56:** 61-86.

102. Liu, W.-K., Belytschko, T., and Mani, A. (1986b), "Random field finite elements." *International Journal for Numerical Methods in Engineering,* **23(10):** 1831-1845.

103. Lopez-Caballero, F., and Modaressi Farahmand-Razavi, A. (2010). "Assessment of variability and uncertainties effects on the seismic response of a liquefiable soil profile." *Soil Dynamics and Earthquake Engineering,* **30(7):** 600-613.

104. Loukidis, D., Bandini, P., and Salgado, R. (2003). "Stability of seismically loaded slopes using limit analysis." *Géotechnique,* **53(5):** 463-479.

105. Lumb, P. (1966). "The variability of natural soils." *Canadian Geotechnical Journal,* **3:** 74-97.

106. Lumb, P. (1970). "Safety factors and the probability distribution of soil strength." *Canadian Geotechnical Journal,* **7:** 225-242.

107. Lumb, P. (1972). "Precision and accuracy of soil tests." *In Statistics and Probability in Civil Engineering,* Hong Kong University Press.

108. Mao, N., Al-Bittar, T., and Soubra, A.-H. (2011). "Probabilistic analysis of shallow foundations on rocks obeying Hoek-Brown failure criterion." *GeoRisk (GSP 224), ASCE,* Atlanta, USA, 26-28 June.

109. Mao, N., Al-Bittar, T., and Soubra, A.-H. (2012). "Probabilistic analysis and design of strip foundations resting on rocks obeying Hoek-Brown failure criterion." *International Journal of Rock Mechanics and Mining Sciences,* **49:** 45–58.

110. Merifield, RS., Lyamin, AV., and Sloan, SW. (2006). "Limit analysis solutions for the bearing capacity of rock masses using the generalized Hoek-Brown criterion." *International Journal of Rock Mechanics and Mining Sciences*, **43:** 920-937.

111. Michalowski, R.L. (2002). "Stability charts for uniform slopes." *Journal of Geotechnical and Geoenvironmental Engineering, ASCE,* **128(4):** 351-355.

112. Mollon, G., Dias, D., and Soubra, A.-H. (2011). "Probabilistic analysis of pressurized tunnels against face stability using collocation-based stochastic response surface method." *Journal of Geotechnical and Geoenvironmental Engineering, ASCE*, **137(4):** 385-397.

113. Morse, R.K. (1972). "The importance of proper soil units for statistical analysis." *In Statistics and Probability in Civil Engineering,* Hong Kong University Press.

114. Myers, R.H., and Montgomery, D.C. (1995). "Response surface methodology: process and product optimization using designed experiments." *Wiley and Sons*.

115. Nataf, A. (1962). "Détermination des distributions de probabilités dont les marges sont données." *CR Acad Sci*, **225:** 42-3 (in French).

116. Niandou, H., and Breysse, D. (2007). "Reliability analysis of a piled raft accounting for soil spatial variability." *Computer and Geotechnics*, **34:** 71-80.

117. Nour, A., Slimani, A. and Laouami N. (2002). "Foundation settlement statistics *via* finite element analysis." *Computers and Geotechnics,* **29:** 641–672.

118. Nour, A., Slimania, A., Laouamia, N., and Afraa, H. (2003). “Finite element model for the probabilistic seismic response of heterogeneous soil profile.” *Soil Dynamics and Earthquake Engineering*, **23:** 331-348.

119. Nova, R., and Montrasio, L. (1991). “Settlements of shallow foundations on sand.” *Géotechnique*, **41(2):** 243 256.

120. Papadimitriou, K. (1990). “Stochastic characterization of strong ground motion and application to structural response.” *Report No. EERL 90-03*, Earthquake Engineering Research Laboratory, California Institute of Technology, Pasadena, CA.

121. Pecker, A. (1984). “Dynamique des Sols.” *Presse*, ENPC: Paris, France.

122. Phoon, K.K., and Kulhawy, F.H., (1999). “Evaluation of geotechnical property variability.” *Canadian Geotechnical Journal,* **36:** 625-639.

123. Phoon, K.K., Kulhawy, F.H., and Grigoriu, M.D. (1995). “Reliability-based design of foundations for transmission line structures.” *Rpt. TR-105000*, Electric Power Research Inst., Palo Alto (CA), 380p.

124. Popescu, R., Deodatis, G., and Nobahar, A. (2005). “Effect of random heterogeneity of soil properties on bearing capacity.” *Probabilistic Engineering Mechanics*, 20: 324-341.

125. Popescu, R., Prevost, J.H., and Deodatis, G. (2005). “3D effects in seismic liquefaction of stochastically variable soil deposits.” *Géotechnique*, **55(1)**: 21-31.

126. Popescu, R., Prevost, J.H., Deodatis, G., and Chakrabortty, P. (2006). “Dynamics of nonlinear porous media with applications to soil liquefaction.” *Soil Dynamics and Earthquake Engineering*, **26(6-7):** 648-665.

127. Prévost, J.H. (1999). “DYNAFLOW. A finite element analysis program for static and transient response of linear and nonlinear two and three dimensional systems.” *User Manual*, Department of Civil Engineering, Princeton University.

128. Rezaeian, S., and Der Kiureghian, A. (2008). “A stochastic ground motion model with separable temporal and spectral nonstationarity.” *Earthquake Engineering and Structural Dynamics*, **37:** 1565-1584.

129. Rezaeian, S., and Der Kiureghian, A. (2010). “Simulation of synthetic ground motions for specified earthquake and site characteristics.” *Earthquake Engineering and Structural Dynamics*, **39:** 1155-1180.

130. Sacks, J., Welch, W. J., Mitchell, T. J. and Wynn, H. P. (1989). “Design and analysis of computer experiments.” *Statistical Science*, **4(4):** 409-435.

131. Sadek, M., and Shahrour, I. (2004). “Three-dimensional finite element analysis of the seismic behavior of inclined micropiles.” *Soil Dynamics and Earthquake Engineering*, **24(6):** 473-485.

132. Sadek, M. (2012). “Problèmes d'Interaction Sol Structure sous chargements statique et dynamique. ” Laboratoire Génie Civil et géo-Environnement, Université Lille 1, France.

133. Saltelli, A., Chan, K., and Scott, E. M. (2000). “Sensitivity Analysis.” *John wiley and sons.*

134. Shinozuka, M., and Deodatis, G. (1988). “Stochastic process models for earthquake ground motion.” *Probabilistic Engineering Mechanics,* **3:** 114-123.

135. Shinozuka, M., and Sato, Y. (1967). “Simulation of nonstationary random process.” *Journal of Engineering Mechanics (ASCE),* **93:** 11-40.

136. Sobol, I.M. (2001). “Global sensitivity indices for nonlinear mathematical models and their Monte Carlo estimates.” *Mathmatics and Computers in Simulation,* **55:** 271-280.

137. Soubra, A.-H., Youssef Abdel Massih, D., and Kalfa, M. (2008). “Bearing capacity of foundations resting on a spatially random soil.” *GeoCongress 2008, ASCE,* GSP N° 178, New Orleans, Louisiana, USA, 9-12 March, 66-73.

138. Spanos, P.D., and Ghanem, R. (1989). “Stochastic finite element expansion for random media.” *Journal of Engineering Mechanics, ASCE,* **115(5):** 1035-1053.

139. Stuedlein, A.,W., Kramer, S., and Arduino, P. (2012). “Geotechnical characterization and random field modeling of desiccated clay.” *Journal of Geotechnical and Geoenvironmental Engineering, ASCE,* http://dx.doi.org/10.1061/(ASCE)GT.1943-5606.0000723

140. Sudret, B. (2008). “Global sensitivity analysis using polynomial chaos expansion.” *Reliability Engineering and System Safety,* **93**: 964-979.

141. Sudret, B., and Berveiller, M. (2008). “Stochastic finite element methods in geotechnical engineering.” *In: Phoon, K.K., ed. Reliability-Based design in Geotechnical Engineering:* Computations and applications. Taylor & Francis: 260-296.

142. Sudret, B., and Der Kiureghian, A. (2000). “Stochastic finite element methods and reliability: A State-of-the-Art Report.” *Report No. UCB/SEMM-2000/08 Structural Engineering, Mechanics and Materials Department of Civil & Environmental Engineering, University of California,* Berkeley

143. Sudret, B., Berveiller, M., and Lemaire, M. (2006). “A stochastic finite element procedure for moment and reliability analysis.” *Eur. J. Comput. Mech.,* **15 (7-8):** 825–866.

144. Uzielli, M.,Vannucchi, G., and Phoon, K.K. (2005). “Normal field characterization of stress-normalised cone penetration testing parameters.” *Geotechnique,* **55(1):** 3-20.

145. Vanmarcke, E.H. (1977). “Probabilistic modeling of soil profiles.” *Journal of the Geotechnical Engineering Division, ASCE,* **103(11):** 1227-1246.

146. Vanmarcke, E.H. (1983). “Random fields: Analysis and synthesis.” M.I.T, *Press, Cambridge, Mass.,* 382 p.

147. Vanmarcke, E., and Grigoriu, M., (1983). “Stochastic finite analysis of simple beams.” *Journal of Engineering Mechanics,* **109:** 1203-1214.

148. Vořechovský, M. (2008). “Simulation of simply cross-correlated random fields by series expansion methods.” *Structural Safety,* **30:** 337-363.

149. Wang, S., and Hao, H. (2002). “Effects of random variations of soil properties on site amplification of seismic ground motions.” *Soil Dynamics and Earthquake Engineering,* **22(7):** 551-564.

150. Widmer, F., Duvernay, B., Fäh, D., and Parriaux, A. (2003). “Projet pilote de microzonage sismique à Yverdon (VD).” *Bulletin for Applied Geology,* **8:** 5-16.

151. Wolff, T.H. (1985). “Analysis and design of embankment dam slopes: A probabilistic approach." *Ph.D thesis, Purdue Univ., Lafayette, Ind.*

152. Wolff, T.H. (1996). “Probabilistic slope stability in theory and practice.” *Uncertainty in Geological Environment, Madison, WI,* ASCE, 419-433.

153. Xiu, D., and Karniadakis, G.E. (2002). “The Wiener-Askey polynomial chaos for stochastic differential equations.” *SIAM J. on Scientific Computing,* **24(2):** 619-44.

154. You, L., and Michalowski, R.L. (1999). “Displacement charts for slopes subjected to seismic loads.” *Computers and Geotechnics,* **25(4):** 45-55.

155. Youssef Abdel Massih, D. (2007). “Analyse du comportement des fondations superficielles filantes par des approches fiabilistes.” *Ph.D thesis,* university of Nantes, France.

156. Yuceman, M.S., Tang, W.H. and Ang, A.H.S. (1973). “A probabilistic study of safety and design of earth slopes.” *Civil Engineering Studies, Structural Research Series 402,* University of Illinois, Urbana.

157. Zerva, A. (2009). “Spatial variation of seismic Ground-Motions.” *Haym Benaroya*.

158. Zerva, A. (1988). “Seismic source mechanisms and ground motion models, review paper.” *Probabilistic Engineering Mechanics,* **3:** 64-74.

159. Zhang, J., and Ellingwood, B. (1994). “Orthogonal series expansion of random fields in reliability analysis.” *Journal of Engineering Mechanics, ASCE,* **120(12):** 2660-2677.

160. Zimbone, S.M., Vickers, A., Morgan, R.P.C., and Vella, P. (1996). “Field investigations of different techniques for measuring surface soil shear strength.” *Soil Technology,* **9:** 101-111.

Appendix A.

Weight functions and deterministic basis of the MP, SF, SA and OLE methods

Method	Weight function ω(X)	Deterministic basis $\varphi_j(X)$
MP	$\delta(X - X_c)$	$1_{\Omega_e}(X)$
SF	$\delta(X - X_j)$	$1_{\Omega_e}(X)$
SA	$\frac{1_{\Omega_e}(X)}{\lvert\Omega_e\rvert}$	Polynomial shape function $N_j(X)$
OLE	$\delta(X - X_j)$	$\left(\Sigma^{-1}_{\chi;\chi}.\Sigma_{Z(X);\chi}\right)_j$

Table A.1. Weight functions and deterministic basis of the MP, SF, SA and OLE methods

In Table A.1, X is the vector of the coordinates of an arbitrary point, X_c is the vector of the coordinates at the centroid element of the finite element/finite difference mesh, X_j is the vector of the coordinates at a node j in the SF method and at a the sample point j in the OLE method, $\delta(.)$ denotes the Dirac function, $1_{\Omega_e} = \begin{cases} 1 & X \in \Omega_e \\ 0 & otherwise \end{cases}$ and Ω_e is the mesh element.

Appendix B.

Generation of cross-correlated non-Gaussian random fields: The illustrative Example

In this illustrative example, one considers a soil for which the shear strength parameters (i.e. the cohesion c and the internal friction angle φ) are modeled as two anisotropic cross-correlated non-Gaussian random fields. These two random fields have the same square exponential autocorrelation function ρ^{NG} (c.f. Equation (I.8) with n=2) and a non-Gaussian cross-correlation matrix C^{NG} given as follows: $C^{NG} = \begin{bmatrix} 1 & -0.5 \\ -0.5 & 1 \end{bmatrix}$.

The soil cohesion c was assumed to be lognormally distributed. Its mean and coefficient of variation values were taken as follows: $\mu_c = 20kPa, Cov_c = 25\%$. On the other hand, the friction angle φ was assumed to have a Beta distribution with a mean value and a coefficient of variation given as follows: $\mu_\varphi = 30^o$, $Cov_\varphi = 10\%$. In this illustrative example, the soil domain was chosen to be small in order to handle small size matrices. For this purpose, the adopted soil domain considered in the analysis is 4m wide by 5m deep (i.e. x_{min}=0m, x_{max}=4m and y_{min}=0m, y_{max}=5m). As for the autocorrelation distances a_x and a_y, the horizontal autocorrelation distance a_x was chosen to be equal to 5m and the vertical autocorrelation distance a_y was fixed to 4m. A stochastic mesh composed of 3 points in both the horizontal and the vertical directions is chosen in this example (cf. Figure B.1).

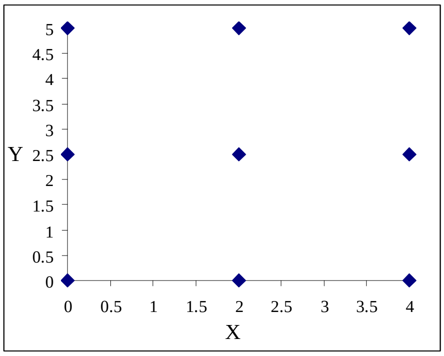

Figure B.1. The stochastic mesh used in the analysis

In order to discretize the two random fields of c and φ, one needs to perform the different steps described in section I.3.4.1 as follows:

a) Evaluate the common non-Gaussian autocorrelation matrix $\Sigma_{\chi\chi}^{NG}$ for which each row gives the correlation between a given gridpoint of the stochastic mesh with all the others gridpoints of this mesh using Equation (I.9). Table B.1 presents the common non-Gaussian autocorrelation matrix $\Sigma_{\chi\chi}^{NG}$ for the stochastic mesh presented in Figure B.1.

	(0,0)	(2.5,0)	(5,0)	(0,2)	(2.5,2)	(5,2)	(0,4)	(2.5,4)	(5,4)
(0,0)	1	0.779	0.368	0.779	0.606	0.286	0.368	0.286	0.135
(2.5,0)	0.779	1	0.779	0.606	0.779	0.606	0.286	0.368	0.286
(5,0)	0.368	0.779	1	0.286	0.606	0.779	0.135	0.286	0.368
(0,2)	0.779	0.606	0.286	1	0.779	0.368	0.779	0.606	0.286
(2.5,5)	0.606	0.779	0.606	0.779	1	0.779	0.606	0.779	0.606
(5,2)	0.286	0.606	0.779	0.368	0.779	1	0.286	0.606	0.779
(0,4)	0.368	0.286	0.135	0.779	0.606	0.286	1	0.779	0.368
(2.5,4)	0.286	0.368	0.286	0.606	0.779	0.606	0.779	1	0.779
(5,4)	0.135	0.286	0.368	0.286	0.606	0.779	0.368	0.779	1

Table B.1. The non-Gaussian autocorrelation matrix $\Sigma_{\chi;\chi}^{NG}$

b) Transform the common non-Gaussian autocorrelation matrix $\Sigma_{\chi\chi}^{NG}$ into the Gaussian space using Nataf correction functions (cf. Equation (I.19)). The obtained Gaussian autocorrelation matrices are respectively $\Sigma_{\chi;\chi}^{c}$ and $\Sigma_{\chi;\chi}^{\varphi}$. It should be mentioned here that both matrices $\Sigma_{\chi;\chi}^{c}$ and $\Sigma_{\chi;\chi}^{\varphi}$ were quasi-similar to $\Sigma_{\chi;\chi}^{NG}$ and thus the number of eigenmodes (number of random variables) which is necessary to discretize each one of the two random fields was similar. Tables B.2 and B.3 present respectively the matrices $\Sigma_{\chi;\chi}^{c}$ and $\Sigma_{\chi;\chi}^{\varphi}$ obtained after transforming the common non-Gaussian autocorrelation matrix into the Gaussian space.

	(0,0)	(2.5,0)	(5,0)	(0,2)	(2.5,2)	(5,2)	(0,4)	(2.5,4)	(5,4)
(0,0)	1	0.782	0.372	0.782	0.611	0.290	0.372	0.290	0.137
(2.5,0)	0.782	1	0.782	0.611	0.782	0.611	0.290	0.372	0.290
(5,0)	0.372	0.782	1	0.290	0.611	0.782	0.137	0.290	0.372
(0,2)	0.782	0.611	0.290	1	0.782	0.372	0.782	0.611	0.290
(2.5,5)	0.611	0.782	0.611	0.782	1	0.782	0.611	0.782	0.611
(5,2)	0.290	0.611	0.782	0.372	0.782	1	0.290	0.611	0.782
(0,4)	0.372	0.290	0.137	0.782	0.611	0.290	1	0.782	0.372
(2.5,4)	0.290	0.372	0.290	0.611	0.782	0.611	0.782	1	0.782
(5,4)	0.137	0.290	0.372	0.290	0.611	0.782	0.372	0.782	1

Table B.2. The Gaussian autocorrelation matrix $\Sigma_{\chi;\chi}^{c}$ of the cohesion random field obtained using the Nataf transformation

	(0,0)	(2.5,0)	(5,0)	(0,2)	(2.5,2)	(5,2)	(0,4)	(2.5,4)	(5,4)
(0,0)	1	0.779	0.368	0.779	0.607	0.287	0.368	0.287	0.135
(2.5,0)	0.779	1	0.779	0.607	0.779	0.607	0.287	0.368	0.287
(5,0)	0.368	0.779	1	0.287	0.607	0.779	0.135	0.287	0.368
(0,2)	0.779	0.607	0.287	1	0.779	0.368	0.779	0.607	0.287
(2.5,5)	0.607	0.779	0.607	0.779	1	0.779	0.607	0.779	0.607
(5,2)	0.287	0.607	0.779	0.368	0.779	1	0.287	0.607	0.779
(0,4)	0.368	0.287	0.135	0.779	0.607	0.287	1	0.779	0.368
(2.5,4)	0.287	0.368	0.287	0.607	0.779	0.607	0.779	1	0.779
(5,4)	0.135	0.287	0.368	0.287	0.607	0.779	0.368	0.779	1

Table B.3. The Gaussian autocorrelation matrix $\Sigma^{\varphi}_{\chi;\chi}$ of the friction angle random field obtained using the Nataf transformation

Then, for these two Gaussian autocorrelation matrices $\Sigma^{c}_{\chi;\chi}$ and $\Sigma^{\varphi}_{\chi;\chi}$ one needs to compute N largest eigenmodes λ^c_j, ϕ^c_j and $\lambda^{\varphi}_j, \phi^{\varphi}_j$ (where j=1,…, N) for which the variance of the error is smaller than a prescribed threshold (say $\varepsilon \approx 10\%$). In this illustrative example, N was found equal to 4 and thus only 4 eigenmodes were considered to be the most influent and their values are presented in Table B.4.

λ^c_1	λ^c_2	λ^c_3	λ^c_4	λ^{φ}_1	λ^{φ}_2	λ^{φ}_3	λ^{φ}_4
5.323	1.450	1.450	0.393	5.296	1.453	1.453	0.399
φ^c_1	φ^c_2	φ^c_3	φ^c_4	φ^{φ}_1	φ^{φ}_2	φ^{φ}_3	φ^{φ}_4
-0.291	0.459	-0.284	0.500	0.291	0.440	-0.312	0.500
-0.348	0.444	0.104	$-1.3\text{x}10^{-17}$	0.348	0.450	0.076	$7.7\text{x}10^{-17}$
-0.291	0.284	0.459	-0.500	0.291	0.312	0.440	-0.500
-0.348	0.104	-0.444	$4.4\text{x}10^{-17}$	0.348	0.076	-0.450	$-1.8\text{x}10^{-16}$
-0.417	$1.3\text{x}10^{-17}$	$3.8\text{x}10^{-17}$	$3.0\text{x}10^{-16}$	0.417	$-3.6\text{x}10^{-17}$	$6.5\text{x}10^{-18}$	$2.8\text{x}10^{-17}$
-0.348	-0.104	0.444	$3.9\text{x}10^{-17}$	0.348	-0.076	0.450	$-2.9\text{x}10^{-16}$
-0.291	-0.284	-0.459	-0.500	0.291	-0.312	-0.440	-0.500
-0.348	-0.444	-0.104	$-2.3\text{x}10^{-16}$	0.348	-0.450	-0.076	$2.2\text{x}10^{-16}$
-0.291	-0.459	0.284	0.500	0.291	-0.440	0.312	0.500

Table B.4. The eigenvalues and eigenvectors λ^c_j, ϕ^c_j and $\lambda^{\varphi}_j, \phi^{\varphi}_j$ of the matrices $\Sigma^{c}_{\chi;\chi}$ and $\Sigma^{\varphi}_{\chi;\chi}$ for an expansion order N=4

c) Transform the non-Gaussian cross-correlation matrix $C^{NG} = \begin{bmatrix} 1 & -0.5 \\ -0.5 & 1 \end{bmatrix}$ into the Gaussian space using the Nataf correction functions (cf. Equation (I.20)). The obtained Gaussian cross-correlation matrix is given as follows: $C = \begin{bmatrix} 1 & -0.504 \\ -0.504 & 1 \end{bmatrix}$. Its corresponding eigenvalues vector and eigenvectors matrix are given as follows: $\Lambda^C = \begin{bmatrix} 1.504 & 0 \\ 0 & 0.496 \end{bmatrix}$ and $\Phi^C = \begin{bmatrix} -0.7071 & -0.7071 \\ 0.7071 & -0.7071 \end{bmatrix}$, where the eigenvalues correspond the diagonal values of the matrix Λ^C and the eigenvectors correspond to the columns of the matrix Φ^C.

d) Simulate the vector κ^D composed of two cross-correlated blocks given by Equation (I.22) as follows: $\left(\kappa^D\right)^T = \Phi^D (\Lambda^D)^{1/2} \xi^T$ where Λ^D and Φ^D are the matrices obtained by multiplying each element of the matrices Λ^C and Φ^C by a unit matrix of dimension N=4, and ξ is a two-block vector of N=4 standard normal random variables $\xi = \left\{ \xi^c = \left(\xi_1^c, \xi_2^c, \xi_3^c, \xi_4^c\right), \xi^\varphi = \left(\xi_1^\varphi, \xi_2^\varphi, \xi_3^\varphi, \xi_4^\varphi\right) \right\}$. This simulation of standard normal random variables is performed using the (randn) command in MATLAB 7.0. A single simulation of this vector and its corresponding vector κ^D are presented in Table B.5 and evaluated as follows:

$$\left(\kappa^D\right)^T = \begin{bmatrix} -0.7071 \times \begin{bmatrix} 1&0&0&0\\0&1&0&0\\0&0&1&0\\0&0&0&1 \end{bmatrix} & -0.7071 \times \begin{bmatrix} 1&0&0&0\\0&1&0&0\\0&0&1&0\\0&0&0&1 \end{bmatrix} \\ 0.7071 \times \begin{bmatrix} 1&0&0&0\\0&1&0&0\\0&0&1&0\\0&0&0&1 \end{bmatrix} & -0.7071 \times \begin{bmatrix} 1&0&0&0\\0&1&0&0\\0&0&1&0\\0&0&0&1 \end{bmatrix} \end{bmatrix} \times \begin{bmatrix} 1.504 \times \begin{bmatrix} 1&0&0&0\\0&1&0&0\\0&0&1&0\\0&0&0&1 \end{bmatrix} & 0 \times \begin{bmatrix} 1&0&0&0\\0&1&0&0\\0&0&1&0\\0&0&0&1 \end{bmatrix} \\ 0 \times \begin{bmatrix} 1&0&0&0\\0&1&0&0\\0&0&1&0\\0&0&0&1 \end{bmatrix} & 0.496 \times \begin{bmatrix} 1&0&0&0\\0&1&0&0\\0&0&1&0\\0&0&0&1 \end{bmatrix} \end{bmatrix} \times \begin{bmatrix} \xi_1^c \\ \xi_2^c \\ \xi_3^c \\ \xi_4^c \\ \xi_1^\varphi \\ \xi_2^\varphi \\ \xi_3^\varphi \\ \xi_4^\varphi \end{bmatrix}$$

ξ	$\xi_1^c = 0.03$	$\xi_2^c = 0.55$	$\xi_3^c = 1.10$	$\xi_4^c = 1.54$	$\xi_1^\varphi =$ -1.49	$\xi_2^\varphi =$ -0.74	$\xi_3^\varphi =$ -1.06	$\xi_4^\varphi = 2.35$
κ^D	$\kappa_{c,1}^D = 0.72$	$\kappa_{c,2}^D =$ -0.11	$\kappa_{c,3}^D =$ -0.43	$\kappa_{c,4}^D =$ -2.51	$\kappa_{\varphi,1}^D = 0.77$	$\kappa_{\varphi,2}^D = 0.85$	$\kappa_{\varphi,3}^D = 1.48$	$\kappa_{\varphi,4}^D = 0.16$

Table B.5. Values of the vector of standard normal random variables ξ and the corresponding cross-correlated vector κ^D

d) Evaluate the values of the two Gaussian cross-correlated random fields c and φ at any arbitrary point (say x=1m, y=1m) which does not belong to the stochastic mesh by applying the formula given by Equation (I.21) as follows:

$$c(x=1,\ y=1) = \sum_{j=1}^{4} \frac{\kappa_{c,j}^D}{\sqrt{\lambda_j^c}} \cdot \left(\phi_j^c\right)^T . \Sigma_{Z(X);\chi}^c \quad \text{and} \quad \varphi(x=1,\ y=1) = \sum_{j=1}^{4} \frac{\kappa_{\varphi,j}^D}{\sqrt{\lambda_j^\varphi}} \cdot \left(\phi_j^\varphi\right)^T . \Sigma_{Z(X);\chi}^\varphi$$

where $\Sigma^{c}_{Z(X);\chi}$ and $\Sigma^{\varphi}_{Z(X);\chi}$ are the two correlation vectors between the arbitrary points (*x*=1m, *y*=1m) and all the other points of the stochastic mesh. Their values are the same in this illustrative example because the same arbitrary point (*x*=1m, *y*=1m) is used for the two random fields *c* and *φ* and they are presented in Table B.6.

	(0,0)	(2.5,0)	(5,0)	(0,2)	(2.5,2)	(5,2)	(0,4)	(2.5,4)	(5,4)
(1,1)	0.9026	0.8586	0.4953	0.9026	0.8586	0.4953	0.5474	0.5207	0.3004

Table B.6. Values of the correlation vectors $\Sigma^{c}_{Z(X);\chi}$ and $\Sigma^{\varphi}_{Z(X);\chi}$ between the arbitrary point (x=1m, y=1m) and all the points of the stochastic mesh

Finally the transformation to the non-Gaussian space is performed using the non-Gaussian distribution function of each random field (cf. Equation (I.23)).

Appendix C.

Determination of the stochastic model parameters

The used stochastic model is a parameterized modulated, filtered white-noise process for which the parameters are calculated by fitting this model to the real recorded target acceleration time history $a(t)$.

The time modulation function $q\ (\alpha, t\ )$ *and its parameters* $\alpha = (\alpha_1,\ \alpha_2,\ \alpha_3)$

The time modulation function given by Equation (I.26) is completely defined by three parameters $\alpha = (\alpha_1,\ \alpha_2,\ \alpha_3)$ which are related to three physically-based parameters $(\bar{I}_a,\ D_{5-95},\ t_{mid})$. The three physical parameters $(\bar{I}_a,\ D_{5-95},\ t_{mid})$ are calculated from the real target acceleration time-historey $a(t)$ as follows:

$$\bar{I}_a = \frac{\pi}{2g} \int_0^T \left[\ a(t)\ \right]^2\ dt \tag{C.1}$$

where g is the acceleration due to gravity and T is the duration of the ground-motion. On the other hand, t_{mid} is the time at the middle of the strong shaking; it corresponds to the time for which 45% of the total I_a is reached. Finally, $D_{5\text{-}95}$ is the effective duration of the target GM; it corresponds to the duration that ranges between 5% and 95% of I_a. Figure C.1 presents the identification of these physical parameters for the target acceleration time history.

For the selected modulation function given by Equation (I.26), Rezaeien and Der Kiureghian (2010) stated that the square value of this function (i.e. $q^2\ (\alpha, t\ )$) is proportional to a gamma probability density function (PDF) having parameter values $2\alpha_2 - 1$ and $2\alpha_3$. Let t_p represent the p-percentile variate of the gamma cumulative distribution function. Then, t_p is given in terms of the inverse of the gamma cumulative distribution function at probability value p%. It follows that t_p is uniquely given in terms of the parameters α_2 and α_3 and probability p%. Consequently, one can write:

$$D_{5-95} = t_{95} - t_5 = \text{Gaminv}(0.95,\ 2\alpha_2 - 1,\ \frac{1}{2\alpha_3}) - \text{Gaminv}(0.05,\ 2\alpha_2 - 1,\ \frac{1}{2\alpha_3}) \tag{C.2}$$

$$t_{mid} = t_{45} = \text{Gaminv}(0.45,\ 2\alpha_2 - 1,\ \frac{1}{2\alpha_3}) \tag{C.3}$$

For given values of D_{5-95} and t_{mid} computed from the target acceleration time-history, parameters α_2 and α_3 can be computed by solving the above two equations. Furthermore, one can easily show that α_1 is directly related to the expected Arias intensity as follows [Rezaeian and Der Kiureghian (2010)]:

$$\alpha_1 = \sqrt{\frac{\bar{I}_a \left(2\alpha_3\right)^{2\alpha_2 - 1}}{\Gamma\left(2\alpha_2 - 1\right)}} \tag{C.4}$$

where $\Gamma(.)$ is the gamma function.

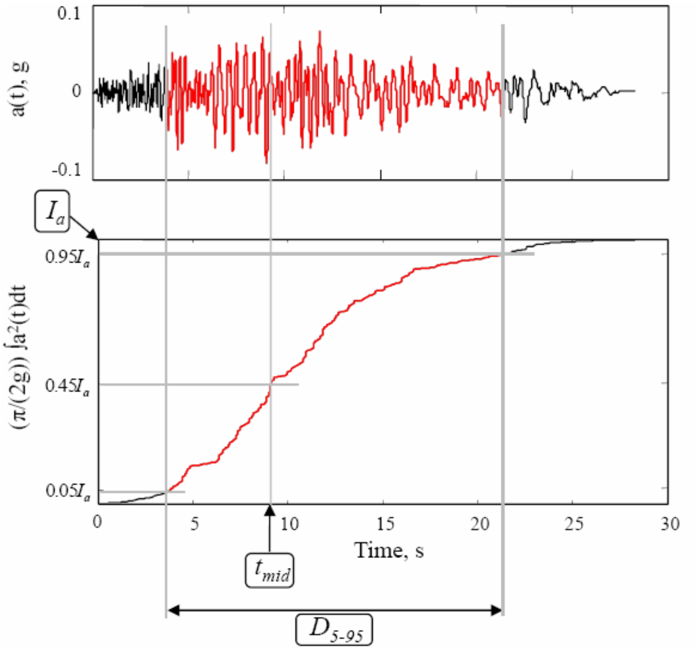

Figure C.1. Modulation function physical parameters identified from the target acceleration time-history a(t)

The Linear filter $h\left[t - t_i, \omega_f(t_i), \zeta_f(t_i)\right]$ *and its parameters* $\omega_f(t_i), \zeta_f(t_i)$

The linear filter function given by Equation (I.27) is completely defined by two parameters $\omega_f(\tau)$ and $\zeta_f(\tau)$ with $\omega_f(\tau)$ denoting the natural frequency and $\zeta_f(\tau)$ denoting the damping ratio, both dependent on the time of application of the pulse. Based on the analysis of a large number of accelerograms, a linear form is adopted for the filter frequency and a constant value is considered for the filter damping ratio as follows:

$$\omega_f(\tau) = \omega_{mid} + \omega'(\tau - t_{mid}) \tag{C.5}$$

$$\zeta_f(t_i) = \zeta_f \tag{C.6}$$

where ω_{mid} is the frequency at the middle of the strong shaking, ω' is the rate of change of the frequency over time (i.e. the slope) and t_{mid} is the time at the middle of the strong shaking.

The parameters ω_{mid}, $\omega^{'}$ and ζ_f have interacting influences. Thus, they cannot be identified independently for a target (real) accelerogram *a*(*t*). Therefore, we follow a procedure that first optimizes the frequency parameters ω_{mid} and $\omega^{'}$ by matching the cumulative count of zero-level up-crossings of the simulated and target motions (notice that the zero-level up-crossings are number of times per unit time that the process crosses the level zero from below [see Figure C.2]). Then use these optimum frequency parameters ω_{mid} and $\omega^{'}$ with a series of constant damping ratio (i.e. $\zeta_f = 0.1, 0.2, ..., 0.9$) and select the optimum damping ratio for which the cumulative count of positive minima and negative maxima of the simulated and target motions fit the most.

For a target acceleration time-history *a*(*t*), the cumulative count of zero-level up-crossings is fitted by a second degree polynomial ($p = p_1 x^2 + p_2 x + p_3$) as shown in Figure C.3(a). The frequency parameters ω_{mid} and $\omega^{'}$ are deduced from the fitted polynomial as follows:

$$\omega_{mid} = 2p_1(t_{mid}) + p_2 \text{ and } \omega^{'} = 2p_1 \tag{C.7}$$

After determining the frequency parameters ω_{mid} and $\omega^{'}$, we generate filtered processes using the frequency parameters ω_{mid} and $\omega^{'}$ with a series of constant damping ratio (i.e. $\zeta_f = 0.1, 0.2, ..., 0.9$) and see for which value of the damping ratio the cumulative count of positive minima and negative maxima of the simulated and target motions fit the most [see Figure C.3(b)]. One can see from Figure C.3(b) that the target cumulative count of positive minima and negative maxima fits the simulated one for $\zeta_f = 0.4$.

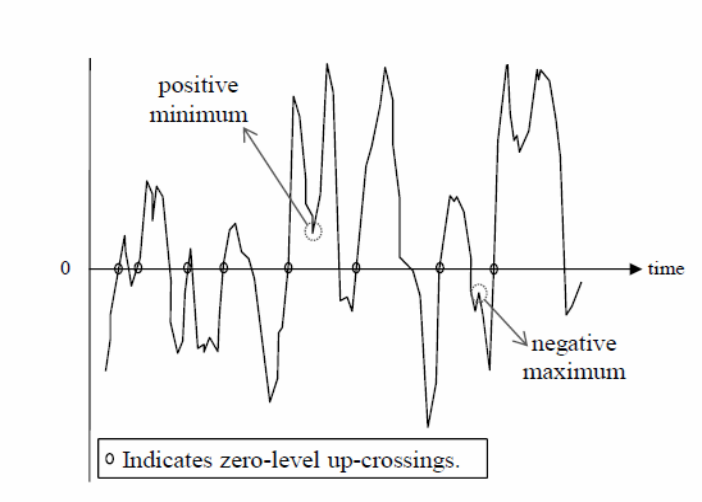

Figure C.2. Sample stochastic process, showing zero-level up-crossings, positive minima, and negative maxima.

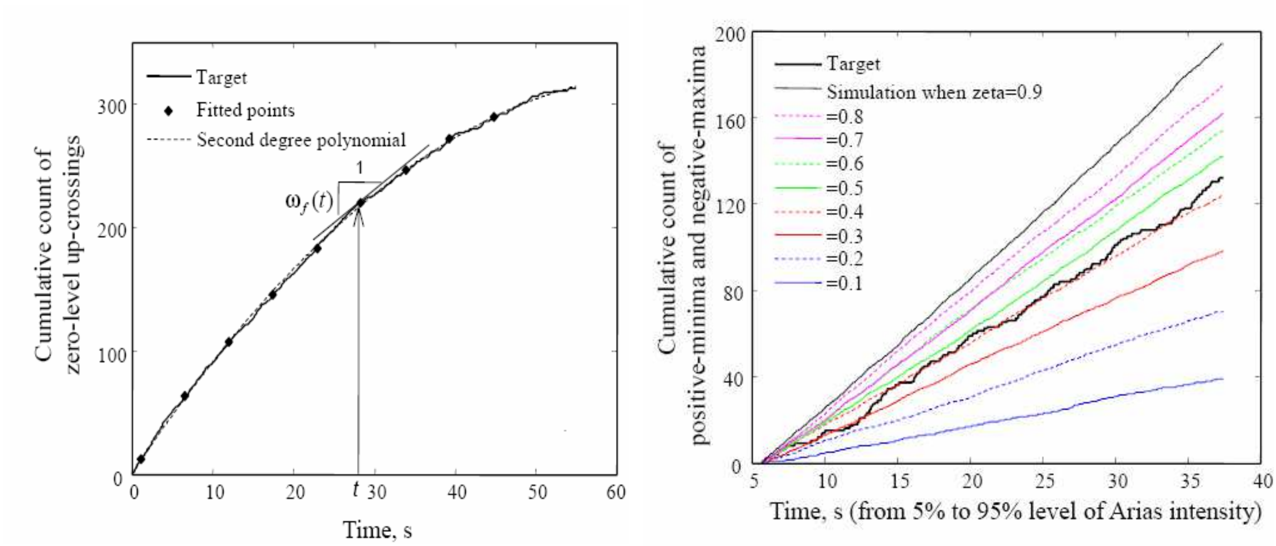

(a) (b)

Figure C.3. Identification of filter parameters, (a) matching the cumulative number of zero level up-crossings (b) matching the cumulative count of negative maxima and positive minima

Appendix D.

Pseudo-acceleration response of a single degree of freedom linear oscillator subjected to an impulsive solicitation

A single degree of freedom (SDOF) system is a spring-mass-damper system in which the spring has no damping or mass, the mass has no stiffness or damping, and the damper has no stiffness or mass. Furthermore, the mass is allowed to move in only one direction (cf. Figure D.1). The SDOF system may be subjected or not to an external time-varying force *f*(*t*).

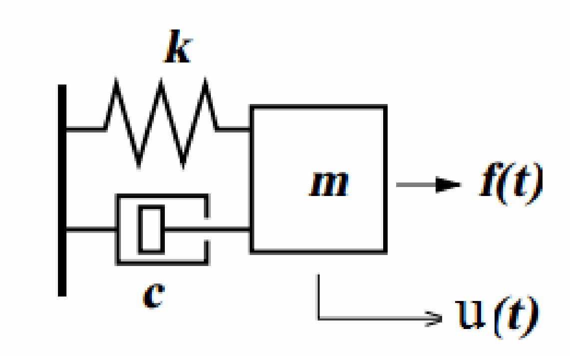

Figure D.1. Single degree of freedom linear oscillator

The general form of the differential equation describing a SDOF oscillator which results from balancing the forces on the mass is given by:

$$M\frac{d^2u}{dt^2}+c\frac{du}{dt}+ku=f(t) \tag{D.1}$$

where u is the displacement of the system, M is the mass of the system, c is the linear viscous damping coefficient, k is the linear elastic stiffness coefficient and $f(t)$ is a time-varying external force. By dividing all the terms of Equation (D.1) by M, one obtains the reduced form of this equation as follows:

$$\frac{d^2u}{dt^2} + 2\xi\omega\frac{du}{dt} + \omega^2 u = \frac{f(t)}{M} \tag{D.2}$$

where $\omega = \sqrt{k/M}$ is the natural frequency of the oscillator, $\xi_c = 2\sqrt{kM}$ is the critical damping of the oscillator and $\xi = c/2\sqrt{kM}$ is its damping ratio.

If the SDOF oscillator is subjected to an impulsive (a single pulse suddenly applied at an instant $t = \tau$) external force $f(t) = \delta(t-\tau)$, the response of the SDOF oscillator $u(t) = h(t-\tau)$ may be obtained by solving Equation (D.2) (cf. Figure D.2).

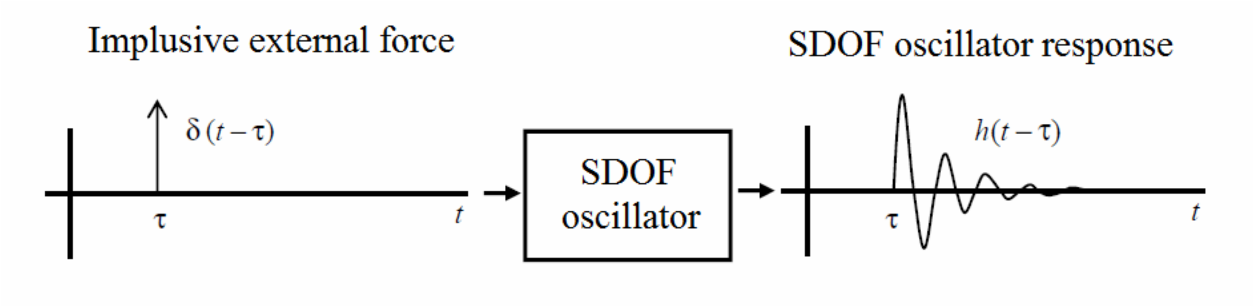

Figure D.2. Impulsive external force and SDOF oscillator response

The solution of Equation (D.2) in the case of an impulsive external force is given as follows:

For $t < \tau$ u=0

For $t \geq \tau$ $$u(t) = h(t-\tau) = \frac{1}{m\,\omega\sqrt{1-\xi^2}}\, e^{-\xi\omega(t-\tau)}\, \sin(\omega\sqrt{1-\xi^2}\,(t-\tau)) \tag{D.3}$$

The pseudo-acceleration response $A(t)$ of the SDOF linear oscillator subjected to an impulsive external force is simply the response $u(t)$ multiplied by the squared natural frequency as follows:

$$A(t) = \omega^2 u(t) = \frac{\omega^2}{m\,\omega\sqrt{1-\xi^2}}\, e^{-\xi\omega(t-\tau)}\, \sin(\omega\sqrt{1-\xi^2}\,(t-\tau)) \tag{D.4}$$

Appendix E.

One-dimensional Hermite polynomials

The one-dimensional Hermite polynomials are given by:

$$H_0(\xi)=1$$
$$H_1(\xi)=\xi$$
$$H_2(\xi)=\xi^2-1$$
$$H_3(\xi)=\xi^3-3\xi$$
$$H_4(\xi)=\xi^4-6\xi^2+3$$
$$H_5(\xi)=\xi^5-10\xi^3+15\xi$$
$$H_6(\xi)=\xi^6-14\xi^4+45\xi^2-15$$
.
.
.
$$H_n(\xi)=\xi H_{n-2}(\xi)-H'_{n-1}(\xi)$$

Illustrative Example

In order to illustrate the PCE theory in a simple manner, a PCE of order p=3 using only M=2 random variables (ξ_1 and ξ_2) will be considered in this illustrative example. As may be easily seen from Table E.1, the PCE basis contains P=10 terms whose expressions $\Psi_\beta\left(\beta=0,...,9\right)$ are computed using Equation (I.38).

β	Order of the term Ψ_β	$\Psi_\beta=\prod_{i=1}^{M}H_{\alpha_i}(\xi_i)$	$E\left(\Psi_\beta^2\right)=\prod_{i=1}^{M}\alpha_i\,!$
0	p=0	$\Psi_0=H_0(\xi_1)xH_0(\xi_2)=1$	$\alpha_1!\ x\ \alpha_2!=0!x0!=1$
1	p=1	$\Psi_1=H_1(\xi_1)xH_0(\xi_2)=\xi_1$	$\alpha_1!\ x\ \alpha_2!=1!x0!=1$
2		$\Psi_2=H_0(\xi_1)\ xH_1(\xi_2)=\xi_2$	$\alpha_1!\ x\ \alpha_2!=0!x1!=1$
3	p=2	$\Psi_3=H_1(\xi_1)\ xH_1(\xi_2)=\xi_1\ \xi_2$	$\alpha_1!\ x\ \alpha_2!=1!x1!=1$
4		$\Psi_4=H_2(\xi_1)\ xH_0(\xi_2)=\xi_1^2-1$	$\alpha_1!\ x\ \alpha_2!=2!x0!=2$
5		$\Psi_5=H_0(\xi_1)\ xH_2(\xi_2)=\xi_2^2-1$	$\alpha_1!\ x\ \alpha_2!=0!x2!=2$
6	p=3	$\Psi_6=H_2(\xi_1)\ xH_1(\xi_2)=\left(\xi_1^2-1\right)\xi_2$	$\alpha_1!\ x\ \alpha_2!=2!x1!=2$
7		$\Psi_7=H_1(\xi_1)\ xH_2(\xi_2)=\xi_1\left(\xi_2^2-1\right)$	$\alpha_1!\ x\ \alpha_2!=1!x2!=2$
8		$\Psi_8=H_3(\xi_1)\ xH_0(\xi_2)=\xi_1^3-3\xi_1$	$\alpha_1!\ x\ \alpha_2!=3!x0!=6$
9		$\Psi_9=H_0(\xi_1)\ xH_3(\xi_2)=\xi_2^3-3\xi_2$	$\alpha_1!\ x\ \alpha_2!=0!x3!=6$

Table E.1. Basis Ψ_β (β=0, …, 9) of the PCE and values of $E\left(\Psi_\beta^2\right)$ for a PCE with M=2 and p=3

By using Table E.1, one can write the PCE as function of the input random variables (ξ_1 and ξ_2) as follows:

$$\begin{aligned}&\Gamma_{PCE}(\xi)=a_0\Psi_0+a_1\Psi_1+...+a_9\Psi_9=\\&a_0+a_1\xi_1+a_2\xi_2+a_3\xi_1\xi_2+a_4(\xi_1^2-1)+a_5(\xi_2^2-1)+a_6\left(\xi_1^2-1\right)\xi_2+a_7\xi_1\left(\xi_2^2-1\right)+a_8(\xi_1^3-3\xi_1)+a_9(\xi_2^3-3\xi_2)\end{aligned} \tag{E.1}$$

where the unknown coefficients can be computed using Equation (I.41). Once the PCE coefficients are computed, the first order Sobol indices for the two random variables (ξ_1 and ξ_2) can be easily obtained using Equation (I.47). The only additional step is to compute $E\left(\Psi_\beta^2\right)$ corresponding to these two random variables. Table E.1 provides the values of $E\left(\Psi_\beta^2\right)$ computed using Equation (I.49) for the different Ψ_β terms. The expressions of the first order Sobol indices of the two random variables ξ_1 and ξ_2 can thus be written as follows:

$$\begin{aligned}S(\xi_1)&=\frac{a_1^2+2a_4^2+6a_8^2}{a_1^2+a_2^2+a_3^2+2a_4^2+2a_5^2+2a_6^2+2a_7^2+6a_8^2+6a_9^2}\\S(\xi_2)&=\frac{a_2^2+2a_5^2+6a_9^2}{a_1^2+a_2^2+a_3^2+2a_4^2+2a_5^2+2a_6^2+2a_7^2+6a_8^2+6a_9^2}\end{aligned} \tag{E.2}$$

where $I_1=(1,4,8)$ and $I_2=(2,5,9)$.

Appendix F.

Introduction

The seismic stability of slopes is widely investigated in literature using deterministic approaches. However, the material properties of soils are known to vary greatly from point to another, and many of these older pen and paper methods have difficulty to successfully model this heterogeneity. Things are more complicated when dealing with dynamic loading situations. In this paper, the effect of both the soil spatial variability and the time variability of Ground-Motion (GM) on the dynamic responses of a simple slope are studied. Few authors have worked on the analysis of the dynamic horizontal soil behavior using probabilistic approaches where the spatial variability of soil properties and the time variability of seismic excitations were considered [Koutsourelakis et al (2002), Popescu et al (2006), ...]. In these works, three main deficiencies can be detected: First, the classical Monte Carlo Simulation (MCS) methodology with a small number of realizations is used to determine the probability density function (PDF) of the system responses (e.g. 50 simulations). It is well known that in order to be a rigorous approach, MCS is very time-expensive. Second, the stochastic model for generating synthetic acceleration time-histories is based on the spectral representation in order to simulate accelerograms which are compatible with a prescribed response spectrum and not real GM acceleration. Finally, the spatial variability of soil properties is studied for specific autocorrelation distances.

In this study, the three mentioned deficiencies will be improved by (i) using a more efficient probabilistic approach instead of the crude MCS which is the Sparse Polynomial Chaos Expansion (SPCE) [Blatman and Sudret (2010), Al-Bittar and Soubra (2011)]; (ii) simulating the stochastic accelerogram using the method given by Rezaeian and Der Kiureghian (2010). This method has the advantage of solving the majority of problems encountered in the previous models [Rezaeian and Der Kiureghian (2008)]; (iii) considering a large range of autocorrelation distances for the soil shear modulus G modeled as an isotropic non-Gaussian random field. The Expansion Optimal Linear Estimation (EOLE) methodology proposed by Li and Der Kiureghian (1993) is used to generate this random field.

The deterministic model is based on numerical simulations using the dynamic option of the finite difference code FLAC^{3D}. Samples of the synthetic GM time-histories were generated and a dynamic stochastic calculation for each realization was performed to compute the dynamic responses (i.e. the permanent displacement at the toe of the slope and the maximum amplification of the acceleration at the top of the slope). The paper is organized as follows: The first three sections aim at presenting (i) the method used to generate the random field of the shear modulus *G*, (ii) the method used to generate the stochastic synthetic accelerograms based on a real target one and finally (iii) the SPCE methodology employed to determine the analytical expression of the dynamic system responses. These sections are followed by a presentation of the probabilistic numerical results in which only the soil spatial variability is first considered and then combined with the time variability of the GM in order to highlight its effect on the variability of the dynamic responses.

Generation of non-Gaussian random field

Let's consider the non-Gaussian random field $Z_G^{NG}(x, y)$ (where *G* represents the soil shear modulus) described by: (i) constant mean μ_G and standard deviation σ_G, (ii) non-Gaussian marginal cumulative distribution function F_G, and (iii) a square exponential autocorrelation function ρ_Z^{NG} [(x, y), (x', y')] which gives the values of the correlation function between two arbitrary points *(x, y)* and *(x', y')*. This autocorrelation function is given as follows:

$$\rho_z^{NG}[(x, y), (x', y')] = \exp\left(-\left(\frac{x-x'}{a_x}\right)^2 - \left(\frac{y-y'}{a_y}\right)^2 \right) \quad \text{(F.1)}$$

where a_x and a_y are the autocorrelation distances along *x* and *y* respectively. The EOLE method proposed by Li and Der Kiureghian (1993) is used herein to generate the random field of *G*. In this method, one should first define a stochastic grid composed of *q* grid points (or nodes) obtained from the different combination of *H* points in the *x* (or horizontal) direction, and *V* points in the *y* (or vertical) direction assembled is a vector $Q=\{Q_n=(x_h, y_v)\}$ where *h=1, …, H, v=1, …, V* and *n=1, …, q*. Notice that for the vector Q composed of q elements, the values of the field are assembled in a vector $\chi=\{\chi_n=Z(x_h, y_v)\}$ where *h=1, …, H, v=1, …, V* and *n=1, …, q*. Then, one should determine the correlation matrix for which each element $\left(\Sigma_{\chi;\chi}^{NG}\right)_{i,j}$ is calculated using Equation (F.1) as follows:

$$\left(\Sigma_{\chi;\chi}^{NG}\right)_{i,j} = \rho_z^{NG}\left[Q_i, Q_j\right] \quad \text{(F.2)}$$

where *i=1, …, q* and *j=1, …, q*. Notice that the matrix $\Sigma_{\chi;\chi}^{NG}$ in equation (F.2) provides the correlation between each point in the vector χ and all the other points of the same vector. The non-Gaussian autocorrelation matrix $\Sigma_{\chi;\chi}^{NG}$ should be transformed into the Gaussian space using the Nataf transformation. As a result, one obtains a Gaussian autocorrelation matrix $\Sigma^{G}_{\chi;\chi}$ that can be used to discretize the random field of the shear modulus G as follows:

$$\tilde{Z}_G(x, y) = \mu_G + \sigma_G \sum_{j=1}^{N} \frac{\xi_j}{\sqrt{\lambda_j}} .\phi_j .\Sigma_{Z(x,y);\chi} \qquad \text{(F.3)}$$

where (λ_j, ϕ_j) are the eigenvalues and eigenvectors of the Gaussian autocorrelation matrix $\Sigma^{G}_{\chi;\chi}$, $\Sigma_{Z(x,y);\chi}$ is the correlation vector between each point in the vector χ and the value of the field at an arbitrary point (x, y), ξ_j is a standard normal random variable, and *N* is the number of terms (expansion order) retained in EOLE method.

Once the Gaussian random field is obtained, it should be transformed into the non-Gaussian space by applying the following formula:

$$\tilde{Z}_G^{NG}(x, y) = F_G^{-1}\left\{\Phi\left[\tilde{Z}_G(x, y)\right]\right\} \qquad \text{(F.4)}$$

where $\Phi(.)$ is the standard normal cumulative density function.

It should be mentioned here that the presented method can be applied for both Gaussian and non-Gaussian random fields. Since non-negative values must be obtained for *G*, a non-Gaussian (lognormal) random field was used in this paper.

Generation of stochastic Ground Motion accelerograms

In this paper, the method proposed by Rezaeian and Der Kiureghian (2010) was used to generate stochastic acceleration time histories from a target accelerogram. This method consists in fitting a parameterized stochastic model that is based on a modulated, filtered white-noise process to a recorded ground motion. The parameterized stochastic model in its continuous form is defined as:

$$x(t) = q(t, \alpha)\left[\frac{1}{\sigma_f(t)} \int_{-\infty}^{t} h\left[t-\tau, \lambda(\tau)\right] w(\tau) d\tau\right] \qquad \text{(F.5)}$$

In this expression, $q(t, \alpha)$ is a deterministic, positive, time-modulating function with parameters α controlling its shape and intensity; $w(\tau)$ is a white-noise process; the integral inside the curved brackets is a filtered white-noise process with $h\left[t-\tau, \lambda(\tau)\right]$ denoting the Impulse-Response Function (IRF) of the filter with time-varying parameters $\lambda(\tau)$; and $\sigma_h^2(t) = \int_{-\infty}^{t} h^2\left[t-\tau, \lambda(\tau)\right] d\tau$ is variance of the integral process. Because of the normalization by $\sigma_h(t)$, the process inside the curved brackets has unit variance. As a result, $q(t, \alpha)$ equals the standard deviation of the resulting process x(t). It should be clear that the modulating function $q(t, \alpha)$ completely defines the temporal characteristics of the process, whereas the form of the filter IRF and its time-varying parameters define the spectral characteristics of the process. In this study, a 'Gamma' modulating function is used:

$$q(t, \alpha) = \alpha_1 t^{\alpha_2 - 1} \exp(-\alpha_3 t) \tag{F.6}$$

where $\alpha = (\alpha_1, \alpha_2, \alpha_3)$, $\alpha_1, \alpha_3 > 0$, and $\alpha_2 > 1$. Of the three parameters, α_1 controls the intensity of the process, α_2 controls the shape of the modulating function and α_3 controls the duration of the motion. These parameters $\alpha = (\alpha_1, \alpha_2, \alpha_3)$ are related to three physically based parameters $(\bar{I}_a, D_{5-95}, t_{mid})$ which describe the real recorded GM in the time domain; where $\bar{I}_a$, is the Arias Intensity (AI), D_{5-95} represents the effective duration of the motion. It is defined as the time interval between the instants at which the 5% and 95% of the expected AIs are reached respectively. t_{mid} is the time at the middle of the strong-shaking phase. It is selected as the time at which 45% level of the expected AI is reached. The relations between $\alpha = (\alpha_1, \alpha_2, \alpha_3)$ and $(\bar{I}_a, D_{5-95}, t_{mid})$ are given in details in Rezaeian and Der Kiureghian (2010).

For the filter IRF, we select a form that corresponds to the pseudo-acceleration response of a single-degree-of-freedom linear oscillator:

$$\begin{aligned} h\left[t-\tau, \lambda(\tau)\right] &= \frac{\omega_f(\tau)}{\sqrt{1-\zeta_f^2(\tau)}} \exp\left[-\zeta_f(\tau)\omega_f(\tau)(t-\tau)\right] \times \sin\left[\omega_f(\tau)\sqrt{1-\zeta_f^2(\tau)}(t-\tau)\right] \qquad t \le \tau \\ &= 0 \qquad \text{otherwise} \end{aligned} \tag{F.7}$$

where $\lambda(\tau) = (\omega_f(\tau), \zeta_f(\tau))$ is the set of time-varying parameters of the IRF with $\omega_f(\tau)$ denoting the frequency of the filter and $\zeta_f(\tau)$ denoting its damping ratio. These two parameters, $\omega_f(\tau)$ and $\zeta_f(\tau)$ are related to two physical parameters that describe the recorded GM in the frequency domain and which are respectively the predominant frequency and the bandwidth of the GM. For more details about the identification procedure between the recorded GM and the stochastic model described previously, the reader may refer to Rezaeian and Der Kiureghian (2008, 2010).

Sparse Polynomial Chaos Expansion (SPCE) methodology

The polynomial chaos expansion (PCE) methodology aims at replacing a complex deterministic model whose input parameters are modeled by random variables by a meta-model which allows one to calculate the system response using an approximate analytical equation [Blatman and Sudret (2010)]. The coefficients of the PCE are computed herein using a regression approach.

For a deterministic numerical model with *M* input uncertain parameters, the uncertain parameters should be represented first by independent standard normal random variables $\{\xi_i\}_{i=1,\ldots,M}$ gathered in a random vector *ξ*. The random response *Γ* of our mechanical model can then be expressed by a PCE of order p fixed by the user as follows:

$$\Gamma_{PCE}(\xi) = \sum_{\beta=0}^{\infty} a_\beta \Psi_\beta(\xi) \cong \sum_{\beta=0}^{P-1} a_\beta \Psi_\beta(\xi) \tag{F.8}$$

where *P* is the number of terms retained in the truncation scheme, a_β are the unknown PCE coefficients to be computed and Ψ_β are multivariate (or multidimensional) Hermite polynomials which are orthogonal with respect to the joint probability distribution function of the standard normal random vector *ξ*. These multivariate polynomials are given by $\Psi_\beta = \prod_{i=1}^{M} H_{\alpha_i}(\xi)$, where $H_{\alpha_i}(.)$ is the α_i-th one-dimensional Hermite polynomial and α_i are a sequence of M non-negative integers $\{\alpha_1, \ldots, \alpha_M\}$. In practice, one should truncate the PCE representation by retaining only the multivariate polynomials of degree less than or equal to the PCE order *p*. For this reason, a classical truncation scheme based on the determination of the first order norm is generally adopted in the literature. This first order norm is defined as follows: $\|\alpha\|_1 = \sum_{i=1}^{M} \alpha_i$. The classical truncation scheme suggests that the first order norm should be less than or equal to the order *p* of the PCE. Using this method of truncation, the number *P* of the unknown PCE coefficients is given by $P = \frac{(M+p)!}{M!\,p!}$. Thus, the number *P* of the PCE coefficients increases dramatically with the number *M* of the random variables and the order *p* of the PCE. To overcome such a problem, it was shown that the number of significant terms in a PCE is relatively small since the multidimensional polynomials Ψ_β corresponding to high-order interaction are associated with very small values for the coefficients a_β. Thus, a truncation strategy based on this observation was developed in which the multidimensional polynomials Ψ_β corresponding to high-order interaction were penalized. This was performed by considering the hyperbolic truncation scheme that considers the q-norm instead of the first order norm. The *q*-norm is given by $\|\alpha\|_q = \left(\sum_{i=1}^{M} \alpha_i^q\right)^{1/q}$ where *q* is a coefficient (0<*q*<1). The hyperbolic truncation scheme suggests that the q-norm should be less than or equal to the order p of the PCE. The proposed methodology leads to a SPCE that contains a small number of unknown coefficients which can be calculated from a reduced number of calls of the deterministic model. This is of particular interest in the present case of random fields which involve a significant number of random variables. This strategy will be used in this paper to build up a SPCE of the system response using an iterative procedure [Blatman and Sudret (2010)]. Once the unknown coefficients of the SPCE are determined, the PDF of the dynamic responses can be estimated using Monte Carlo technique.

Numerical results

The aim of this section is to present the probabilistic results. It should be remembered here that the dynamic system responses involves the permanent displacement at the toe and the maximum amplification of the acceleration at the top of the slope. In this study, the effect of both the soil spatial variability and the time variability of Ground-Motion (GM) on the dynamic responses are considered. The soil shear modulus G is considered as an isotropic lognormal random field. The mean and the coefficient of variation of G are respectively $\mu_G = 112.5MPa$ and $Cov_G = 40\%$. In order to simulate the stochastic synthetic time histories, the Kocaeli (Turkey 1999) earthquake is used as the target accelerogram (see Figure F.1). The deterministic model is based on numerical simulations using the dynamic option of the finite difference code FLAC^{3D}. The slope geometry considered in the analysis is 10m in height and 45^{o} in inclination angle (see Figure F.2). It should be noted that the size of a given element in the mesh depends on both the autocorrelation distances of the soil properties and the wavelength λ associated with the highest frequency component f_{max} of the input signal. For the autocorrelation distances of the soil properties, Der Kiureghian and Ke (1988) have suggested that the length of the smallest element in a given direction (horizontal or vertical) should not exceed 0.5 times the autocorrelation distance in that same direction. As for the wavelength λ associated with the highest frequency component f_{max} of the input signal, Itasca (2000) has suggested that the smallest element should not exceed 1/10 to 1/8 this wavelength λ in order to avoid numerical distortion of the propagating waves. Respecting these two conditions, a size element of 2m was chosen to perform the dynamic analysis. For the boundary conditions, the bottom horizontal boundary was subjected to an earthquake acceleration signal and free field boundaries were applied to the right and left vertical boundaries. The numerical simulations are performed using an elastoplastic model based on the Mohr-Coulomb failure criterion. The corresponding model parameters are the shear modulus G which is modeled as a random field, the bulk modulus K, the cohesion c, the friction angel φ, the dilation angel ψ, and the soil unit weight which are considered as deterministic. The values of these deterministic parameters are as follows: K=133MPa, c=10kPa, φ=30^o, ψ =20^o, and γ =18kN/m^3.

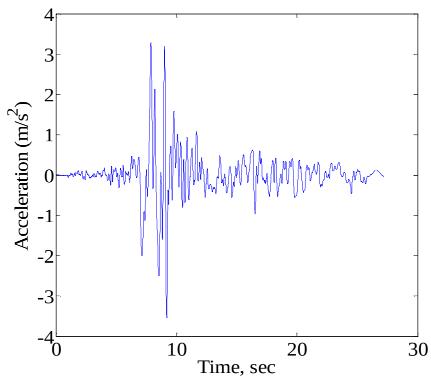

Figure F.1. Kocaeli (Turkey 1999) accelerogram

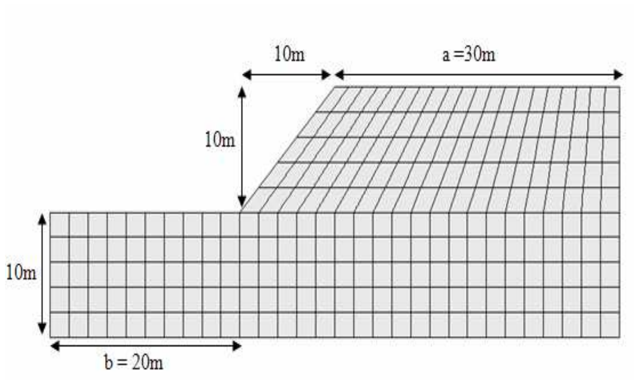

Figure F.2. The slope geometry and FLAC^{3D} mesh

In the following sections, one examines the effect of the soil spatial variability on both the amplification at the top and the permanent displacement at the toe of the slope using deterministic and stochastic GM accelerograms.

Effect of the soil spatial variability on the amplification at the top of the slope using deterministic and stochastic GM accelerograms

The effect of the soil spatial variability on the amplification at the top of the slope using deterministic and stochastic GM accelerograms is studied and presented in Figures F.3, F.4 and Table F.1. Different values of the isotropic autocorrelation distance (θ=0.5, 1, 2, 3, 5) were considered in the analyses. Notice that in the current study, the autocorrelation distance has been nondimensionalized by dividing it by the height of the slope. Figures F.3 and F.4 show that the PDF is less spread out when the isotropic autocorrelation distance θ decreases. The variability of the amplification at the top of the slope decreases with the increase in the soil heterogeneity (i.e. small values of θ). This can be explained by the fact that the fluctuations of the shear modulus are averaged to a mean value along the seismic wave's path propagation. This mean is close to the probabilistic mean value of the random field G. This leads to close values of the responses amplification and thus to a smaller variability in this response. Notice however that adding the randomness of the earthquake GM has a significant incidence on the variability of the amplification. Table F.1 shows that for the range of the autocorrelation distances considered in this study, the coefficient of variation COV of the amplification is between 2.78% and 10.91% when deterministic GM accelerogram is used. This range of COV increases significantly when the randomness of the earthquake GM is introduced. In this case, the COV of the amplification have values between 4.23% and 31.78%. One can notice that for the largest autocorrelation distance θ=5, the variability of the amplification in the case where stochastic GM accelerograms were used is 2.9 time larger than the one obtained with the deterministic GM accelerogram.

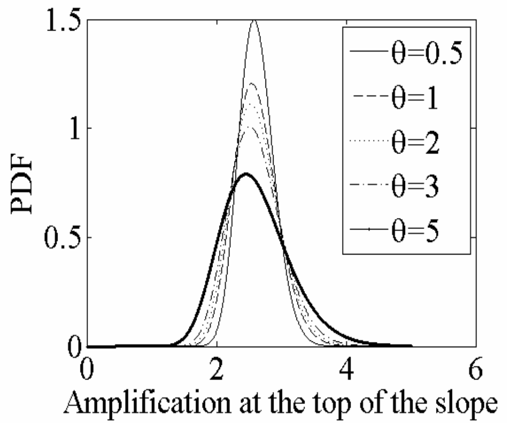

Figure F.3. Amplification at the top of the slope with deterministic GM

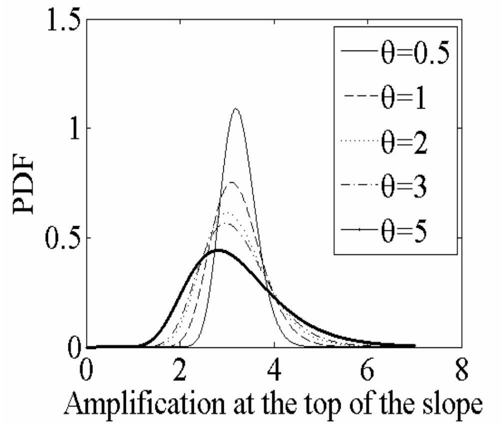

Figure F.4. Amplification at the top of the slope with stochastic GM

Table F.1 also shows that the autocorrelation distance θ has practically no effect on the mean value of the amplification. This mean value is shown to be larger than the corresponding deterministic value. This means that the probabilistic results are much more critical than the deterministic value with a difference of 5% in the case where deterministic GM accelerogram is is used, and 29% in the case where stochastic GM accelerograms are used.

	θ	Mean μ x 10^{-2} (m)	Standard deviation σ	*COV* (%)	Deterministic amplification
Deterministic GM	0.5	2.6	0.073	2.784	2.48
	1	2.6	0.114	4.364	
	2	2.6	0.135	5.176	
	3	2.6	0.166	6.362	
	5	2.6	0.285	10.915	
	θ	Mean μ x 10^{-2} (m)	Standard deviation σ	*COV* (%)	Deterministic amplification
Stochastic GM	0.5	3.2	0.138	4.237	2.48
	1	3.2	0.301	9.301	
	2	3.2	0.472	14.610	
	3	3.2	0.567	17.565	
	5	3.2	1.030	31.780	

Table F.1. Effect of the autocorrelation distance θ on the statistical moments (μ, σ) of the amplification

Effect of the soil spatial variability on the permanent displacement at the toe of the slope using deterministic and stochastic GM accelerograms

The effect of the soil spatial variability on the permanent displacement at the toe of the slope using deterministic and stochastic GM accelerograms is studied and presented in Figures F.5, F.6 and Table F.2. The same values of the isotropic autocorrelation distance θ used in the previous section are also used herein. Figures F.5 and F.6 show that the PDFs are very close to each other and thus the shear modulus variability has a small influence on the permanent displacement. This is because the permanent displacement appears only when the plastic phase is reached which means that the effect of the shear modulus *G* on this response is relatively small. Table F.2 confirms this observation because very small values of the *COV* of the permanent displacement are obtained when only the spatial variability of *G* is considered. On the other hand, one can see that introducing the randomness of the earthquake GM considerably affects the permanent displacement. High values of the *COV* are detected because of the important increase in the mean value of the permanent displacement due to the variability of the GM.

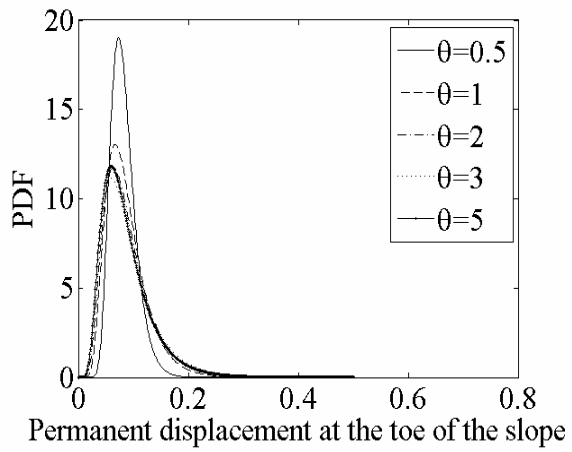

Figure F.5. Permanent displacement at the toe of the slope with deterministic GM

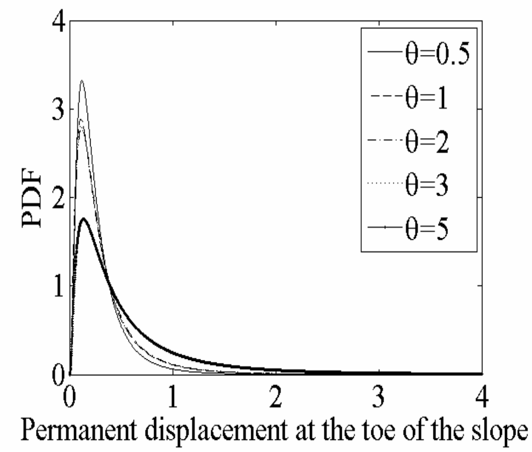

Figure F.6. Permanent displacement at the toe of the slope with stochastic GM

Table F.2 also shows that the mean value of the permanent displacement presents a maximum. This maximum was detected when θ=2, i.e. when the isotropic autocorrelation distance is equal to the height of the soil domain. When θ decreases from 5 to 2, one can notice that the mean of the permanent displacement increases. This can be explained by the fact that increasing the soil heterogeneity introduces weak zones with small values of the shear modulus *G*, thus leading to larger values of the permanent displacement. The decrease in the permanent displacement for values of θ smaller than 2 may be explained by the fact that as the autocorrelation distance decreases, the propagating wave can face some stiff zones which reduce the permanent displacement. Finally, on can notice also that introducing the soil spatial variability and the randomness of GM lead to more critical results since all the mean values of the permanent displacement obtained in the probabilistic study are larger than the corresponding deterministic value.

	θ	Mean μ x 10^{-2} (m)	Standard deviation σ	*COV* (%)	Deterministic permanent displacement
Deterministic GM	0.5	8.20	0.0005	0.610	0.0407
	1	8.62	0.0014	1.624	
	2	8.84	0.0020	2.262	
	3	8.75	0.0021	2.400	
	5	8.55	0.0025	2.924	
	θ	Mean μ x 10^{-2} (m)	Standard deviation σ	COV (%)	Deterministic permanent displacement
Stochastic GM	0.5	26.20	0.0596	22.75	0.0407
	1	26.46	0.1248	47.16	
	2	27.40	0.1267	46.24	
	3	27.17	0.1359	50.02	
	5	25.57	0.2793	109.23	

Table F.2. Effect of the autocorrelation distance θ on the statistical moments (μ, σ) of the permanent displacement

Conclusions

The effect of both the soil spatial variability and the Ground-Motion (GM) time variability on the dynamic responses is studied. The soil shear modulus *G* is considered as an isotropic non-Gaussian random field. The simulation of variable acceleration time histories based on a real target accelerogram is done using a fully nonstationary stochastic model. The deterministic model was based on numerical simulations using the dynamic option of the finite difference code FLAC^{3D}. The methodology adopted in this paper makes use of a non-intrusive approach to build up a sparse polynomial chaos expansion (SPCE) for the dynamic system responses. The main conclusions can be summarized as follows: (i) the decrease in the autocorrelation distance of *G* (i.e. the soil heterogeneity) leads to a small variability of the dynamic responses; the amplification being more affected; (ii) adding the randomness of the earthquake GM has a significant incidence on the variability of the dynamic responses; (iii) the isotropic autocorrelation distance affects the probabilistic mean values of plastic responses (eg. the permanent displacement); its effect being negligible on elastic responses (eg. the amplification).

Appendix G.

The purpose of this Appendix is to check if the possible reason for which relatively small values of Q^2 were obtained (when the SPCE methodology was applied in chapter V) is linked to the chosen system response (i.e. A_{max}). Notice that the test was performed using the 'column' model and the reference case where $\mu_{G_1} = 72MPa$ and a_y=2m.

The test consists in constructing the SPCE not only for A_{max} at the top of the soil column but for all the accelerations at the top of the soil column at the different time steps (the value of A_{max} can be deduced from the different SPCEs constructed at the different time steps). This test allows one to detect if the fact of considering directly A_{max} as a system response is the reason for which the relatively small values of Q^2 were obtained.

Notice that a seismic loading of total duration T=15s and time step Δt=0.05s was considered in the analysis. Thus, it is composed of 301 registration points (or acceleration values). The construction of the SPCE 301 times is a difficult task. Blatman and Sudret (2011) have suggested an efficient and fast alternative approach. To obtain the SPCEs for all the accelerations at the different time steps, Blatman and Sudret (2011) have proposed the use of the so-called *principal component analysis* (PCA). The aim is to capture the main stochastic feature of the response using a small number of (non physical) variables compared to the original number of variables (i.e. 301 in the present analysis). This enormously reduces the computational cost since the SPCEs are no longer evaluated for all the accelerations at the different time steps, but on a small number of non physical variables. In the next section, one presents the so-called *principal component analysis* (PCA). It is followed by the obtained numerical results.

Principal component analysis (PCA)

Consider an experimental design (ED) $\{\xi^{(1)} = (\xi_1,...,\xi_M),...,\xi^{(K)} = (\xi_1,...,\xi_M)\}$ and the corresponding set of model evaluations $\Gamma = \left\{\Gamma\left(\xi^{(1)}\right),...,\Gamma\left(\xi^{(K)}\right)\right\}$ where K is the number of realizations. Notice here that each element $\Gamma\left(\xi^{(i)}\right)$ is a vector composed of Q elements where Q is the number of response components. In our case where the acceleration at the top of the column at different time steps is considered, Q=301 which is the number of registration points. Thus, Γ is a matrix composed of K rows and Q columns. In order to perform the principal components analysis, the following steps must be considered:

- For each column in matrix Γ, one needs to compute the mean value and then to subtract this mean value from each element in this same column. This provide a new matrix Γ'.

- Compute the covariance matrix as follows: $C_{\Gamma'} = \Gamma' x \Gamma'^T$

  Compute the eigenvalues and eigenvectors of $C_{\Gamma'}$ by solving the matrix system $C_{\Gamma'} V = VD$ where *V* is a matrix whose columns are the eigenvectors and *D* is a diagonal matrix whose entries are the eigenvalues ($\lambda_1, \ldots, \lambda_K$).

- Sort the eigenvalues and the corresponding eigenvectors in a descending order and retain only the *K'* largest eigenvalues. Notice that the value of *K'* may be selected such that the relative PCA induced error given by $\varepsilon_{PCA} = 1 - \sum_{i=1}^{K'} \lambda_i \Big/ \sum_{i=1}^{K} \lambda_i$ is less than a prescribed value (say $\varepsilon_{PCA} \leq 5\%$). Notice that $V_{K'}$ of dimensions [*Q*, *K'*] is a matrix whose columns are the eigenvectors of the *K'* largest eigenvalues.

- Compute the transformed and reduced response matrix (called PCA matrix) as follows: $Y_{K'} = \Gamma' V_{K'}$.

  where $Y_{K'}$ is a matrix composed of *K* rows and *K'* columns.

Notice that obtaining the orginal model from the PCA matrix $Y_{K'}$ is straighforwad. This can be performed by applying the following equation: $\Gamma' = V_K Y_{K'}$. Thus, characterizing the model response Γ' or Γ can be achieved indirectly by identifying a functional relationship between the input random vector ξ and the PCA output matrix $Y_{K'}$.

Numerical results

In this section, one presents the numerical results obtained using the PCA which was previously presented. The aim is to capture the main stochastic feature of the response using a small number of (non physical) variables compared to the original number of variables (i.e. 301 in the present analysis). This enormously reduces the computational cost since the SPCEs are no longer evaluated for all the accelerations at the different time steps, but on a small number of non physical variables. The SPCEs computed for the non-physical variables are then used to deduce the SPCEs for all the accelerations at the different time steps.

In the present work, the original matrix Γ is composed of K=500 rows (corresponding to 500 realisations of the input random vector ξ) and Q=301 columns (corresponding to 301 registration points of the acceleration). This original matrix was then used to deduce the matrix Γ' (as presented in the previous section) which will be used to perform the PCA. The PCA has lead to a reduced number K'=5 of most influent eigenmodes for the prescribed error of $\varepsilon_{PCA} \approx 5\%$. This means that for the 301 registration points, only five SPCEs must be evaluated in order to estimate the SPCEs of the 301 registration points. The SPCE methodology was applied on the five most influent eigenmodes, and the deduced SPCEs of the 301 registration points were computed (not presented herein). Notice that the values of Q^2 obtained for the five most influent eigenmodes (when using the 500 MC simulations) were respectively 0.65, 0.6, 0.2, 0.2 and 0.2.

Table G.1 presents the first two statistical moments as obtained from the direct determination of the SPCEs at three different arbitrary times (t_1=2.5s, t_2=5s and t_3=10s). In the same table, one also presents the first two statistical moments as obtained from the SPCEs deduced after performing a PCA on the output matrix Γ. This table shows that the presented results using the PCA are in good agreement with those obtained form the direct determination of the SPCE at the three chosen times. Even though satisfactory results for the fist two statistical moments were obtained, unsatisfactory values of Q^2 were obtained when using either the PCA or the direct determination of the SPCE. Thus, for such types of problems, one needs to find more advanced stochastic models in order to obtain more rigorous meta-models for the highly non-linear problems.

	Direct determination of the SPCEs			Determination of the SPCEs using the PCA	
	μ_A (m/s^2)	σ_A (m/s^2)	Q^2	μ_A (m/s^2)	σ_A (m/s^2)
t_1=2.5s	0	0.80	0.66	-0.05	0.71
t_2=5s	-1.58	3.33	0.81	-1.52	3.82
t_3=10s	0.9	2.67	0.69	0.87	2.90

Table G.1. Values of the first two statistical moments and the coefficient of determination Q^2

Appendix H.

Mathematical description of the macro-element

The purpose of this Appendix is to describe a theoretical model based on strain hardening plasticity theory which is capable of describing the behavior of a shallow footing when it is subjected to all possible combinations of vertical, horizontal and moment loading using the macro-element.

In the framework of the macro-element theory, any load or deformation path can be applied to the footing and the corresponding unknowns (deformations or loads) can be calculated.

The foundation is assumed to be rigid and the nonlinearities of the soil and interface are assumed to be condensed in a representative point which is the footing centre. Within that framework, it is suggested to work with generalized (global) variables: (i) the force resultants, i.e. the vertical force V, the horizontal forces H_x, H_y, and the moments M_x, M_y and (ii) the corresponding displacements; i.e. the vertical displacement u_z, the horizontal displacements u_x and u_y, and the rotations θ_x and θ_y. The torque moment (M_z) and the corresponding displacement are not taken into account in the present analysis.

The three-dimensional SSI macro-element takes into account three different mechanisms: the soil elasticity, the possible soil plasticity and the possible uplift of the foundation. The total displacement can thus be considered as a sum of three components related to the elastic and plastic behavior of the soil and the uplift behavior of the foundation. These three different mechanisms and their mathematical development are extensively presented in Crémer et al. (2002), Grange et al. (2009a) and Grange et al. (2009b) and are briefly described herein.

Elastic behaviour

The elastic constitutive model can be written as $\vec{F} = K^{el}\left(\vec{u} - \vec{u}^{\,pl}\right)$ where $\vec{u} = \left(u'_z \quad u'_x \quad \theta'_y \quad u'_y \quad \theta'_x\right)$ and $\vec{F} = \left(V' \quad H'_x \quad M'_y \quad H'_y \quad M'_x\right)$ are the vectors that represent the dimensionless generalized displacements and forces and K^{el} is the elastic stiffness matrix [Grange et al. (2009a)].

Plastic behaviour - failure criterion and loading surface

The loading surface used was initially developed in Crémer et al. (2001) to describe the behaviour of a 2D shallow foundation. The extension of this loading surface to cover the case of a 3D shallow foundation is a five-dimensional surface. It is given as follows:

$$\begin{aligned} f_c(F,\vec{\tau},\rho,\gamma) \equiv & \left(\frac{H'_x}{\rho a V'^c \left(\gamma - V'\right)^d} - \frac{\alpha}{\rho} \right)^2 + \left(\frac{M'_y}{\rho b V'^e \left(\gamma - V'\right)^f} - \frac{\beta}{\rho} \right)^2 \\ & + \left(\frac{H'_y}{\rho a V'^c \left(\gamma - V'\right)^d} - \frac{\delta}{\rho} \right)^2 + \left(\frac{M'_x}{\rho b V'^e \left(\gamma - V'\right)^f} - \frac{\eta}{\rho} \right)^2 - 1 = 0 \end{aligned} \qquad \text{(H.1)}$$

The coefficients *a* and *b* define the size of the surface in the plane (*H'-M'*), and the coefficients *c*, *d*, *e* and *f* define the parabolic shape of the surface in the planes (*V'-M'*) and (*V'-H'*). Theses parameters can be obtained by fitting this equation to the experimental results. On the other hand, the vector $\vec{\tau} = (\alpha, \beta, \delta, \eta)$ is the kinematics hardening vector. It is composed of 4 kinematics hardening variables and ρ is the isotropic hardening variable. The variable γ is chosen to parameterize the second intersection point of the loading surface with the *V'* axis and its evolution in the *V'* axis (the other point is the origin of the space). The evolution of the hardening variables is obtained by considering experimental results and numerical simulations [Crémer et al. (2001)]. Notice finally that the failure criterion is given by Equation (H.1) with $(\alpha, \beta, \delta, \eta, \rho, \gamma) = (0,0,0,0,1,1)$.

Uplift behaviour - failure criterion and loading surface

The uplift behaviour is not influenced by the horizontal forces. For the uplift mechanism, the failure criterion is given by Grange et al. (2009) as follows:

$$f_\infty \equiv M'^2 - \left(\frac{V'}{q_1} \left(e^{-AV'} + q_2 \right) \right)^2 = 0 \qquad \text{(H.2)}$$

where *A* is a parameter of the constitutive model and (q_1, q_2) is a couple of integers that takes into account the shape of the foundation. As for the loading surface, its evolution is more complicated than for a classical plasticity model. Thus, it is not presented herein. For more details, the reader may refer to Grange et al. (2009a). The uplift mechanism is coupled with the plasticity mechanism by using the classical multi-mechanism approach.